The role of Biophotons in cellular senescence.

Kalampouka, Ifigeneia, Kalampouka, Ifigeneia and Kalampouka, Ifigeneia

https://doi.org/10.34737/wy80y

THE ROLE OF BIOPHOTONS IN CELLULAR SENESCENCE

IFIGENEIA KALAMPOUKA

PhD Thesis

Awarded by the University of Westminster

A thesis submitted in partial fulfilment of the requirements of the University of Westminster for the degree of Doctor of Philosophy

July 2024

Acknowledgements

Among everyone who supported me through my PhD, I want to thank first my greatest source of encouragement, my beloved Nikos.

I am deeply grateful to my dedicated supervisors:

Prof Jimmy Bell, who initially recruited me to our research group, opened doors, introduced me to the field of Quantum Biology, and has been my academic mentor for over five years.

Prof Louise Thomas, who has always bolstered my confidence and applied her extensive experience to facilitate every one of my academic needs throughout my PhD journey.

Dr Rhys Mould, who has been a leading figure in the lab, included me in various projects and consistently challenged my understanding of complex concepts and methods.

I extend my sincere appreciation to my honorary supervisor, Prof Alistair Nunn, for honing my approach to scientific thinking, and to Prof Geoffrey Guy for placing his trust in me as a scientist by providing the funding for my PhD.

My heartfelt thanks go to those who have been instrumental in my academic journey: Dr Meliz Sahuri Arisoylu for teaching me good laboratory practices; Dr Bradley Elliott, my MSc supervisor who inspired my pursuit of research; Grace Pennelli for her invaluable assistance in the lab; and Nina Copping for her support through the Guy Foundation.

I'm grateful to my caring friends Lili, Anna, and Yvoni for their moral support throughout this journey.

Lastly, thank you to my dearly loved family, Nikos, Vicky, and Christina, for their continuous support in every facet of my life. You are the foundation for each of my achievements.

Abstract

Senescence is the irreversible arrest of cell proliferation. While serving as a natural barrier against mutation progression, senescence's metabolic activity and elevated ROS levels can pose significant health risks. Concurrently, cellular metabolic processes, including mitochondrial respiration, are known to emit ultra-weak photons (biophotons), primarily generated through ROS production. There is increasing evidence that cells can influence each other non-chemically via biophotons. In this study, I aim to elucidate the potential impact of both intrinsic biophotonic emissions and extrinsic light exposure on cellular senescence. To achieve this, I developed, utilising doxorubicin (Dox), four different senescence models: two cancer (MCF7 breast and A549 lung) and two non-cancer cell lines (MCF10A breast and IMR-90 lung fibroblasts). Dox-treated cells showed senescent-related physiological changes, including decreased proliferation ($P \leq 0.05$), increased beta-galactosidase activity ($P \leq 0.001$), increased ROS ($P \leq 0.01$), mitochondrial membrane potential ($P \leq 0.01$) and calcium (Ca^{2+}) levels ($P \leq 0.01$). Then, to investigate potential biophotonic communication, I utilised a customised assay to detect non-chemical signalling, showing an increasing oxygen consumption rate in isolated mitochondria from senescent MCF10A (0.0029% per second; $P < 0.0001$), MCF7 (0.0042% per second; $P < 0.0001$) and A549 cells (0.0017% per second; $P < 0.0001$). Additionally, photons emitted by isolated mitochondria from senescent MCF10A cells were monitored via an ultra-sensitive light detector, confirming biophotonic activity (1.86 ± 0.82 photons per 10 seconds; $P \leq 0.05$). Further comparison of mitochondrial non-chemical signalling between senescent and non-senescent cells revealed distinct biophotonic communication across the three tested senescent cell lines, with significant differences compared to their non-senescent cellular controls (MCF10A and MCF7: $P \leq 0.0001$; A549: $P \leq 0.05$). In addition, I have shown that cells interact with external light, as exposure to near-infrared (NIR) light (734 nm) increased senescent levels in the cancer cell lines ($P \leq 0.01$), associated with increased ROS production ($P \leq 0.05$), mitochondrial membrane potential ($P \leq 0.05$), and intracellular Ca^{2+} levels ($P \leq 0.05$), but not in the two non-cancer populations. My work demonstrates that biophotons and extracellular light (NIR light exposure) may play a significant role in senescence and open novel insights for non-invasively influencing cellular processes.

List of Content

List of Figures

List of Tables

Abbreviations

ADP: adenosine diphosphate

AMPK: AMP-activated protein kinase

ATCC: American type culture collection

ATP: adenosine triphosphate

BSA: bovine serum albumin

CCO: cytochrome C oxidase

CDK: cyclin dependent kinases

DAPI: 4′-6-diamidino-2-phenylindole

DCFDA: 2',7' –dichlorofluorescin diacetate

DCF: 2',7' –dichlorofluorescin

DDR: DNA damage response

DI: autoclave deionized

DMEM: Dulbecco's modified eagle medium

DMSO: dimethyl sulfoxide

Dox: doxorubicin

ELISA: enzyme-linked immunosorbent assay

EMEM: eagle's minimum essential medium

FACS: fluorescence-activated cell sorting

FBS: fetal bovine serum

HGPS: Hutchinson–Gilford progeria syndrome

HIF-1α: hypoxia-inducible factor 1α

H_2O_2: hydrogen peroxide

IL: interleukin

LED: light emitting diode

LLLT: low level laser therapy

MAB: mitochondrial assay buffer

MAPK: mitogen-activated protein kinase

MIM: mitochondrial inner membrane

MMP: mitocondrial membrane potential

mtDNA: mitochondrial DNA

mTOR: mammalian target of rapamycin

MTT: 3-(4,5-dimethylthiazol-2-yl)-2,5-diphenyltetrazolium bromide

NADPH: Nicotinamide adenine dinucleotide phosphate

NF-κB: nuclear factor-κB

NIR: near-infrared

O_2^-: anion superoxide

OCR: oxygen consumption rate

OIS: oncogene-induced senescence

OXPHOS: oxidative phosphorylation

PBM: photobiomodulation

PBS: phosphate-buffered saline

PD: population doubling

PI: propidium iodide

pRb: p16/Retinoblastoma

qPCR: quantitative real-time polymerase chain reaction

Raf: fibrosarcoma

Ras: rat sarcoma

RIPA: radioimmunoprecipitation assay

ROS: reactive oxygen species

SASP: secretory associated senescence phenotype

SA β-gal: senescence-associated beta-galactosidase

SD: standard deviation

SEM: standard error of the mean

SIPS: stress-induced premature senescence

SMS: senescence messaging secretome

TMRE: tetramethylrhodamine ethyl ester

UV: ultraviolet radiation

UPE: ultraweak photon emission

List of accompanying material

Publications arising from this thesis:

Kalampouka, I., Mould, R. R., Botchway, S. W., Mackenzie, A. M., Nunn, A. V., Thomas, E. L., & Bell, J. D. (2024). Selective induction of senescence in cancer cells through near-infrared light treatment via mitochondrial modulation. *Journal of Biophotonics*. https://doi.org/10.1002/jbio.202400046

General authorship publications:

Mould, R. R., Mackenzie, A. M., **Kalampouka, I**., Nunn, A. V. W., Thomas, E. L., Bell, J. D., & Botchway, S. W. (2024). Ultra weak photon emission—a brief review. *Frontiers in Physiology*, *15*. https://doi.org/10.3389/fphys.2024.1348915

Mould, R. R., **Kalampouka, I**., Thomas, E. L., Guy, G. W., Nunn, A. V. W., & Bell, J. D. (2023). Non-chemical signalling between mitochondria. *Frontiers in Physiology*, *14*. https://doi.org/10.3389/fphys.2023.1268075

Presentation, conference and research awards:

Three Minute Thesis Competition 2024, University of Westminster – "*Talking through light*" Winner & People's Choice Award

Mitox Conference 2023, University of Oxford, UK – "*NIR light exposure induces senescence to breast cancer cells but not healthy breast cells*" Best Poster Award

Quantum Effects in Biological Systems Workshop 2023, University of Surrey, UK – "*NIR light induces senescence in cancer but not healthy cells*" Best Poster Award

Authors declaration

I declare that all material contained in this thesis is my own work. Any assistance and collaborations are detailed in the “Declaration of Contributors”.

Declaration of Contributors:

Dr Rhys Mould (University of Westminster) produced the data for the mitochondrial assay buffer (MAB) photonic emission (N=3) using the ultra-sensitive light detector and shared the raw data of non-chemical communication assay for non-senescent MCF10A and MCF7 (Mould et al., 2023).

Dr Brandon Whitcher and Dr Rhys Mould wrote the statistical analysis code in RStudio to calculate the mitochondrial oxygen consumption rate.

LED light characterization was performed by Prof Stan Botchway and Dr Alasdair Mackenzie at the Research Complex at Harwell, Science & Technology Facilities Council.

The LED NIR light was provided by Prof Margaret Ahmad (University of Sorbonne).

Chapter 1 : Introduction

1.1 Senescence

Cells possess a variety of strategies to manage stress and strive to maintain their internal physiological and chemical conditions. They can overcome environmental and internal stress through multiple homeostatic mechanisms and DNA repair pathways when the stressors cause mild damage. However, when the stress is prolonged and/or highly intense, and the cells cannot recover from the damage, they will signal the process of apoptosis (programmed cell death) and eventually die (Vasileiou et al., 2019). Cells do have, however, also intermediate responses to stress; when the stressor is not damaging enough to induce apoptosis, or the cell is unable to ensure tissue homeostasis and organismal health after exposure to the stressor, it undergoes a transition into a senescent state (Myrianthopoulos et al., 2019; Vasileiou et al., 2019).

The senescent cell is a highly metabolically active cell that has permanently lost its ability to proliferate (Hayflick & Moorhead, 1961; Quijano et al., 2012). The first senescent cell culture was reported by Hayflick and Moorhead more than 60 years ago when they observed human diploid fibroblasts entering permanent cell cycle arrest following extensive *in vitro* serial passaging (Hayflick & Moorhead, 1961). The molecular trigger that induced senescence in diploid fibroblasts used by Hayflick and Moorhead was telomere attrition (Harley et al., 1990). As cells undergo repeated rounds of proliferation, the progressive shortening of telomeres reaches a critical length, known as the Hayflick limit, after which the cells enter a proliferation arrest state: senescence (Hayflick & Moorhead, 1961).

Cellular senescence can be induced by different stressors, both environmental and intrinsic. For example, senescence can be triggered by extensive replication due to telomere attrition. This is known as ***replicative senescence***, with the population doublings (PD) required for reaching senescence depending on the cell line and/or the origin of cells (Fumagalli et al.,

2014; Hayflick & Moorhead, 1961). Cellular senescence can be triggered by other stressors, such as oxidative or DNA damage (Gorgoulis & Halazonetis, 2010; Herskind & Rodemann, 2000; Myrianthopoulos et al., 2019). The second type of senescence, caused by stressors other than and before telomere shortening, is called ***premature senescence*** (Kuilman et al., 2010). Interestingly, there is not one senescence-specific physiological characteristic observed in all types of senescence, and the senescent cellular response is highly dependent on the cell type and stress inducer (Hernandez-Segura et al., 2018a; Kumari & Jat, 2021; Lujambio, 2016). Even when cells are exposed to the same stressor, such as oxidative stress, the resulting senescence response can differ significantly based on environmental factors. For instance, when IMR-90 fibroblasts were subjected to varying levels of oxidative stress, the degree of senescence observed was directly proportional to the intensity of the stress. In other words, the severity of the senescence response varied depending on the magnitude of the oxidative stress (Chen et al., 1995). Although senescence has gained significant ground in the fields of cellular and cancer biology (see Section 1.3.3) and ageing research (Section 1.4), there is still debate about how "senescence" should be defined due to its heterogeneous phenotype (Sharpless & Sherr, 2015). The highly complex and dynamic profile of senescent cells is what makes the senescence state so interesting to study.

1.2 Senescence-associated secretory phenotypes (SASP)

Second to proliferation arrest, a significant characteristic of senescent cells is the production of a complex mixture of distinctive pro-inflammatory, proteolytic secretory factors (Coppé et al., 2010). These include cytokines, chemokines, growth factors, and proteases, which are collectively called the senescence-associated secretory phenotype (SASP) or senescence messaging secretome (SMS) (Coppé et al., 2010; Evan & d'Adda di Fagagna, 2009; Kuilman & Peeper, 2009). SASP production is another example of senescence heterogenicity because the secretome's time of secretion and exact composition depend

on the cell origin and the stage of senescence (Coppé et al., 2008; He & Sharpless, 2017). However, from a molecular point of view, all produced SASPs are mutually controlled by nuclear factor-κB (NF-κB) and by one of the three mitogen-activated protein kinase (MAPK) families, $p38^{MAPK}$ signalling pathways—activation of which initiates downstream induction of transcription factors which play a role in cellular programs such as proliferation, differentiation, and inflammation. SASPs are also regulated by the mammalian target of rapamycin (mTOR), which is a serine-threonine protein kinase inhibited by rapamycin and controlling cell growth and proliferation (Chien et al., 2011; Freund et al., 2011; Laberge et al., 2015).

SASPs communicate actively between senescent and neighbouring cells and the wider tissue microenvironment. During this secretory function, senescence is induced via an autocrine and/or paracrine manner, maintaining the senescence phenotype and influencing the phenotype of neighbouring senescent and non-senescent cells (Acosta et al., 2013; Kuilman & Peeper, 2009). Interestingly, SASPs can reinforce both replicative or premature senescence in a cell-autonomous manner and independent from DNA damage (Freund et al., 2011). They can bind to cell-surface receptors of non-senescent cells and activate or inhibit different signal transduction pathways. These membrane activities in normal cells activated by SASPs demonstrate how senescent cells can modify their tissue microenvironment (Coppé et al., 2010). Another function of SASPs, besides senescence induction, is the recruitment of immune cells to eliminate the senescent and stressed cells (Muñoz-Espín & Serrano, 2014). Although this acts as a positive effect on the tissues because it clears out the damage caused by stress cells, the accumulation of immune cells results in increased inflammation, which is detrimental to the organism (Lujambio, 2016). More details about the opposing effects of senescence regarding proliferation arrest and SASP secretion are discussed in Section 1.3.

1.3 Effects of senescence

1.3.1 Acute vs chronic senescence

Senescence has many different physiological effects, both negative and positive. The heterogeneous senescence functionality is exhibited by the two senescence sub-categories: acute (short-term) and chronic (long-term). Acute senescence is observed both in embryonic and adult life and ensures organismal health through preserving homeostasis and tissue/organ development and repair (Muñoz-Espín & Serrano, 2014; van Deursen, 2014). On the other hand, chronic senescence, the result of prolonged exposure to stress, causes significant damage to the cell, resulting in pathological conditions and ageing (Burton & Krizhanovsky, 2014; López-Otín et al., 2013; van Deursen, 2014). In contrast to acute senescence, chronic senescence is not programmed and appears to occur randomly, targeting cells of any origin. Furthermore, senescence (replicative through telomere attrition and chronic) is considered one of the nine hallmarks of ageing (López-Otín et al., 2013).

1.3.2 Opposing effects of senescence

The opposing effects of senescence and its direct association with organismal ageing make senescence an example of antagonistic pleiotropy (Figure 1) (Campisi, 2003; Campisi & d'Adda di Fagagna, 2007; Williams, 1957). This theory refers to progressive loss of fitness with age and postulates that younger organisms increase their health and survival rate thanks to senescence. In contrast, as they grow older, they face negative implications. The beneficial and detrimental results of senescence are discussed in more detail in Sections 1.3.3 and 1.3.4.

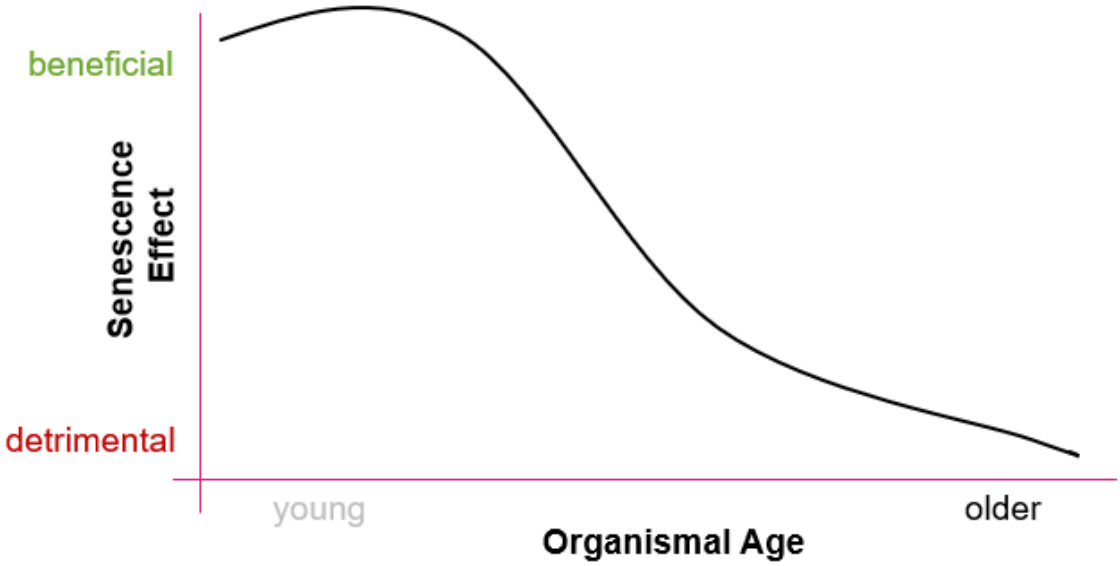

Figure 1.1: *The opposing effects of senescence explained by antagonistic pleiotropy.* The graph demonstrates the relationship between organismal age (x-axis) and the impact of senescence (y-axis). The curve illustrates how senescence is highly beneficial in young organisms (shown by the peak at young age) but progressively becomes detrimental as the organism ages (shown by the declining curve). This relationship exemplifies Williams' antagonistic pleiotropy theory (1957), where the same biological process (senescence) that provides evolutionary advantages in youth becomes increasingly harmful with age. The continuous decline in the curve represents the gradual shift from protective effects (such as tumor suppression and wound healing) to detrimental outcomes (such as chronic inflammation and tissue dysfunction).

1.3.3 Positive effects of senescence: cancer and other clinical conditions

Senescence plays an important role as a natural protection against cancer progression. Initially, cellular senescence was described as a cell-autonomous tumour suppression mechanism (He & Sharpless, 2017). However, it is now known that it also acts in a paracrine manner to induce senescence in nearby healthy cells (He & Sharpless, 2017; Lujambio, 2016). While cancerous cells carry mutations on cell cycle regulatory genes that promote cancer progression and advance survival of a cancer cell population, the permanent arrest in senescence stops the proliferation of such cells, ensuring that mutated genomes are not perpetuated to subsequent generations and limiting malignant tumorigenesis (Campisi & d'Adda di Fagagna, 2007; Leite de Oliveira & Bernards, 2018). DNA damage that can potentially cause tumorigenesis triggers the senescence response, a process known as oncogene-induced senescence (OIS) (Bartkova et al., 2006; Courtois-Cox et al., 2008; Di Micco et al., 2006) and is the result of activated oncogenes or deactivated tumour suppressor genes, in a similar manner to apoptosis (Dimri et al., 2000; Serrano et al., 1997). Indeed, apoptosis and senescence are mediated by common signalling pathways, such as the p53/p21 (Herbig et al., 2004) and the p16/Retinoblastoma (pRb) (Serrano et al., 1997) tumour suppressor pathways, which have been demonstrated to control the induction and maintenance of senescence (Campisi & d'Adda di Fagagna, 2007; Lowe et al., 2004). From a pharmacological point of view, although apoptosis is the core of current anti-cancer therapy, synthetic chemical triggers of OIS can act as a secondary cancer treatment (Gorgoulis & Halazonetis, 2010). Therapeutic drugs, such as palbociclib, which induces p21 expression through the p53 signalling pathway, are already being used in anti-cancer therapy to suppress cancer cell replication (Leite de Oliveira & Bernards, 2018; Wang et al., 2021).

In addition to OIS, acute and developmental senescence are as beneficial to many physiological processes, such as normal development, as they contribute to pathological processes (He & Sharpless, 2017). Cellular senescence plays a critical role in embryonic

development both directly and indirectly. First, as a direct role, it participates in regulating embryonic growth, tissue remodelling and organ patterning (Muñoz-Espín et al., 2013; Rajagopalan & Long, 2012; Storer et al., 2013). Secondly, it is involved in the physiological function and growth of the placenta (Bowen et al., 2002; Chuprin et al., 2013) and in maintaining placenta homeostasis (Mizutani & Tomoda Y, 1996), thus assisting indirectly in embryonic development. Additionally, senescent cells are responsible for wound healing (Demaria et al., 2014; Jun & Lau, 2010) and tissue repair (Kim et al., 2013; Krizhanovsky et al., 2008), and they limit tissue damage by preventing and limiting tissue fibrosis. Restriction of the fibrotic response is achieved by activating senescence and through SASPs, which signal an immune response resulting in the clearance of damaged cells (Muñoz-Espín & Serrano, 2014). Furthermore, the senescence phenotype plays a positive role in diseases such as atherosclerosis and ageing: For instance, senescent paracrine induction by pancreatic beta cells promotes insulin secretion during tissue maturation with ageing (Helman et al., 2016), while proliferation arrest in senescent cells decreases plaque formation. The reduction in plaque formation can lead to improved blood flow and less arterial stiffness, which in turn improves mobility and, hence, fitness in patients with atherosclerosis (Childs et al., 2016).

1.3.4 Negative effects of senescence: heart and neurodegenerative conditions

Senescence, particularly chronic senescence, can result in detrimental physiological changes, including development of disease (He & Sharpless, 2017; Muñoz-Espín & Serrano, 2014; Myrianthopoulos et al., 2019). As discussed in Section 1.3.1, these adverse effects are observed mostly in aged organisms, since during ageing, the accumulation of stress increases the proportion of senescent cells (Dimri et al., 1995). A persistent and increasingly senescent cell population, accompanied by a higher volume of SASP production, result in the inability of the immune system to achieve the clearance of damaged cells from the tissue. Thus, not only is senescent cell clearance not achieved, but SASPs

induce more cells into senescence (McHugh & Gil, 2018). Altogether, this leads to the accumulation of senescence and damaged cells, which results in the disruption of homeostasis and the onset of diseases, including cancer, heart conditions and neurodegenerative diseases (da Silva et al., 2019; McHugh & Gil, 2018; von Kobbe, 2019). In the case of cancer, as mentioned in section 1.3.3, senescence can act as a natural anti-cancer response, mostly in younger organisms. However, the risk of cancer increases with age, and when senescent cells accumulate in aged organisms, senescence promotes tumorigenesis and metastasis through inflammation (Baker et al., 2016; DePinho, 2000). Specific removal of senescent cells from *in vivo* animal models results in a delay in the progression of cancer and neurodegenerative pathologies (Bussian et al., 2018), atherosclerosis (Childs et al., 2016), osteoarthritis (Jeon et al., 2017), kidney and heart diseases (Baker et al., 2016), pulmonary fibrosis (Schafer et al., 2017), cataracts (Baker et al., 2016) and other age-related diseases (Rabinowitz & Cui, 2023).

The SASP plays a significant role in the detrimental effects of senescence, not only because it assists in the accumulation of senescent cells through its paracrine effect but also because it causes inflammation. Clinical research has demonstrated the harmful effects of inflammation in ageing and the correlation between the ageing phenotype and increased levels of inflammation (McHugh & Gil, 2018). Inflammatory SASP content can influence senescent fibroblasts and myeloid cells into pro-inflammatory and pro-tumorigenic cells (Coppé et al., 2010; Di Mitri et al., 2014). Similarly, by targeting senescent cells to delay disease, the elimination of senescent cells results in decreased levels of inflammatory biomarkers, such as IL-6 and IL-1β – these markers are associated with chronic inflammation in different organs, such as the kidney, heart, liver, and lung (Baker et al., 2016). Hence, the accumulation of senescent cells acts synergistically with SASP-induced inflammation to reduce health in ageing.

The delay of disease onset and the reduced inflammation that results from eliminating senescence make targeting senescence an effective therapeutic strategy. Three major

classes of drugs target senescence: senolytic drugs, which eliminate senescent cells; senomorphic compounds that inhibit SASP and thus decrease senescence induction; and drugs that enhance the immune system (immunosurveillance) to assist with the natural clearance of senescence (Gasek et al., 2021; von Kobbe, 2019). A key target of senolytic and senomorphic drugs are the BCL-2 anti-apoptotic protein family located in mitochondria (Yosef et al., 2016) and the mTOR pathway (Thapa et al., 2017), respectively, whose role is the maintenance of proliferative potential. While senotherapeutics have been used and are being explored for specific age-related diseases, such as diabetic macular edema, the Translational Geroscience Network is conducting Phase 1 and Phase 2 trials using compounds such as Dasatinib, Quercetin, and Fisetin to address conditions like sepsis, chronic kidney disease, lung fibrosis, and Alzheimer's disease (Quarta & Demaria, 2024). The field is also expanding to explore other potential indications, with companies like Rubedo Life Sciences and Boehringer-Ingelheim developing novel senolytic molecules for skin and muscle dysfunctions in pre-clinical models (Quarta & Demaria, 2024). Despite these advancements, challenges remain in harnessing the full therapeutic potential of targeting cellular senescence. There is still a need for more sensitive and localised/targeted drugs because the heterogeneity of senescent cell populations and their varied physiological roles necessitate precise therapeutic approaches to minimise potential off-target effects and maximise therapeutic efficacy (Quarta & Demaria, 2024).

As mentioned in Sections 1.3.3 and 1.3.4, senescence can positively or negatively affect different physiological conditions. The dual nature of senescence, summarised in Figure 1.2, explains why senescence is so physiologically relevant to health and disease (Rabinowitz & Cui, 2023).

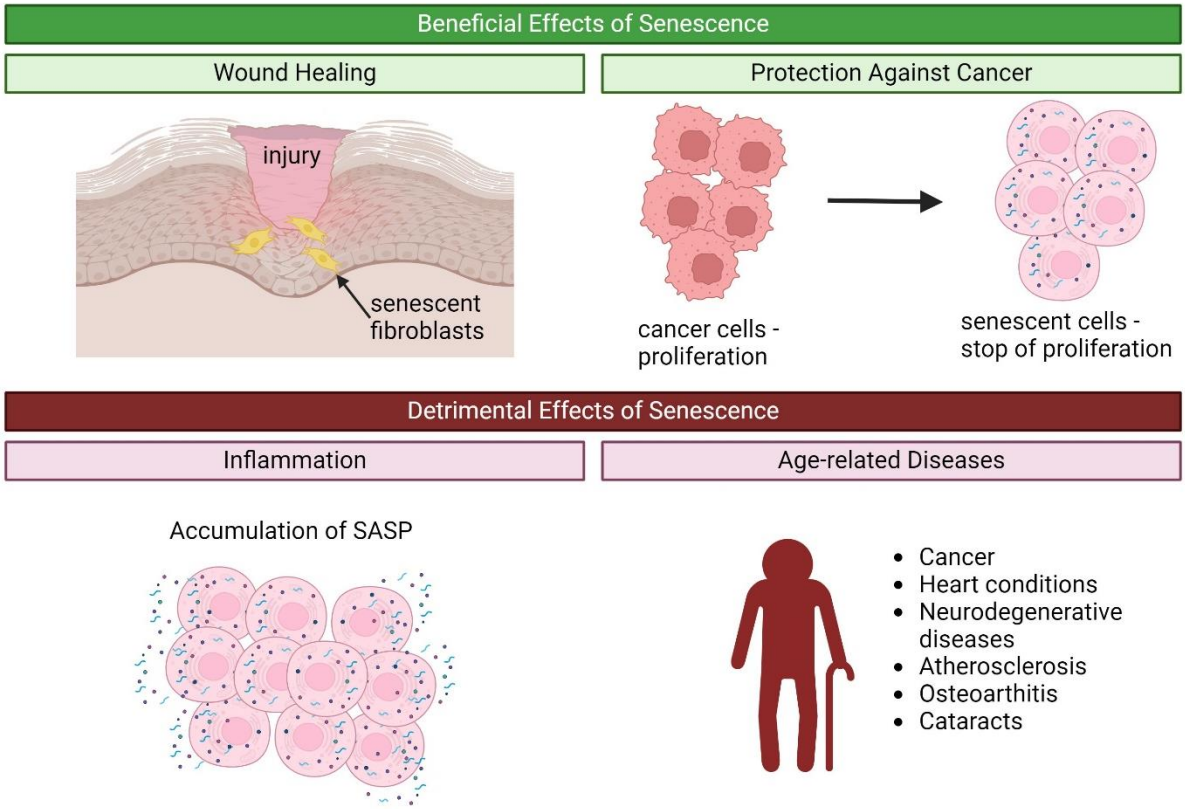

Figure 1.2: A summary of the dual role of senescence. The comparative table highlights the contrasting effects of senescence, emphasizing on how the same biological process can have opposing outcomes depending on the physiological context and duration of the senescent response. The top section (in green) illustrates the beneficial effects, subdivided into two key processes: (1) wound healing acceleration through senescent fibroblasts and (2) protection against cancer through tumour suppression mechanisms. The bottom section (in red) presents the detrimental effects, categorized into two main outcomes: (1) chronic inflammation driven by SASP accumulation and (2) increased susceptibility to age-related diseases, including cancer and other degenerative conditions. (Image created with biorender.com)

1.4 Senescence and ageing

Ageing, characterized by the organismal decrease in physiological function over time, is a complex process affecting all multicellular organisms and prokaryotes (López-Otín et al., 2013). Cellular senescence, an antagonistic hallmark of ageing, contributes to both normal ageing and age-related diseases (Childs et al., 2015; López-Otín et al., 2013; McHugh & Gil, 2018). The accumulation of senescent cells in tissues of older organisms results from increased senescence induction, lack of apoptosis and insufficient immunoclearance (Herbig et al., 2006; Muñoz-Espín & Serrano, 2014; Wang et al., 2009).

Targeting senescence is a major goal of ageing research, with approaches including genetic interference to eliminate senescence and use of senolytic drugs to delay or reverse the ageing phenotype (Baker et al., 2011, 2016; Zhu et al., 2015). Senolytic and senomorphic therapies have been proposed as human geroprotectors, pharmacological agents that decrease the ageing process, decrease age-associated diseases, and increase lifespan (Di Micco et al., 2021; Moskalev et al., 2022). Interestingly, a recent review on the potential benefits of addressing senescence in clinical settings suggests that, in addition to senolytic and senostatic drugs, exercise and nutrition may induce senotherapeutic effects, highlighting the multifaceted approach to combating age-related conditions (Witham et al., 2023). For example, Minuzzi et al reported that master athletes engaged in lifelong training and competition showed lower levels of senescent T-cells compared with control subjects, meaning a lower ageing marker (Minuzzi et al., 2018).

Ageing and senescence share common hallmarks, such as epigenetic factors, DNA damage, telomere erosion and mitochondrial dysfunction (discussed in Section 1.7.2) (López-Otín et al., 2013; McHugh & Gil, 2018). Chronic senescence during natural ageing results from a complex combination of these stressors (Childs et al., 2015). Aged and senescent cells share common phenotypic characteristics with similarities in nuclear architecture: cells from ageing tissue and some senescent cells have nuclei with an irregular structure, such as larger in size and loss of nuclear envelope integrity (Pathak et al., 2021).

This results from the abnormal function of lamin fibers, the proteinaceous meshwork of inner nuclear membrane; mutations in genes producing the lamin proteins lead to lamin-deficient cells (Pathak et al., 2021). For example, the loss of the lamin A/C gene is a biomarker of ageing and the loss of lamin B1 is a biomarker of senescence (Pathak et al., 2021).

1.4.1 Progeria disease

Progeroid syndromes are premature ageing disorders, and progeroid models (usually mice models or human cell donors) are used in ageing research to study cellular senescence and other phenotypic characteristics of ageing (Childs et al., 2015; Dreesen, 2020; López-Otín et al., 2013). Progeroid diseases have a variety of effects in young children, such as rapid symptom progression in Hutchinson–Gilford progeria syndrome (HGPS) or slower progression with longer life expectancy in Nestor-Guillermo progeria syndrome (NGPS) (Foo et al., 2019). HGPS, or “progeria disease”, is the most studied progeroid condition caused by a point mutation in the *LMNA* gene that encodes the A-type lamins (Foo et al., 2019). Progeria patients show clinical ageing characteristics as early as their 12^{th} to 18^{th} month of life (Foo et al., 2019; Sangita Devi & Thokchom, 2017). They exhibit aged-looking skin, alopecia, bone defects, loss of joint mobility and other severe age-related symptoms, which can result in premature death from stroke or heart failure due to severe artery thickening during the teenage years (Foo et al., 2019). Treatment of progeria requires drug inhibitors that help with cellular repair and anticoagulants to prevent strokes and heart conditions, with early detection considered essential to delay disease progression (Sangita Devi & Thokchom, 2017).

These phenotypic abnormalities result from cells carrying the mutated lamin A gene, called progerin. These cells demonstrate irregular nuclear morphology, genetic instability, and DNA damage—the latter two cause accelerated induction of premature senescence in progeria cells (Wheaton et al., 2017). Additionally, the accumulation of progerin expression

results in elevated levels of senescence (Ashapkin et al., 2019), suggesting that progeria cells are good models of both ageing and senescence.

1.5 Experimental induction of senescence

Senescence is a multi-step process initiated via various stressors: intrinsic stimuli, including telomere attrition and oxidative damage, and extrinsic stimuli, including chemotherapeutic drugs and ultraviolet (UV) radiation (Gorgoulis et al., 2019). These triggers usually activate senescence via DNA damage, which can also occur via protein or lipid damage (Gorgoulis et al., 2019). For example, telomere shortening peaks after extensive replication and activates telomere dysfunction-induced foci, which signal the DNA damage response (DDR), leading to cell cycle arrest (Shay & Wright, 2019). Other senescence inducers include reactive oxygen species (ROS) and mitochondrial dysfunction, which can lead to proteotoxicity (protein damage) and ROS-driven lipid damage, respectively (Correia-Melo et al., 2016; Höhn et al., 2017).

1.5.1 Replicative senescence

As proposed by Hayflick and Moorhead, sequential shortening of telomeres accompanies cellular division and increases with cell culture time (Hayflick & Moorhead, 1961). Telomeres determine the proliferation capacity of the cell as they can reach a critical short length (Hayflick limit) (Shay & Wright, 2000). Reaching the Hayflick limit is recognised by telomere dysfunction response or DDR through telomere dysfunction-induced foci, which signals proliferation arrest (Fagagna et al., 2003). P53 and p16 signalling molecules are involved in the pathway that leads to replicative senescence cycle arrest (Fagagna et al., 2003; Smogorzewska, 2002).

Extensive replication *in vitro* is widely used to induce senescence. Hayflick showed replicative senescence to be independent of cell culture conditions, although it largely

depends on the origin of the cell line used (Fumagalli et al., 2014; Hayflick & Moorhead, 1961). For example, the PD for foreskin fibroblasts to reach senescence has been reported to be 80-90, whereas lung fibroblasts WI-38 reach complete cultural senescence at a PD of 50 (Fumagalli et al., 2014). WI-38 and IMR-90 lung fibroblasts are commonly used cell lines in senescence and are considered the gold-standard model to use for *in vitro* replicative senescence (Hernandez-Segura et al., 2018b; Hooten & Evans, 2017).

1.5.2 Premature senescence

Premature senescence is the cellular response to stresses, and it is not linked to the extensive replication of telomere attrition. The permanent cellular proliferation arrest induced by telomere-shortening-independent cytotoxic stresses or stress-induced premature senescence (SIPS) can be triggered by many extracellular factors, such as cellular exposure to UV, γ-radiation, hyperoxia, chemotherapeutic drugs, H_2O_2 (Gorgoulis et al., 2019; Toussaint et al., 2002). These chemical stressors result in DDR (Fumagalli et al., 2014), chromatin remodelling (Narita et al., 2003), spindle stress (Schmidt et al., 2010) and other cellular mechanisms that eventually lead to senescent cell cycle arrest. Although the overall phenotype of senescent cells is similar, it depends on the senescence induction mechanism, the molecular pathway and the origin of the cell (Toussaint et al., 2002; Gorgoulis et al., 2019).

The largest group of senescence stimuli is the DDR, which is activated following the generation of DNA damage; when cells cannot repair or overcome that damage, they enter a DDR-induced senescent state (Fumagalli et al., 2014). Dysfunction due to oxidative damage can activate DDR and induce senescence (Gorgoulis et al., 2019). Oxygen is a major stressor that induces oxidative DNA damage (Wiley & Campisi, 2021) and higher oxygen concentrations, which result in the accumulation of senescent cells (Chen et al., 1995). ROS has also been described as a major senescence regulator (Höhn et al., 2017). For example, treating cells with H_2O_2 is commonly used to induce senescence in cancerous

and non-cancerous cell lines (Hernandez-Segura et al., 2018b; Höhn et al., 2017; Petrova et al., 2016). Additionally, over 50 small chemical compounds have been identified to induce premature senescence via eight functionally different DDR activation mechanisms, including DNA damaging agents, inhibitors of cyclin-dependent kinase, epigenetic modifiers, etc (Petrova et al., 2016). One example is the active anti-cancer DNA damaging agent doxorubicin (Dox). This chemical compound activates DDR via intercalating into the DNA and inhibiting DNA topoisomerase II, which is essential for creating the breaks in the DNA double-strand (Nitiss, 2009). Dox is widely used for *in vitro* senescence induction (Chang et al., 1999; Hernandez-Segura et al., 2018b).

Although the principal cause of senescence induction appears to be DDR (Huang et al., 2022), there are examples where senescence is initiated without the involvement of DDR. For instance, recent research has uncovered a significant link between plasma membrane damage and cellular senescence in both yeast and human cells. Scientists found that plasma membrane damage can induce long-term cell cycle arrest, contributing to cellular ageing. In yeast, enhancing membrane repair mechanisms extends replicative lifespan. In human fibroblasts, plasma membrane damage triggered premature senescence through a calcium (Ca^{2+}) - p53 pathway, independent of the typical DDR. Upregulating certain repair factors suppressed this plasma membrane damage-induced senescence. These findings reveal a previously underappreciated subtype of senescent cells, suggesting a novel mechanism in cellular ageing processes (Suda et al., 2024).

Another significant premature senescence sub-group is the OIS generated by introducing oncogenic drugs and activating oncogenes in normal cells. In this case, DDR is activated by cellular hyper-replication or ROS over-production, which is the result of overexpression of oncogenic *ras* and accumulation of rat sarcoma (Ras) proteins (Di Micco et al., 2006; Lee et al., 1999; Serrano et al., 1997). Overexpression of *ras* results in cell cycle arrest similarly to, but independent from, p53/p21 and p16 (Serrano et al., 1997). Mechanistically, OIS acts as a cancer progression defender while it is activated by inhibition of tumour-suppressor

cellular mechanisms (Di Mitri & Alimonti, 2016). Oncogenic stimuli have been traditionally used *in vitro* to induce senescence, with examples of expression of Ras, fibrosarcoma (Raf) and p53 oncogenic proteins (Höhn et al., 2017; van Deursen, 2014).

1.6 Detecting senescence

The complexity of the senescence phenomenon is mirrored in its detection. Firstly, no single marker is unique to all senescent cells, so multiple tests and assays are required to establish senescence (Campisi, 2013). Secondly, senescent cells have different characteristics that depend on cell type and senescence induction pathway (Crowe et al., 2014; Sharpless & Sherr, 2015). However, due to different phenotypic and molecular changes in senescent cells, some distinctive markers can be used to distinguish between senescent and replicating cells. Phenotypic changes associated with senescence include low proliferation rate, cellular morphological changes, senescence-associated beta-galactosidase (SA β-gal) activity, senescence-associated heterochromatin foci (SAHF) formation, and secretion of SASPs. In contrast, molecular markers of senescence include the expression of cyclin-dependent kinases (CDKs) such as p16, p53, inflammatory molecules and heterochromatin markers (Salama et al., 2014). These markers and their detection are discussed in Sections 1.6.1, 1.6.2 and 1.6.3.

1.6.1 Senescence associated β-galactosidase

The most widely used senescence marker detects SA β-gal activity under sub-optimal conditions of pH 6.0 (Dimri et al., 1995). While testing for senescence *in vivo* can be challenging, SA β-gal assays can be employed for both *in vitro* cultures and histochemical detection in tissue sections. This method has been used to test for replicative or premature senescence in multiple cell lines from different origins and in mammalian tissues (Debacq-Chainiaux et al., 2009). A feature of the SA β-gal assay is that it does not test positive for

cells that can reverse from cycle arrest; thus, it can distinguish between senescence and quiescence (Dimri et al., 1995). This is because β-gal activity indicates increased lysosomal content, a feature of senescent cells (Kurz et al., 2000), although the lysosomes of senescent cells can increase in both number and size. The increase in β-gal enzymatic activity results from the expansion of the lysosomal compartment and increased lysosome biogenesis (Hernandez-Segura et al., 2018a; Kurz et al., 2000; Lee et al., 2006).

Although SA β-gal is an attractive first choice for senescence detection, it has several limitations; while β-gal activity is characteristic of senescent cells, it is not an essential characteristic of senescence (Lee et al., 2006). Thus, false-negative results from cells that senesce but do not express β-gal enzymatic activity are possible. Secondly, a few conditions can result in false-positive SA β-gal activity, including highly confluent cell cultures (Severino et al., 2000) and cultures under serum starvation conditions (Yegorov et al., 1998). Additionally, this assay cannot be used in cells that have been frozen or/and fixed with formalin for an extended amount of time, as the enzymatic activity is disturbed (Debacq-Chainiaux et al., 2009).

1.6.2 Other phenotypic markers

The primary hallmark of senescence is growth arrest; thus, senescent cells can be tested for an absence of proliferation markers (Campisi, 2013). Examples of testing for loss of proliferation potential include simple cell number counting, cell cycle or DNA synthesis analysis (Crowe et al., 2014). Replicative senescence can determine PD by assessing the proliferation rate via the cell division number (Crowe et al., 2014) or by examining cellular morphology. Senescent cells are typically enlarged and adopt a flattened or spindle-shaped morphology (Campisi, 2013; Kuilman et al., 2010). There may also be changes in the cell nucleus, which may be refractile, or cells may have multiple nuclei. However, changes in morphology are highly dependent on the senescence induction pathway (Kuilman et al., 2010). Changes in chromatin structure are also an indication of cellular senescence

(Adams, 2007). Senescent cells have highly condensed sections of heterochromatin called SAHF. Simple cell nuclear staining with 4′-6-Diamidino-2-phenylindole (DAPI) efficiently indicates SAHF formation as DAPI stains brighter in senescent cells due to compact chromatin foci (Adams, 2007). Lastly, changes in mitochondrial function and homeostasis are also markers of senescence, discussed in detail in Section 1.7.2.

1.6.3 Molecular senescent markers

Different molecular changes are observed in senescent cells and can be used to detect senescence (Coppé et al., 2010). As mentioned, p53, p21, and p16/Rb signalling proteins control the senescence activation pathway, thus, the accumulation of these molecular proteins indicates activation of senescence (Kuilman et al., 2010). Quantitative real-time polymerase chain reaction (qPCR) can be used to measure the expression of these biomarkers. Immunophenotyping methods test different CDKs activated during senescence induction pathways (Adewoye et al., 2020). SASP expression is also a distinct characteristic of senescence, and changes in the specialised secretory activity can be used as a senescence detection method (Campisi, 2013). For example, when multiplex enzyme-linked immunosorbent assay (ELISA) assays detect increased expression of interleukin 8 and 6 (IL8 and IL6) inflammatory molecules, then there is a positive indication of senescent cells in culture (Adewoye et al., 2020). Lastly, senescence detection also includes examining changes in proteins that affect chromatin structure, such as heterochromatin protein 1 (HP1) group of proteins (Adams, 2007).

To conclude, each senescence biomarker can detect aspects of senescence (Sharpless & Sherr, 2015), although none are senescent specific, necessitating the use of multiple detection markers. For example, Gorgoulis et al. (2019) suggest a three-step senescence detection multi-marker: screening for senescence via positive SA β-gal staining, use of additional molecular biomarkers, such as p16 or proliferation arrest markers, and use of a

cell-type specific marker of senescence, such as examining SASP factors or molecules specific to induction pathway, such as DDR markers (Gorgoulis et al., 2019).

Detecting senescence quickly and accurately is becoming increasingly important, especially for assessing senolytic drugs (Duran et al., 2024). Excitingly, research into senescence detection is advancing, with new methods including machine learning algorithms that can predict senescence in various cell types and tissues based on nuclear morphology features (Duran et al., 2024) and small molecule imaging probes (Rabinowitz & Cui, 2023). Molecular imaging probes, in particular, increase the ability to study senescence in living organisms by providing various detection methods, including optical probes for laboratory research and MRI, SPECT, and PET for clinical applications (Rabinowitz & Cui, 2023). Despite challenges, combining multiple biomarkers shows promise for better senescence detection. These new approaches, such as the senescence classifiers, can help identify pathophysiological senescence and aid in discovering and validating potential senotherapies.

1.7 Mitochondria

Mitochondria are multifunctional cellular organelles, and they are highly affected during senescence. Mitochondria are semi-autonomous, double membrane-bound organelles of the cell which play a critical role in cell homeostasis (Chinnery & Schon, 2003). Widely recognised as the “powerhouse of the cell”, mitochondria are essential for energy production, and in parallel, they control cellular processes such as cellular metabolism, intracellular signalling, and cell death (apoptosis) (Murata et al., 2020). The role of mitochondria in apoptosis is critical, as most apoptotic signals are initiated in mitochondria. For example, apoptosis is initiated by different stimuli, such as the B-cell lymphoma 2 (Bcl-2) family of pro-apoptotic proteins (including Bax and Bak), which regulate mitochondrial membrane permeabilisation. Activation of such proteins allows other apoptogenic proteins (such as cytochrome c) to be released into the cytoplasm to engage in apoptotic protein

cascade activation for apoptosome formation and, finally, cellular destruction (Suh et al., 2013; Vermeulen et al., 2005).

Although the mitochondrion is usually illustrated as an oval-shaped organelle, its morphology is highly dynamic, and the shape, size, and total number of mitochondria within a cell constantly change, reflecting the ever-changing cellular function of the mitochondria (Lackner, 2013; Roy et al., 2015). Mitochondria continually divide and fuse to create smaller individual mitochondria or form more extensive interconnected networks (Bereiter-Hahn, 1990). This balance between mitochondrial fusion and division maintains cellular homeostasis and ensures a healthy mitochondria population by controlling the degradation of dysfunctional mitochondria. Disruption of this balance leads to severe disorders, such as metabolic syndromes and neurodegenerative conditions (Murata et al., 2020).

One of the most essential mitochondrial functions is energy production. Mitochondria are responsible for 90% of the energy produced in the cell via oxidative phosphorylation (OXPHOS) (Birch-Machin, 2006). The principal purpose of OXPHOS is oxygen respiration, which generates energy for the cell (Cole, 2016). OXPHOS is an electrochemical mechanism that takes place in the respiratory chain—this is composed of 5 multi sub-unit protein complexes (I – V) found on the mitochondrial inner membrane (MIM) (Figure 1.3) (Stoldt et al., 2018). Electrons flow between electron-transporting complexes (I-IV) down an energy gradient providing a membrane potential, which is utilised by H^+-translocating adenosine triphosphate (ATP) synthetic complex V. ATP, which is the energy source for all cellular metabolic processes, is synthesised via phosphorylation of adenosine diphosphate (ADP) by complex V and then released into to the cytoplasm (Chinnery & Schon, 2003).

The OXPHOS complexes result from dual-origin protein units encoded from nuclear and mitochondrial DNA (mtDNA) (Stoldt et al., 2018). Mitochondria, one of the oldest evolutionary endomembrane systems in eukaryotic cells, contain their own genetic material as mitochondrial DNA (mtDNA). The human mtDNA genome spans just 16.5 kilobases and encodes 13 proteins, specifically subunits of the electron transport chain complexes I, III,

IV, and ATP synthase (complex V) (Giles et al., 1980). The majority of the mitochondrial proteome originates from nuclear DNA. These proteins are translated on cytosolic ribosomes and actively imported into mitochondria through outer and inner membrane translocase machines, a process dependent on the electrochemical potential (Friedman & Nunnari, 2014). Mutations in mtDNA or nuclear-encoded mitochondrial genes can lead to dysfunctional OXPHOS complexes, resulting in various mitochondrial diseases that can affect any organ in the body (Friedman & Nunnari, 2014).

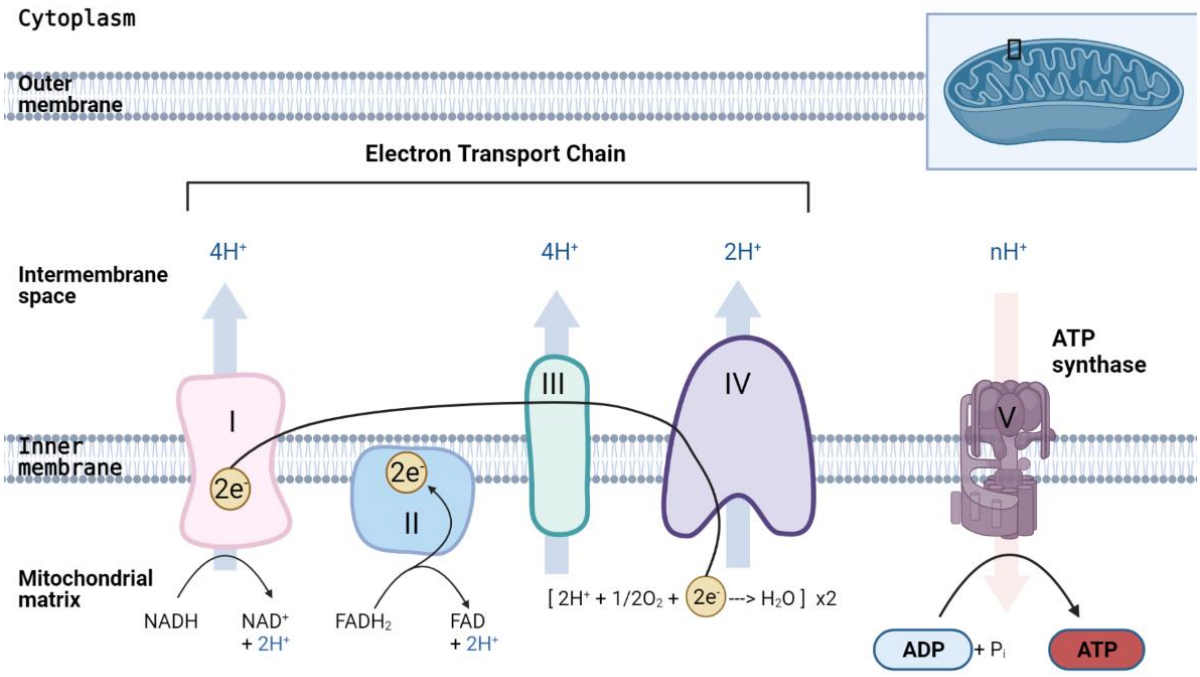

Figure 1.3: Mitochondrial OXPHOS across the inner membrane. The diagram shows the electron transport chain components and ATP synthesis in mitochondria. The five OXPHOS complexes (I-V) are embedded in the mitochondrial inner membrane, with clear demarcation of the four compartments: outer membrane, intermembrane space, inner membrane, and mitochondrial matrix. The electron transport chain (Complexes I-IV) facilitates the movement of electrons ($2e^-$) through a series of redox reactions: Complex I oxidizes NADH to NAD^+, Complex II oxidizes $FADH_2$ to FAD, Complex III facilitates electron transfer via cytochrome c, and Complex IV reduces O_2 to H_2O. Simultaneously, protons (H^+) are pumped from the matrix into the intermembrane space at specific quantities ($4H^+$ at Complex I, $4H^+$ at Complex III, and $2H^+$ at Complex IV, with no proton pumping at Complex II), establishing an electrochemical gradient. Complex V (ATP synthase) harnesses this gradient by allowing protons (nH^+) to flow back into the matrix, coupling this energy to the phosphorylation of ADP to ATP. This process illustrates the chemiosmotic coupling between electron transport and ATP synthesis. (Image created with biorender.com)

1.7.1 Reactive oxygen species (ROS)

ROS, such as the anion superoxide (O_2^-) and H_2O_2 radicals, are by-products of cellular metabolism (Fridovich, 1995) and are the result of reduced oxygen levels (Correia-Melo & Passos, 2015). ROS levels are usually controlled in the cell via mitochondrial and antioxidant systems (Koopman et al., 2012). Dysfunctions in redox complexes and incomplete oxygen metabolism in the cellular mitochondrial OXPHOS can lead to the accumulation of ROS. ROS are produced in the mitochondrial respiratory chain due to electron leakage from complexes I and III (Figure 1.3) (Birch-Machin, 2006). Accumulation of intracellular ROS leads to oxidative damage of nuclear and mitochondrial DNA, which is increased in old age (Barja & Herrero, 2000). This is described as the “free-radical theory of ageing” proposed by Harman (1956), which explains that the DNA mutations that accumulate with age lead to a higher volume of impaired OXPHOS complexes, resulting in the production of more ROS and increased oxidative damage (Birch-Machin, 2006; Harman, 1956). Indeed, there is evidence reporting a link between ROS and cellular senescence (Passos & von Zglinicki, 2005); Section 1.7.2.

Besides the natural ageing process, oxidative stress is characteristic in age-related diseases, including cancer, Parkinson’s disease, and type-2 diabetes, where ROS levels are elevated (Scialò, Fernández-Ayala and Sanz, 2017). On the other hand, it is also accepted that ROS exhibit an example of a hormetic effect, as positive effects are associated with lower ROS levels. The biological characteristic of hormesis describes a biphasic response where low doses of inhibitors or mild stress stimulate beneficial effects (Calabrese & Mattson, 2017). Such examples are found in the physiological roles of low/controlled levels of ROS, which is an important contributor to apoptosis and organismal defence against infection (Schieber & Chandel, 2014).

1.7.2 Mitochondria from senescent cells

Defective mitochondria are a hallmark of senescence (Hernandez-Segura et al., 2018a; Miwa et al., 2022), exhibiting dynamics, morphological characteristics, and functional alterations. An imbalance between mitochondrial fusion and fission and decreased mitophagy during senescence results in changes in morphology (highly elongated mitochondria with changes in cristae structure) and increased mitochondrial content, respectively (Tai et al., 2017; Yoon et al., 2006). Interestingly, despite higher mitochondrial biogenesis, ATP production is reduced (Birch & Passos, 2017) while mitochondrial ROS is increased in senescent cells. This is due to impaired OXPHOS, increased membrane potential and increased proton leak in the electron-transport chain during senescence (Allen et al., 1999; Hutter et al., 2004).

Increased ROS and mitochondrial dysfunction result from senescence and are necessary for senescence induction, cell arrest, and senescent phenotype maintenance (Figure 1.4) (Birch & Passos, 2017; Miwa et al., 2022). Mitochondria are drivers of senescence, both *in vivo* and *in vitro*, and play a role in maintaining senescence (Correia-Melo & Passos, 2015; Passos et al., 2010). Interestingly, mitochondrial dysfunction-associated senescence activates a distinct molecular mechanism that leads to cycle arrest (Wiley et al., 2016). Increased mitochondrial ROS production, dysfunctional mitochondrial OXPHOS complexes, imbalance between fission and fusion in mitochondria and dysregulation of mitochondrial metabolic profile and Ca^{2+} levels are some mechanisms that trigger p53/p21 and/or Rb signalling pathways and induce and/or promote cellular senescence (Ziegler et al., 2015). Evidence shows that mitochondrial ROS results in oxidative stress that enhances telomere attrition, leading to paracrine senescence via DDR (von Zglinicki, 2002; von Zglinicki et al., 1995). To sum up, there is a bidirectional mechanism of dysfunctional mitochondria and senescence, since one can trigger the other (Figure 1.4).

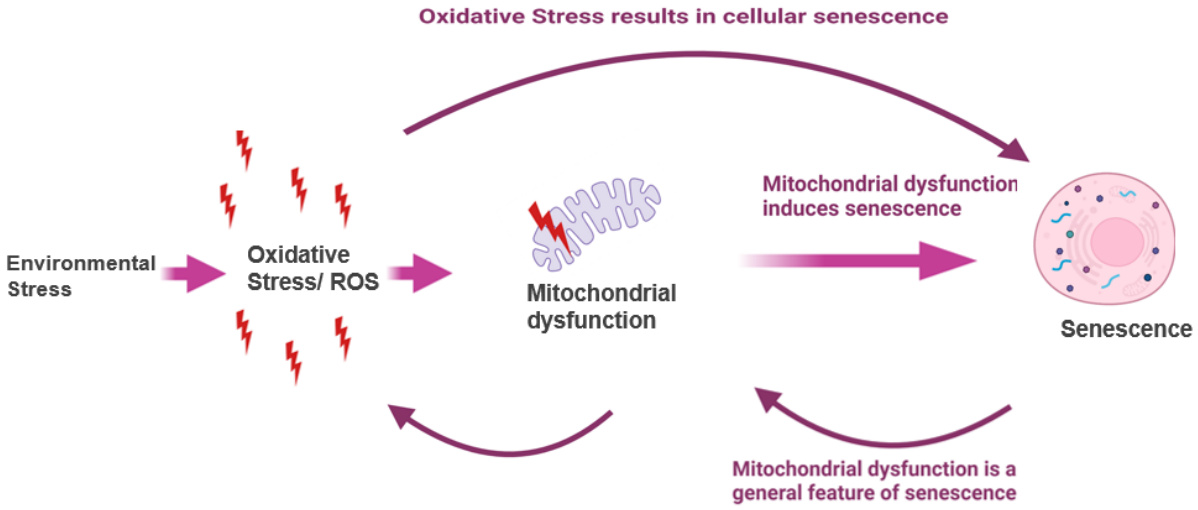

Figure 1.4: The relationship between senescence and mitochondria. This flow diagram illustrates the complex bidirectional relationship between cellular senescence, mitochondrial function, and oxidative stress. The primary pathway (middle) demonstrates how environmental stressors trigger oxidative stress and ROS production, leading to mitochondrial dysfunction, which subsequently induces senescence. A parallel feedback loop (bottom) shows how senescence itself produces mitochondrial dysfunction as one of its characteristic features, which in turn generates more oxidative stress/ROS. The direct pathway (top) represents how oxidative stress can independently trigger cellular senescence without requiring mitochondrial dysfunction as an intermediary. Together, these interconnected pathways create a self-reinforcing cycle where mitochondrial dysfunction and senescence can perpetuate each other through ROS-mediated mechanisms. This diagram emphasizes the central role of mitochondria in both the initiation and maintenance of the senescent state, highlighting how multiple pathways can converge to promote and sustain cellular senescence.

1.8 Biophotons

Living organisms constantly exchange energy and particles with their environment to maintain homeostasis and meet their living needs. While biological processes have been studied in classical dynamic models on a nano- to larger-metre scale, the role of quantum mechanics in biology has been less examined. Quantum biology investigates ions, atoms, and molecules whose behaviour defies classical laws of physics and chemistry. In this field, quantum mechanics theories are used to explain biological processes (Marais et al., 2018). Photons are quantum light particles, which are considered key players in these processes, as they have a significant role in physical interactions at an atomic and molecular level (Niggli, 1992).

In the early 1920s, Einstein proposed that light radiation could exhibit both wave-like and particle-like behaviour, introducing the concept of the “photon” (Marais et al., 2018). A few years later, another German scientist, Gurwitsch, discovered the possibility of non-contact, non-chemical cellular communication, now referred to as “biphotonic communication”, where living organisms emit light (Gurwitsch, 1923). Gurwitsch demonstrated this phenomenon using two onion rootlets: an inductor and a detector. When the inductor was in a high cell division state, the nearby detector, shielded by quartz glass allowing UV light to pass through, showed an increase in cell division rate. In contrast, separating the detector and inductor with a regular glass tube (which typically blocks most UV light) resulted in no change in the division rate (Gurwitsch, 1923). Traditional biological and physical laws could not explain this phenomenon, but it is possible that photon emission from the onion rootlets stimulated cell division. After a hiatus due to the Second World War, it was discovered that this effect was not only limited to cell division but applied to other cellular processes, including intracellular interactions (Kaznacheev et al., 1980) and mitochondrial oxygen consumption (Bat’yanov, 1984).

Over 60 years after its initial experimental evidence, German biophysicist Fritz-Albert Popp introduced the term “biophotons” describing them as low-energy photons emitted by

biological systems in the UV range (Popp et al., 1984). Popp proposed that biophotons are produced in a coherent electromagnetic field and are influenced by cellular activities (Popp, 1992, 2003a). It is important to note here that while spontaneous biophotonic emission is closely linked to delayed luminescence produced by biological tissues, it is distinct from delayed luminescence, which is the ultra-weak delayed light (or photon) emission that appears in biological organisms in response to light exposure (Fleiss & Sarkisyan, 2019; Popp, 2003b).

In my recent collaborative review on biophotons, it was highlighted that scientists have employed various terms over the years to describe the phenomenon initially termed "biophotons" by Popp, including biological autoluminescence, metabolic photon emission, and ultraweak photon emission (UPE), with the latter being the focus of our review (Mould et al., 2024). Notably, a book published recently by field experts entitled "Ultra-Weak Photon Emission from Biological Systems" further emphasises the use of "UPE" to characterise this effect (Volodyaev et al., 2023). However, the term "biophotons" will be employed to ensure consistency within this thesis.

1.8.1 Biophotonic production

Today, there is compelling evidence that biophotons are spontaneous, ultra-weak emissions of light produced by living cells of microbial, plant or animal origin (Cifra & Pospíšil, 2014; Prasad & Pospíšil, 2013). The intensity of biophotons is reported to be from several to tens of photons per sec^{-1} cm^{-2} within the 200-800 nm range of the spectrum (Cifra & Pospíšil, 2014). However, there is evidence that abiotic or biotic stress on biological systems enhances the biophotonic intensity to hundreds of photons sec^{-1} cm^{-2} (Burgos et al., 2017; Kamal & Komatsu, 2016; Kobayashi et al., 2009). This occurs becasue biophotons are produced during oxidative metabolic reactions (Bókkon et al., 2010; Prasad & Pospíšil, 2013; Van Wijk et al., 2008), including mitochondrial respiration, lipid peroxidation, peroxisome and catecholamine biochemistry and oxidation of tyrosine and

tryptophan residues in proteins. While ROS are considered the primary source of biophotons, both biotic (e.g., viral or bacterial infection) and abiotic stressors (e.g., temperature changes, ionizing radiation, mechanical or light damage) can increase oxidative stress. This enhanced oxidative stress leads to greater ROS production, which in turn explains the observed changes in biophotonic intensity under stress conditions (Cifra & Pospíšil, 2014).

Fundamentally, the production of biophotons is characterised by electronically excited species, which include singlet oxygen ($^1O_2$) and carbonyl species ($^3R{=}O$), moving from a high to lower energy state, releasing a photon each time (Figure 1.5) (Cifra & Pospíšil, 2014). Interestingly, research suggests that biophoton emission is primarily associated with regulated intracellular redox processes, particularly those occurring in mitochondria (Bókkon et al., 2010). This is notable because the concentration of biophotons within cells can significantly exceed that of the extracellular environment. The main sites of ROS generation and other redox reactions - mitochondria, cell membranes, and chloroplasts - are thought to be the principal cellular sources of biophotons (Pospíšil et al., 2019).

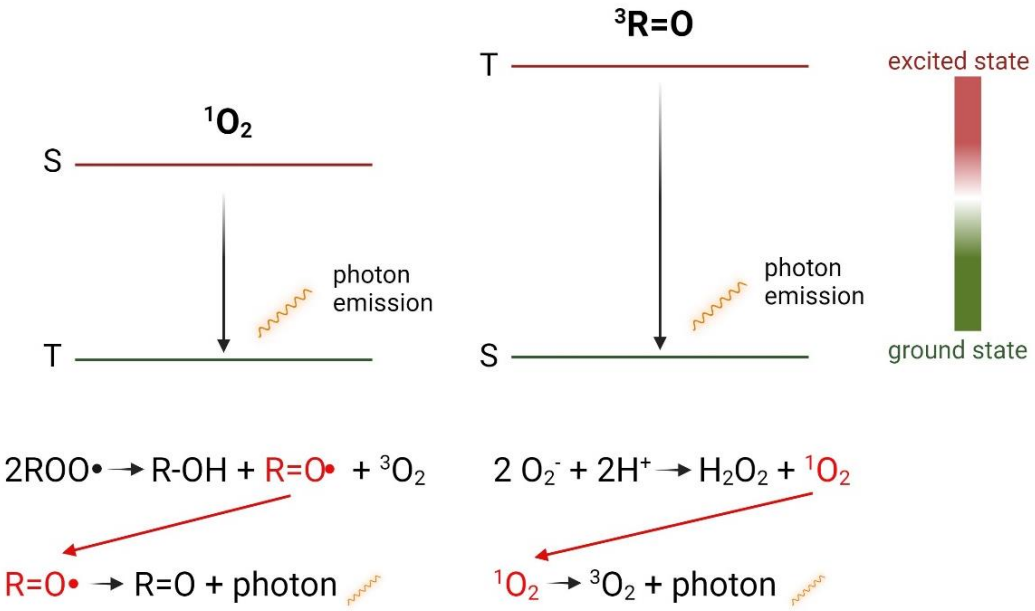

Figure 1.5: Biophotonic emission during oxidative metabolic processes and their mechanistic pathways. Oxidative metabolism results in biophotonic emission through two parallel pathway. Left pathway: The transition of carbonyl radical (R=O•) to ground state carbonyl (R=O) with photon emission, initiated by the reaction of two peroxyl radicals (2ROO•) forming alcohol (R-OH), carbonyl radical (R=O•), and triplet oxygen ($^3O_2$). Right pathway: The conversion of singlet oxygen ($^1O_2$) to ground state triplet oxygen ($^3O_2$) with photon emission, generated from the reaction of superoxide radicals (O_2^-) with protons (H^+) via hydrogen peroxide (H_2O_2) formation. Both pathways are represented by energy level diagrams showing the transition from high-energy excited states (S, shown in red) to lower-energy ground states (T, shown in green), with photon emission occurring during this energy state transition. Each transition is accompanied by the release of a photon, visualized by the emission symbol between the energy levels. Modified from Mould et al. (2024). Key: R represents any alkyl group or hydrogen atom; S denotes a singlet state; T denotes a triplet state; O represents oxygen; $^1O_2$ is singlet oxygen; 3R=O represents a triplet state carbonyl group. (Image created with biorender.com)

1.8.2 Biophotonic detection

The correlation between biophotons and oxidative stress has led to investigations into its potential as a non-invasive tool for detecting and monitoring oxidative stress dynamics (Section 1.8.4) (Du et al., 2023). However, detecting and measuring biophotons remains a significant challenge due to their extremely low intensity (Mould et al., 2024).

Historically, researchers have employed various sophisticated detection methods to capture these weak light emissions. Two primary technologies have been the photomultiplier tubes and charge-coupled device cameras. For example, previous studies using photomultiplier tubes technology have demonstrated elevated biophotonic levels in human skin following UVA exposure, with dose-dependent reductions observed upon application of antioxidants such as vitamin C and alpha-glucosyl rutin (Hagens et al., 2008). While these findings suggest a relationship between biophoton emission and oxidative stress, it's important to note that biophoton measurement is not yet a routine method for assessing oxidative stress due to the technical challenges involved. Both detection techniques offer ways to visualize biophotons temporally and spatially, but each comes with limitations in terms of sensitivity and resolution (Cifra & Pospíšil, 2014).

A recent study by Mackenzie et al. (2024) marks a significant advancement in the field of biophoton detection. By employing highly sensitive detection systems and optimizing experimental conditions, Mackenzie and colleagues successfully detected biophotons in growing mung beans. This work enhances the evidence for the intrinsic metabolic photon emission phenomenon first observed by Gurwitsch a century ago (Mackenzie et al., 2024). The advancements made by Mackenzie et al. include improvements in light-tight experimental chambers, reduction of background noise, and careful management of delayed luminescence effects. Their setup demonstrated the ability to detect changes as small as 0.1 average counts per second using a photomultiplier tube with an average dark count of 15 - 17 counts per second, which is quite low. This level of sensitivity allowed them

to measure signal changes of fractions of a count per second by averaging 1000 seconds of data.

It's worth noting that current detection techniques still face limitations regarding the need for complete darkness during experiments, the challenge of discriminating biophotons from other light sources, and the difficulty in obtaining fully resolved spectra due to the low photon count (Mould et al., 2024). Mackenzie et al.'s work represents progress in overcoming some of these challenges, providing valuable insights into the dynamic emission patterns of UPE and its potential implications in biological processes. This pioneering work provides valuable insights into the dynamic emission patterns of UPE and its potential implications in biological processes, such as metabolism.

1.8.3 Biophotonic communication

During the 20th century, when it was proposed that biological systems emit biophotons (Gurwitsch, 1923), early experimental evidence of non-chemical cellular communication by light was reported, postulating biophotonic communication for the first time: Non-chemical light signalling has been suggested to play a role in the orientation of baby hamster kidney cells in experiments undertaken by Albrecht-Buehler, with the distribution and orientation of newly grown cells, modulated by cultivated baby hamster kidney cells placed on the opposite surface of glass slides. An effect was no longer observed when a thin piece of metal which blocked the passage of light was added between cell populations (Albrecht-Buehler, 1992). Similarly, a cellular response was demonstrated in neutrophils (from pig blood) after non-chemical, optical contact with a second neutrophil population exposed to an oxidative burst (Shen et al., 1994). More recently, researchers have developed more advanced set-ups to demonstrate non-chemical communication, including intestinal epithelial cells separated by a custom-made container (Farhadi et al., 2007) and a “dish-on-dish” design containing endothelial cell populations (Rossi et al., 2011). In both cases, physically disconnected cell populations were shown to influence each other by changing

protein content and altering cellular growth and morphology, supporting the role of biophotons as a method of cellular communication.

The mechanism of non-chemical cell-cell communication has been postulated to take place within mitochondria as the primary source of ROS production, which can lead to biophotonic emission (Kurian et al., 2017). Mitochondria are thought to act as "optical waveguides," guiding light within the cell due to their elongated shape and high refractive index contrast with the surrounding cytoplasm (Thar & Kühl, 2004). Similarly, the microtubule network within cells has also been proposed to function as waveguides, channelling light along their length due to their tubular structure and ability to support guided modes of light propagation. Rahnama et al. and Kurian et al. investigated this interaction between mitochondrial biophotons and microtubules, using a quantum mechanical approach, suggesting that coherent energy is transferred within the microtubule network, absorbed from a chromophore in cytochrome c or aromatic amino acids, and is regulated during ROS production (Kurian et al., 2017; Rahnama et al., 2011).

Bokkon et al. suggested that biophotonic production is regulated by redox and free-radical processes within mitochondria, which can induce the polymerisation of microtubules and can be used as a cross-talk between mitochondria via microtubule networks (Bókkon et al., 2010). More recently, Mould et al. adapted Gurwitsch's original non-chemical communication experimental protocol, incorporating knowledge regarding mitochondria's potential role as waveguides for light and their capacity for redox-driven biophotonic production (Mould et al., 2023). and investigated potential non-chemical signalling between isolated mitochondria from MCF7 (cancer) and MCF10A (non-cancer) mammalian cell lines. By inducing oxidative stress in one population of mitochondria using antimycin, Mould et al. observed significant changes in the oxygen consumption rate of physically separated mitochondria, suggesting the existence of non-chemical signalling pathways. This experiment used a bespoke assay designed to measure mitochondrial respiration responses in quartz cuvettes, importantly ensuring chemically isolated environments to

exclude potential transmission via volatile solvents. Light-absorbing opaque barriers and dark conditions further emphasised the potential light-based nature of the observed communication. Mould et al.'s study provides the most recent and robust evidence for non-chemical communication between mitochondria and represents a groundbreaking advancement in our understanding of cellular communication mechanisms

1.8.4 Potential applications of biophotonic emission in biological systems

Since cells in close proximity can influence each other using biophotons and cellular generation of ROS controls the intensity of biophotonic production, measuring biophotonic emission is postulated to be a non-invasive tool for measuring stress levels in animals and plants. That could, in turn, give valuable information in different disease diagnoses, such as ageing-related diseases where ROS levels significantly increase. In theory, detecting the intensity of the spontaneous biophotonic emission will provide information about the oxidative processes of the organisms (Cifra & Pospíšil, 2014; Cohen & Popp, 2003). Initial and more recent experiments support that idea by demonstrating that plants, such as mug beans exposed to H_2O_2, and animals, such as experiments using injured or cancer-diseased mice, result in altered biophotonic emission (Mackenzie et al., 2024; Ohya et al., 2002; Takeda et al., 2004a).

Pioneering experimental results reveal a potential role of biophotonic emission in several fields, such as agriculture, with biophotonic emission providing information about plant health regarding pathogenic infections (Kobayashi et al., 2006; Rastogi & Pospíšil, 2012), salt stress (Ohya et al., 2000), herbicides resistance (Inagaki et al., 2008) and food quality control (Iida et al., 2002). Changes in biophotonic emission have been shown in human skin tissue exposed to oxidative stress (Murugan et al., 2020; Prasad & Pospišil, 2011; Rastogi & Pospíšil, 2010). Potential applications to non-invasive detection in human diseases related to increased oxidative stress include oncological (Cohen & Popp, 2003; Takeda et al., 2004b), neurodegenerative (Kurian et al., 2017) and dermatological (Rastogi & Pospíšil,

2010) conditions. Biophotonic detection would provide an advanced but non-invasive, label-free, real-time diagnostic tool.

1.9 Photobiomodulation

In addition to intrinsic sources such as intracellular biophotonic production, cells can also interact with extrinsic light emission sources. Photobiomodulation (PBM) is the term used to describe the changes in cellular activity and transformation that occur in response to irradiation with extrinsic light under certain conditions (Tam et al., 2020). Light has been utilized since very early years; sunlight has been used to treat ailments throughout history, a treatment known today as heliotherapy. In the late nineteenth century, Niels Ryberg Finsen pioneered the use of red and blue light to treat Lupus vulgaris, leading to his Nobel Prize in 1903 (Anders et al., 2015; Finsen, 1902; Finsen, 2023). The modern term PBM therapy (formerly low-level laser therapy – LLLT) is a non-thermal use of light that is distinguished from other light-based therapies that rely on thermal effects, and it was first introduced by Endre Mester in 1967 (Mester et al., 1968a). Mester observed increased wound healing and hair growth in mice treated with low-level applications (Mester, Ludany, et al., 1968; Mester et al., 1968b). The term "photobiomodulation therapy", specifically for this type of light therapy, to distinguish it from other forms that generate thermal effects, which may have adverse side effects for the organism The term could reduce confusion and promote a positive image of its clinical applications (Hamblin, 2016a; Tam et al., 2020).

1.9.1 Cellular mechanisms of PBM

The electromagnetic spectrum encompasses a range of wavelengths, including visible light, ultraviolet, and infrared radiation. Visible light, the only portion of the spectrum that humans can see, falls between 400-700 nm. UV radiation ranges from 100-400 nm and near-infrared (NIR) to infrared radiation between 700 nm and 1000 nm. UV, visible light, and NIR to

infrared are the three different types of radiation that make up the optical region of the electromagnetic spectrum (de Sousa, 2017). The depth to which light can penetrate human skin varies depending on its wavelength. Red light, for instance, can penetrate up to 4-5 mm below the surface of the skin, whereas UV radiation has a limited ability to penetrate, and blue light can only penetrate up to 1 mm into the tissue (Ash et al., 2017; Clement et al., 2005).

PBM therapy utilises light, most commonly in the red to NIR range (600 – 1000 nm), to facilitate therapeutic effects and promote health. It is employed for wound healing, decreasing inflammation, reducing pain, and managing age-related symptoms (de Freitas and Hamblin, 2016; Wang et al., 2016; Hamblin, 2017). Mechanistically, PBM is a photochemical reaction during which a cell absorbs photons of red to infrared wavelengths and induces biomodulation. For this to occur, a molecule or part thereof known as a chromophore must be present within the cell, and it must possess electrons in a low-energy orbit that can be excited by photons to transition to a higher-energy orbit (de Sousa, 2017). Tina Karu's research in Russia was crucial in establishing a solid foundation for understanding the mechanism behind PBM (Karu, 2008). She identified cytochrome c oxidase (CCO) in the mitochondrial respiratory chain and suggested it as a primary chromophore. Karu also introduced the concept of "retrograde mitochondrial signalling" to explain how a short exposure to light could result in long-lasting effects on the organism, spanning from hours to even weeks (Karu, 2008).

The CCO is the terminal enzyme in the mitochondrial OXPHOS (located in the IV complex; Figure 1.3), and it is responsible for catalysing the reduction of oxygen to produce energy for cellular metabolism (Cardoso et al., 2022; Hatefi, 1985; Wang et al., 2016). The level of metabolic energy generated via mitochondrial oxidative phosphorylation is directly related to the activity of CCO; as CCO activity increases, so does oxygen consumption and energy production (Rojas & Gonzalez-Lima, 2013).

Today, the exact mechanism of PBM is still not fully understood. Currently, the leading theory is that light excitation affects the activity of the CCO molecule in the mitochondria. COO absorbs photons, leading to changes in the cell's electrochemical proton gradient, ROS levels, mitochondrial membrane potential (MMP), ATP synthesis, and redox changes (Karu, 2008; Passarella & Karu, 2014). By up-regulating CCO concentration, PBM therapy can induce longer-lasting effects on mitochondria oxygen metabolism, which in turn enhances the overall capacity for cellular energy metabolism (Wang et al., 2016). A second suggested pathway involves ion channels that are sensitive to photonic stimulation. These ion channels allow increased calcium ions (Ca^{2+}) to pass through the cellular membrane, altering cellular homeostasis (de Freitas and Hamblin, 2016; Hamblin, 2017). A third mechanism, proposed by Sommer et al. (2015), suggests that PBM could modulate the viscosity of nanoscopic water layers within and around mitochondria, potentially affecting the efficiency of the ATP synthase motor and overall mitochondrial function.

To sum up, the absorption of photons in the cell leads to the activation of several molecules, including ROS and Ca^{2+} (Dompe et al., 2020; Hamblin, 2017; Yadav and Gupta, 2017), which can change the ultrastructure of mitochondria (mitochondrial fission and fusion) (de Freitas and Hamblin, 2016). Mitochondrial ultrastructure and dynamics change can lead to a further increase of mitochondrial Ca^{2+}, ROS, ATP production, and various other signalling molecules, which can activate different transcription factors in the nucleus due to mitochondria-nucleus communication (de Freitas & Hamblin, 2016; Foo et al., 2020; Hamblin, 2018b). These transcription factors can, in turn, result in gene expression affecting improved cell survival, such as cell migration and proliferation, wound healing, anti-inflammatory signalling and protein synthesis (de Freitas & Hamblin, 2016; Hamblin, 2018b; Kim et al., 2017; Zamani et al., 2020).

1.9.2 PBM applications

PBM has made significant advancements and gained recognition from various entities, including biomedical researchers, scholarly journals, medical practitioners, and the media. The number of publications relating to PBM research increased dramatically after 2002 (Figure 1.6), and the efforts to raise awareness and acceptance of PBM are ongoing. The interest in PBM has been increased mainly due to the non-invasiveness of this methodology (de Sousa, 2017); Standard PBM therapy involves the use of red to NIR light, which can penetrate deeper into the human tissue than other wavelengths (Ash et al., 2017). The beneficial effects of PBM have been observed in the treatment of diabetes (Bodnar et al., 1999), neural diseases and injuries (Cardoso et al., 2022; Foo et al., 2020; Hamblin, 2018b; Naeser et al., 2014; Rojas & Gonzalez-Lima, 2013), ophthalmology (Rojas et al., 2008; Shinhmar et al., 2021; Sivapathasuntharam et al., 2017; Zhu et al., 2021), dermatology (Avci et al., 2013; Barolet et al., 2009), treatment of alopecia (Roets, 2023; Wikramanayake et al., 2012), applications in dentistry (Grzech-Leśniak, 2017; Świder et al., 2019) and managing ageing-related health implications (see Section 1.9.3).

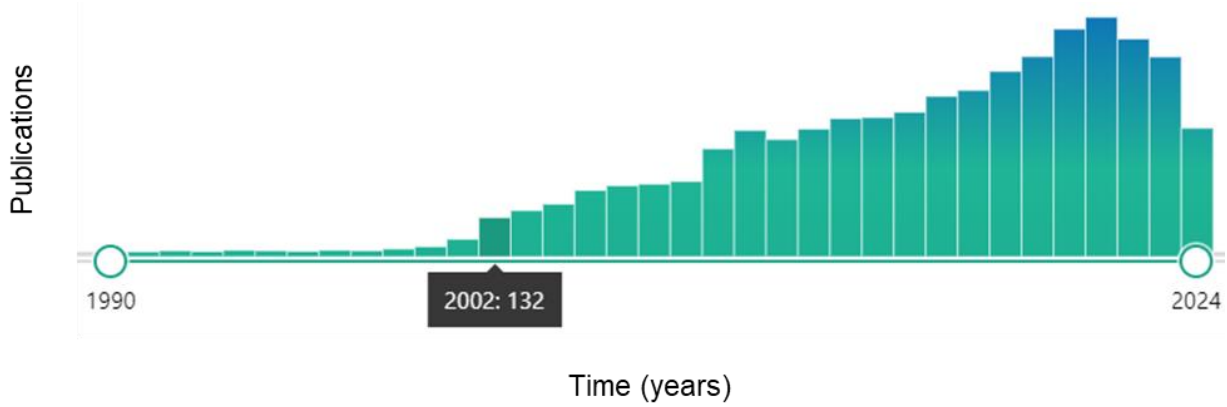

Figure 1.6: Published research in PBM between 1990 and 2024 in Pubmed. Bar graph showing the annual publication count of PBM-related research over a 34-year period. The graph demonstrates three distinct phases: (1) Initial phase (1990-2001) with minimal research output (<50 publications/year), (2) Growth phase beginning in 2002 with a significant jump to 132 publications (83 more than 2001), marking the start of increased research interest, and (3) Rapid expansion phase (2002-2024) showing consistent year-over-year growth. Notable milestones include exceeding 500 annual publications in 2013 and reaching a historic peak of 904 publications in 2021. This trend reflects the growing scientific interest in PBM and its emerging applications in various fields of medicine and biology. Data was obtained through a Pubmed search of PBM-related publications, including earlier terminology such as 'low-level laser therapy' (LLLT).

1.9.3 PBM and ageing

Among the applications described in Section 1.9.2, PBM with red to NIR light has also gained attention for its potential to improve age-related pathologies. Several recent studies have demonstrated the beneficial effects of PBM, particularly with 670 nm light, on mitigating age-related cellular and functional deficiencies in the central nervous system (Mitrofanis & Jeffery, 2018; Sivapathasuntharam et al., 2017). The proposed underlying mechanism of PBM (see Section 1.9.1) against age-related decline agrees with the literature (Karu, 2008) (see Section 1.9.1). That includes the absorption of these long wavelengths by CCO in the mitochondrial respiratory chain, which enhances CCO activity, increasing mitochondrial membrane potential and ATP production (Karu, 2008; Powner & Jeffery, 2024). PBM can improve mitochondrial function, reduce oxidative stress, and decrease inflammation associated with ageing (Sivapathasuntharam et al., 2017).

In the retina, a tissue with high metabolic demand and mitochondrial density, PBM treatment using 670 nm light has been shown to decrease age-related photoreceptor loss and improve retinal function in aged mice (Sivapathasuntharam et al., 2019). Similar benefits have been observed in human participants (over 40 years old), with 670 nm light exposure improving rod and cone photoreceptor function (Shinhmar et al., 2020, 2021). Additionally, *in vivo* measurements using NIR spectroscopy have demonstrated that PBM exposure increases the oxidation of CCO and improves retinal hemodynamics in aged rats, which further supports the mechanism proposed by Passarella and Karu (Kaynezhad et al., 2016; Passarella & Karu, 2014). These studies suggest that PBM can modulate mitochondrial function and cellular metabolism, potentially slowing or reversing age-related declines.

Moreover, a recent study by Powner and Jeffery demonstrates that PBM with 670 nm light reduces blood glucose spikes following glucose intake in normal human participants (Powner & Jeffery, 2024). This finding suggests that PBM may have potential applications in managing various metabolic disorders associated with ageing, including but not limited to diabetes. The study's results indicate that PBM could be a promising approach for

regulating blood glucose levels and potentially mitigating the harmful effects of glucose fluctuations on overall health (Powner & Jeffery, 2024).

Lastly, PBM has also been emerging as a potential neuroprotective treatment against age-related conditions that affect the brain, such as memory loss, Alzheimer's and Parkinson's disease. NIR light has been proposed to be capable of arresting neuronal death in these conditions (Johnstone et al., 2016). Preliminary clinical studies have reported improvements in symptoms, such as cognitive function and speech difficulties, in Parkinson's disease patients treated with transcranial PBM (Hamblin, 2016b). Moreover, transcranial NIR light exposure is being explored as a promising non-pharmacological treatment for cognitive impairment in Alzheimer's disease, owing to its low cost, safety profile, and ease of self-administration (Garcia-Pardo et al., 2023). Recent advances in transcranial PBM, combined with new drug delivery systems and nanotechnologies, offer new methods for rejuvenating the central nervous system and overcoming protective brain barriers in the treatment of Alzheimer's disease (Ailioaie et al., 2023).

To conclude, despite the advances and advantages of PBM, this type of therapy has not yet been incorporated into standard treatment practices due to a limited understanding of how the mechanism works at the molecular, cellular, and tissue level (de Freitas & Hamblin, 2016). Additionally, the effectiveness of PBM on a particular target tissue can depend on various factors, including the light source, wavelength, energy density, light pulse structure, and duration of the laser application. These parameters significantly determine the optimal treatment outcomes (Kujawa et al., 2014). Tackling these methodological uncertainties, PBM could serve as a non-invasive health strategy.

1.10 Aims

The primary aim of this thesis was to characterize changes in biophotonic emission during cellular senescence. This involved investigating the relationship between senescence and biophotonic production, with a focus on the role of ROS, as primary source of biophotons. A secondary aim was to explore potential non-chemical communication between senescent cells, examining whether biophotons play a role in this process. Finally, this research aimed to investigate the interaction between NIR light and cells in the context of senescence induction. This involved studying how PBM might influence senescence levels in different cell types, considering the potential bidirectional effects mediated by ROS. Through these aims, I seeked to contribute to our understanding of the biophysical aspects of senescence and their potential implications for cellular communication and light-based therapies.

1.11 Hypothesis

Senescence alters the biophotonic non-chemical communication effect on cellular mitochondrial function, and this phenomenon can be modulated by exposure to NIR light.

Chapter 2 : Methods

2.1 Cellular models selection

This study employed a diverse range of cell lines to investigate senescence across different cellular contexts. The selection of these cell lines was based on their relevance to senescence research, their representation of both cancerous and non-cancerous tissues, and their established use in the field.

The non-cancerous breast MCF10A cell line was chosen as the primary senescent model for this thesis. This selection was made to establish a main model that is not diseased, allowing for the study of senescence in a non-pathological context. MCF10A was specifically chosen among other non-cancer models due to its direct cancer analogue, MCF7. MCF7 is widely used in senescence studies (El-Far et al., 2020; Srdic-Rajic et al., 2017), and having this paired set of cell lines enables comparative analyses between cancerous and non-cancerous breast tissue responses to senescence induction. This pairing provides valuable insights into how senescence mechanisms might differ between normal and cancerous cells of the same tissue origin.

IMR-90 lung fibroblasts were employed as a control senescent gold standard model (Hernandez-Segura et al., 2018b; Hooten & Evans, 2017), with the lung cancer cell line A549 serving as a cancerous counterpart. This pairing allowed for the examination of senescence in a different tissue type. Furthermore, the progeria cell line AG01972 was used as a model for premature ageing disease, characterized by high levels of senescent cells (Ashapkin et al., 2019).

It is important to note that not all tests were performed on all cell lines due to time constraints and the specific focus of each experimental phase. For instance, IMR-90 cells were primarily used to validate the senescence induction protocol, serving as a control cell line. A549 cells were not subjected to all mitochondrial function tests (such as mitochondrial

membrane potential, mitochondrial Ca^{2+}, and intracellular Ca^{2+} measurements) because they were primarily employed for the NIR light study in Chapter 6. For A549 cells, the focus was on Dox-induced senescence characteristics and ROS levels, which were also critical for the subsequent biophotonic production study.

2.2 Cell lines

Human breast cell line **MCF10A** was grown in Dulbecco's modified eagle's medium (DMEM): F12 (Life Sciences, UK), supplemented with 5% horse serum (ThermoFisher, UK), 1% penicillin/streptomycin, 20 ng/mL epidermal growth factor (Merck, UK), 0.5 mg/mL hydrocortisone (Merck, UK), 100 ng/mL cholera toxin (Merck, UK) and 10 µg/mL insulin (Merck, UK). Human breast adenocarcinoma cell line **MCF7**, human lung fibroblast cell line **IMR-90** purchased from American Type Culture Collection (ATCC) and human Hutchinson-Gilford progeria fibroblast cell line **AG01972** purchased from the Coriell Institute for Medical Research were grown in eagle's minimum essential medium (EMEM; ThermoFisher, UK), supplemented with 10% fetal bovine serum (FBS), 1% l-glutamine and 1% penicillin/streptomycin. All cells were incubated at 37°C with 5% CO_2. Human lung cancer cell line **A549** purchased from ATCC were grown in DMEM high glucose (ThermoFisher, UK), supplemented with 10% FBS and 1% penicillin/streptomycin.

2.3 Reagents

Palbociclib (Merck, UK) was dissolved in dimethyl sulfoxide (DMSO) to a stock concentration of 100 mM. 30% volume by volume hydrogen peroxide (H_2O_2) (ThermoFisher, UK) was diluted in autoclaved deionised (DI) water (H_2O) to a stock concentration of 100 mM. Doxorubicin (Dox) (Tocris, Bio-techne, Bristol) was dissolved in autoclaved DI H_2O to a stock concentration of 100 mM. Dox was diluted for experimentation on the day of the experiment in fresh media.

2.4 Cell culture

All work with cell lines was carried out in a laminar flow hood with an aseptic technique. Cells were grown in sterile T75 or T175 flasks and passaged at 80-90% confluency. Confluency was estimated by microscopical observation. Regarding passage protocol, media was removed from the flask and cells were washed with half the media volume of sterile phosphate-buffered saline (PBS). Cells were then detached from the surface of the flask using 1-2 mL TrypLE for 15 minutes for the MCF10A cell line and 7 minutes for other cell lines. Following detachment, cells could be resuspended in fresh media and diluted into new flasks. Cells were only used for experimentation between passages between 5 and 25. Regarding cell seeding protocol, cells were detached as described above, counted using a Countess 2 automated cell counter (ThermoFisher, UK), and added to wells with the appropriate volume of media for the plate being used (100 µL total for 96-well plates and 2 mL for 6-well plates).

2.5 Treatment protocols for senescence induction

To induce cellular premature senescence, three chemical agents known for their potential to induce senescence were tested: Dox, hydrogen peroxide (H_2O_2), and palbociclib. These agents were selected based on previous literature reporting their senescence-inducing capabilities in various cell types, including MCF7 breast cancer cells (Hernandez-Segura et al., 2018b; Jost et al., 2021; Zhong et al., 2019).

Dox treatment involved exposing cells to 0.25 µM for 24 hours, followed by culture in drug-free media for an additional 5 days to allow a senescent population to develop fully. For H_2O_2 treatment, a range of concentrations (100, 200, 300, and 500 µM) were tested of 30% H_2O-soluble H_2O_2 for 24 hours. Palbociclib was applied at a concentration of 10 µM for 72 hours. All three treatments were conducted in parallel under the same experimental conditions. This approach allowed for a comprehensive evaluation of different senescence induction methods in this experimental system.

Cells were passaged for a minimum of 25 passages for replicative senescence induction. Under the conditions described in Section 2.3, the cells were split every 3 - 4 days until they reached passage 25 or until they were no longer able to replicate and reach confluency.

2.6 Cell viability in response to treatment

Cell viability was assessed by using the 3-(4,5-dimethylthiazol-2-yl)-2,5-diphenyltetrazolium bromide (MTT) assay kit (Sigma, UK). The assay is based on the conversion of MTT (yellow) to formazan (purple) by nicotinamide adenine dinucleotide phosphate (NADPH)-dependent reductases in the cell. 10,000 cells were seeded onto 96-well plates and treated as described in Section 2.4. Cell viability was determined according to the manufacturer's guidelines. Following drug treatment, cells were washed with PBS and replaced with phenol red-free media (prepared as described in Section 2.1). Cells were treated with 10 µL 5 mg/mL MTT solution for 3 hours at 37°C. Media was removed, and resultant crystals dissolved in 100 µL DMSO. Absorbance at 690 nm was subtracted from absorbance at 570 nm with a microplate reader (SPECTROstar Nano, BMG Labtech, Germany). Cell viability is presented as a percentage of the vehicle control.

2.7 Flow cytometry assay for senescence quantification

Flow cytometry was used to quantify intracellular nanoparticles and examine senescent levels in cellular populations (Cahu & Sola, 2013). Similar to the procedures described in Sections 2.3 and 2.4, 100,000 cells were seeded in a 6-well plate and treated with Dox/palbociclib/H_2O_2 for senescence induction. CellEvent™ Senescence Green Flow Cytometry Assay Kit (ThermoFisher, UK) was employed to detect cellular senescence via flow cytometry. This assay quantifies senescence-associated β-galactosidase (SA-β-gal) activity by measuring the hydrolysis of a fluorescein-based substrate containing galactoside moieties. The kits reagent is specifically cleaved by β-galactosidase in lysosomes under

acidic conditions, yielding a fluorescent product. This product is retained within the cell due to its interaction with intracellular proteins, emitting a green, fluorescent signal detectable by flow cytometry. The assay allows for the quantitative assessment of senescent cells based on their elevated β-galactosidase activity, a widely recognized biomarker of cellular senescence, and was conducted according to the manufacturer's protocol (ThermoFisher Scientific, 2019).

Briefly, cells were detached by TrypLE, fixed with 1:1 Formalin:PBS, stained with CellEvent green probe (1,000x) diluted in buffer, and incubated for 90 minutes in a CO_2-free incubator at 37°C. After staining, cells were washed with PBS and prepared for flow cytometry. Flow cytometry measurements were performed with a BD LSRFortessa™ X-20 Analyser flow cytometer (BD Biosciences, New Jersey-USA), and data were recorded/analysed using a BD FACSDiva™ Software. The AlexaFluor channel (488 nm laser) was used to capture the uptake of stained cells. For the analysis, the cell population was selected on a forward/scatter/sideward scatter plot to exclude debris cellular aggregates and 10,000 gated events were recorded. The median fluorescent intensity was determined from a histogram, and the results were recorded as a median value.

2.8 SA β-gal staining

SA β-gal staining was performed using the Beta-Galactosidase Staining Kit (Cell Signaling Technology, US) following the manufacturer's instructions. Similar to the procedures described in Sections 2.3 and 2.4, 100,000 cells were seeded in a 6-well plate and treated with Dox for senescence induction. On the day of the experiment, cells were fixed with 1:10 fixative solution for 15 minutes, washed twice with PBS, and stained with the staining solution (pH: 6) overnight at 37°C without CO_2. After staining, samples were rinsed with PBS and imaged using an EVOS FL2 fluorescent microscope (ThermoFisher, UK).

2.9 Cell cycle analysis

The stages of the cell cycle were assessed using propidium iodide (PI) staining (ThermoFisher, UK), which binds to double-stranded DNA following flow cytometry (Krishan, 1975). 100,000 cells were seeded in a 6-well plate and treated with Dox for senescence induction. On the day of the experiment, cells were detached using TrypLE and centrifuged at 1,000 RCF for 5 minutes, washed with PBS, and centrifuged again at 1,000 RCF for another 5 minutes. The pellet was resuspended in 300 µL ice-cold PBS, and 700 µL ice-cold 100% ethanol was added while the sample was shaken. Cells were then incubated at -20°C for a minimum of 2 hours. After incubation, samples were centrifuged at 2,000 RCF for 5 minutes and resuspended in 500 µL fluorescence-activated cell sorting (FACS) buffer containing 1% bovine serum albumin (BSA) in PBS. Following an additional centrifugation step, 50 µL of 100 µg/mL RNAase and 450 µL of 50 µg/mL PI solution were added to the pellet. Cells were then incubated in the dark at room temperature for 15 minutes, and flow cytometry measurements were performed (similar to the protocol described in Section 2.7). The PE channel (575 nm laser) was used to capture the uptake of stained cells. For the analysis, the cell population was selected on a forward/scatter/sideward scatter plot to exclude debris cellular aggregates and doublet exclusion was employed. The percentage of the total population was determined from a histogram in each cell cycle phase, and results from G1, M and G2 phases were recorded.

2.10 Detection and quantification of ROS

The 2',7'–dichlorofluorescin diacetate (DCFDA) stain was used to detect changes in the levels of ROS in live cells. The presence of ROS in the cell converts DCFDA into the highly fluorescent compound 2',7'–dichlorofluorescin (DCF). 100,000 cells were seeded in a 6-well plate and treated with Dox for senescence induction. After treatment, cells were washed with PBS and incubated with 30 µM DCFDA (Sigma, UK) at 37°C 5% CO_2 for 30 minutes, protected from light. In the presence of ROS, DCFDA forms the highly fluorescent

compound DCF, quantified by flow cytometry (similar to the protocol described in Section 2.7) –the AlexaFluor channel (488 nm laser) was used to capture the uptake of stained cells.

2.11 Assessment of mitochondrial membrane potential

The cell-permeant tetramethylrhodamine, ethyl ester (TMRE) stain was used to label active mitochondria in live cells. TMRE is a positively charged dye that accumulates in active, negatively charged mitochondria, reflecting the increased mitochondrial membrane potential in live cells. 100,000 cells were seeded in a 6-well plate and treated with Dox for senescence induction. After treatment, cells were washed with PBS and incubated with 500 nM TMRE (Sigma, UK) in Phenol Red Free media at 37°C with 5% CO_2 for 30 minutes and then protected from light. Activated mitochondria sequester TMRE, quantified by flow cytometry (similar to the protocol described in Section 2.7) – the PE channel (575 nm laser) was used to capture the uptake of stained cells.

2.12 Assessment of intracellular Ca^{2+} levels

The cell-permeant Fluo-4 stain was used to label the total cellular Ca^{2+} in live cells (Gee et al., 2000). 100,000 cells were seeded in a 6-well plate and treated with Dox for senescence induction. After treatment, cells were incubated with 1 μM Fluo-4 (ThermoFisher, UK) in Phenol Red Free media, at 37°C 5% CO_2 for 30 minutes, protected from light. Fluo-4 fluorescence signals were quantified by flow cytometry – the PE channel (575 nm laser) was used to capture the uptake of stained cells.

2.13 Assessment of mitochondrial Ca^{2+} levels

The cell-permeant Rhod-2 stain was used to label mitochondrial Ca^{2+} in live cells (Fonteriz et al., 2010). Rhod-2 is a labelled Ca^{2+} indicator that exhibits a fluorescence increase when

binding to Ca^{2+}. 100,000 cells were seeded in a 6-well plate and treated with Dox for senescence induction. After treatment, cells were washed with PBS and incubated with 1 µM Rhod-2 (ThermoFisher, UK) in Phenol Red Free media at 37°C 5% CO_2 for 30 minutes, protected from light. Mitochondrial Ca^{2+} within the cells released Rhod-2 fluorescence signals, which were quantified by flow cytometry (similar to the protocol described in Section 2.7) - the PE channel (575-nm laser) was used to capture the uptake of stained cells.

2.14 Mitochondrial isolation

Mitochondria were extracted from whole cells utilising the Mitochondria Isolation Kit for Cultured Cells (Abcam, UK), as described by Mould et al. (2023). 2,000,000 cells were seeded in 2 T175 flasks and treated with Dox for senescence induction. After treatment, cells were detached with TrypLE and centrifuged at 1,000 RCF for 5 minutes, then washed with PBS and re-centrifuged. The pellet was frozen at -80°C overnight to facilitate membrane weakening. Upon thawing, cells were resuspended to a concentration of 5 mg/mL in kit reagent A and maintained on ice for 10 minutes. Following this, cell homogenisation was performed with 30 strokes using a Dounce homogeniser equipped with pestle B, followed by centrifugation at 1,000 RCF for 10 minutes at 4°C. The supernatant was retained, while the pellet was resuspended in kit reagent B, homogenised again using the Dounce homogeniser, and subjected to a subsequent centrifugation step at 1,000 RCF for 10 minutes at 4°C. The two resulting supernatants were combined and centrifuged at 12,000 RCF for 15 minutes at 4°C. The pellet was resuspended in 500 µL kit reagent C after discarding the supernatant. The isolated mitochondria were quantified utilising a Bradford assay.

2.15 Mitochondrial assay buffer

Following isolation as described in Section 2.13, mitochondria were resuspended in mitochondrial assay buffer (MAB) prepared as follows: 110 mM mannitol, 70 mM sucrose, 10 mM KH_2PO_4, 5 mM $MgCl_2$, 2 mM HEPES, 1 mM EGTA, 0.2% weight/volume BSA (Merck, United Kingdom) in ultrapure H_2O (Rogers et al., 2011).

2.16 Bradford protein assay

Cellular protein levels, quantified by Bradford protein colorimetric assay (BioRad, UK), were used to assess the cell number post-treatment or post-senescence induction. Briefly, each cellular sample underwent two washes with ice-cold PBS. Cells were then lysed using ice-cold radioimmunoprecipitation assay (RIPA) buffer from Sigma, UK, for 15 minutes while agitated on a shaker. After lysis, samples were centrifuged at maximum speed for 15 minutes at 4°C, after which the supernatant was carefully decanted into new tubes. A 5 µL aliquot of each sample was dispensed into the wells of a 96-well plate in triplicate. Following this, 200 µL of Bradford reagent was added to each well, and the absorbance at 595 nm was determined using a plate reader. A series of protein standards BSA (BioRad, UK) was employed to generate a standard curve via linear regression to facilitate quantification of the unknown samples.

2.17 Non-chemical communication assay

Building upon the protocol outlined by Mould et al., 2023, in which I had first-hand training as I contributed to the publication, a customised non-chemical communication assay was developed to investigate potential inter-mitochondrial non-chemical signalling from senescent cells (Figure 2.1). The assay's fundamental principle involved inducing oxidative stress in one group of mitochondria and evaluating the response, specifically in terms of mitochondrial respiration, among chemically isolated mitochondria populations.

Mitochondria from senescent cells were evenly distributed across three quartz cuvettes (Helma, Germany). Each cuvette held a final volume of 2 mL, comprising 166 µL of isolated mitochondria suspended in 1,834 µL of MAB. Equipped with a magnetic stirrer bar, each cuvette was securely sealed with parafilm to prevent potential chemical transmission between them. These cuvettes were arranged linearly, with one pair separated by an opaque aluminium foil barrier, serving as a light-absorbing shield. The central cuvette underwent treatment with antimycin A, which is a complex III inhibitor of the mitochondrial electron transport chain, thereby disrupting the production of ATP by oxidative phosphorylation and significantly reducing oxygen consumption in isolated mitochondria (Kim et al., 1999). The shielded and the unshielded cuvettes remained untreated. Oxygen consumption in each cuvette was monitored using a FireSting O_2 meter (PyroScience, Germany) equipped with individual needle-like probes and a temperature probe to compensate for temperature fluctuations. Oxygen consumption was recorded over a 120-second interval, after which 50 µL of 10 mM antimycin A was introduced into the central ("treated") cuvette using a Hamilton syringe, achieving a final concentration of 244 µM. Oxygen consumption was then measured for 300 seconds in each cuvette, resulting in a total measurement duration of 420 seconds. The oxygen consumption rate was calculated by using a linear model (see Section 2.20). This whole assay was conducted under dark/lightproof conditions.

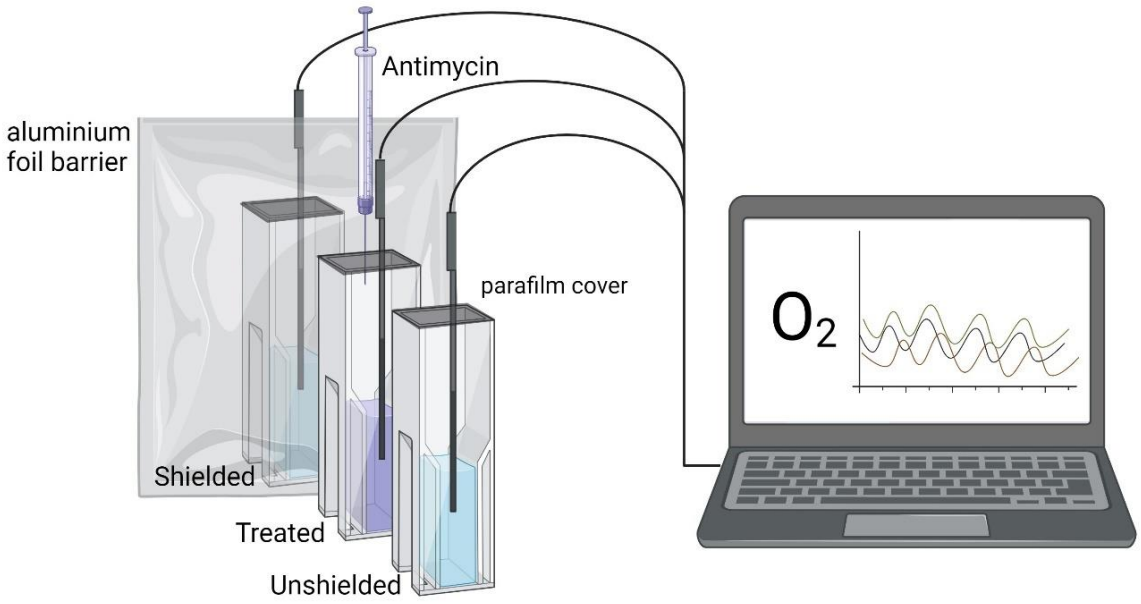

Figure 2.1: Schematic representation of non-chemical communication assay. Mitochondria from senescent cells were placed into three quartz cuvettes: “shielded”, "treated", and “unshielded”, positioned with 0 cm distance between them (in direct contact with each other). An aluminium foil barrier was placed between the “shielded” and “treated” cuvettes to block any light transmission between them, while the “unshielded” cuvette remained in direct contact with the “treated” cuvette without any barrier. Oxygen consumption probes monitored the oxygen levels continuously for 420 seconds, with antimycin injection into the central ("treated") cuvette occurring at the 120-second timepoint. Each cuvette contained isolated mitochondria in mitochondrial assay buffer and was sealed with parafilm to prevent chemical exchange. Each cuvette was equipped with a magnetic stir bar to maintain continuous mitochondrial suspension throughout the experiment. The entire assay was conducted under strict dark conditions to enable the effect of potential light-based signalling between mitochondrial populations. (Image created with biorender.com)

2.18 Biophotonic detection

Biophotons were detected using an ultra-sensitive light detector, which was built, tested, and published by Mackenzie et al., 2024. A single photomultiplier tube detector was positioned within a light-tight, aluminium dark box, with the sample (cells or isolated mitochondria) above within a 35 mm ibidi dish containing a total volume of 3 mL. The photomultiplier tube detectors converted the ultra-weak photon signals into electrical pulses, which were then recorded using the Hamamatsu C8855-01 Photon Counter Unit and accompanying software (Hamamatsu Photonics, Japan). The dark box was covered with a black cloth and then placed within a dark room with a double door system to ensure minimal light interference (Figure 2.2). The room remained dark for at least 24 hours before each recording to avoid false detection of noise and light not originating from the samples. The photon acquisition time was 10 seconds for a total of 72 hours of recording per sample, to a minimum of N=3 biological repeats, with appropriate corrections applied to account for detector dark counts and experimental interruptions.

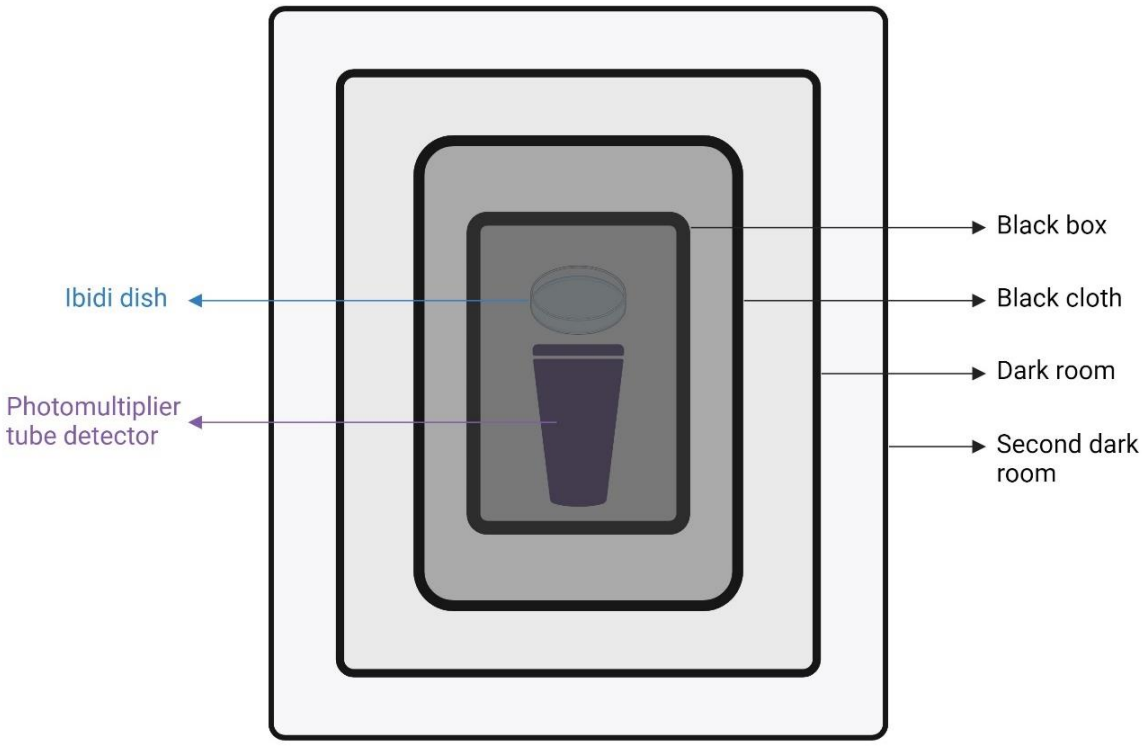

Figure 2.2: *Schematic representation of the ultra-sensitive light detector set-up*. The innermost compartment contains the photomultiplier tube (PMT) with the ibidi dish containing isolated mitochondria positioned directly above it for maximum photon detection sensitivity. This core detection unit is housed within an aluminium dark box (shown as the darkest grey middle square), which is wrapped in a black cloth (represented by the next layer). The entire apparatus is situated within a system of two consecutive dark rooms (depicted by the two outermost, lighter grey squares), creating multiple layers of light protection. This multi-layered isolation system ensures minimal light noice and enables detection of ultra-weak biophotonic emissions from the mitochondrial samples. Each successive layer of containment is represented by increasingly darker shading, illustrating the progressive light isolation from the outer environment to the central detection area. (Image created with biorender.com)

2.19 NIR LED light characterization

Near-infrared (NIR) light emitting diode (LED) exposure was achieved by using a pre-mounted 7 – LED array of NIR (734 nm) Rebel LEDs (Luxeon Star LED, Alberta – Canada) mounted on a SinkPAD-II 40 mm Round 7-Up base with a power output of between 0.328 to 0.420 mW (Fluence ≈ 63 mJ/cm^2, Power density ≈ 0.05 mW/ cm^2), as provided by Professor Margaret Ahmad and described by (Pooam et al., 2021).

LED light characterisation was performed at the Research Complex at Harwell Science & Technology Facilities Council. The wavelength range was measured using a portable USB high-resolution fibre optic HR2000CG UV-NIR spectrometer (Ocean Optics Inc, Florida - USA), and the output power was recorded on a PM100D power meter with an S120VC photodiode power sensor (Thorlabs Inc, New Jersey - USA). LED light thermal effects on media were measured with a FireSting optical temperature sensor and recorded by an FSO_2 temperature meter (Pyroscience, Germany). The temperature sensor was positioned at the centre of the plate well containing cell-free media, and temperature readings were taken every 5 seconds over 1,440 seconds (24 minutes). The LED was switched on at 240 seconds. Media for both cancer and non-cancer cell lines were utilised and compared against control media with no NIR light irradiation.

2.20 NIR light treatment

The cells were seeded in a 6-well plate with a density of 100,000 and left in the incubator for 24 hours. One plate (“control”) was left in the dark, and a second (“treated”) received the NIR light treatment (Figure 2.3). The treatment included a daily 20-minute exposure to NIR light over a six-day period, similar to the NIR light treatment described by Pooam et al. (2021).

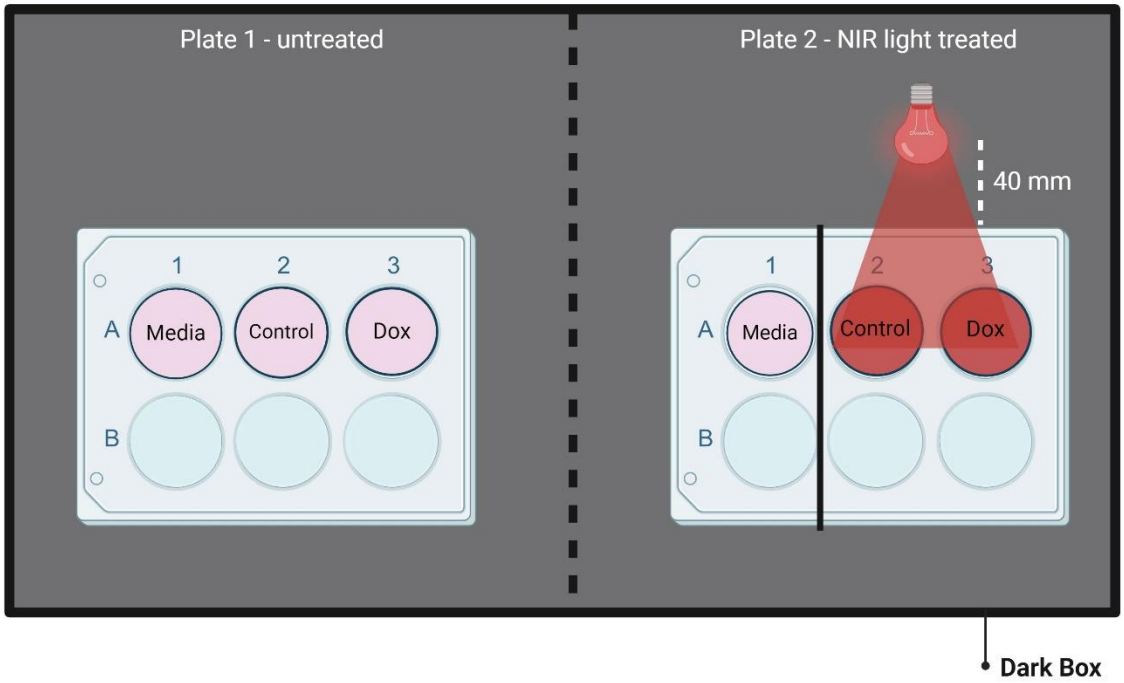

Figure 2.3: Experimental design for NIR light exposure method. The illustration shows a dark box containing two experimental setups: Left side – control untreated condition with a 6-well plate (Plate 1) kept in darkness, containing three populated wells (untreated cells, vehicle control, and Dox-treated senescent cells). Right side – plate (Plate 2) where vehicle control and Dox-treated wells receive 20-minute NIR light exposure from an LED source positioned 40 mm below the plate, while the untreated cell well remains shielded from the light. Both plates were shielded from ambient light by the dark box enclosure for 20 minutes. The 40 mm distance between the LED source and plate was maintained to ensure consistent light exposure across treated wells. (Image created with biorender.com)

The LED array was placed 40 mm below the 6-well culture plate and between two wells receiving the treatment, to create a uniform beam to illuminate the plate. The well with the “control” population was covered, and any other cell treatment (e.g. Dox treatment for senescence induction) was performed normally during these six days before the light treatment. Figure 2.4 outlines the different experimental treatments applied parallel to one cellular population.

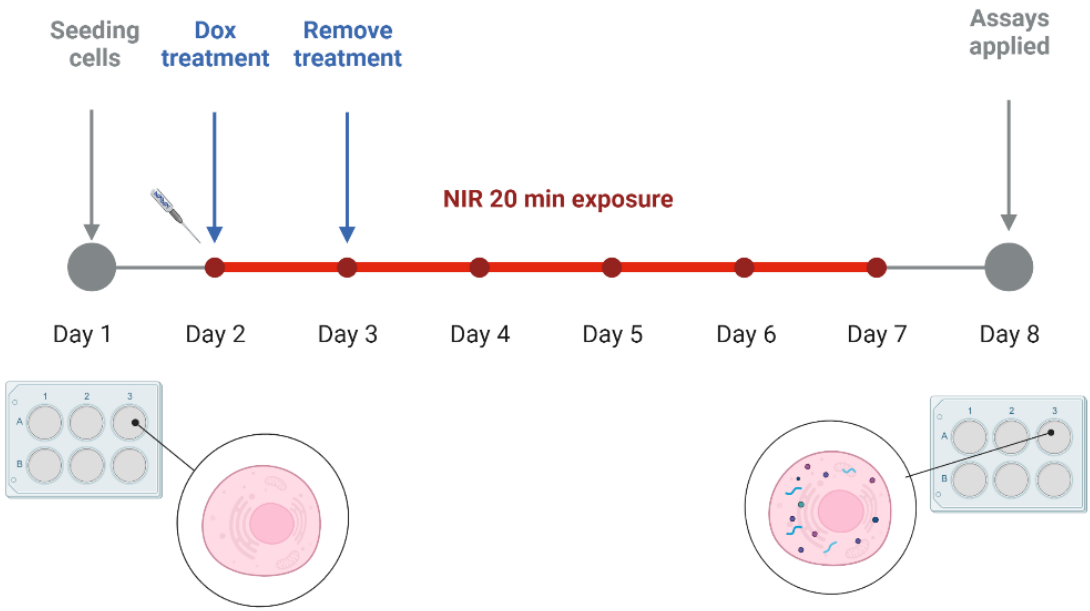

Figure 2.4: *Outline of the experimental design for cellular treatments.* The timeline diagram illustrates the sequence of interventions: cells were first seeded (Day 1), followed by initiation of treatments 24 hours later (Day 2). For Dox-treated populations, a 24-hour Dox exposure was followed by 5 days (Days 3 to 8) in drug-free media to allow senescence development. NIR light treatment consisted of daily 20-minute exposures for 6 consecutive days (Days 2-7). Cells receiving both treatments underwent concurrent Dox and NIR light exposure protocols. Analysis was performed on Day 7, allowing full development of the senescent phenotype while maintaining consistent timing across all treatment conditions. (Image created with biorender.com)

2.21 Statistical analysis

For each experiment, data from a minimum of three biological repeats (N=3) under the same exposure conditions were averaged with the determination of standard deviation (SD) and standard error of the mean (SEM). For each MTT experiment, the data from a minimum of 3 technical repeats at each treatment were averaged with the determination of SD and SEM. Statistical analyses were performed with GraphPad Prism (United States) version 10.0.2. Results are expressed as the mean ± SEM. All data sets were tested for significant outliers (Alpha=0.05) via Grubbs' test– if outliers were detected, they were excluded from the analysis.

For comparison between two groups (control and senescent populations; isolated mitochondria and buffer), statistical analysis was performed using the non-parametric Mann-Whitney U test when appropriate. For comparisons with N=3 biological repeats, a two-tailed unpaired t-test was applied. For multiple group comparisons, one-way ANOVA with post hoc Bonferroni testing was performed.

The effect of NIR light treatment in control and senescent populations in senescence induction (CellEvent fluorescent assay); ROS levels (DCFDA fluorescent assay); mitochondrial membrane potential (TMRE fluorescence assay), intracellular Ca^{2+} levels (Fluo-4 fluorescent assay) mitochondrial Ca^{2+} levels (Rhod-2 fluorescent assay) were compared with a mixed-model two-way ANOVA, with *post hoc* Bonferroni testing.

Differences in the mitochondrial oxygen consumption rate between pre- and post-injection of antimycin were analysed using a linear model using the 'lm' function in the R statistical software (version 4.3.2) (R Core Team, 2021). The model included the predictors “time”, “state” (pre or post-injection), and “time_since”, representing the time elapsed since treatment. The formula used for the model was “value ~ time + state + time_since”, where “value” means the observed outcome variable.

Differences in the rate of oxygen consumption between mitochondria from shielded and unshielded cuvettes were analysed using a linear mixed-effects model using the “lme” function from the “nlme” package (Pinheiro J et al., 2020) in the R statistical software (version 4.3.2) (R Core Team, 2021). The analysis was restricted to data collected post-injection (“ state == 'post' “) and included the predictors “time” and “shielded”, as well as their interaction term “time * shielded”. The random effect’s structure incorporated random intercepts for each “run” nested within “time”, accounting for repeated measures within each run.

For the ultra-sensitive light detector analysis, the mean recorded photons per 10 seconds were processed in R (version 4.3.2) (R Core Team, 2021). For visualisation purposes, a 1000 point rolling mean was calculated over the dataset to reduce noise and highlight underlying trends. A scatter plot was created with the smoothed data (rolling means). The mean emission per 10 seconds was calculated by averaging the recording counts per 10 seconds of each sample minus the background dark count rate, measured to be an average of 160 counts per 10 seconds.

Plotted graphs were constructed in GraphPad Prism, and schematic diagrams and digital figures were generated via Microsoft PowerPoint (Microsoft 365, Washington – USA) or BioRender (BioRender, Toronto – Canada). A P value of less than 0.05 was used as the criteria for statistical tests were statistically significant. This is represented graphically as follows: * $P \leq 0.05$, ** $P \leq 0.01$, *** $P \leq 0.001$, **** $P \leq 0.0001$.

Chapter 3 : Senescence Induction

3.1: Aims

Senescence, as a complex cellular process, requires specific approaches for detection and induction due to its multifaceted nature (Campisi, 2013). This chapter investigates three distinct chemical inducers of senescence across five diverse cell lines, including cancerous and non-cancerous models. Since senescent cells exhibit a spectrum of cellular changes, including SA β-gal activity, cellular proliferation, cell cycle distribution, intracellular Ca^{2+} levels and morphology, these indicators were assessed in the senescent models to validate senescence induction. The overall aim of this chapter was to determine which cell lines, and methods of both inducing and detecting senescence would provide the most robust and reproducible model for the subsequent experimental work in chapters 5 and 6.

3.2: Results

3.2.1 Dox-induced senescence optimisation

Four cell lines were treated with doses of Dox to induce cellular premature senescent populations. Figures 3.1 to 3.5 describe the different Dox treatments in the MCF10A breast cell line (Figure 3.1), MCF7 breast cancer cell line (Figure 3.2), IMR-90 lung fibroblasts (Figure 3.3), A549 lung cancer cell line (Figure 3.4) and AG01972 progeria fibroblasts (Figure 3.5).

MCF10A breast cells: Following Dox treatment (0.25 μM for 24 hours and then 6 days in Dox-free media) the level of senescence in MCF10A breast cells, increased by 90.56% ± 10.17 ($P < 0.0001$; Figure 3.1) compared to vehicle control. While 24 hours of Dox treatment at a higher dose (0.5 μM) resulted in a mean increase in the level of senescence of 73.69% ± 14.38 ($P = 0.0003$) compared with the vehicle control. Interestingly, a shorter treatment of 3 hours using 0.5 μM Dox treatment increased the senescent population by 63.08% ± 14.38 ($P = 0.0015$) in MCF10A cells, compared to vehicle controls. There were no significant differences between Dox dosages or exposure times (24 or 3 hours).

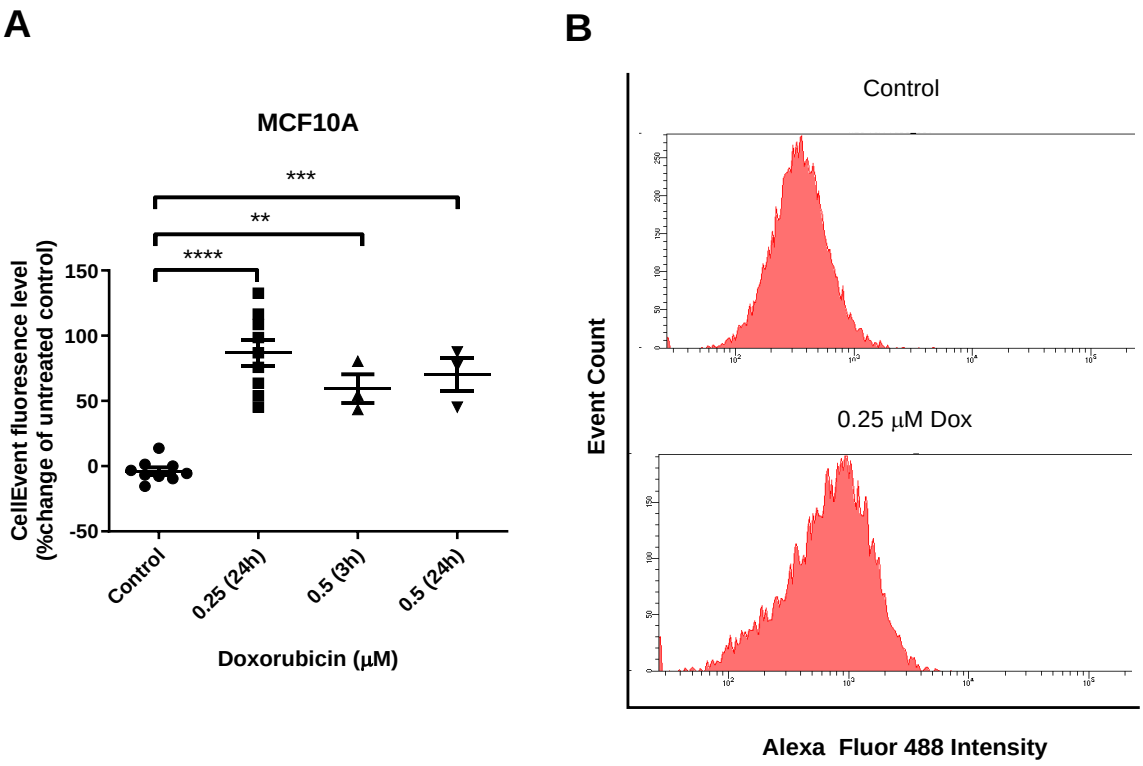

Figure 3.1: *The effect of Dox on MCF10A senescence induction – Flow cytometry.* (A) MCF10A breast cells were treated with 0.25 and 0.5 µM Dox for 24 hours, or with 0.5 µM Dox for 3 hours, followed by 6 days in drug-free media. Senescent levels were quantified with CellEvent fluorescence intensity and expressed as a percentage change from untreated control (N=9 independent biological repeats). Statistical significance was determined using one-way ANOVA with post-hoc Bonferroni testing. (B) Representative histograms showing univariate plot intensity of Alexa Fluor-488 against event count in flow cytometry, demonstrating the distribution of senescent cells across different treatment conditions. Data are presented as mean changes compared to an untreated control ± SEM. ** : $P \leq 0.01$, *** : $P \leq 0.001$ **** : $P \leq 0.0001$.

MCF7 breast cancer cells: Following Dox treatment (0.25 μM for 24 hours and then 6 days in Dox-free media), the level of senescence in MCF7 breast cancer cells increased by 51.07% ± 7.74 ($P < 0.0001$; Figure 3.2) compared to vehicle control. 24 hours of treatment with 0.5 μM Dox resulted in a mean increase in senescence of 55.63% ± 10.61 ($P = 0.0003$) compared to the vehicle control. Additionally, 3 hours of 0.5 μM Dox treatment increased the senescent population by 37.94% ± 10.61 ($P = 0.0100$) in MCF7 cells, compared to vehicle controls. There were no significant differences between Dox dosages or exposure times (24 or 3 hours).

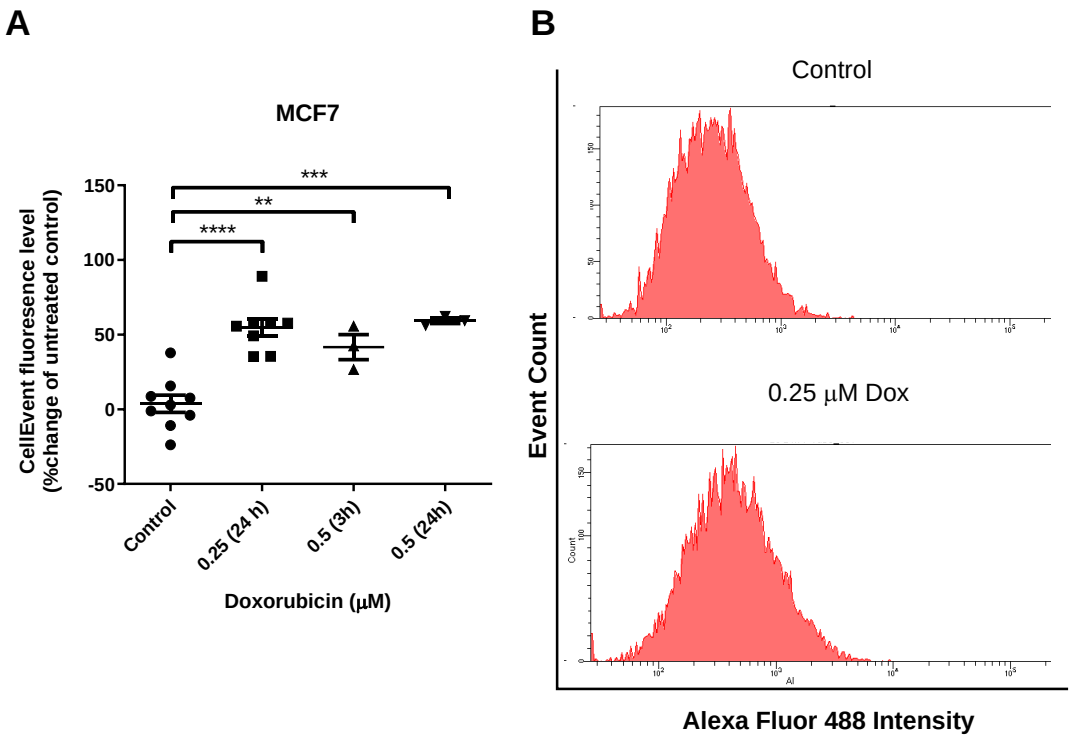

Figure 3.2: The effect of Dox on MCF7 senescence induction – Flow cytometry. (A) MCF7 breast cancer cells were treated with 0.25 and 0.5 µM Dox for 24 hours, or with 0.5 µM Dox for 3 hours, followed by 6 days in drug-free media. Senescent levels were quantified with CellEvent fluorescence intensity and expressed as a percentage change from untreated control (N=8 independent biological repeats). Statistical significance was determined using one-way ANOVA with post-hoc Bonferroni testing. (B) Representative histograms showing univariate plot intensity of Alexa Fluor-488 against event count in flow cytometry, demonstrating the distribution of senescent cells across different treatment conditions. Data are presented as mean changes compared to an untreated control ± SEM. ** : $P \leq 0.01$, *** : $P \leq 0.001$, **** : $P \leq 0.0001$.

IMR-90 lung fibroblasts: Following Dox treatment (0.25 μM for 24 hours and then 6 days in Dox-free media), the level of senescence in IMR-90 lung fibroblasts increased by 50.44% ± 9.93 (P = 0.0006; Figure 3.3) compared to vehicle control. 24 hours of treatment with 0.1 μM Dox resulted in a mean increase in senescence of 37.39% ± 10.63 (P = 0.0098) compared to the vehicle control. There was no significant difference among the different Dox dosages.

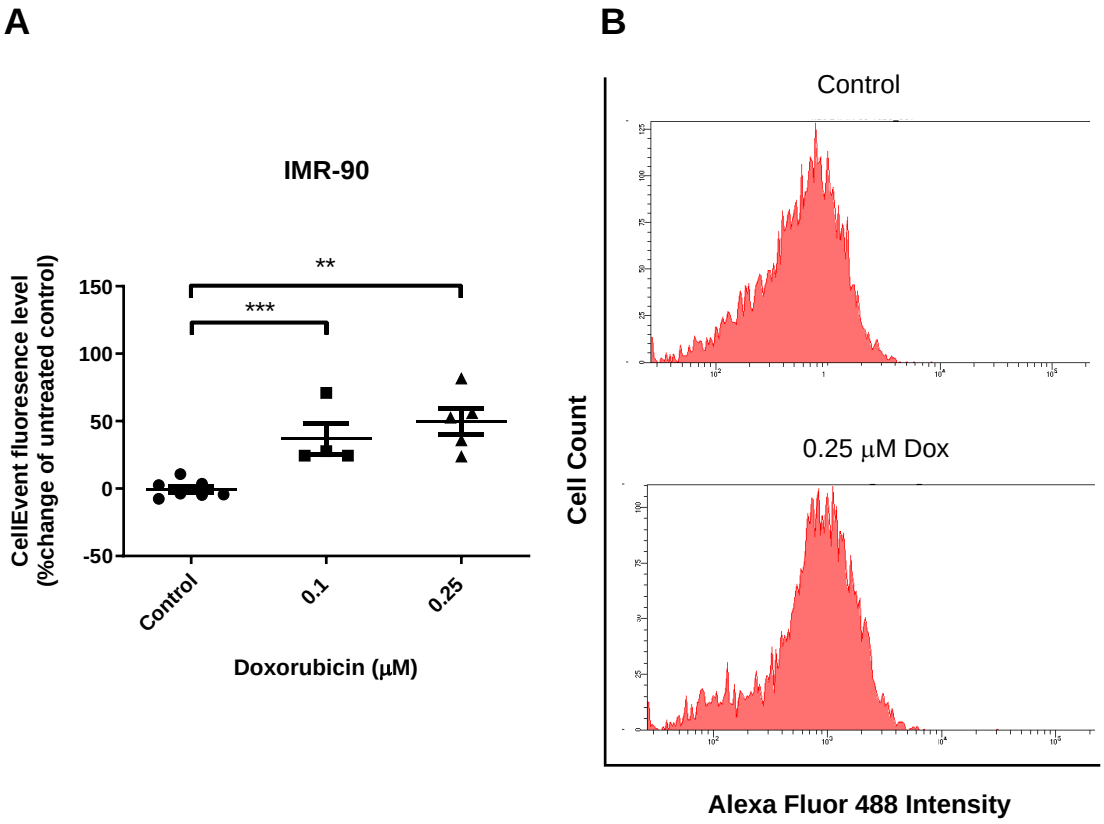

Figure 3.3: The effect of Dox on IMR-90 senescence induction – Flow cytometry. (A) IMR-90 lung fibroblasts were treated with 0.1 and 0.25 µM Dox for 24 hours, followed by 6 days in drug-free media. Senescent levels were quantified with CellEvent fluorescence intensity and expressed as a percentage change from untreated control (N=5 independent biological repeats). Statistical significance was determined using one-way ANOVA with post-hoc Bonferroni testing. (B) Representative histograms showing univariate plot intensity of Alexa Fluor-488 against event count in flow cytometry, demonstrating the distribution of senescent cells across different treatment conditions. Data are presented as mean changes compared to an untreated control ± SEM. ** : $P \leq 0.01$, *** : $P \leq 0.001$.

A549 lung cancer cells: Following Dox treatment (0.25 µM for 24 hours and then 6 days in Dox-free media), the level of senescence in A549 lung cancer cells increased by 244.20% ± 30.00 (P < 0.0001; Figure 3.4) compared to vehicle control.

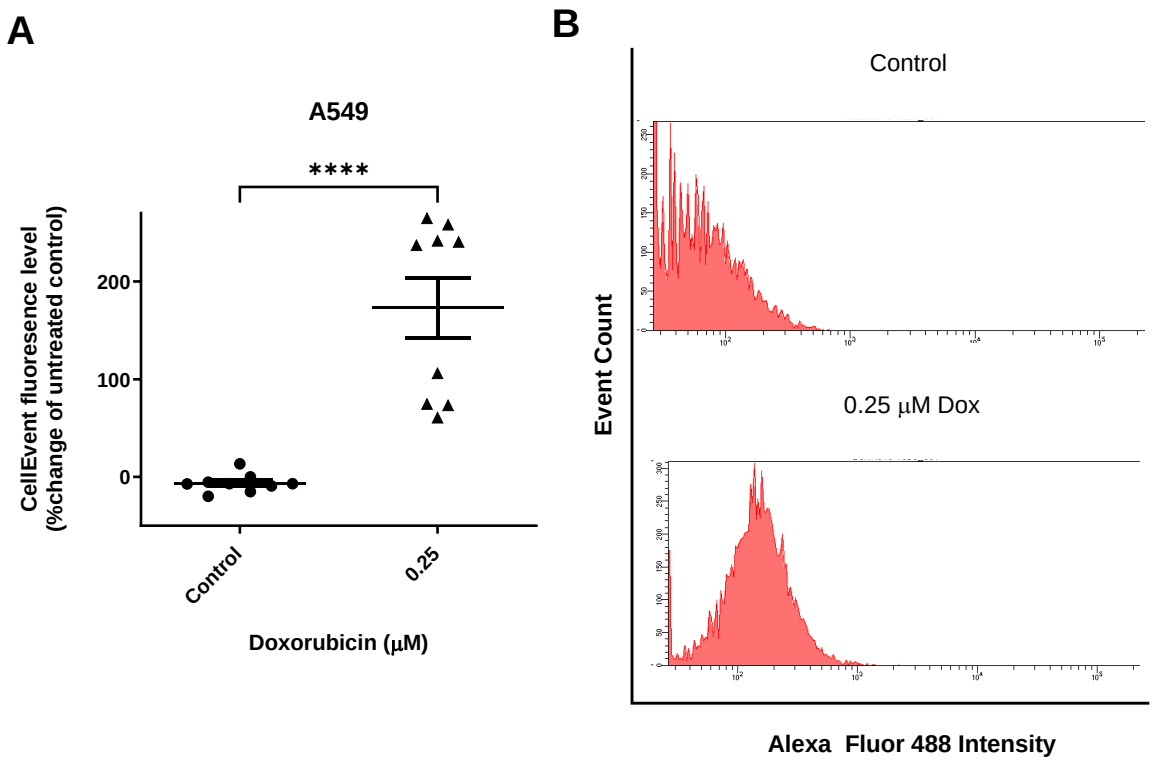

Figure 3.4: The effect of Dox on A549 senescence induction – Flow cytometry. (A) A549 lung cancer cells were treated with 0.25 µM Dox for 24 hours, followed by 6 days in drug-free media. Senescent levels were quantified with CellEvent fluorescence intensity and expressed as a percentage change from untreated control (N=9 independent biological repeats). Statistical significance was determined using Mann-Whitney U test. (B) Representative histograms showing univariate plot intensity of Alexa Fluor-488 against event count in flow cytometry, demonstrating the distribution of senescent cells across different treatment conditions. Data are presented as mean changes compared to an untreated control ± SEM. **** : P < 0.0001.

AG01972 progeria fibroblasts: Dox treatment had no effect on the induction cellular senescence in AG01972 progeria fibroblasts ($P > 0.05$ at 0.25 µM and 0.5 µM Dox concentrations; Figure 3.5). Furthermore, neither the 24 or 48-hour treatment of 0.25 µM Dox nor the three or 24-hour treatment of 0.5 µM Dox significantly induced senescence in the AG01972 cell line.

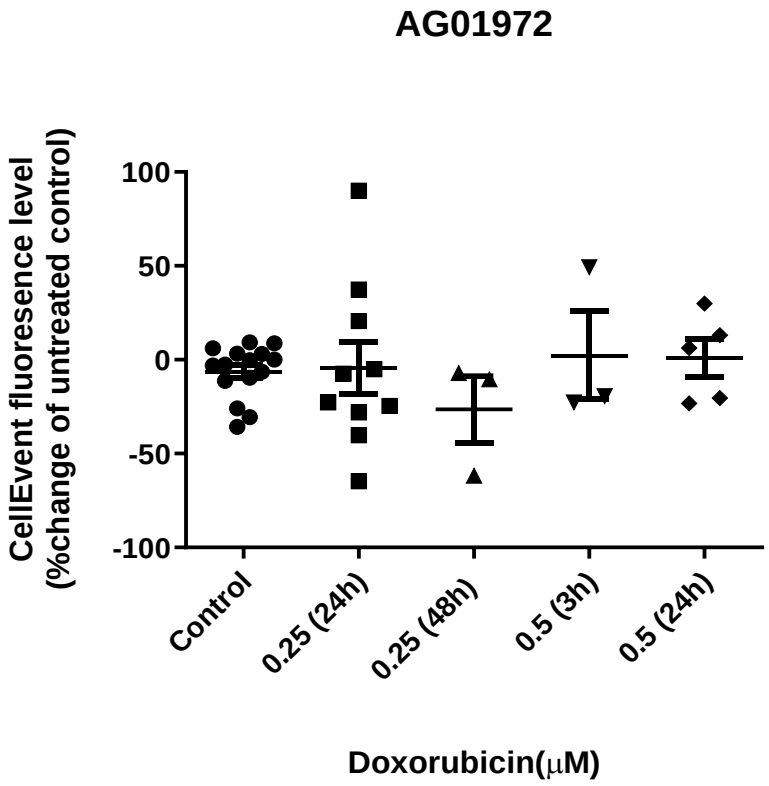

Figure 3.5: The effect of Dox on AG01972 senescence induction – Flow cytometry. AG01972 progeria fibroblasts were treated with 0.25 µM Dox for 24 and 48 hours or with 0.5 µM Dox for 3 and 24 hours, followed by 6 days in drug-free media. Senescent levels were quantified with CellEvent fluorescence intensity and expressed as a percentage change from untreated control (N=10 independent biological repeats). Statistical significance was determined using one-way ANOVA with post-hoc Bonferroni testing. Data are presented as mean changes compared to an untreated control ± SEM, and no significance was detected.

3.2.2 Examination of other chemical senescence inducers

Additional chemical inducers were also explored while testing for Dox-induced senescence. Published data reported H_2O_2- (Zhong et al., 2019) and palbociclib-induced (Jost et al., 2021) senescence in MCF7 cells. Therefore, the breast cancer MCF7 cell line was treated with these two chemical candidates to induce premature senescence, in parallel with Dox (Section 3.2.1). The data shown in Figure 3.6 indicates that H_2O_2 and palbociclib did not increase senescence. In more detail, seven days after 24 hours of 100, 300 and 500 μM H_2O_2 treatment, the cell population was not significantly more senescent ($P = 0.7800$). Similarly, 72 hours of 10 μM palbociclib treatment did not significantly induce a senescent population ($P = 0.6700$).

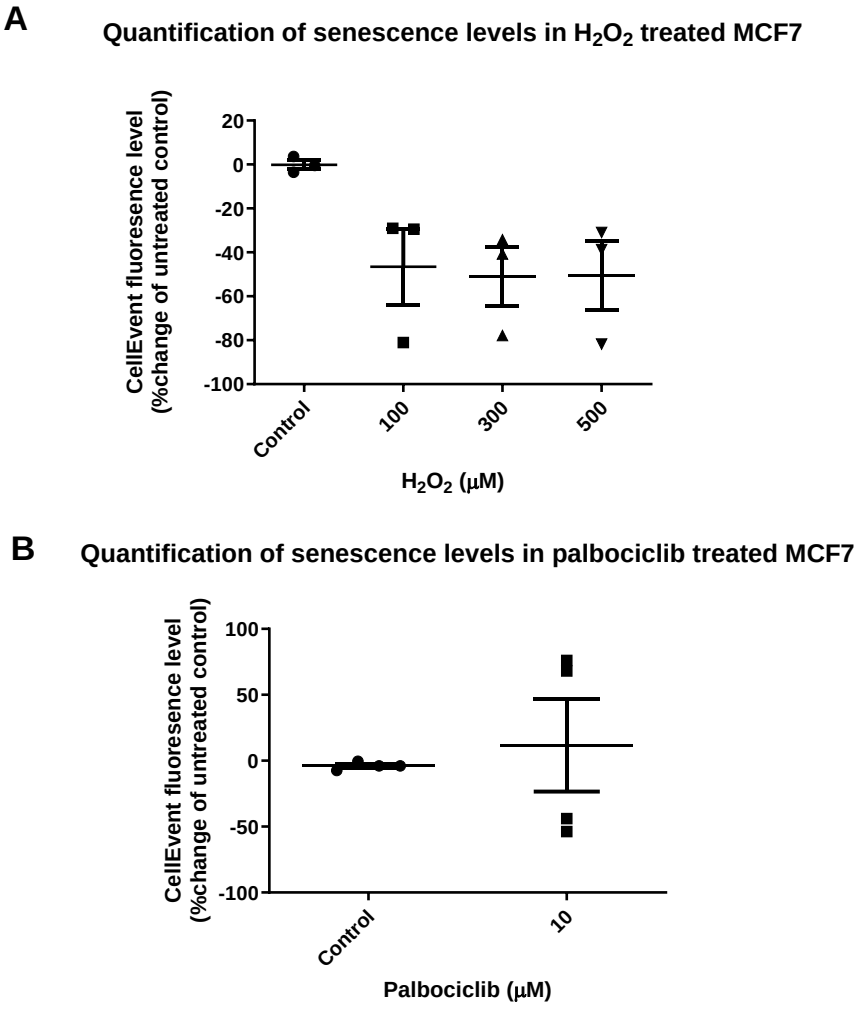

Figure 3.6: The effect of drug senescence inducers in MCF7 cells – Flow cytometry. (A) MCF7 breast cancer cells were treated with 100, 300 and 500 μM H_2O_2 for 24 hours (N=3 independent biological repeats), followed by 6 days in drug-free media. Senescent levels were quantified with CellEvent fluorescence intensity and expressed as a percentage change from untreated control. Statistical significance was determined using one-way ANOVA with post-hoc Bonferroni testing. (B) MCF7 cells were treated with 10 μM palbociclib for 72 hours (N=4 independent biological repeats), followed by 6 days in drug-free media. Senescent levels were quantified with CellEvent fluorescence intensity and expressed as a percentage change from untreated control. Statistical significance was determined using Mann-Whitney U test. Data are presented as mean changes compared to an untreated control ± SEM, and no significance was detected.

3.2.3 Cell Viability in Response to Dox treatment

The MTT assay was employed to examine the impact of various Dox concentrations on cell viability. In MCF10A breast cells, which in this thesis is the main senescent cellular model, exposure to doses ranging from 0.05 to 1.0 μM of Dox for 24 hours had no significant effect on cellular viability ($P > 0.05$ for all concentrations; Figure 3.7).

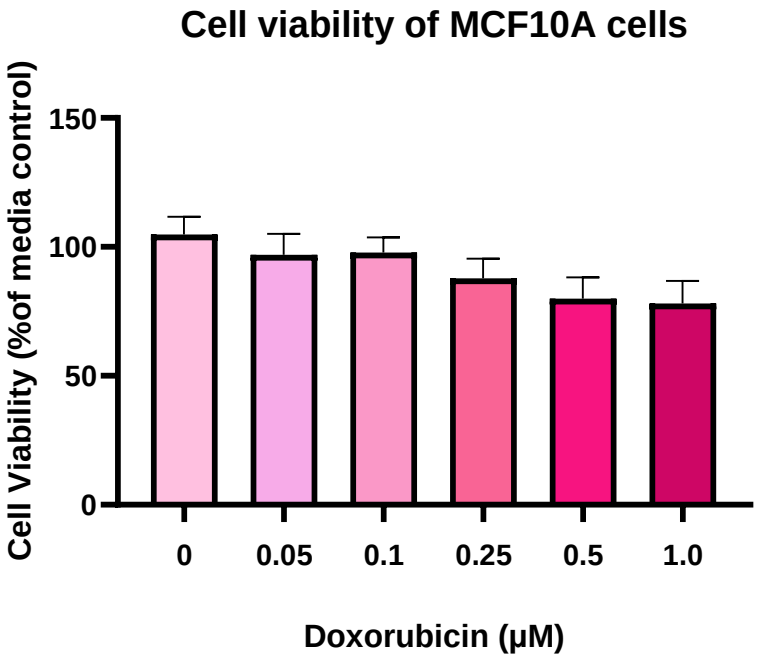

Figure 3.7: The effect of Dox on MCF10A cell viability. MCF10A breast cells were exposed to increasing Dox concentrations (0.05, 0.1, 0.25, 0.5, 1.0 μM) and one drug-free control (0 μM) for 24 hours, followed by MTT assay measurement of cell viability (N=3 independent biological repeats). Statistical significance was determined using one-way ANOVA with post-hoc Bonferroni testing. Data are presented as mean changes compared to an untreated control ± SEM, and no significance was detected.

3.2.4 Cellular characteristics of Dox-induced senescent cells

Once Dox-senescence induction was established, the cellular and molecular characteristics of the senescent cells were examined. Figures 3.8 and 3.9 describe the changes in cell count (Figure 3.8) and cell cycle (Figure 3.9)

Six days after 24 hours of 0.25 μM Dox treatment, cell number decreased significantly in all cell lines: MCF10A breast 297,700 ± 34,480 (83.62% decrease, P = 0.0003), MCF7 breast cancer 217,300 ± 42,010 (75.56% decrease, P = 0.0050), and A549 lung cancer 595,600 ± 89,600 (74.10% decrease, P = 0.0014) (Figure 3.8).

The cell cycle of MCF10A breast cells was further analysed to assess senescent proliferation arrest. During Dox-induced senescence, the percentage of cells in the G1 (P = 0.0094) and S (P = 0.0116) phases were decreased by 9.19% ± 2.37 and 2.48% ± 0.66, respectively. In contrast, the percentage of senescent MCF10A cells in the G2 phase (P = 0.0059) was higher than the non-senescent control cells by 11.68% ± 2.78 (Figure 3.9).

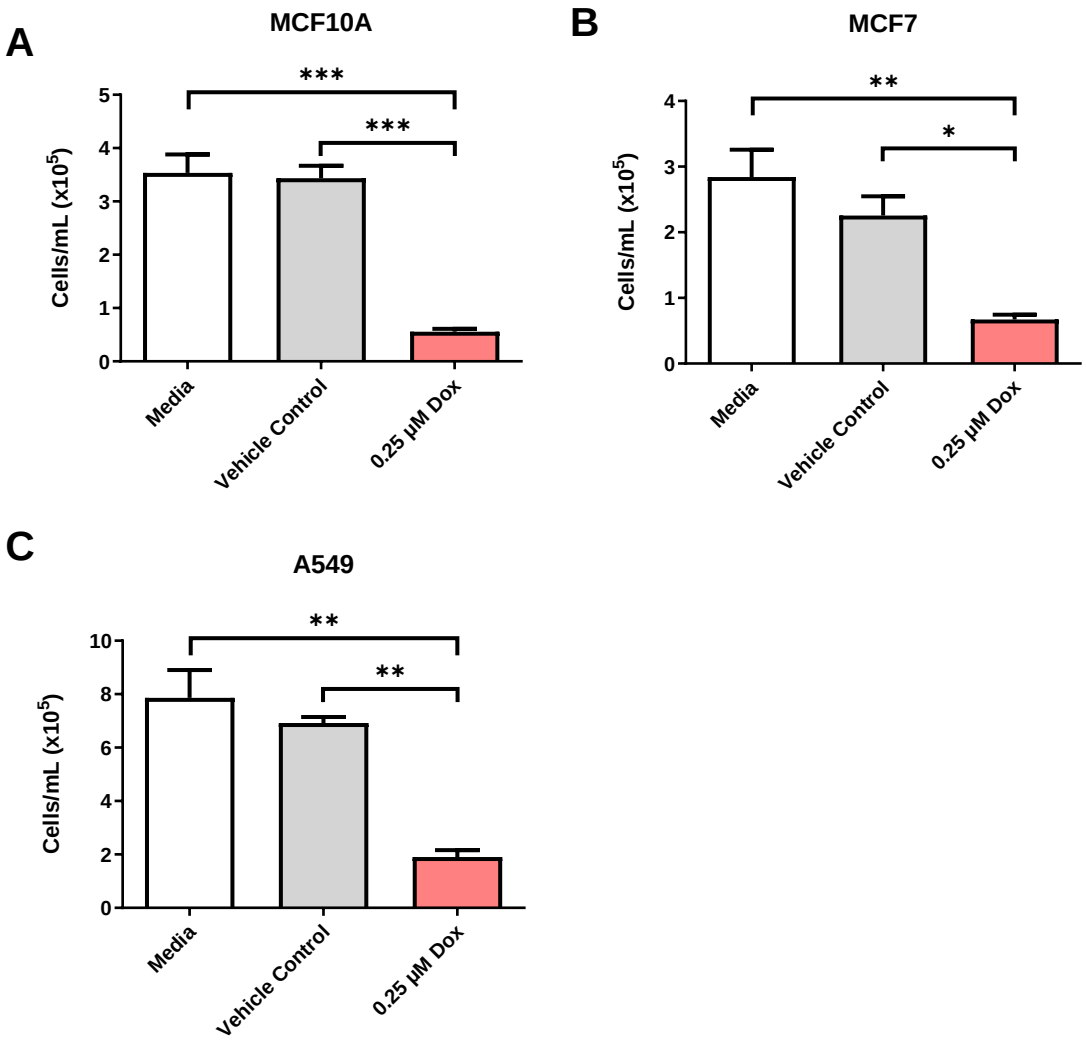

Figure 3.8: Cell count post-senescence induction. MCF10A breast (A), MCF7 cancer (B), and A549 lung cancer (C) cells were treated with media alone, H_2O vehicle control, or 0.25 µM Dox for 24 hours, followed by 6 days in drug-free media. Cell counts were performed using a Countess 2 automated cell counter (N=3 independent biological repeats for each cell line). Statistical significance was determined using one-way ANOVA with post-hoc Bonferroni testing. Data are presented as average counts ± SEM. * : P ≤ 0.05, ** : P ≤ 0.01, *** : P ≤ 0.001.

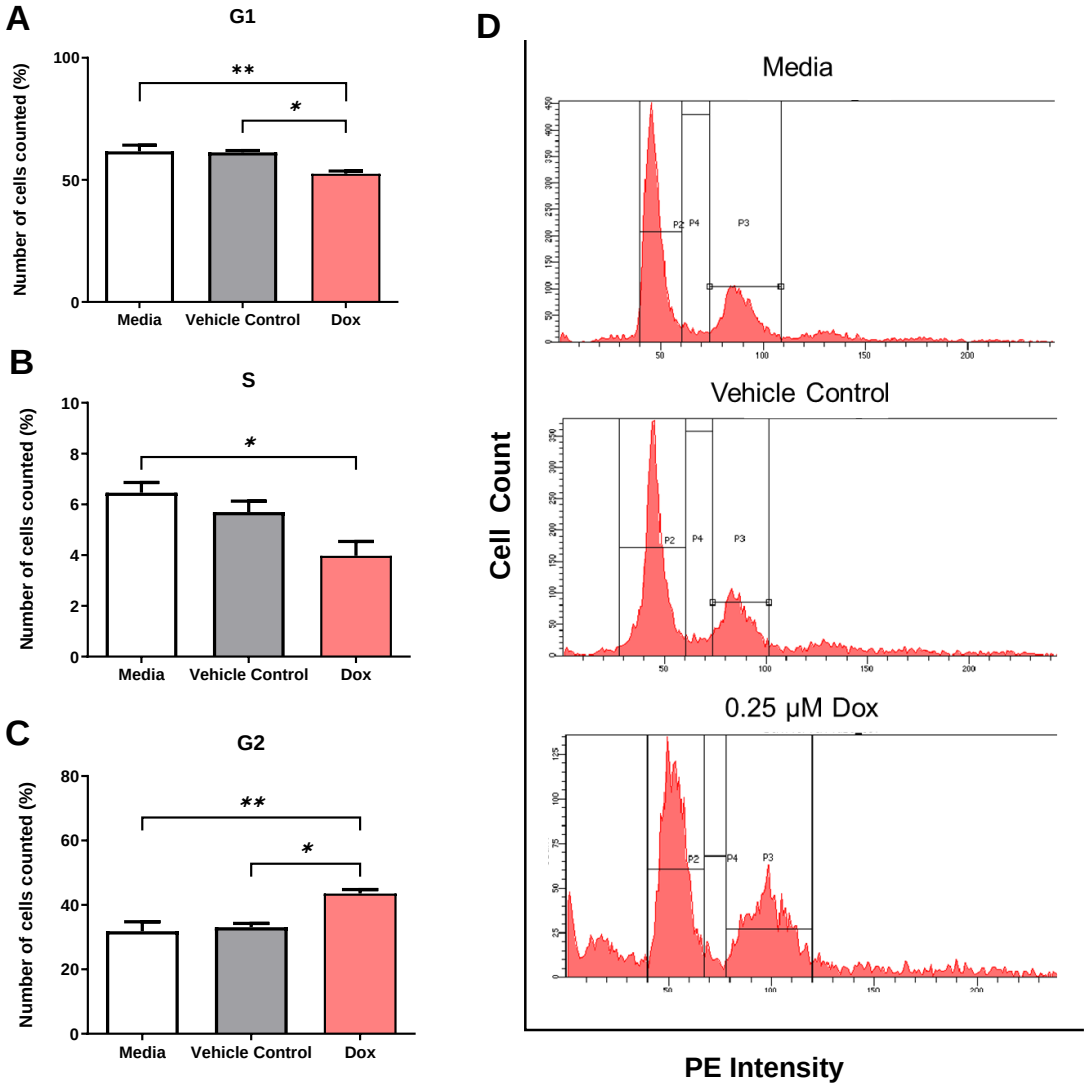

Figure 3.9: Cell cycle analysis post-senescence induction. MCF10A breast cells were treated with Media alone, H_2O vehicle control, or 0.25 µM Dox for 24 hours, followed by 6 days in drug-free media. Cell cycle was aanalysed using propidium iodide staining and flow cytometry (N=3 independent biological repeats). The percentage of cells in (A) G1, (B) S, and (C) G2 phases was determined. Statistical significance was determined using one-way ANOVA with post-hoc Bonferroni testing. (D) Representative histograms showing univariate plot intensity of PE gate against event count in flow cytometry, demonstrating the distribution of cells across different cell cycle phases. Data are presented as percentages of the total number of cells ± SEM. * : $P \leq 0.05$, ** : $P \leq 0.01$.

3.2.5 β-galactosidase activity of Dox-induced senescent cells

To further characterize the senescent phenotype in Dox-treated cells, I assessed β-galactosidase (β-gal) activity using senescence-associated β-gal (SA β-gal) staining. This widely accepted biomarker has been extensively used in senescence research due to its reliability in identifying senescent cells (Dimri et al., 1995; Debacq-Chainiaux et al., 2009). Cells were stained with X-gal, and the presence of blue-stained cells was quantified to indicate senescence. A statistically significant increase of senescent, blue-stained cells was observed in Dox-treated populations of MCF10A (56% ± 4.50; $P = 0.0002$), MCF7 (70% ± 1.40; $P < 0.0001$) and A549 (64% ± 3.50; $P < 0.0001$) in comparison to control populations (Figures 3.10 and 3.11). Furthermore, the morphology of Dox-treated populations was altered, with enlarged and swollen cells.

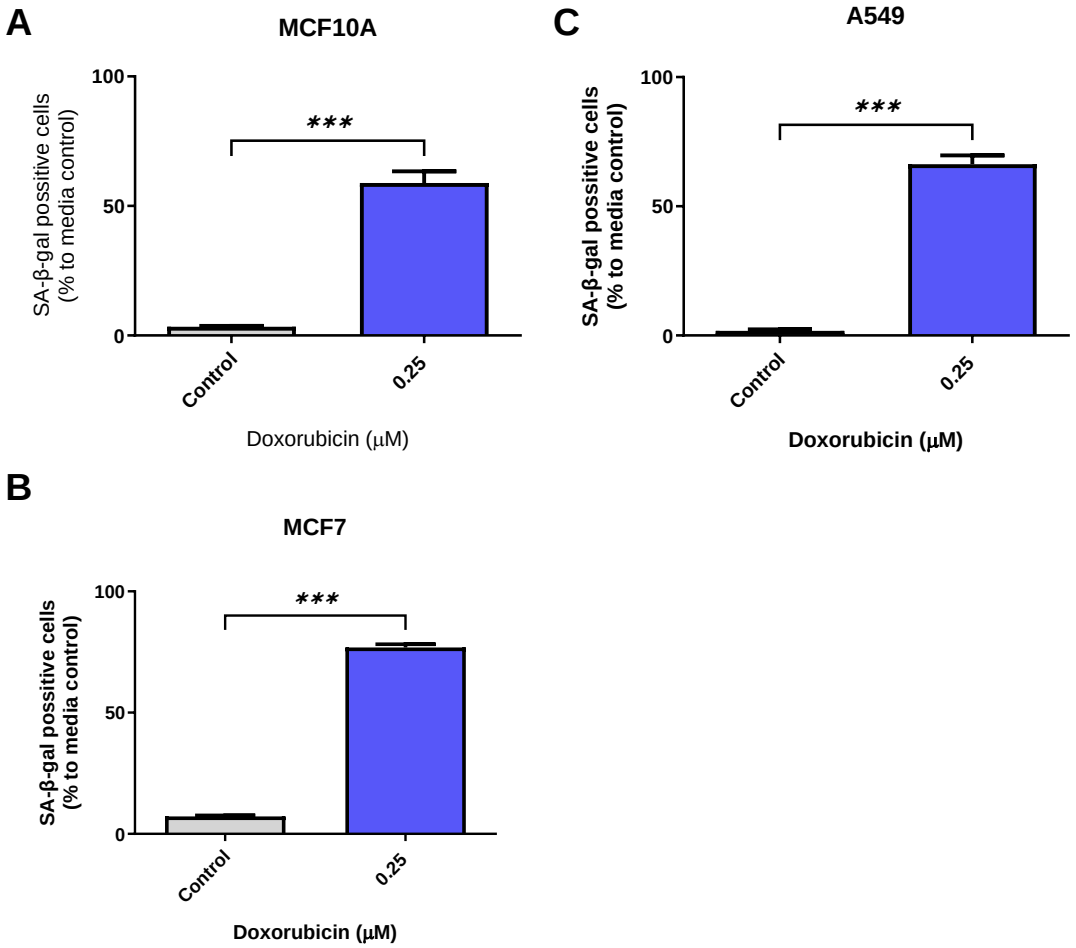

Figure 3.10: Detection of positively stained cells for SA β-gal activity. MCF10A breast (A), MCF7 breast cancer (B), and A549 lung cancer (C) cells were treated with media alone, H_2O vehicle control, or 0.25 μM Dox for 24 hours, followed by 6 days in drug-free media. Cells were stained with X-gal solution at pH 6.0, and positively stained cells were counted and expressed as percentage change from untreated control (N=3 independent biological repeats for each cell line). Statistical significance was determined using an unpaired two-tailed t-test. Data are presented as mean changes compared to an untreated control ± SEM. *** : $P \leq 0.001$.

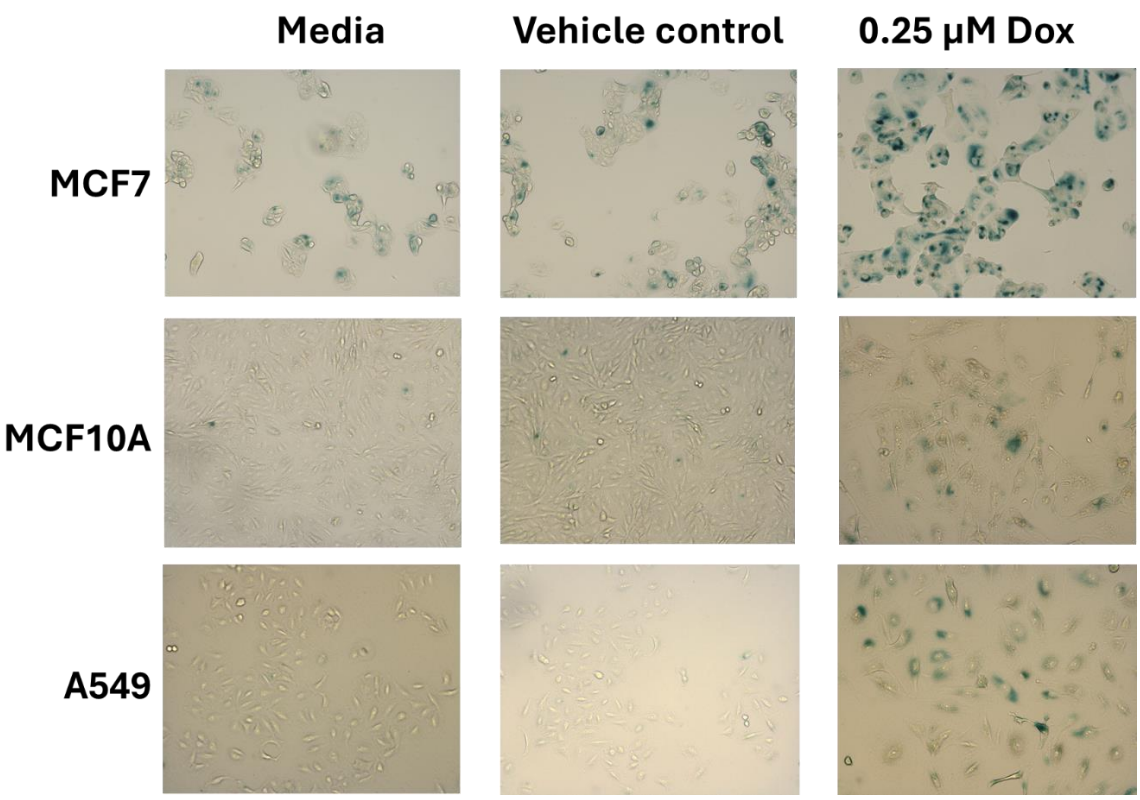

Figure 3.11: Microscopic imaging of SA β-gal activity in stained cells. MCF7 breast cancer, MCF10A breast and A549 lung cancer cells were treated with media alone, H_2O vehicle control, or 0.25 µM Dox for 24 hours, followed by 6 days in drug-free media. Cells were stained with X-gal solution at pH 6.0 for detection of SA β-gal activity and imaged using the EVOS FL2 fluorescent microscope with the EVOS 20X, fluorite, LWD, 0.45NA/6.23WD objective (microscopic images were acquired on day 8 post-seeding). Representative images show adherent cells with characteristic senescent features in Dox-treated populations: positive blue X-gal staining, enlarged and flattened morphology, and reduced cell density compared to control conditions. Scale bar: 100 µm.

3.2.6 Assessment of intracellular Ca^{2+} levels of Dox-induced senescent cells

Given literature reports of increased intracellular Ca^{2+} concentrations in senescent cells (Martin et al., 2018), total intracellular Ca^{2+} levels were measured as an additional senescence marker. Ca^{2+} levels were quantified in MCF10A breast and MCF7 breast cancer cells. The results showed a significant increase in both cell lines' Ca^{2+} levels after 0.25 μM Dox treatment for 24 hours and six days of culture with Dox-free media. Senescent MCF10A cells increased Ca^{2+} by 117.80% ± 13.05 (P = 0.079; Figure 3.12) and senescent MCF7 cells by 94.74% ± 17.44 (P = 0.0002; Figure 3.13).

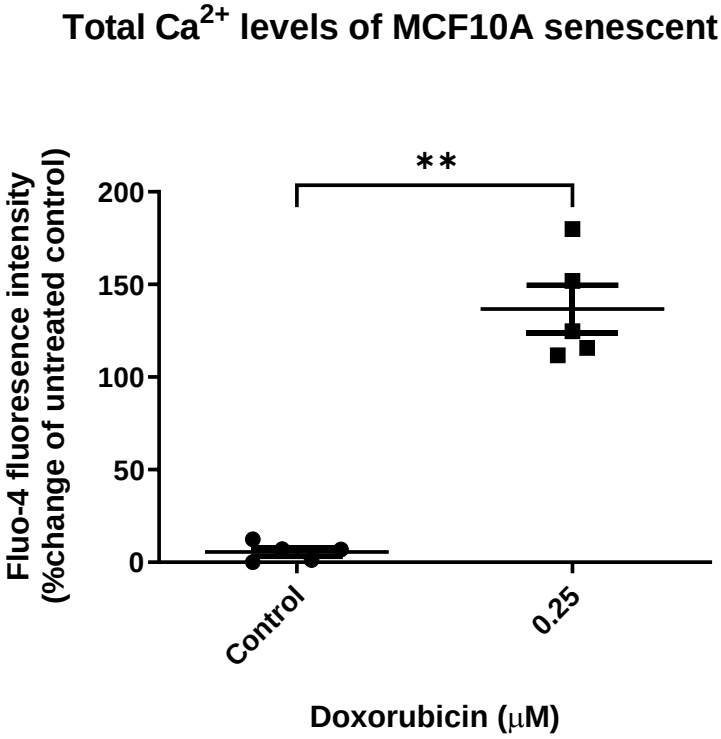

Figure 3.12: The effect of senescence in MCF10A total Ca^{2+} levels – Flow cytometry. MCF10A breast cells were treated with 0.25 μM Dox for 24 hours, followed by 6 days in drug-free media. Media (untreated) and vehicle (H_2O) control were included for comparison. Total intracellular Ca^{2+} levels were quantified by flow cytometry in live cells stained with Fluo-4 fluorescent dye and expressed as a percentage change from untreated control (N=5 independent biological repeats). Statistical significance was determined using Mann-Whitney U test. Data are presented as mean changes compared to an untreated control ± SEM. ** : $P \leq 0.01$.

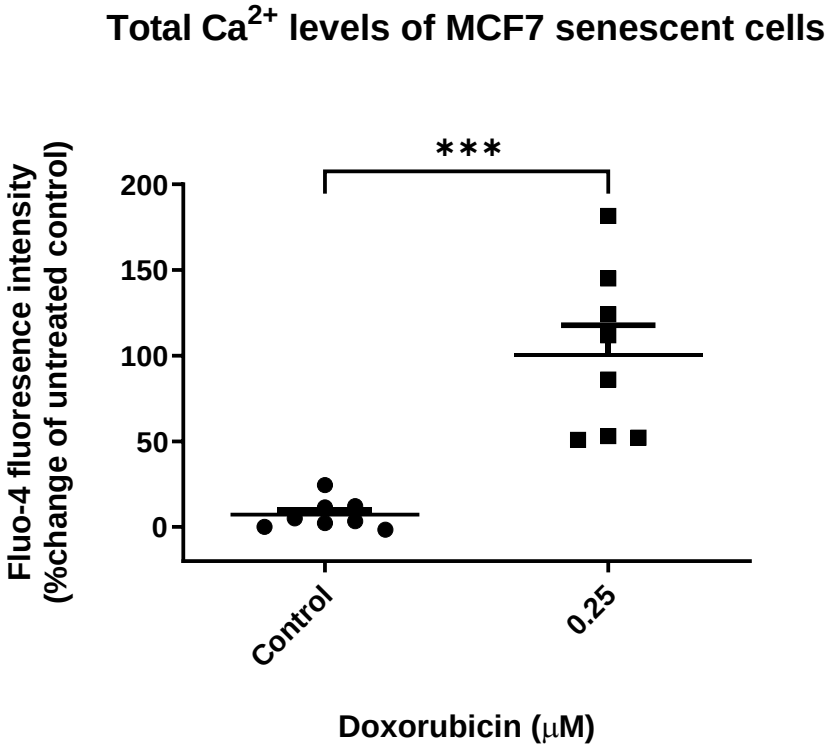

Figure 3.13: The effect of senescence in MCF7 total Ca^{2+} levels – Flow cytometry. MCF7 breast cancer cells were treated with 0.25 μM Dox for 24 hours, followed by 6 days in drug-free media. Media and vehicle (H_2O) controls were included for comparison. Total intracellular Ca^{2+} levels were quantified by flow cytometry in live cells and expressed as a percentage change from untreated control (N=8 independent biological repeats). Statistical significance was determined using Mann-Whitney U test. Data are presented as mean changes compared to an untreated control ± SEM. *** : P ≤ 0.0001.

3.3: Discussion

3.3.1 Dox treatment as senescence-induction protocol for three different senescent models.

In this chapter, the aim was to establish robust and reproducible senescence models across various cell lines for subsequent experimental work. Specifically, the objective was to determine the most effective method for inducing and detecting senescence in different non-cancer and cancer cell lines. Additionally, the chapter aimed to characterize the cellular and molecular features of the induced senescent cells to validate the models.

Senescence is a complex cellular phenomenon reflected in both its detection and induction, which require different tests and assays to establish whether a population is senescent (Campisi, 2013). Senececent phenotypes are dependent on cell type, and therefore the protocol for senescent induction may vary from cell line to cell line. Furthermore, cell lines may exhibit different senescence cell characteristics depending on the induction pathway (Sharpless and Sherr, 2015). This variability in senescence response presents a challenge when designing senescence induction protocols.

Three different chemical inducers of senescence were tested on five cell lines: MCF10A breast non-cancer, MCF7 breast cancer, A549 lung cancer, AG01972 progeria skin fibroblasts and IMR-90 lung fibroblasts. The senescence inducers Dox (Hernandez-Segura et al., 2018b; Hou et al., 2019; Jochems et al., 2021), H_2O_2 (Arnandis et al., 2018; Hernandez-Segura et al., 2018b; Zhong et al., 2019; Zhou et al., 2015) and palbociclib (Jost et al., 2021; Leite de Oliveira & Bernards, 2018) have been widely used for *in vitro* induction of senescence. Dox, a topoisomerase II inhibitor, and palbociclib, a selective CDK4/6 inhibitor, are both anti-cancer chemical agents which activate DDR, leading to permanent cell cycle arrest (Nitiss, 2009; Wang et al., 2021), while H_2O_2 leads to oxidative stress-induced premature senescence (Chen et al., 2007). Previous studies of cancer cellular models, such as MCF7 and A549, have utilised Dox (Bojko et al., 2019; Jochems et al.,

2021; Srdic-Rajic et al., 2017), H_2O_2 (Zhong et al., 2019) and palbociclib (Leite de Oliveira & Bernards, 2018) to induce senescence.

Among the three chemical inducers tested, only exposure to Dox induced senescence in breast and lung cancer cells, breast non-cancer cells, and lung fibroblasts without reducing the cell viability 24 hours after exposure (Figure 3.7). Dox is one of the most common senescent inducers in chemotherapies against cancers and is also used as a positive control for senescence *in vitro* studies (Milczarek, 2020). Based on these results, Dox treatment was selected as the primary method for inducing senescence in this research, based on its consistent effectiveness and the clear senescent phenotype it produced (Figures 3.1, 3.2, 3.3 and 3.4).

MCF10A non-cancer breast cells were chosen as the primary senescent model for several reasons. Firstly, as a non-cancer cell line, it provides a more appropriate model for studying general senescence mechanisms compared to cancer cell lines. Secondly, it has a clear cancer cell analogue (MCF7), allowing for comparative studies. Additionally, MCF10A cells showed a more pronounced senescent response to Dox treatment compared to the commonly used IMR-90 fibroblasts, making them a suitable model for my research objectives.

The complexity and heterogeneous state of senescence (Campisi, 2013; Sharpless & Sherr, 2015) and variability between cell lines may explain why chemicals reported to induce senescence in some cell lines in the literature did not significantly induce senescence in this study. Recent studies have shown that cancer cells can escape senescence, and some senescent cells can regain their proliferative capacity, including tumour cells induced by chemotherapy (Liao et al., 2020). This may explain why breast cancer MCF7 showed no senescence effect after treatment with commonly used senescence inducers, such as H_2O_2 and palbociclib. In addition, a study showed that in patient-derived glioma stem cell-enriched cell lines, palbociclib induced a senescent-like quiescence instead of true senescence, as evidenced by the cell lines resuming normal

proliferation after palbociclib removal, suggesting they maintained their replicative potential (Morris-Hanon et al., 2019), possibly explaining why palbociclib did not lead to a senescent MCF7 population. In contrast, a study on various chemotherapeutic senescence inducers describes Dox, along with irinotecan and methotrexate, as the most effective inducers of senescence in cancer cells (Bojko et al., 2019).

While progeria cell lines are widely considered a valuable model for studying ageing and senescence, there is limited literature investigating premature senescence induction in the progeria population (Ashapkin et al., 2019). The results provide new insights into this area, particularly regarding the response of progeria cells to Dox treatment. Based on my results, it appears that progeria cells may not be an ideal model for studying Dox-induced senescence. This unexpected finding raises important questions about the mechanisms of senescence induction in cells already predisposed to premature ageing. The distinct response of progeria cells to Dox compared to normal fibroblasts suggests that the underlying genetic mutation in LMNA and the resulting accumulation of progerin may alter cellular pathways involved in stress-induced senescence.

3.3.2 Senescence associated β-gal activity as senescence detection method

Flow cytometry analysis demonstrated positive staining results with a fluorescence dye for SA β-gal activity, a distinctive feature of senescence, in the four cell populations in which I established a reproducible senescence model. The SA β-gal activity detection method is widely used to confirm senescence induction (Dimri et al., 1995). It has been applied to test senescence induction caused by various stressors in multiple cell lines from diverse origins, both *in vivo* and *in vitro* (Debacq-Chainiaux et al., 2009). One advantage of the SA β-gal assay is its ability to distinguish senescence from quiescence, as only the former exhibits increased lysosomal content and β-gal enzymatic activity (Dimri et al., 1995). Senescent cells display an increase in both lysosome number and size, leading to an expansion of the lysosomal compartment and lysosome biogenesis (Hernandez-Segura et al., 2018a; Kurz

et al., 2000; Lee et al., 2006). Thus, the result indicates non-reversible proliferation arrest in cellular populations.

SA β-gal emerges as a robust detection technique for cellular senescence, often regarded as "simple and reproducible" in recent publications (Faragher, 2021). In this thesis, flow cytometry has been effectively employed for SA β-gal senescence detection, presenting the opportunity for flow sorting of viable senescent cells. Flow cytometry offers advantages over traditional colourimetric β-gal assays, such as enhanced sensitivity, automated quantitative analysis and avoidance of operator error (Faragher, 2021; Noppe et al., 2009). Although flow cytometry is the primary method to confirm senescence, a colourimetric assay was applied to three cell lines (Figures 3.10 and 3.11). The positively stained results were consistent with previous studies using Dox-induced senescent MCF10A (Hou et al., 2019), MCF7 (El-Far et al., 2020; Milczarek, 2020) and A549 (Fan et al., 2023; Jochems et al., 2021) cells, validating flow cytometry as an accurate test in this thesis. This integration of techniques highlights the reliability of the senescence detection method.

In conclusion, as senescence is a complex cellular phenomenon, an appropriate methodology for detection and induction is required. The results of this chapter describe that among the three chemical senescence inducers tested, only Dox was found to induce senescence in breast cancer, breast non-cancer, lung cancer cells, and lung fibroblasts. Additionally, the SA β-gal activity detection via flow cytometry confirmed senescence induction in all four cell populations, indicating non-reversible proliferation arrest. This method was employed to test senescent levels in the following chapters.

3.3.3 Cellular characteristics of senescent cells

Defining a senescent cell requires more than just a single marker. As Lee et al. (2006) noted, reliance solely on SA β-gal may present limitations, given its non-essential nature for senescence (Lee et al., 2006). Although senescent cells exhibit various characteristics,

these often depend on the induction method and cell origin (Sharpless & Sherr, 2015); one characteristic that all senescent populations exhibit is growth arrest (Campisi, 2013; Faragher, 2021). In this study, alongside SA β-gal detection, cellular proliferation was assessed through cell number quantification before and after Dox-senescence induction. The results revealed a significant decrease in cell number (Figure 3.8), confirming the proliferation arrest characteristic of senescent cells. This finding aligns with the approach suggested by Crowe et al. (2014), where simple cell counting serves as a reliable indicator of proliferation arrest. All four cell lines, MCF7, MCF10A, A549, and IMR-90, significantly decreased cell number, further confirming the observed senescent phenotype.

Senescence was induced in four cell lines, including the primary MCF10A breast cell model, using Dox, a DNA-damaging agent known to activate DDR pathways by inhibiting DNA topoisomerase II, as described in Section 1.5.2 (Nitiss, 2009). Consistent with previous findings by Srdic-Rajic et al. (2017) in MCF10A and MCF7 cell models, results demonstrate a significant alteration in the cell cycle phase distribution of MCF10A cells following Dox treatment (Srdic-Rajic et al., 2017). Flow cytometry analysis reveals an increased accumulation of cells in the G2 phase of the cell cycle (Figure 3.9), indicating that senescent cells blocked their proliferation in the G2 phase. This G2 cell cycle arrest aligns with the concept proposed by Afifi et al. (2023), supporting the senescent, irreversible, terminal cell fate (Afifi et al., 2023). The confirmation of G2 phase cell cycle arrest confirms the efficacy of Dox in inducing senescence in MCF10A cells and provides mechanistic insights into Dox-induced senescent models. Interestingly, this G2 phase arrest in Dox-induced senescence differs from the cell cycle arrest observed in replicative senescence. Bielak-Zmijewska et al. (2014) reported that while 32% of Dox-treated vascular smooth muscle cells were arrested in the G2/M phase, 73% of replicative senescent cells were arrested in the G1 phase (Bielak-Zmijewska et al., 2014). This distinction in cell cycle arrest patterns between drug-induced premature senescence and replicative senescence suggests that these two categories of senescence might have different physiological characteristics. It is important

to note that due to time limitations, I could not explore the full range of differences between drug-induced and replicative senescence. However, future studies would benefit from a more comprehensive investigation of these distinctions.

Another characteristic of senescent cells is their altered morphology, consistent with the observed SA β-gal staining results. As demonstrated in Figure 3.11, MCF10A, MCF7, and A549 cells demonstrate elongated and swollen morphology compared to their non-senescent control populations. Although size cannot be used as a senescence marker alone (Faragher, 2021), this altered morphology is characteristic in cells with increased SA β-gal activity, as previously described (Kurz et al., 2000). The enlarged cell mass reflects the increased lysosomal compartment and lysosome biogenesis in senescent cells (Hernandez-Segura et al., 2018a; Lee et al., 2006). These morphological changes provide further evidence of senescence induced by Dox treatment in MCF10A, MCF7, and A549 cell lines, reinforcing the findings from SA β-gal staining and highlighting the effectiveness of senescence induction in this thesis.

Finally, intracellular Ca^{2+} levels are increased due to senescence (Martin et al., 2023). My results show that Dox-induced senescent MCF10A (Figure 3.12) and MCF7 (Figure 3.13) cells exhibit increased intracellular Ca^{2+} levels. These results are consistent with recent publications highlighting the importance and involvement of increased Ca^{2+} levels in senescence (Martin et al., 2023; Martin & Bernard, 2018). Ca^{2+} signalling plays an essential role in the cell cycle, modulating various molecular processes, including gene expression, cell proliferation, and migration (Martin & Bernard, 2018), while senescent cells increase their intracellular Ca^{2+} levels in response to various senescence-inducing stresses (Martin et al., 2023). The increase in intracellular Ca^{2+} concentration in senescent cells can be attributed to Ca^{2+} influx through plasma membrane channels and Ca^{2+} release from intracellular stores such as endoplasmic reticulum or mitochondria (Martin et al., 2023).

Moreover, the rise in intracellular Ca^{2+} concentration has been linked to regulating crucial senescence effector pathways (Martin et al., 2023). For example, elevated intracellular Ca^{2+}

levels trigger cellular senescence by contributing to DNA damage response activation and p53/p21/RB pathway activation (Borodkina et al., 2016), which also control the senescence activation pathways, as described in Section 1.6.3. Additionally, the Ca^{2+}-binding protein calbindin 1 is upregulated as a response to senescence-inducing stresses, and its overexpression has been found to reduce the increase in intracellular Ca^{2+} levels and prevent senescence in cancer cells (Raynard et al., 2022). And importantly, Ca^{2+} regulates the SASP by controlling the processing of interleukin 1 alpha (IL1α), an important positive regulator of SASP (McCarthy et al., 2013).

Interestingly, it has been suggested that there is a shift in the sensitivity to intracellular Ca^{2+} levels with ageing, as Martin et al. exhibited increased responses to intracellular Ca^{2+} stimulation despite decreased receptor expression in senescent cells (Martin et al., 2023). Mijares et al., 2021, further support these findings by demonstrating an age-dependent increase in intracellular Ca^{2+} concentration in skeletal muscle during normal ageing (Mijares et al., 2021). Additionally, Witcher et al., 2021, reported increased intracellular Ca^{2+} signalling in senescent airway smooth muscle cells, suggesting a potential role in promoting fibrosis and altered cellular contractility associated with ageing (Wicher et al., 2021). These findings highlight that increased Ca^{2+} levels are essential for the senescent phenotype at a cellular level and contribute to why senescence is a hallmark of ageing at an organism level.

3.3.4 Conclusion

In conclusion, this chapter investigates the potential candidates for senescence induction in various non-cancerous and cancerous cell lines. Among the drugs tested, Dox was the most effective senescence drug inducer for four different cell lines, including breast non-cancer, breast and lung cancer and lung fibroblasts. Senescence was confirmed and validated by detecting SA β-gal activity via flow cytometry. Senescent populations demonstrated specific cellular characteristics, such as proliferation arrest, altered

morphology and increased Ca^{2+} intracellular levels (Table 3.1), which align with the literature and confirm the senescent models for this thesis.

Despite the successful establishment of senescence models, this study has some limitations. Dox-induced senescence represents premature senescence, which reflects only one of the two senescent categories. An additional replicative senescence model would be beneficial to better model ageing. However, inducing replicative senescence requires extensive cell replication over several months, which was not feasible within the time constraints of this study. The stress-induced chemical senescence model using Dox was chosen as the most practical approach given the time limitations and the need to explore multiple aspects of senescence. Furthermore, while multiple senescence markers were assessed, the study could benefit from examining additional markers and pathways to provide a more comprehensive characterization of the senescent phenotype, such as epigenetic changes and SASP characterisation.

Change	Markers
Increased lysosomal content	↑ **SA β-galactosidase**
Proliferation arrest	↓ **cell count**
Cell cycle arrest	↑ **G2 phase of cell cycle**
Morphology	↑ **cell size**
Homeostasis	↑ **Ca^{2+} concentration**

Table 3.1: Summary of cellular characteristics in senescent models. Dox-induced senescence is confirmed by changes in cellular characteristics, which are experimentally confirmed *in vitro* by different cellular markers. ↑ : increase ↓ : decrease.

Chapter 4 : Mitochondria Function from Senescent Cells

4.1 Aims

Mitochondria have a dual role in cellular senescence; they are both drivers and effectors (Correia-Melo & Passos, 2015). Increased ROS levels are essential for maintaining the senescent phenotype in cellular populations (Correia-Melo et al., 2016), while changes in MMP are not just a result of cellular senescence but also have a role in ROS increased levels (Correia-Melo & Passos, 2015). Additionally, in recent years, the role of Ca^{2+} and Ca^{2+} signalling has a clear role in cellular senescence, as Ca^{2+}, Ca^{2+}-binding proteins and Ca^{2+} channels are key players in the regulation of senescence (Martin et al., 2023). Therefore, the aim of this chapter was to characterise the mitochondrial function of senescent cellular models.

4.2 Results

4.2.1 Detection and quantification of ROS

The mitochondria of MCF10A breast and MCF7 breast cancer and A549 lung cancer cells were further assessed to determine whether cellular ROS levels were altered following the induction of senescence with 0.25 μM Dox treatment for 24 hours and six days culture with Dox-free media. The results showed that senescence significantly increased cellular ROS levels in all cell lines; by 91.68% ± 24.90 ($P = 0.0079$) in MCF10A breast senescent cells (Figure 4.1); by 130.60% ± 21.60 ($P = 0.0079$) in MCF7 breast cancer cells (Figure 4.2) and by 1,235% ± 14.45 ($P < 0.0001$) in A549 lung cancer cells (Figure 4.3).

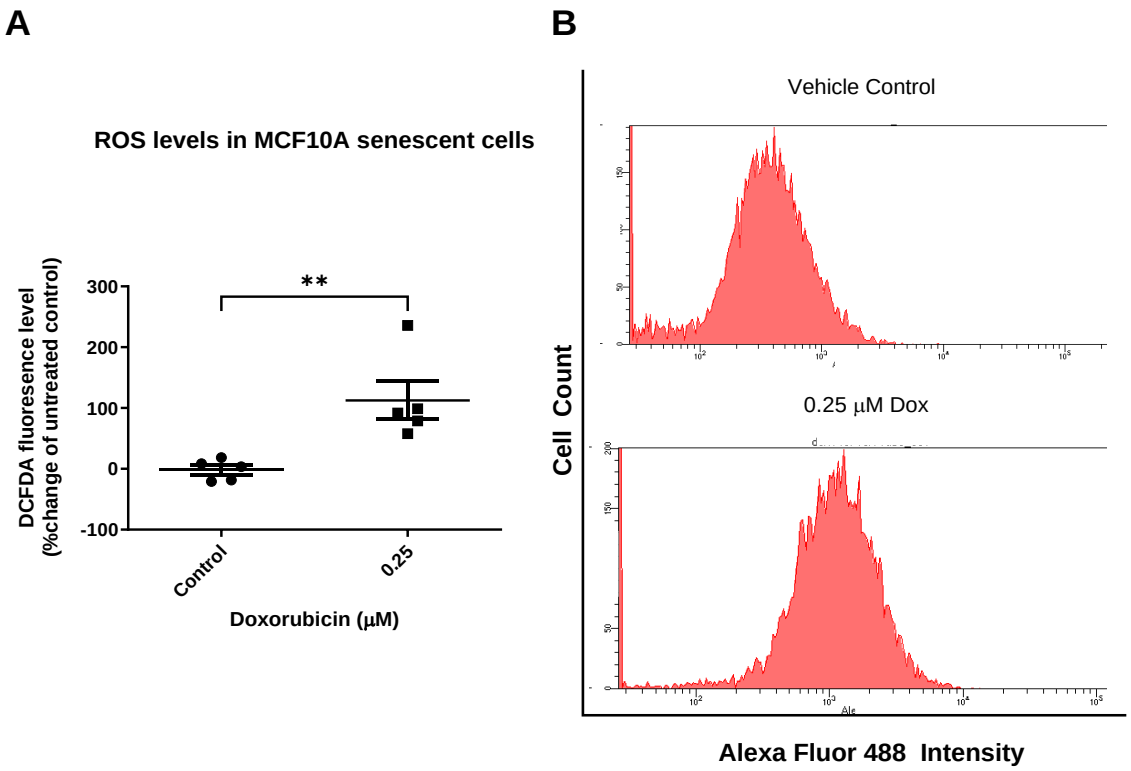

Figure 4.1: The effect of senescence on cellular ROS levels in MCF10A – Flow cytometry. (A) MCF10A breast cells were treated with 0.25 µM Dox for 24 hours, followed by 6 days in drug-free media. Media and vehicle (H_2O) controls were included for comparison. ROS levels were quantified by flow cytometry in live cells following DCFDA staining and expressed as a percentage change from untreated control (N=12 independent biological repeats). Statistical significance was determined using Mann-Whitney U test. (B) Representative histograms showing univariate plot intensity of Alexa Fluor-488 against event count in flow cytometry, demonstrating the distribution of ROS levels across different treatment conditions. Data are presented as mean changes compared to an untreated control ± SEM. ** : $P \leq 0.01$.

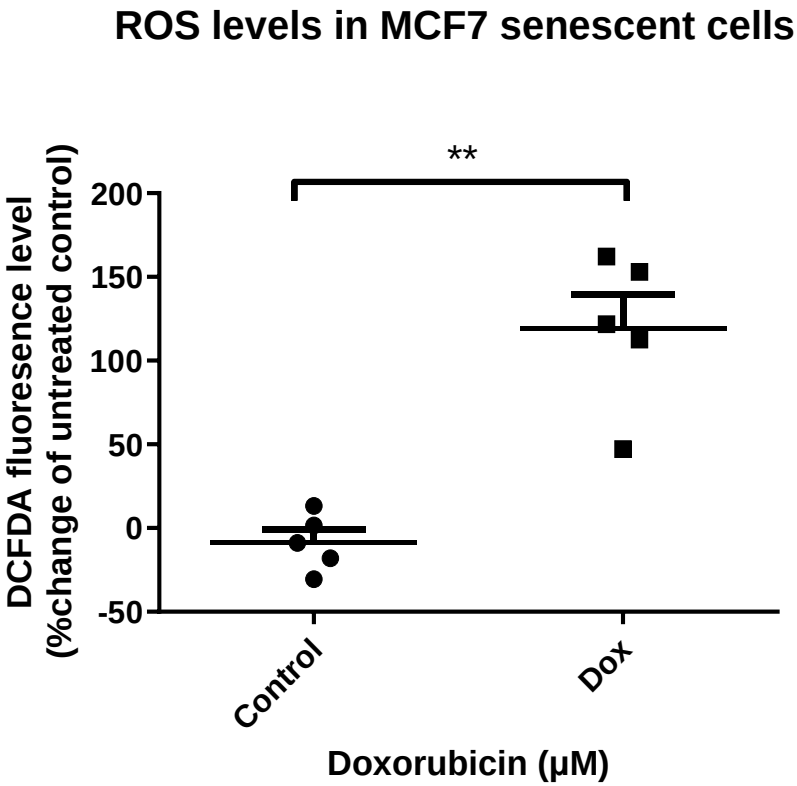

Figure 4.2: The effect of senescence on cellular ROS levels in MCF7 – Flow cytometry. MCF7 breast cancer cells were treated with 0.25 μM Dox for 24 hours, followed by 6 days in drug-free media. Media and vehicle (H_2O) controls were included for comparison. ROS levels were quantified by flow cytometry in live cells following DCFDA staining and expressed as a percentage change from untreated control (N=5 independent biological repeats). Statistical significance was determined using Mann-Whitney U test. Data are presented as mean changes compared to an untreated control ± SEM. ** : $P \leq 0.01$.

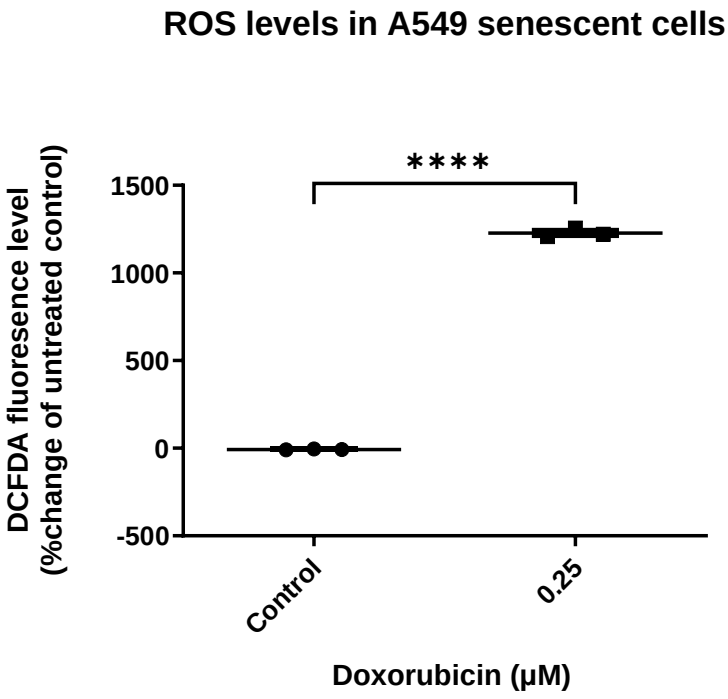

Figure 4.3: The effect of senescence on cellular ROS levels in A549 – Flow cytometry. A549 lung cancer cells were treated with 0.25 μM Dox for 24 hours, followed by 6 days in drug-free media. Media and vehicle (H_2O) controls were included for comparison. ROS levels were quantified by flow cytometry in live cells following DCFDA staining and expressed as a percentage change from untreated control (N=3 independent biological repeats). Statistical significance was determined using unpaired two-tailed t-test. Data are presented as mean changes compared to an untreated control ± SEM. **** : $P < 0.0001$.

4.2.2 Assessment of mitochondrial membrane potential

MCF10A breast and MCF7 breast cancer cells were further assessed to determine whether senescence altered MMP. The results showed that MMP increased by 122.30% ± 25.10 ($P = 0.0082$; Figure 4.4) in MCF10A, while no significant MMP change was observed in senescent MCF7 cells ($P = 0.3095$, Figure 4.5).

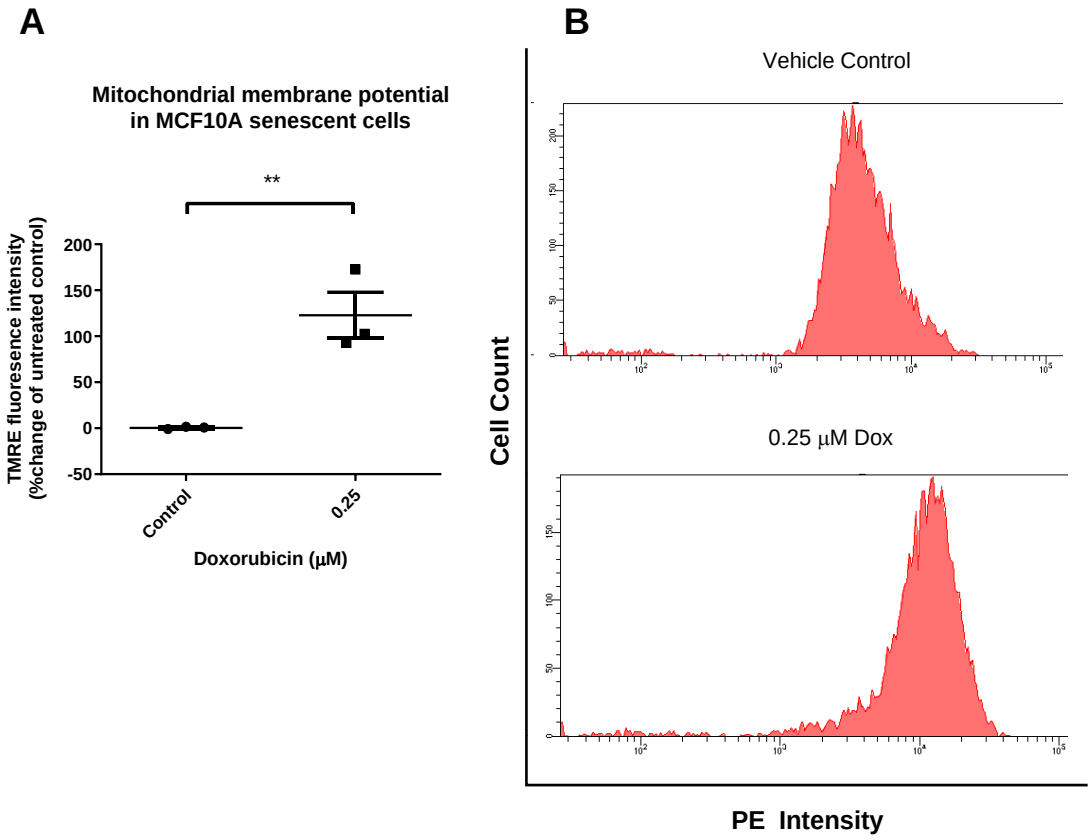

Figure 4.4: The effect of senescence in MCF10A MMP – Flow cytometry. (A) MCF10A breast cells were treated with 0.25 µM Dox for 24 hours, followed by 6 days in drug-free media. Media and vehicle (H_2O) controls were included for comparison. Mitochondrial membrane potential was quantified by flow cytometry in live cells following TMRE staining and expressed as a percentage change from untreated control (N=3 independent biological repeats). Statistical significance was determined using unpaired two-tailed t-test. (B) Representative histograms showing univariate plot intensity of PE against event count in flow cytometry, demonstrating the distribution of MMP across different treatment conditions. Data are presented as mean changes compared to an untreated control ± SEM. ** : $P \leq 0.01$.

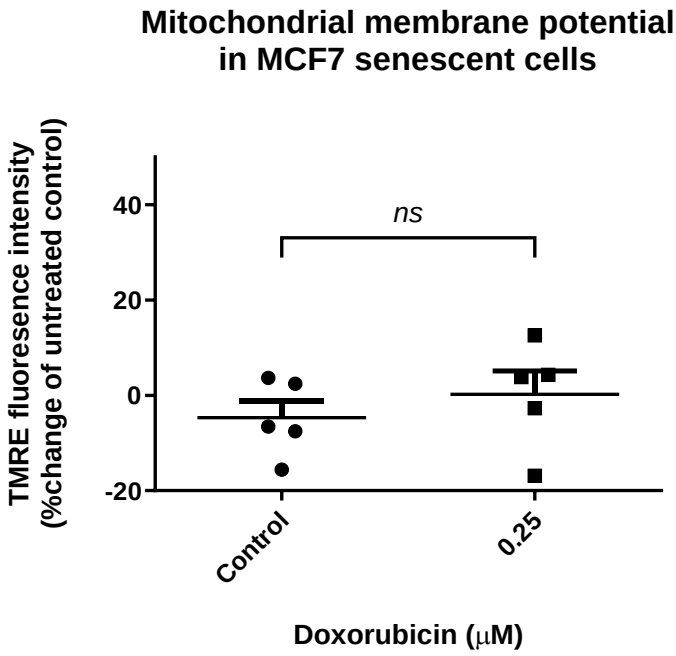

Figure 4.5: The effect of senescence in MCF7 MMP – Flow cytometry. MCF7 breast cancer cells were treated with 0.25 μM Dox for 24 hours, followed by 6 days in drug-free media. Media and vehicle (H_2O) controls were included for comparison. Mitochondrial membrane potential was quantified by flow cytometry in live cells following TMRE staining and expressed as a percentage change from untreated control (N=4 independent biological repeats). Statistical significance was determined using Mann-Whitney U test. Data are presented as mean changes compared to an untreated control ± SEM. non-significant: P > 0.05.

4.2.3 Assessment of mitochondrial Ca^{2+} levels

MCF10A breast and MCF7 breast cancer cells were further analysed to determine whether senescence increased mitochondrial Ca^{2+} levels. The results showed a significant increase of Ca^{2+} levels in both MCF10A and MCF7 after 0.25 μM Dox treatment for 24 hours and six days of culture with Dox-free media. Ca^{2+} levels increased by 96.29% ± 13.40 (P = 0.0022) in mitochondria isolated from senescent MCF10A breast cells (Figure 4.6), and by 23.45% ± 8.24 (P = 0.0079) in mitochondria from senescent MCF7 cancer breast cells (Figure 4.7).

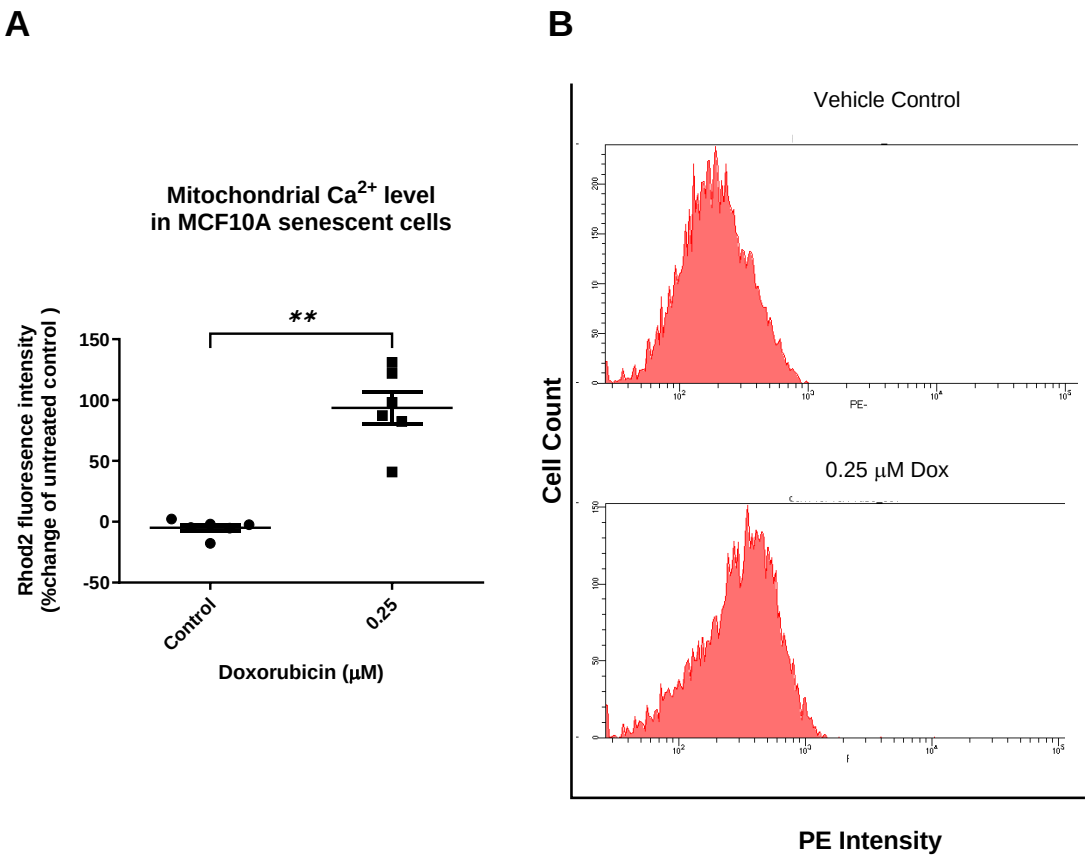

Figure 4.6: The effect of senescence in MCF10A mitochondrial Ca^{2+} levels – Flow cytometry. (A) MCF10A breast cells were treated with 0.25 µM Dox for 24 hours, followed by 6 days in drug-free media. Media and vehicle (H_2O) controls were included for comparison. Mitochondrial Ca^{2+} levels were quantified by flow cytometry in live cells following Rhod-2 staining and expressed as a percentage change from untreated control (N=6 independent biological repeats). Statistical significance was determined using Mann-Whitney U test. (B) Representative histograms showing univariate plot intensity of PE against event count in flow cytometry, demonstrating the distribution of mitochondrial Ca^{2+} levels across different treatment conditions. Data are presented as mean changes compared to an untreated control ± SEM. ** : $P \leq 0.001$.

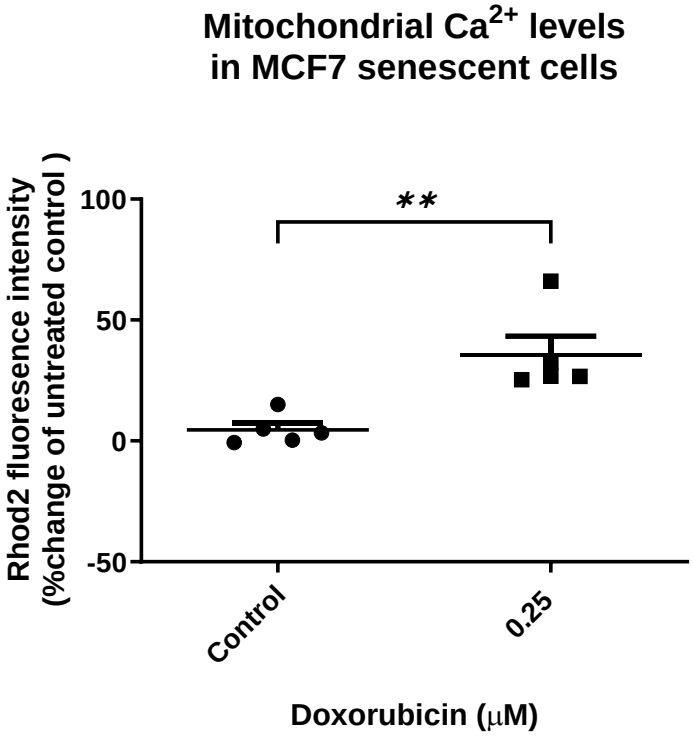

Figure 4.7: The effect of senescence in MCF7 mitochondrial Ca^{2+} levels – Flow cytometry. MCF7 breast cancer cells were treated with 0.25 μM Dox for 24 hours, followed by 6 days in drug-free media. Media and vehicle (H_2O) controls were included for comparison. Mitochondrial Ca^{2+} levels were quantified by flow cytometry in live cells following Rhod-2 staining and expressed as a percentage change from untreated control (N=5 independent biological repeats). Statistical significance was determined using Mann-Whitney U test. Data are presented as mean changes compared to an untreated control ± SEM. ** : P ≤ 0.01.

4.3: Discussion

4.3.1 ROS increase in senescent cells

The overall aim of this chapter was to investigate the changes in mitochondrial function following Dox-induced senescence. I have demonstrated that cellular senescence induces significant alterations in various mitochondrial characteristics, including ROS levels, MMP and mitochondrial Ca^{2+} levels. These changes were observed across multiple characteristic markers of senescence, providing a comprehensive view of the senescent phenotype.

Consistent with previous studies, I observed increased cellular ROS levels in Dox-induced senescent MCF10A, MCF7, and A549 cells. This finding aligns with the work of Fan et al. (2023), who demonstrated elevated ROS levels in Dox-induced senescent A549 cells (Fan et al., 2023). The agreement between my results and those of Fan et al. confirms the reliability of my methods and reinforces the significance of ROS as a hallmark of senescence across different cell types. Indeed, ROS elevation is widely recognized as a key feature of senescence (Hernandez-Segura et al., 2018a).

As previously mentioned (Section 1.7.2), both mitochondria and ROS are drivers of senescence *in vivo* and *in vitro* (Correia-Melo & Passos, 2015; Höhn et al., 2017; Passos et al., 2010). Increased ROS levels and oxidative stress are two of the most established inducers of senescence (Petrova et al., 2016; Hernandez-Segura et al., 2018b). Studies have shown that mitochondrial ROS can result in oxidative stress, which enhances telomere attrition and leads to paracrine senescence via DNA damage response (DDR) activation (Chen et al., 1995; Petrova et al., 2016). For example, treating cells with H_2O_2 is a common technique to induce senescence in cancerous and non-cancerous cell lines (Passos et al., 2010). While I initially attempted to induce senescence with H_2O_2 in MCF7 cells, this approach did not yield conclusive results in this thesis. However, having successfully established three senescent models using Dox, and demonstrating increased levels of ROS across these models, I confirmed the overall senescence phenotype. This aligns with the

work of Passos et al. (2010), who showed that ROS contributes to establishing, maintaining, and stabilizing the cycle arrest in senescent cells. Their research, among others, demonstrates the various ways to induce senescence and highlights the crucial role of ROS in the senescent state. Thus, the increased level of ROS observed in my Dox-induced senescent cells suggests a consistent and irreversible senescence model, further validating the approach used in this study.

4.3.2 MMP increase in senescent MCF10A but not MCF7 cells

In this study, MMP increased during senescence in breast non-cancer cells but not in breast cancer cells (Figures 4.4 and 4.5). This contrasts with the general literature, which typically reports MMP decreases during senescence (Ashapkin et al., 2019; Correia-Melo & Passos, 2015; Martini & Passos, 2023; Passos et al., 2010; Stab et al., 2016). However, recent research indicates that elevated MMP drives ATP synthesis within mitochondria and significantly influences ROS production (Zorova et al., 2018). It is generally accepted that extreme or prolonged changes in the MMP can negatively affect cell viability and contribute to various pathologies due to excessive ROS levels. Maintaining a stable MMP is crucial for mitochondrial homeostasis and eliminating dysfunctional mitochondria. Deviations from normal levels of MMP can have detrimental consequences for the cell (Zorova et al., 2018).

Indeed, as mentioned in Section 4.1.2 (Figure 4.1), MCF10A senescent cells exhibit a more than 100% increase in ROS. This increase could be influenced by the increased levels of MMP, increasing the ROS levels within the mitochondria (Zorova et al., 2018). Measuring ATP levels of MCF10A after Dox senescence induction would provide more information on the pathway involved during senescence. However, for this thesis, I did not test for ATP levels due to time limitations. The tests performed to establish senescence were deemed sufficient for the scope of this research without including ATP level measurements. Nevertheless, this represents a limitation of the current study, and future research could benefit from examining the ATP levels in Dox-induced senescent cells to further investigate

the metabolic changes associated with senescence. Additionally, due to the unique secondary effects that occur during senescence and the fact that cells from different origins exhibit distinct senescent characteristics (Sharpless & Sherr, 2015), my results demonstrate that MCF7 breast cancer cells react differently to Dox-induced senescence than MCF10A breast non-cancer cells. Specifically, MCF7 cells do not show any effect on MMP.

4.3.3 Mitochondrial Ca^{2+} levels increase in senescent cells

Mitochondrial Ca^{2+} levels were increased in Dox-induced senescent cell populations of non-cancer and cancer models (Figures 4.6 and 4.7). This is consistent with the altered mitochondrial Ca^{2+} homeostasis observed in the general senescent cellular profile (Ziegler et al., 2015). The increase in intracellular Ca^{2+} levels in senescent cells can come from Ca^{2+} influx through plasma membrane Ca^{2+} channels or from Ca^{2+} release from the endoplasmic reticulum or mitochondria. This increase in Ca^{2+} levels triggers cellular senescence and is sustained during senescence (Martin & Bernard, 2018).

Ca^{2+} dynamics have also been shown to mediate the communication between mitochondria and the nucleus in response to stress. They can activate signalling factors such as NF-kB (Butow & Avadhani, 2004). According to Ziegler et al. (2021), changes in the transfer of Ca^{2+} from the endoplasmic reticulum to the mitochondria can lead to mitochondrial dysfunction and eventually cause cellular senescence. Additionally, accumulation of Ca^{2+} is observed in cells with increased levels of ROS, which can induce oxidative stress-induced senescence. During senescence, a rapid release of Ca^{2+} occurs, which activates pathways signalling senescence and maintains cell cycle arrest (Borodkina et al., 2016).

As previously mentioned (Section 3.2.3), the increased intracellular Ca^{2+} levels may be attributed to Ca^{2+} release from intracellular stores, such as mitochondria (Martin et al., 2023). The increased MMP in senescent MCF10A cells could contribute to the significant increase in intracellular Ca^{2+} levels. In contrast, the more modest increase in mitochondrial Ca^{2+} levels in MCF7 cells, combined with no increase in MMP, would not contribute to the

elevated intracellular Ca^{2+} levels. This suggests that MMP plays a regulatory role in Ca^{2+} channelling and, subsequently, in Ca^{2+} signalling within the cell (Duchen, 2000).

4.3.4 Conclusion

In this chapter, the impact of senescence on mitochondria in non-cancer and cancer cell models was investigated. The findings confirm that during senescence, there is a consistent pattern of changed mitochondrial homeostasis characterised by increased levels of ROS and Ca^{2+}. These changes in ROS and Ca^{2+} levels indicate mitochondrial stress, which is commonly associated with the senescence of different cell types. The disruption of MMP homeostasis observed in MCF10A cells further demonstrates the impact of senescence on mitochondrial function. MMP disruption can compromise the energy-producing capacity of mitochondria and contribute to cellular dysfunction while increasing Ca^{2+} levels intracellularly.

The differential response of MMP homeostasis between MCF10A breast non-cancer and MCF7 breast cancer cells suggests that the regulation of MMP during senescence may vary depending on the cellular context or cell origin. While MCF10A senescent cells demonstrated MMP disruption, indicating a compromised mitochondrial function, no changes were observed in MCF7 cells. This difference may reflect distinct mechanisms underlying senescence induction and regulation in non-cancer versus cancer cell lines. The regulatory pathways controlling MMP and mitochondrial function during senescence may be cell-type specific and affected by cellular metabolism and oncogenic signalling pathways.

Finally, it is important to acknowledge the limitations of this Chapter. Firstly, ATP levels were not measured due to time constraints, which could have provided additional insights into the metabolic changes associated with senescence. However, it's crucial to note that mitochondrial function and metabolic alterations during senescence, as well as the establishment of a senescent phenotype, can be comprehensively characterized without

direct ATP measurements. Furthermore, MMP, mitochondrial Ca^{2+}, and intracellular Ca^{2+} were not tested in A549 lung cancer cells. This decision was made because A549 cells were primarily employed for the NIR light study in Chapter 6, which occurred later in the research timeline. For A549 cells, only Dox-induced senescence (including primary senescent characteristics such as SA β-gal activity increase; Figure 3.8.C, and cell count decrease; Figure 3.10.C) and ROS levels (Figure 4.3) were examined, as ROS increase is critical for biophotonic production (explored in Chapter 5). While I established that Dox treatment induces a senescent model in A549 cells, the comprehensive mitochondrial function tests were limited to one non-cancer (MCF10A) and one cancer (MCF7) cell model due to time constraints. Future studies could benefit from expanding these analyses to include ATP measurements and a more comprehensive evaluation of mitochondrial parameters across all cell lines, including A549, to provide a more complete picture of altered mitochondrial homeostasis in senescence across different cell types.

Chapter 5 : Non-Chemical Communication During Senescence

5.1 Aims

Biophotonic communication, a phenomenon involving the emission and reception of ultra-weak photons by biological systems, represents a novel field of understanding cellular interactions and signalling mechanisms. Biophotons are produced primarily through oxidative processes within cells, particularly by ROS, reflecting the dynamic metabolic activities and redox balance within the cellular microenvironment. Previous research has demonstrated the existence of non-chemical communication among mitochondria, revealing their potential role in intercellular signalling and coordination.

In this chapter, I aimed to investigate the existence of non-chemical mitochondrial signalling during cellular senescence. Specifically, my objectives were to examine whether mitochondria from senescent cells can respond to stress signals from neighbouring mitochondria without direct chemical contact. This involved quantifying changes in the oxygen consumption rate of mitochondria from senescent cells when exposed to antimycin-induced stress in nearby mitochondria. By comparing these responses to those from non-senescent cells, I aimed to determine if senescence alters this form of mitochondrial communication. Additionally, I aimed to directly measure biophotons from isolated mitochondria from senescent cells.

5.2 Results

5.2.1 Non-chemical communication assay optimisation

To validate the experimental protocol for the non-chemical communication assay, two control experiments were conducted. First, the oxygen consumption rate of isolated mitochondria from senescent MCF10A cells was monitored over a 400-second period without any treatment. No significant change was observed in the oxygen consumption rate, confirming the stability of mitochondrial oxygen consumption under basal conditions (Figure 5.1).

Second, the effect of antimycin on oxygen consumption rate in isolated mitochondria from senescent MCF10A cells was assessed. Oxygen consumption rate was recorded for 2 minutes before and 5 minutes after antimycin treatment. Results demonstrate a statistically significant decrease in oxygen consumption of 2.25% over the 5-minute post-antimycin period (pre-antimycin: 100.02% ± 0.86 SEM, post-antimycin: 97.77% ± 1.30 SEM; $P < 0.0001$; Figure 5.2). Comparable results were obtained for MCF7 and A549 cell lines, demonstrating the consistency of the assay across different cell types.

These validations, conducted on MCF10A cells and replicated with consistent outcomes across other cell lines used in this thesis, demonstrate the reliability of the non-chemical communication assay protocol. The results establish a robust baseline for interpreting subsequent experimental findings, with the MCF10A data serving as a representative example of the validation process applied to all cell lines in this study.

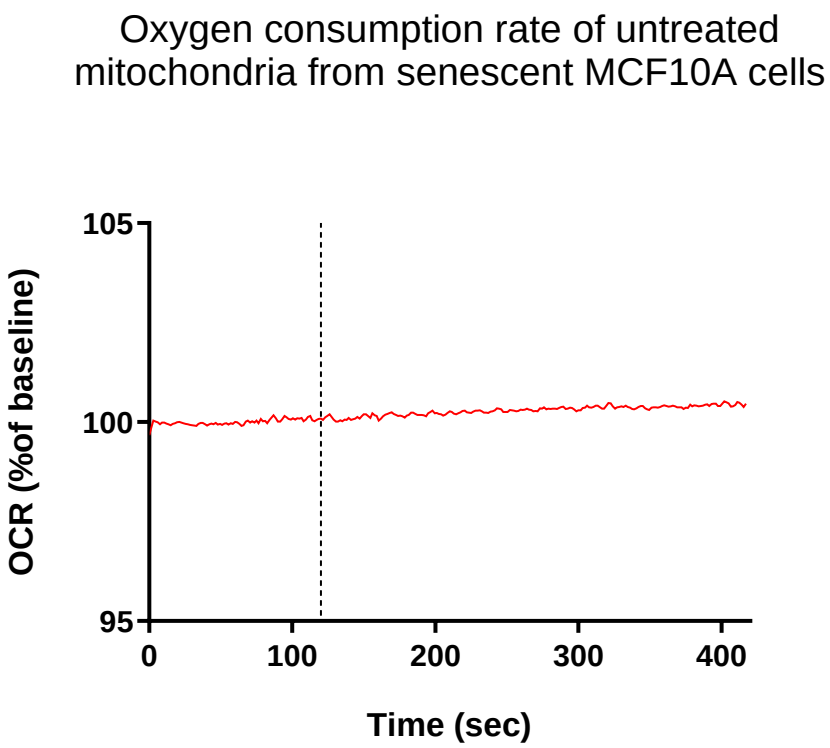

Figure 5.1: Oxygen consumption rate of isolated mitochondria from senescent MCF10A cells. Mitochondria were isolated from Dox-induced senescent MCF10A breast cells. The graph shows the oxygen consumption rate (OCR) measured continuously over 400 seconds in mitochondrial assay buffer under control conditions with no treatment (N=8 independent biological repeats). The red line represents the oxygen consumption rate maintained at 100% of baseline. A vertical dashed line at 120 seconds indicates the timepoint corresponding to antimycin injection in experimental conditions, though no injection was performed in this control. This control experiment demonstrates stable baseline oxygen consumption in isolated mitochondria. Data are presented as mean changes compared to baseline oxygen consumption rate.

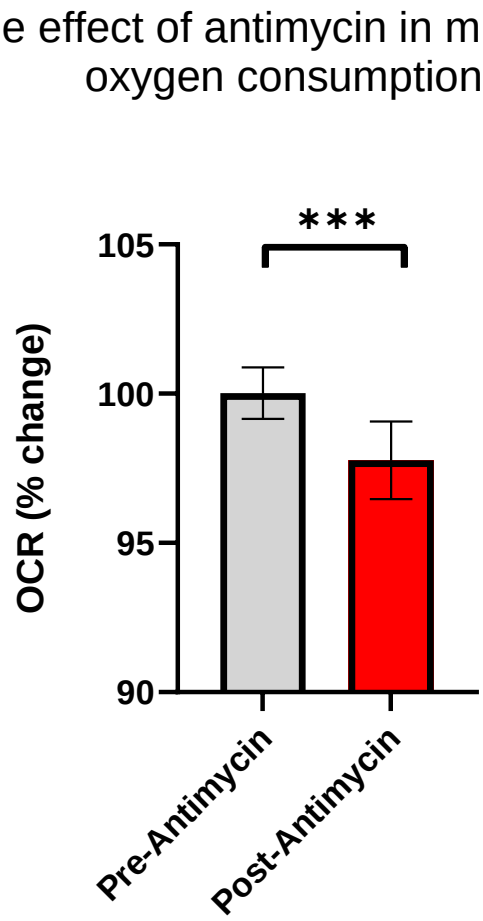

Figure 5.2: The effect of antimycin in isolated mitochondria from senescent MCF10A cells. Mitochondria were isolated from Dox-induced senescent MCF10A breast cells. The oxygen consumption rate was recorded for 2 minutes before (pre-antimycin) and 5 minutes after (post-antimycin) treatment with 244 μM antimycin, a specific inhibitor of mitochondrial complex III (N=8 independent biological repeats). Statistical significance was determined using a linear model analysis. Data are presented as percentage changes compared to baseline oxygen consumption rate ± SEM. *** : $P \leq 0.0001$.

5.2.2 The effect of non-chemical communication on mitochondria from MCF10A breast cells

Comparison of oxygen consumption rate in mitochondria between shielded and unshielded cuvettes demonstrated a significant increase of 0.00268% per second in isolated mitochondria of senescent MCF10A cells (unshielded: 0.00443% ± 0.00012, shielded: 0.00175% ± 0.00018; $P < 0.0001$; Figure 5.3). These results are complemented by data from non-senescent MCF10A cells, previously published by our group (Mould et al., 2023). This work showed a decrease of 0.00420% per second in non-senescent MCF10A cells (unshielded: 0.00261% ± 0.00030, shielded: -0.00120% ± 0.00040; $P < 0.0001$) as demonstrated in Figure 5.4. The inclusion of these published data provides a direct comparison between senescent and non-senescent cells without necessitating the repetition of experiments.

To confirm a differential effect of non-chemical communication during senescence, the oxygen consumption rates of the unshielded cuvettes were compared between isolated mitochondria from senescent and non-senescent populations. Results from MCF10A mitochondria indicate that senescence changes the effect of oxygen consumption by 0.00556% per second (non-senescence: -0.00260 ± 0.00023, senescence: 0.00388 ± 0.00037; $P < 0.0001$; Figure 5.5). At the same time, the oxygen consumption rate of isolated MCF10A mitochondria (shielded cuvettes) was compared between non-senescent and senescent populations. Senescence increased the mitochondrial consumption rate by 0.00169% per second (non-senescence: 0.00033% ± 0.00018, senescence: 0.00202% ± 0.00032; $P < 0.0001$; Figure 5.6).

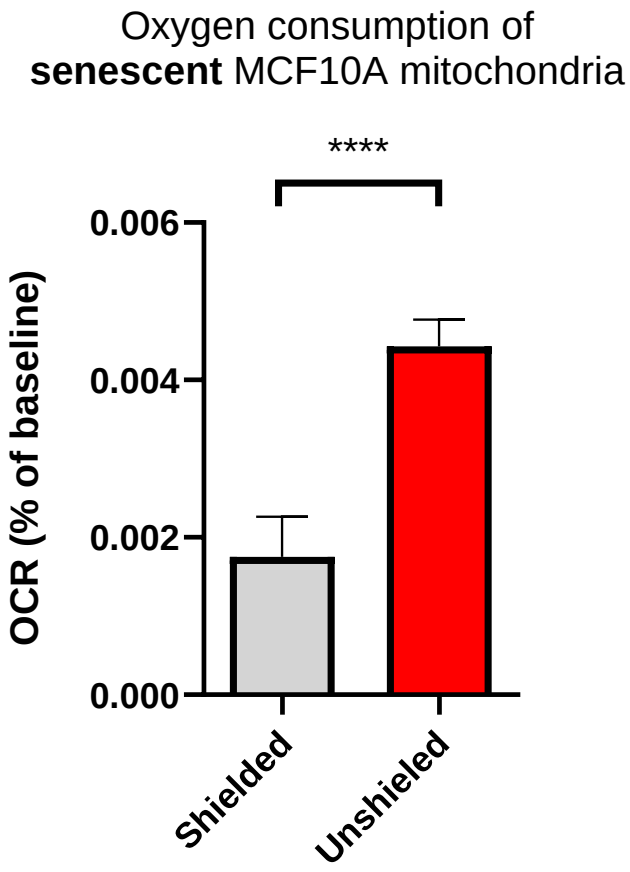

Figure 5.3: The effect of non-chemical communication on mitochondria from senescent MCF10A cells. Mitochondria isolated from Dox-induced senescent MCF10A breast cells were equally distributed into three quartz cuvettes (2 mL total volume each). The oxygen consumption rate was measured in shielded and unshielded cuvettes for 5 minutes following addition of 244 μM antimycin to the central treated cuvette (N=8 independent biological repeats). Statistical significance between shielded and unshielded conditions was determined using linear mixed-effects model analysis. Data are presented as percentage changes compared to baseline oxygen consumption rate ± SEM. **** : $P < 0.0001$.

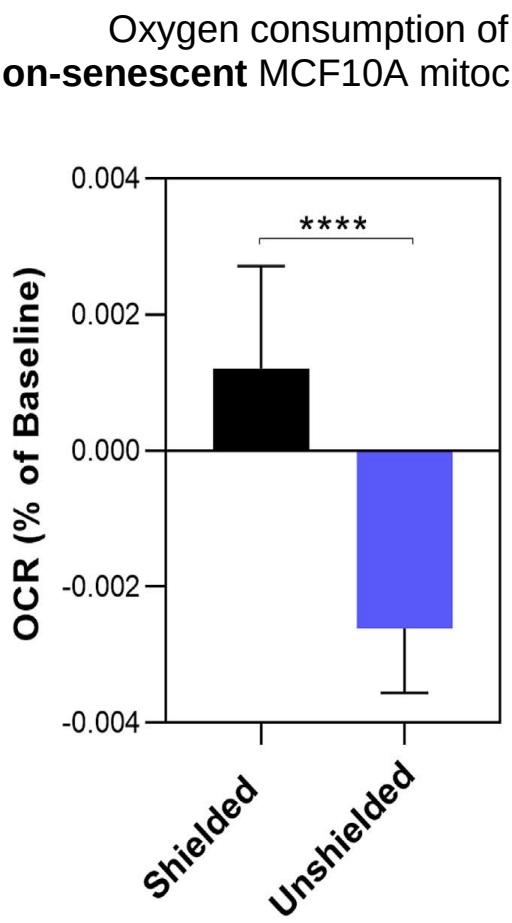

Figure 5.4: The effect of non-chemical communication on mitochondria from non-senescent MCF10A cells. Mitochondria isolated from non-senescent MCF10A breast cells were equally distributed into three quartz cuvettes (2 mL total volume each). The oxygen consumption rate was measured in shielded and unshielded cuvettes for 5 minutes following addition of 244 μM antimycin to the central treated cuvette (N=8 independent biological repeats). Statistical significance between shielded and unshielded conditions was determined using linear mixed-effects model analysis. Data adapted from Mould et al (2023) are presented as percentage changes compared to baseline OCR ± SEM. **** : P < 0.0001..

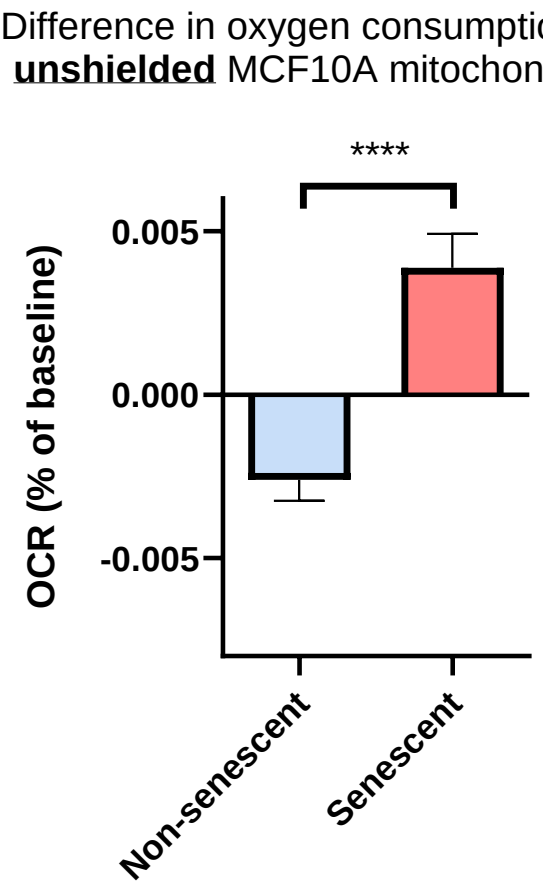

Figure 5.5: The differential effect of non-chemical communication on mitochondrial oxygen consumption rate between senescent and non-senescent MCF10A cells. Oxygen consumption rate data were obtained from independent experiments with Dox-induced senescent and non-senescent MCF10A breast cells, comparing the responses in unshielded cuvettes following antimycin addition to their respective treated cuvettes. The oxygen consumption rate measurements from both experiments' unshielded cuvettes were compared (N=8 independent biological repeats). Statistical significance was determined using linear mixed-effects model analysis. Data are presented as percentage changes compared to baseline OCR ± SEM. **** : $P < 0.0001$.

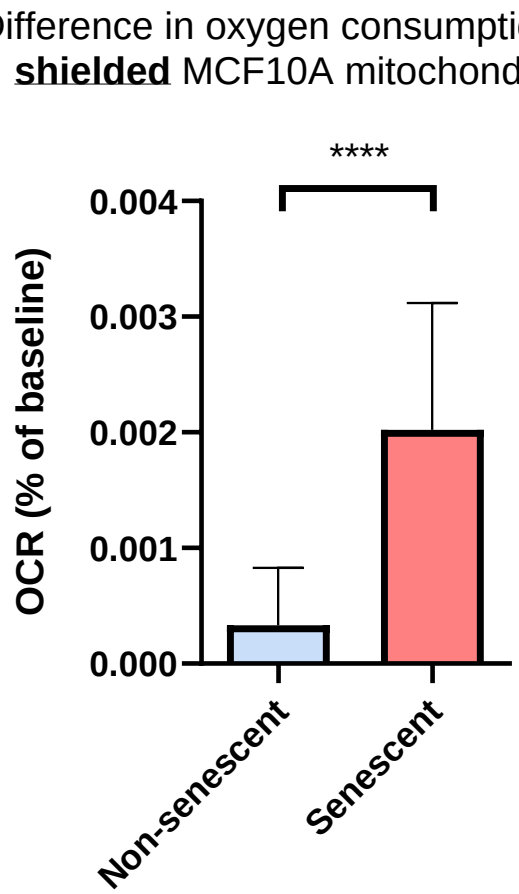

Figure 5.6: The effect of senescence on MCF10A mitochondrial oxygen consumption rate. Oxygen consumption rate data were obtained from independent experiments with Dox-induced senescent and non-senescent MCF10A breast cells, comparing the responses in shielded cuvettes following antimycin addition to their respective treated cuvettes. The oxygen consumption rate measurements from both experiments' shielded cuvettes were compared (N=8 independent biological repeats). Statistical significance was determined using linear mixed-effects model analysis. Data are presented as percentage changes compared to baseline OCR ± SEM. **** : $P < 0.0001$.

5.2.3 The effect of non-chemical communication on mitochondria from MCF7 breast cancer cells

Comparison of oxygen consumption rate in mitochondria between shielded and unshielded cuvettes demonstrated a significant increase of 0.00118% per second in isolated mitochondria of senescent MCF7 cells (unshielded: 0.00287% ± 0.00016, shielded: 0.00169 ± 0.0002404; $P < 0.0001$; Figure 5.7). These results are complemented by data from non-senescent MCF7 cells, previously published by our group (Mould et al., 2023). This work showed an increase of 0.0042% per second in non-senescent MCF7 cells (unshielded: −0.00052% ± 0.0005, shielded: −0.00167% ± 0.0003; $P = 0.0016$) as demonstrated in Figure 5.8. The inclusion of these published data provides a direct comparison between senescent and non-senescent cells without necessitating the repetition of experiments.

To confirm a differential effect of non-chemical communication during senescence, the oxygen consumption rates of the unshielded cuvettes were compared between isolated mitochondria from senescent and non-senescent populations. Results from MCF7 mitochondria indicate that senescence changes oxygen consumption by 0.00977% per second (non-senescence: -0.00111 ± 0.00033, senescence: 0.00401 ± 0.00054; $P < 0.0001$; Figure 5.9). At the same time, the oxygen consumption rate of isolated MCF7 mitochondria (shielded cuvettes) was compared between non-senescent and senescent populations. Senescence increases the mitochondrial consumption rate by 0.00589% per second (non-senescence: -0.00188% ± 0.00031019, senescence: 0.00401% ± 0.00051; $P < 0.0001$; Figure 5.10).

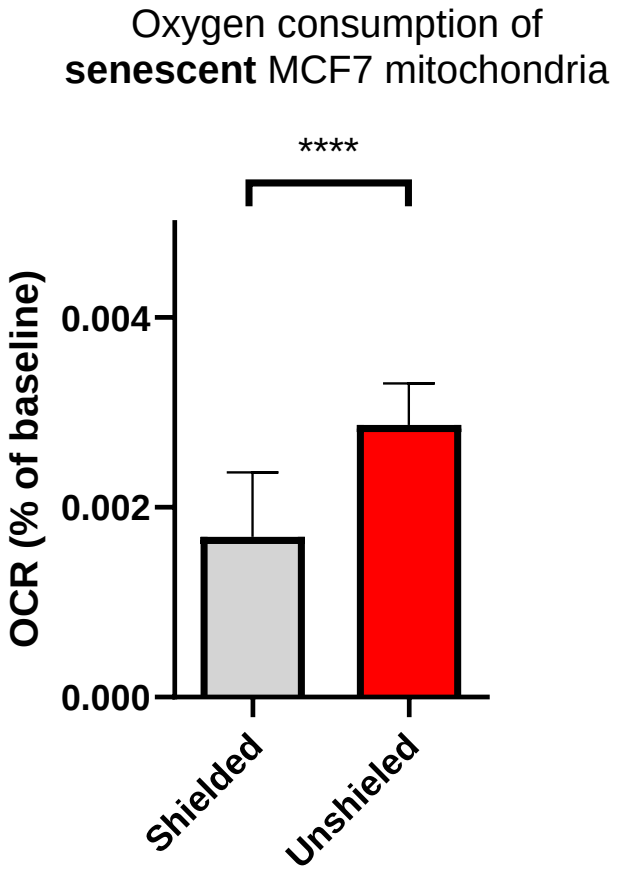

Figure 5.7: The effect of non-chemical communication on mitochondria from senescent MCF7 cells. Mitochondria isolated from Dox-induced senescent MCF7 breast cancer cells were equally distributed into three quartz cuvettes (2 mL total volume each). The oxygen consumption rate was measured in shielded and unshielded cuvettes for 5 minutes following addition of 244 μM antimycin to the central treated cuvette (N=8 independent biological repeats). Statistical significance between shielded and unshielded conditions was determined using linear mixed-effects model analysis. Data are presented as percentage changes compared to baseline OCR ± SEM. **** : $P < 0.0001$.

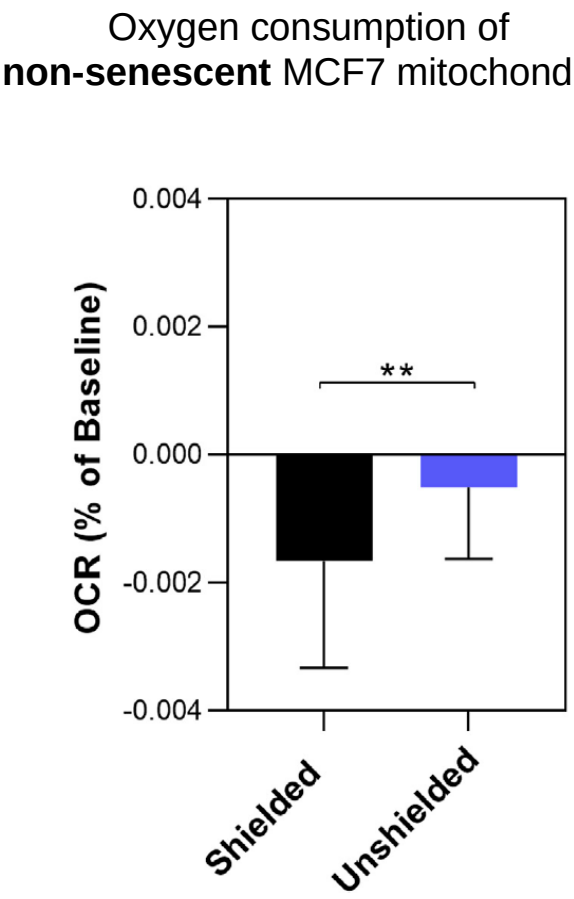

Figure 5.8: The effect of non-chemical communication on mitochondria from non-senescent MCF7 cells. Mitochondria isolated from non-senescent MCF7 breast cancer cells were equally distributed into three quartz cuvettes (2 mL total volume each). The oxygen consumption rate was measured in shielded and unshielded cuvettes for 5 minutes following addition of 244 μM antimycin to the central treated cuvette (N=8 independent biological repeats). Statistical significance between shielded and unshielded conditions was determined using linear mixed-effects model analysis. Data adapted from Mould et al (2023) are presented as percentage changes compared to baseline OCR ± SEM. ** : $P \leq 0.01$.

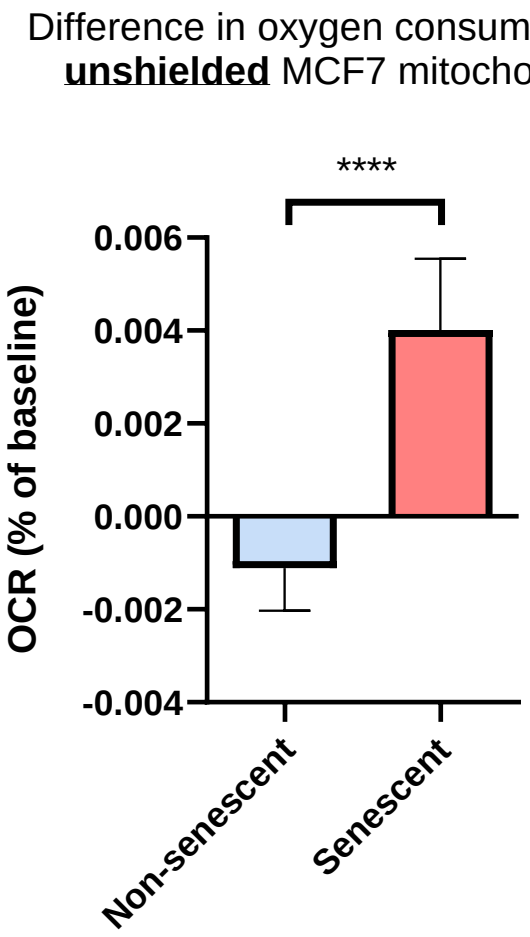

Figure 5.9: The differential effect of non-chemical communication on mitochondrial oxygen consumption rate between senescent and non-senescent MCF7 cells. Oxygen consumption rate data were obtained from independent experiments with Dox-induced senescent and non-senescent MCF7 breast cancer cells, comparing the responses in unshielded cuvettes following antimycin addition to their respective treated cuvettes. The oxygen consumption rate measurements from both experiments' unshielded cuvettes were compared (N=8 independent biological repeats). Statistical significance was determined using linear mixed-effects model analysis. Data are presented as percentage changes compared to baseline OCR ± SEM. **** : $P < 0.0001$.

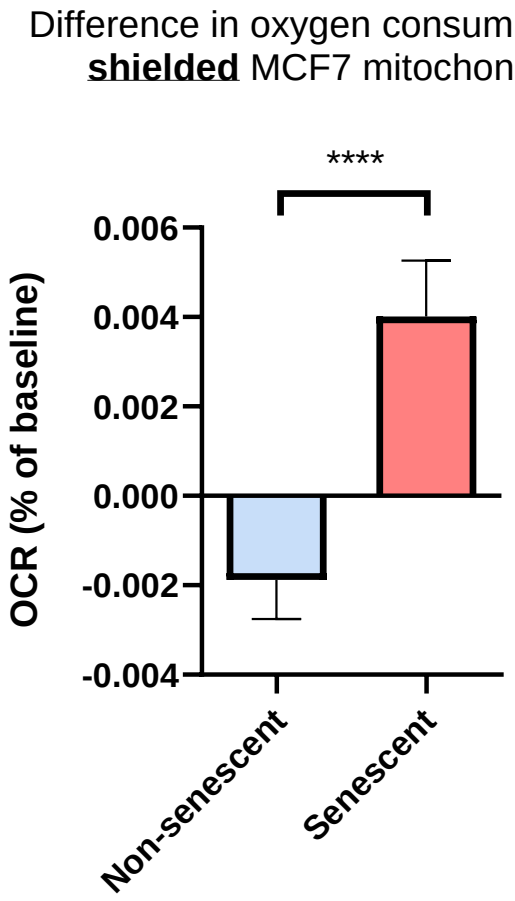

Figure 5.10: The effect of senescence on MCF7 mitochondrial oxygen consumption rate. Oxygen consumption rate data were obtained from independent experiments with Dox-induced senescent and non-senescent MCF7 breast cancer cells, comparing the responses in shielded cuvettes following antimycin addition to their respective treated cuvettes. The oxygen consumption rate measurements from both experiments' shielded cuvettes were compared (N=8 independent biological repeats). Statistical significance was determined using linear mixed-effects model analysis. Data are presented as percentage changes compared to baseline OCR ± SEM. **** : P < 0.0001.

5.2.4 The effect of non-chemical communication on mitochondria from A549 lung cancer cells

Comparison of the oxygen consumption rate of isolated mitochondria in shielded versus unshielded cuvettes demonstrated a significant difference of 0.00168% per second in isolated mitochondria of senescent A549 cells (unshielded: 0.00358% ± 0.00090, shielded: 0.00190 ± 0.00015; $P < 0.0001$; Figure 5.11), and, a significant difference of 0.00216% per second in isolated mitochondria of non-senescent A549 cells (unshielded: 0.00395% ± 0.0001173, shielded: 0.00179 ± 0.00019032; $P < 0.0001$; Figure 5.12).

To confirm a differential effect of non-chemical communication, the oxygen consumption rate of the unshielded cuvette was compared between isolated mitochondria from senescent and non-senescent populations. Results from A549 mitochondria indicate that senescence increases oxygen consumption by 0.00241% per second (non-senescence: 0.00227 ± 0.00015, senescence: 0.00468 ± 0.00026; $P \leq 0.001$; Figure 5.13). At the same time, the oxygen consumption rate of isolated A549 mitochondria (shielded cuvettes) was compared between non-senescent and senescent populations. There was no significant difference in the mitochondrial consumption rate between senescent and non-senescent A549 mitochondria ($P = 0.072$; Figure 5.14).

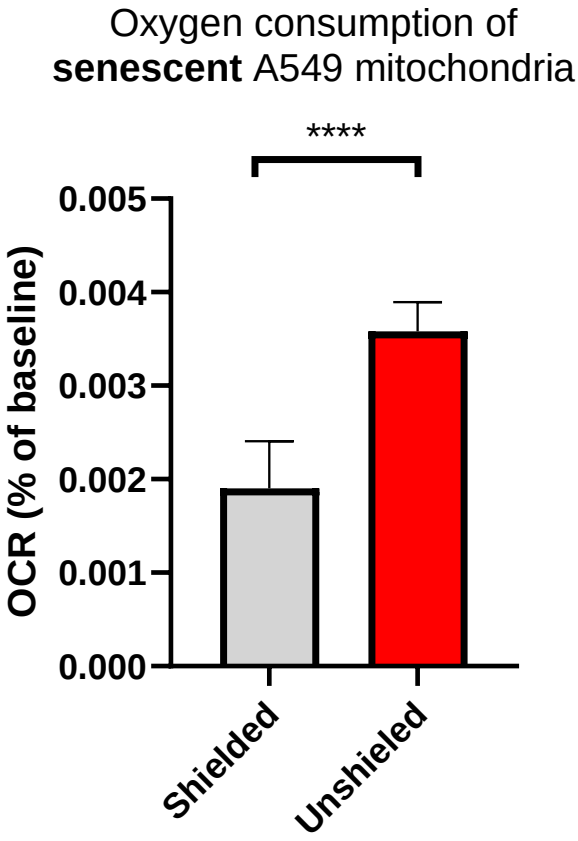

Figure 5.11: The effect of non-chemical communication on mitochondria from senescent A549 cells. Mitochondria isolated from Dox-induced senescent A549 lung cancer cells were equally distributed into three quartz cuvettes (2 mL total volume each). The oxygen consumption rate was measured in shielded and unshielded cuvettes for 5 minutes following addition of 244 μM antimycin to the central treated cuvette (N=12 independent biological repeats). Statistical significance between shielded and unshielded conditions was determined using linear mixed-effects model analysis. Data are presented as percentage changes compared to baseline OCR ± SEM. **** : $P < 0.0001$.

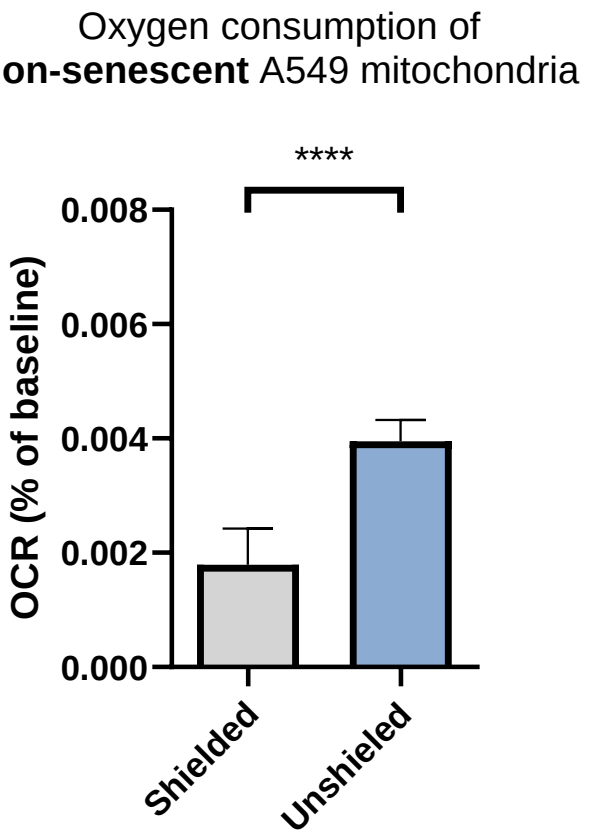

Figure 5.12: The effect of non-chemical communication on mitochondria from non-senescent A549 cells. Mitochondria isolated from non-senescent A549 lung cancer cells were equally distributed into three quartz cuvettes (2 mL total volume each). The oxygen consumption rate was measured in shielded and unshielded cuvettes for 5 minutes following addition of 244 μM antimycin to the central treated cuvette (N=11 independent biological repeats). Statistical significance between shielded and unshielded conditions was determined using linear mixed-effects model analysis. Data are presented as percentage changes compared to baseline OCR ± SEM. **** : $P < 0.0001$.

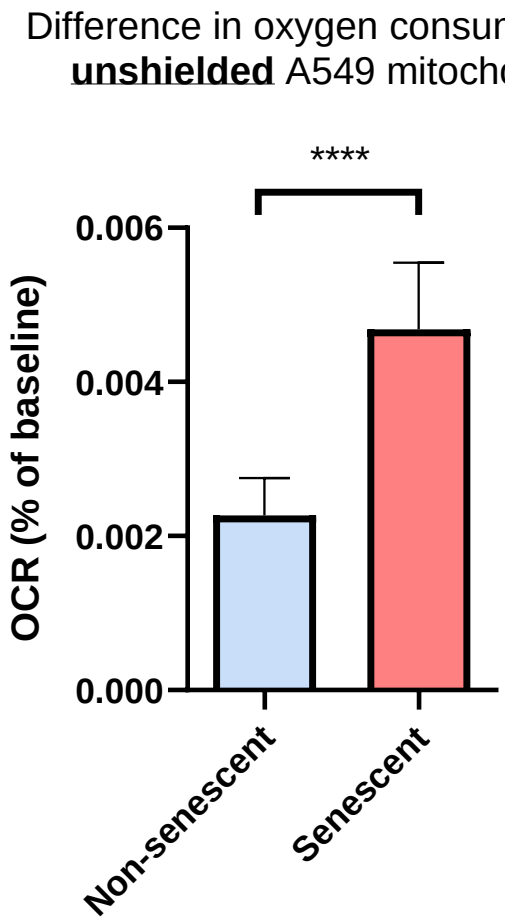

Figure 5.13: The differential effect of non-chemical communication on mitochondrial oxygen consumption rate between senescent and non-senescent A549 cells. Oxygen consumption rate data were obtained from independent experiments with Dox-induced senescent and non-senescent A549 lung cancer cells, comparing the responses in unshielded cuvettes following antimycin addition to their respective treated cuvettes. The oxygen consumption rate measurements from both experiments' unshielded cuvettes were compared (N=11 independent biological repeats). Statistical significance was determined using linear mixed-effects model analysis. Data are presented as percentage changes compared to baseline OCR ± SEM. **** : $P < 0.0001$.

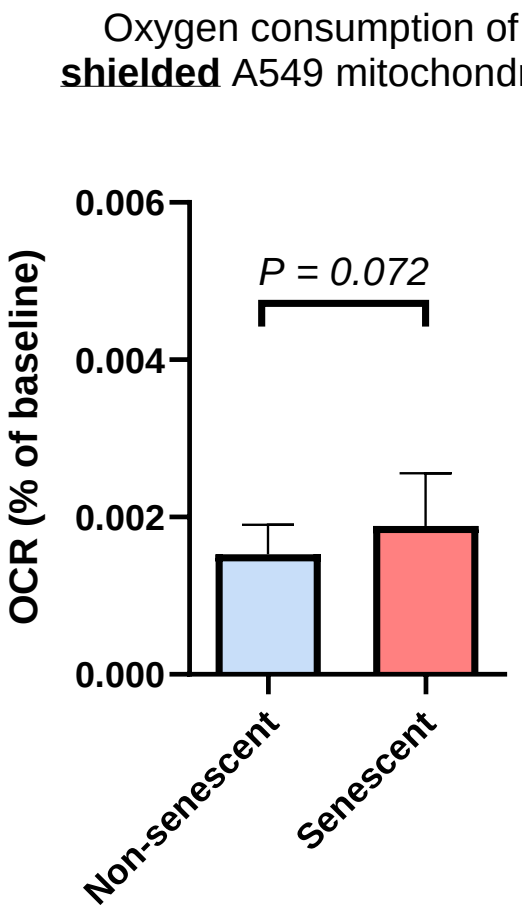

Figure 5.14: The effect of senescence on A549 mitochondrial oxygen consumption rate. Oxygen consumption rate data were obtained from independent experiments with Dox-induced senescent and non-senescent A549 lung cancer cells, comparing the responses in shielded cuvettes following antimycin addition to their respective treated cuvettes. The oxygen consumption rate measurements from both experiments' shielded cuvettes were compared (N=11 independent biological repeats). Statistical significance was determined using linear mixed-effects model analysis. Data are presented as percentage changes compared to baseline OCR ± SEM.

Summary of non-chemical communication effects on oxygen consumption rate

Populations	Oxygen Consumption Rate (unshielded)		
	MCF10A	MCF7	A549
Non-senescent	↓	↑	↑
Senescent	↑	↑	↑
Senescent vs non-senescent	↑	↑	↑

Table 5.1: Summary of mitochondrial non-chemical communication effects on oxygen consumption rate. Summary of directional changes in oxygen consumption rate under three experimental conditions: unshielded cuvettes from non-senescent mitochondria experiments, unshielded cuvettes from senescent mitochondria experiments, and comparison between senescent versus non-senescent mitochondria in unshielded conditions. Upward arrows (↑) indicate increased OCR, downward arrows (↓) indicate decreased OCR. Results are shown for MCF10A breast cells, MCF7 breast cancer cells, and A549 lung cancer cells, derived from antimycin treatment experiments.

5.2.5 Biophotonic detection protocol optimisation

Detecting biophotons is challenging due to their extremely weak emission (only tens of photons per second; Section 1.8.1). An ultra-sensitive detector was employed to address this (Mackenzie et al., 2024). However, the ultra-sensitivity of the detector also captures photons from materials exhibiting delayed luminescence, background noise, and even slight changes in electrical devices within the room. In the controlled dark conditions, the ultra-sensitive detector recorded an average of 160 photons per 10 seconds in the absence of a sample, establishing a dark background noise baseline.

An additional test was conducted to establish a baseline of non-biological photonic emission. This involved recording photons emitted from the mitochondrial assay buffer (MAB) alone. As shown in Figure 5.15, the average photon count from MAB (N=5) was 7.58 ± 0.73 photons per 10 seconds. This baseline allows for differentiation between non-biological photonic emissions and those from isolated mitochondria in subsequent experiments.

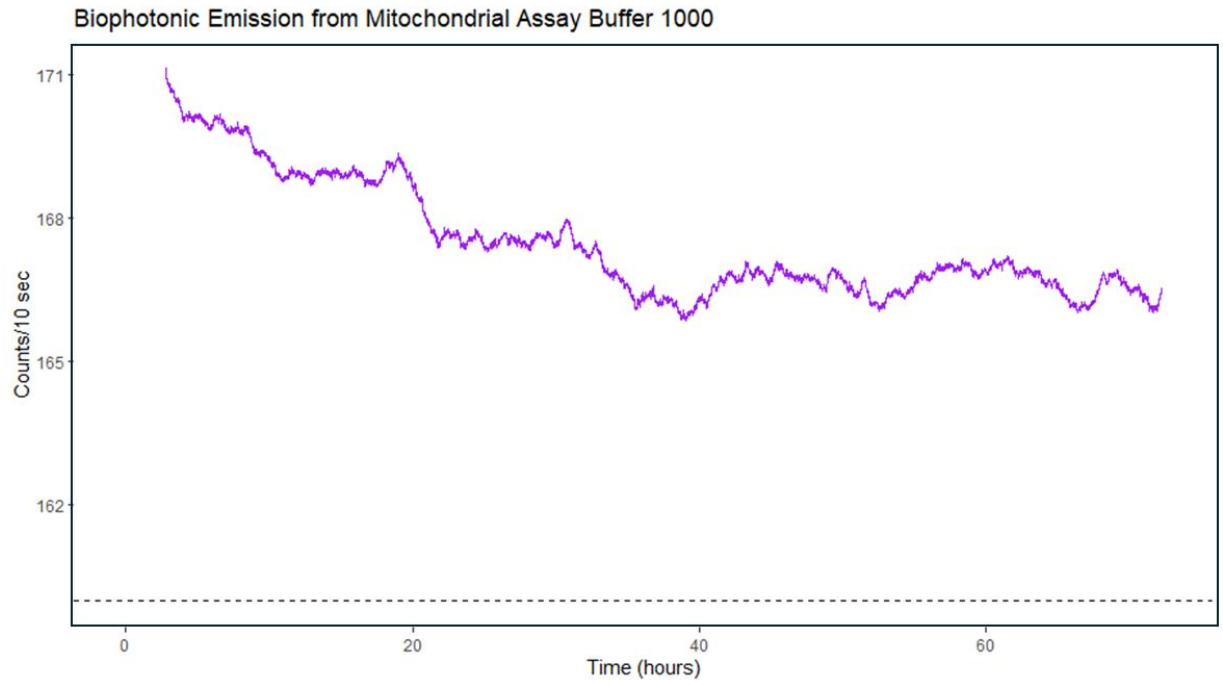

Figure 5.15: The recorded photon counts per 10 seconds emitted from MAB. MAB sample (3 mL) was kept in 35 mm ibidi dish in complete darkness for 24 hours to eliminate delayed luminescence effects. The dish was then positioned directly above an ultra-sensitive photomultiplier tube detector within a light-tight aluminium box for continuous 72-hour measurement of photonic emission. The graph shows photon emission from MAB samples (purple line; N=5) presented as rolling means using a 1000-point window to reduce noise in the signal. The dashed black line at y=160 represents the established background dark count rate (average photon counts per 10 seconds with no sample present).

5.2.6 Detection of biophotons from senescent MCF10A mitochondria

The biophotons emitted from isolated mitochondria from senescent MCF10A breast cells were recorded over 72 hours using the ultra-sensitive light detector to identify the primary means of non-chemical communication. A baseline (background noise) of 160 photons per 10 seconds was established. Figure 5.16 shows the smoothed rolling means for isolated senescent MCF10A mitochondria in MAB (N=5) and MAB alone (N=5), confirming the occurrence of biological biophotonic production. As demonstrated in Figure 5.17, the mean photon counts per 10 seconds from isolated mitochondria of senescent cells were significantly higher than those from MAB alone (9.10 vs 7.60 counts per 10 seconds ± 0.73; P = 0.0397). This difference indicates a measurable biophotonic emission from the senescent MCF10A mitochondria above the non-biological baseline.

To ensure consistency in our experiments and to provide a basis for comparing results across different biological repeats, the mitochondrial samples used in these experiments were characterised by quantifying their protein content. Using a standard Bradford protein assay, the average protein concentration in the isolated mitochondrial samples was determined to be 518.21 ± 138.39 µg/mL. This protein quantification serves multiple purposes: it confirms the consistency of the mitochondrial isolation procedure, enables the normalization of biophoton emission and oxygen consumption data, and provides a reference point for future studies.

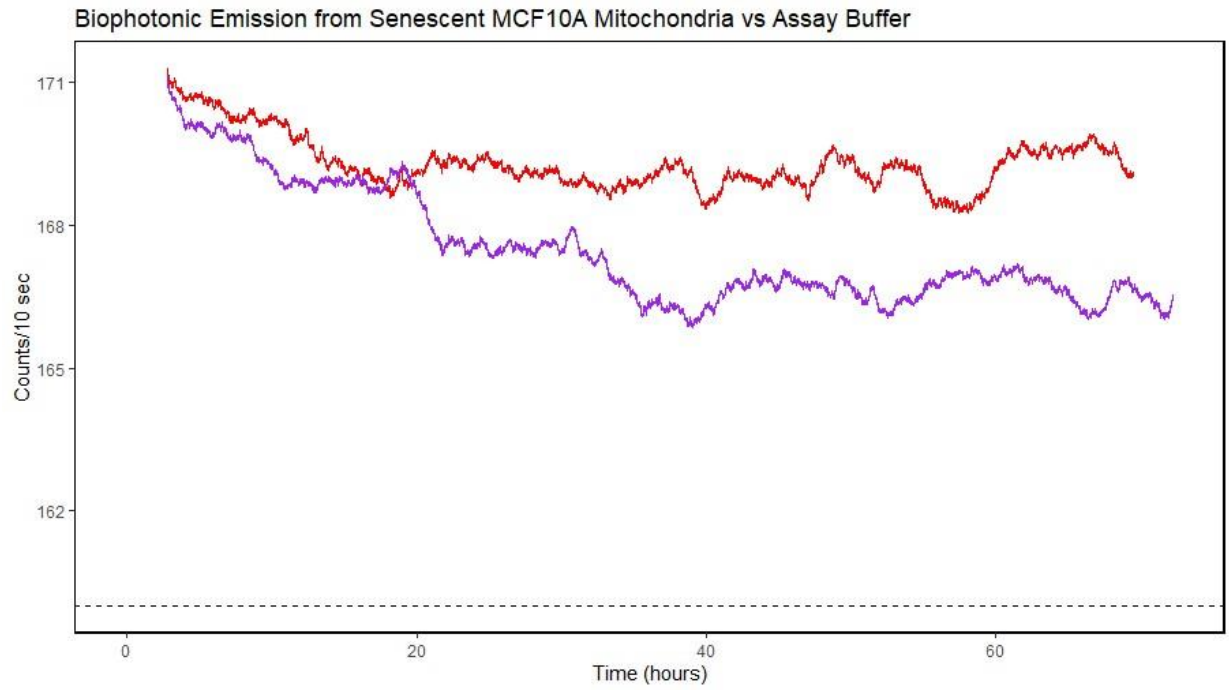

Figure 5.16: The recorded photon counts per 10 seconds emitted from mitochondria from senescent MCF10A cell. Mitochondria isolated from Dox-induced senescent MCF10A breast cells (in 3 mL MAB) were kept in a 35 mm ibidi dish in complete darkness for 24 hours to eliminate delayed luminescence effects. The dish was then positioned directly above an ultra-sensitive photomultiplier tube detector within a light-tight aluminium box for continuous 72-hour measurement of photonic emission. The graph shows photon emission from isolated mitochondria (red line; N=5) and MAB alone (purple line; N=5) presented as rolling means using a 1000-point window to reduce noise in the signal. The dashed black line at y=160 represents the established background dark count rate (average photon counts per 10 seconds with no sample present).

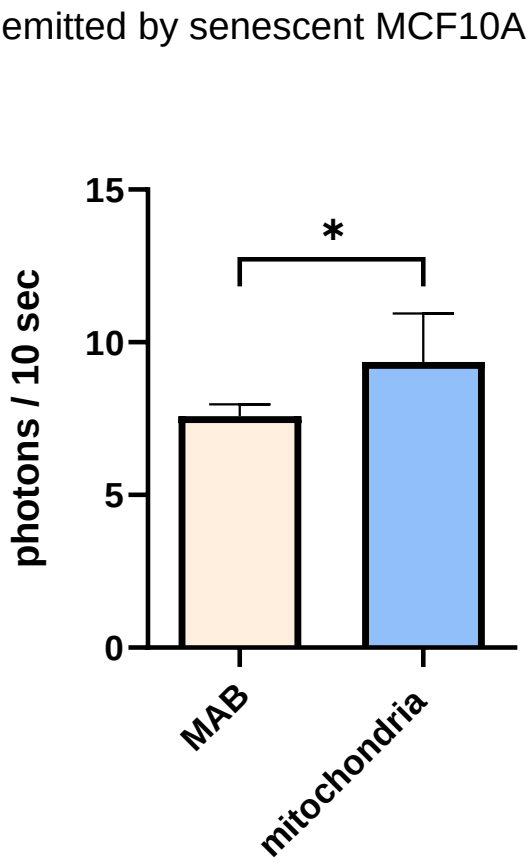

Figure 5.17: Emission of biophotons per 10 seconds from isolated mitochondria and MAB. Average photon counts were compared between mitochondria isolated from Dox-induced senescent MCF10A breast cells and MAB alone following 72-hour continuous measurement using an ultra-sensitive photomultiplier tube detector. Samples (3 mL) were kept in 35 mm ibidi dishes in complete darkness for 24 hours before measurement to eliminate delayed luminescence effects (N=5 independent biological repeats). Statistical significance was determined using Mann-Whitney U test. Data are presented as mean photon counts per 10 seconds ± SEM. * : $P < 0.05$.

5.3 Discussion

5.3.1 Photons recorded from mitochondria of senescent cells

In this chapter, I aimed to investigate non-chemical communication in mitochondria isolated from senescent cells. The primary objectives were to measure biophotonic emission from senescent mitochondria directly, demonstrate the existence of biophotonic communication, and explore the differential effects of non-chemical signalling during senescence compared to non-senescent states.

It has been hypothesised that the existence of non-chemical communication described in the literature (Mould et al., 2023) results from light (biophotons) emitted by mitochondria. Despite the challenge of detecting biophotons directly, I was able to confirm light emission by using an ultra-sensitive light detector. I recorded very low light emission (up to 1.86 photons per 10 seconds) from the mitochondria isolated from senescent MCF10A breast cells.

The methodological setup of this experiment was critical to differentiating delayed luminescence from biophotonic emission. As has been explained previously (Section 1.8), delayed luminescence is weak light emission induced by exposure to external light sources, and that emission can occur from seconds to several hours after light exposure (Cifra & Pospíšil, 2014; Scordino et al., 2014). Although delayed luminescence has been proposed to serve the purpose of communication (Fleiss & Sarkisyan, 2019), it does not appear to be spontaneous or produced by ROS, as in the way that biophotons are.

Lack of experimental control of delayed luminescence can be a barrier to research claiming to record biophotonic emission (Cifra & Pospíšil, 2014; Mould et al., 2024). Thus, different studies employ strict dark conditions to eliminate the delayed luminescence effect when measuring biophotons. For example, in a study by Kobayashi et al. (2009), who imaged diurnal changes in human UPE (biophotons) using a cryogenic charge-coupled device

camera, subjects were dark-adapted for 15 minutes before 20-minute imaging sessions in a darkroom (Kobayashi et al., 2009). Additionally, Ortega-Ojeda et al. (2018) measured the spectral distribution of UPE from the human hand using an electron multiplying, charge-coupled device sensor and liquid crystal tuneable filter. In their study, human participants wore a light-tight sleeve on the selected arm for at least 20 minutes prior to measurements in a darkroom with controlled temperature and humidity (Ortega-Ojeda et al., 2018). These tightly controlled dark conditions were crucial for accurately detecting the extremely weak biophotonic signals without interference from delayed luminescence. Thus, in this thesis, the isolated mitochondria from senescent cells were maintained in a dark box within the incubator (at 37°C with 5% CO_2) for 24 hours before being placed in the detector, which itself is located in a double darkroom (Figure 2.2), to eliminate the effect of delayed luminescence completely.

Detecting and quantifying biophotonic emission presents a significant challenge due to the extremely low photon emission rate, typically ranging from tens to a few hundred photons per second per cm^2 (Cifra & Pospíšil, 2014). Traditional detection methods, such as low-noise photomultiplier tubes and charge-coupled device cameras, have been employed for temporal and spatial visualization of biophotons. However, these methods have sensitivity and signal-to-noise ratio limitations when dealing with such low light signals (Mould et al., 2024). Two strategies were employed to overcome this obstacle, which are described below.

Firstly, isolated mitochondria from senescent cells were used for biophotonic emission detection. Since the main sources of biophotonic production are ROS and redox processes (Bókkon et al., 2010), and these processes mainly occur within the mitochondria, the biophotonic emission was measured specifically from isolated mitochondria rather than whole senescent cells to maximize the detected emission.

Secondly, an innovative and recently published technology was used; a recent study by Mackenzie et al. (2024) marks a significant advancement in biophotonic detection

instrumentation. They employed an ultra-sensitive light detection system placed in an ultra-dark lab to minimize noise and they utilized a photomultiplier tube design with a low count rate and wide active area to maximize sensitivity. Using this approach, Mackenzie successfully detected biophotons in growing mung beans, thereby providing compelling evidence for the intrinsic metabolic photon emission phenomenon (Mackenzie et al., 2024).

The core challenge in recording biophotons with such sensitive equipment is the ability to distinguish the weak biophotonic signals from other photon sources, such as environmental light or instrumentation noise. Thus, rigorous experimental setups are crucial, including the use of sealed, light-tight containers placed in pitch-black rooms with no external light sources. In the present study, I accounted for these parameters, by measuring and subtracting the background noise (160 photons per 10 seconds) and photon emissions from non-biological samples (7.58 photons per 10 seconds; Figure 5.15).

By using the innovative instrumentation developed and validated by Mackenzie et al. and by controlling for all sources of photonic noise and delayed luminescence, I was able to detect and quantify biophotonic emission from mitochondria from senescent cells. This approach not only verifies the reliability of the results but also contributes to the broader field of biophoton research because the feasibility of detecting these ultra-weak signals is demonstrated. Furthermore, the successful detection of biophotons in this study provides a solid foundation for interpreting future results related to non-chemical communication between biological systems. Any observed effects of non-chemical communication in later discussions can now be more confidently attributed to biophotonic emissions.

5.3.2 Non-chemical communication in senescence

Non-chemical communication between mitochondria isolated from senescent cells was demonstrated in this thesis. By replicating the experimental protocol described by Mould et al (2023), significant differences in the oxygen consumption rate in “unshielded” cuvettes, in comparison to “shielded” ones, were exhibited in mitochondria isolated from Dox-induced

senescent MCF10A (Figure 5.3), MCF7 (Figure 5.7) and A549 (Figure 5.11) cells, following antimycin treatment of the “treated” cuvette, where light exchange between these two cuvettes was possible (Mould et al., 2023).

In more detail, two fundamental changes were confirmed from the experimental results to establish non-chemical communication during senescence. Firstly, I observed a significant change in the oxygen consumption rate of mitochondria following the introduction of antimycin (Figure 5.2). Antimycin, a well-known complex III inhibitor, disrupts mitochondrial OXPHOS by binding to the Qi site of cytochrome b in complex III (cytochrome bc1 complex). This binding blocks the electron transfer from ubiquinol to cytochrome c, leading to inhibition of the mitochondrial respiration. As a result, antimycin treatment leads to decreased oxygen consumption, as the final electron acceptor (oxygen) in the electron transport chain can no longer receive electrons. Additionally, this blockage causes an accumulation of reduced electron carriers upstream of complex III, leading to increased electron leakage and ROS production (Kim et al., 1999; Turrens, 2003). This stressed mitochondrial population provides an ideal model for testing non-chemical communication. According to current theories, increased ROS levels are associated with enhanced biophotonic production (Pospíšil et al., 2014). Therefore, the antimycin-treated mitochondria of this study, with interrupted OXPHOS, should theoretically emit more biophotons.

Secondly, the experimental results demonstrate significant changes in the oxygen consumption rate between mitochondria of the “unshielded” and “shielded” cuvette post-antimycin induction in the “treated” cuvette. In particular, the oxygen consumption rate in the “unshielded” cuvette increased for mitochondria isolated from all three senescent models: breast non-cancer and breast and lung cancer cells (Table 5.2). This difference highlights the influence of light exchange between the “unshielded” and “treated” cuvettes in the mitochondrial function.

Since there is low photon emission from mitochondria isolated from senescent cells, the non-chemical communication between “unshielded” and “treated” cuvette is attributed to

biophotons. Additionally, the experiments of this thesis were conducted in “dark” conditions to eliminate potential confounding variables and ambient light influences (Section 2.17) (Mould et al., 2023). These dark parameters ensured that any changes in mitochondrial oxygen consumption rate in the “unshielded” cuvettes could solely be attributed to changes occurring in the “treated” cuvette post-antimycin, independent from external factors.

It is important to note that, in the past, research findings claiming non-chemical cellular communication pathways have encountered scepticism and criticism because of flawed experimental setups. For example, Potapovich and Kostyuk (2021) supported the existence of biophotons in living organisms by claiming non-chemical signals from cellular models with increased oxidative stress post-duroquinone treatment (Potapovich & Kostyuk, 2021). However, Mould et al. (2022) revisited these claims by replicating Potapovich and Kostyuk's experiments, and they found that although the oxidative duroquinone-induced stress indeed led to significant cell death in neighbouring detector cells, this effect was dependent on volatility of the solvent used to dissolve the induction drug. Specifically, the use of a less volatile solvent negated the observed cell death, indicating that the original findings may have been influenced by volatile solvent-based transmission rather than light-based non-chemical signalling (Mould et al., 2022). Taking this into account for the experimental setup of this thesis, parafilm was used to shield all cuvettes containing the isolated mitochondria to avoid confounding variables of potential gas exchange (Section 2.17). This experimental design provided a more controlled environment and ensured that any effect recorded did not result as a consequence of volatile transmission.

In summary, non-chemical communication between mitochondria isolated from senescent cells was confirmed in multiple cell lines (MCF10A, MCF7, and A549), with the observed changes in oxygen consumption rates in the "unshielded" cuvettes, coupled with optimised experimental setup - including dark conditions and parafilm sealing to prevent volatile transmission - to strongly suggest that biophotons mediate this communication. These

findings contribute significantly to the field of biophoton research and provide new insights into understanding the complex interactions between mitochondria from senescent cells.

5.3.3 Potential mechanism of biophotonic mitochondrial communication

Biophotonic communication in mitochondria can potentially offer new insights regarding how these organelles coordinate their activities across the cell. Several mechanisms have been proposed for how this communication might occur.

Firstly, the role of ROS in biophotonic production cannot be overlooked. Mitochondria are a major source of ROS in cells, and these ROS can interact with biomolecules to generate electronically excited species, which subsequently emit biophotons upon returning to their ground state (Figure 1.5; Pospíšil et al., 2019). This process could serve as a mechanism for translating metabolic activity into biophotonic signals. My experiments using antimycin to interrupt OXPHOS and induce oxidative stress provide support for this mechanism, as changes in oxygen consumption rates were observed that could be attributed to increased biophotonic emission.

One of the primary mechanisms for how distant mitochondria can communicate via biophotons has been proposed by Thar and Kuhl (2004). They suggested that filamentous mitochondria, having a higher refractive structure compared to the surrounding cytoplasm, could act as “optical waveguides”. This morphological property could allow the directed transmission of biophotons along the mitochondrial network. The mitochondrial reticulum, in conjunction with microtubules, could form a continuous network that could guide electromagnetic radiation, potentially facilitating long-range communication between distant mitochondria within the cell (Thar & Kühl, 2004). Thar and Kuhl (2004) also described mitochondria as a “multi-layer optical system” with alternating refractive indices, particularly in their metabolically active state. This dynamic structure could potentially support coherent propagation and even amplification of that light. This mechanism could allow for the

amplification of low biophotonic signals, potentially increasing the range and efficacy of biophotonic communication (Thar & Kühl, 2004).

Adding to this concept of long-distance mitochondrial communication, Kurian et al. (2017) proposed a mechanism for how biophotons might travel within microtubules, which are cylindrical proteins in the cytoplasm and play a role in regulating mitochondrial dynamics (Moore & Holzbaur, 2018). Kurian et al. suggested that microtubules could act too as "quantum optical waveguides" that are capable of transmitting light signals over long distances within the cell. According to their proposed model, biophotons, possibly generated by mitochondrial metabolic processes, could excite the uniquely arranged aromatic amino acids, especially tryptophan, within tubulin proteins. This excitation could then propagate along the microtubule structure and could be transferred between neighbouring tryptophan residues (Kurian et al., 2017). This quantum coherent energy transfer mechanism could allow efficient propagation of light-based signals along the microtubule network, potentially connecting distant mitochondria within the cell.

The energy transfer mechanism proposed by Kurian et al. aligns with the earlier work of Craddock et al. (2014), who also suggested that the arrangement of aromatic amino acids (such as tryptophan or tyrosine) in tubulin, the microtubule constituent protein, could support such quantum effects (Craddock et al., 2014). The close association of microtubules and tubulin with mitochondria could potentially facilitate the exchange of biophotonic signals in between these structures within the cells. However, both these theories and the mechanism proposed by Thar and Kuhl describe models of mitochondrial communication over distances within intact cells. In the experimental setup of this thesis, the mitochondria, floating free within the MAB, were communicating outside of the cellular environment, thus making these proposed intracellular mechanisms less likely to be the primary mode of mitochondrial biophotonic communication in the observations of this thesis. It is also likely that mitochondria can act as an "optical system" even in isolation. This distinction highlights the

need for additional theories or modifications to existing models examining mitochondria outside of the cell, to explain the non-chemical communication observed between isolated mitochondria.

At a molecular level, mitochondria contain numerous chromophores capable of absorbing and emitting light across a broad spectrum. Biophotons, which range within the 200-800 nm spectrum (Cifra & Pospíšil, 2014), can potentially interact with various cellular components. The electron transport chain components, such as cytochromes, ubiquinone, and NADPH, have absorption spectra spanning from UV to visible light (Nunn et al., 2020). Additionally, flavins and opsins can absorb light in the blue and green spectral regions (Hamblin, 2017). These diverse chromophores could potentially act as both sources and receivers of biophotons within the cellular and mitochondrial networks, facilitating a complex system of light-based communication.

In the specific context of red to NIR light, several mitochondrial components have been identified as potential chromophores. For example, CCO, located in the inner mitochondrial membrane, is widely recognized as the principal photoreceptor for NIR light in the range of 600-850 nm. Absorption of these wavelengths by CCO can potentially increase electron transport chain activity, leading to enhanced ATP production and altered metabolic homeostasis (Hamblin, 2016b; Karu, 2008). Recent research has also highlighted the role of nanoscopic interfacial water layers within and around mitochondria in NIR light absorption (Sommer et al., 2015). These water layers, particularly near hydrophilic surfaces, may be modulated by NIR light, potentially affecting the efficiency of the ATP synthase motor (Sommer et al., 2015). Furthermore, the inner and outer mitochondrial membranes, containing various proteins and lipids, can absorb NIR light, potentially influencing membrane potential, permeability, and the function of membrane-bound proteins (Passarella & Karu, 2014). This chapter's detection of low biophotonic emission from senescent mitochondria supports the involvement of these chromophores in mitochondrial

non-chemical communication, although the specific contributions of each component remain unknown.

While the mechanisms discussed are theoretically plausible, direct experimental evidence for functional biophotonic communication in mitochondria remains limited. The results of this chapter, including the detection of weak biophotonic emission from senescent mitochondria and observed non-chemical communication between mitochondrial populations, contribute to evidence supporting the existence of biophotonic communication. However, the exact mechanism or combination of mechanisms involved is yet to be fully determined.

Future research should focus on developing techniques to detect and manipulate biophotonic emissions in living cells. Such studies could provide valuable insights into the role of biophotonic communication in cellular ageing and related pathologies, potentially opening new avenues for understanding and addressing age-related diseases.

5.3.4 Different effects of non-chemical communication during senescence

This chapter also explored the differential effects of non-chemical communication during senescence. As demonstrated in Mould et al., 2023, previous research has shown significant changes in the oxygen consumption rate of non-senescent models, particularly in MCF10A non-cancer and MCF7 cancer breast cells, as observed in unshielded cuvettes. In addition to that, non-chemical signalling experiments were also undertaken on senescent and non-senescent A549 lung cancer cells (Figure 5.12) to support these findings further. When the oxygen consumption rate of isolated mitochondria was compared between “unshielded” results from non-senescent and senescent populations of all three cell lines (MCF10A: Figure 5.5, MCF7: Figure 5.9 and A549: Figure 5.13), significant variation between cell lines were observed. This suggests that during senescence, the effect of non-chemical communication is different compared to non-senescent cells of the same cell line.

Given that the observed and recorded means of this communication are biophotons, as described previously (Section 5.3.1), that leads to the conclusion that there exists a biophotonic mitochondrial communication during senescence, influencing how cells communicate with each other across varying states, and thus, accepting this part of the hypothesis set at the beginning of this thesis.

Biophotonic emission originates primarily from mitochondria, which play a crucial role in cellular dynamics (Volodyaev et al., 2023), and as explained in Section 5.3.3, ROS serving as the principal driver of such emission (Cifra & Pospíšil, 2014). In mitochondrial biology, ROS has a central role in influencing mitochondrial-nuclear signalling and epigenetic regulations (Van Wijk & Van Wijk, 2023). These dynamics are closely related to cellular senescence, where alterations in ROS levels and changes in mitochondrial homeostasis are characteristics. Additionally, as mentioned in Section 1.7.1, ROS levels not only contribute to senescence induction but are also responsible for maintaining this cellular phenotype (Correia-Melo & Passos, 2015; Miwa et al., 2022; Ziegler et al., 2015). This phenomenon is also observed in the results of this thesis, where the oxygen consumption of isolated mitochondria from the “shielded” cuvettes, indicating mitochondria unaffected by external influences or treatments, exhibited a significant increase over time in senescent cells compared to non-senescent cells (Figures 5.6 and 5.10), confirming once more the increased metabolic profile of senescence in both cancer and non-cancer cell models.

It is important to note that A549 lung cancer cells exhibited a different metabolic pattern during senescence, compared to the other cell lines. Specifically, mitochondria from A549 cells did not show a statistically significant alteration in oxygen consumption rate during senescence. While other indicators of altered mitochondrial homeostasis were observed in this cell line during senescence, the oxygen consumption rate did not align with the patterns seen in the other senescent models examined in this thesis. This could be attributed to the inherent complexity of senescence, as discussed in Section 4.3. Additionally, it's worth noting that the difference in oxygen consumption rate for A549 cells approached, but did

not reach, statistical significance (Figure 5.14; P = 0.072). This suggests that increasing the number of biological replicates in future experiments might potentially reveal a significant difference, aligning the A549 results more closely with the other cell lines studied.

The results on mitochondria homeostasis during senescence (Chapter 4) demonstrated a highly significant change in mitochondrial function and ROS levels in Dox-induced senescent cell models. The findings, demonstrating distinct changes in oxygen consumption rates and non-chemical communication between senescent and non-senescent states, can be attributed to the differential impact of ROS production and mitochondrial dynamics during senescence. This suggests a potential link between ROS and the non-chemical signalling changes, which appear to be driven by differential biophotonic production during senescence. Therefore, I suggest that the variance in biophotonic production may contribute to the alterations in non-chemical communication observed during senescence, which is driven by ROS-mediated changes in mitochondria.

However, while the experimental setup in this study can confirm the existence of non-chemical biophotonic communication and demonstrate a differential effect of such communication during senescence, several limitations and gaps remain in our understanding of why this effect might be cell origin-dependent. For instance, the observed increase in oxygen consumption rate in mitochondria from cancer MCF7 cells contrasts with the decrease demonstrated in mitochondria from non-cancer MCF10A cells. This phenomenon raises questions about the precise mechanisms governing this non-chemical communication and whether that is origin-dependent. Mould et al. acknowledged the origin-specific nature of non-chemical communication, highlighting that the effect of such communication was increased in breast cancer cells (MCF7) compared to breast non-cancer cells (Mould et al., 2023). Future studies should employ a cellular model of non-cancer lung origin to establish a second cancerous-non-cancerous comparison of non-chemical communication. This will increase the evidence of differential biophotonic emission and non-chemical signalling during cancer, firstly observed in Mould et al. (2023).

Furthermore, there are numerous possibilities regarding why the non-chemical communication effect is altered during senescence. One possible scenario is that changes in biophotonic production, influenced by increased ROS levels during senescence, alter the "message" (i.e. different wavelengths of emitted biophotons) or increase the signal (i.e. higher biophotonic production) being communicated. Alternatively, mitochondria in the "unshielded" cuvettes may be dysfunctional due to senescence and may fail to receive the signal. For example, proteins that act as chromophores inside and on the mitochondrial membrane of mitochondria from senescent cells might not interact with the light signal. On the other hand, they may also be overly sensitive to it, resulting in differential responses in oxygen consumption over time. Moreover, considering that biophotons exhibit a range of wavelengths, from UV to NIR light (Cifra & Pospíšil, 2014), the scenario that the wavelength of biophotons during senescence may vary, leading to differences in the conveyed message, is possible. For instance, different light wavelengths have been reported to exhibit different cellular responses cells, such as with red-NIR light promoting proliferation (Hu et al., 2007), while blue-green light inhibits it (Wang et al., 2017b). Although it is essential to recognise that these extracellular light effects are parameter-dependent, the wavelengths of the biophotons emitted remain unknown, and the technology to measure them is not readily available. In conclusion, to tackle the question about the mechanism of biophotonic communication, further research is needed to examine the specific parameters of non-chemical communication and to characterise the wavelength and frequency of biophotonic production during senescence.

5.3.5 Potential biophotonic applications of senescence-associated conditions and ageing

The importance of biophotonic emission in detecting signature signals from diseased organisms holds significant potential for applications in disease diagnosis. Over the years, research has investigated the influence of internal factors, such as age and diseases, on human biophotonic emissions (Zapata et al., 2021). Since biophotonic production is mainly

influenced by oxygen consumption, ROS formation, and excited state formation, it is theoretically possible to utilise biophotonic emission to monitor an organism's oxidative metabolism and stress (Rastogi & Pospíšil, 2010), and many researchers have proposed biophotons as an *in vivo*, non-invasive diagnostic for various diseases and stress-related disorders (Du et al., 2023; Zapata et al., 2021). However, the accuracy and reliability of these measurements remain a subject of debate within the scientific community.

A recent example of the application of biophotonic emission in disease diagnosis is Alzheimer's disease. Sefati et al. (2024) reported detecting biophotons from the hippocampus of rat brains and found significant correlations between Alzheimer's disease, memory decline, oxidative stress, and biophotonic production. They suggested that biophotons produced from neural tissue could provide insights for screening, detecting, diagnosing, and classifying Alzheimer's disease and other neurodegenerative diseases. Interestingly, the researchers even proposed the development of a semi-invasive brain-computer interface photonic chip for monitoring brain activity and diagnosing Alzheimer's disease (Sefati et al., 2024). While these findings and proposals are intriguing, it's important to note the methodological challenges in such studies. Sefati et al. used a photomultiplier tube to detect biophotonic emissions, in a carefully controlled dark environment to minimize external light interference. They also took steps to minimize background noise and the petri dish containing the hippocampal sample was placed in the darkroom for 10 minutes before measurements to minimize detection of delayed luminescence.

Biophotonic emission could also serve as a potential non-invasive tool for detecting ageing and age-related physiological changes. Studies from Gabe et al. (2013) and Zhao et al. (2016) have shown a relationship between biophotonic production and chronological age, suggesting that biophotonic emission could indicate biological age (Gabe et al., 2014; Zhao et al., 2016). Both studies used a photomultiplier tube to measure the biophotonic emission from the skin of the human participants, and both controlled for delayed luminescence by either leaving the participants in a dark room for 15 minutes (Gabe et al., 2013) or by having

the participants cover their hands with lightproof black gloves for 20 minutes (Zhao et al., 2016). In addition, *in vivo* studies of human skin reported regional-dependent biophotonic production with higher intensity of biophotonic production in areas of the skin with higher oxidative stress and more sensitivity to age-associated changes, such as wrinkle formation (Tsuchida & Kobayashi, 2020). This time, the researchers used a highly sensitive cooled charge-coupled device camera and allowed human subjects to rest in a dark room for 15 minutes before measurement, to prevent delayed luminescence effects.

While these studies attempted to control for delayed luminescence, the effectiveness of their methods in eliminating this phenomenon is a significant challenge. The short dark adaptation periods used may not be sufficient to fully eliminate delayed luminescence, especially from deeper tissues. Additionally, the sensitivity and specificity of the detection methods used in these studies for distinguishing true biophotonic emissions from other sources of low-level light remain uncertain. And although the reported results from these studies are promising, the clinical application of biophotonic emission as a diagnostic tool for ageing or age-related changes has not yet been clinically employed. This is partly due to the difficulty in controlling for delayed luminescence in human and general animal models *in vivo*, as well as the challenges in standardizing measurements across different individuals and environmental conditions.

Combining the literature with this thesis's novel results, the differential effect of biophotonic communication observed during senescence may provide valuable insights into age-related processes. The difference in non-chemical communication effects during senescence presented, possibly due to differential biophotonic production, supports the hypothesis that changes in biophotonic emission during senescence contribute to alterations in cellular communication. Considering that senescence is a biochemical biomarker for predicting human ageing (Levine, 2013), the findings of this thesis could contribute to measuring senescence levels and predicting ageing-related changes. This finding opens avenues for utilising biophotonic emission as a biomarker for assessing age-related changes and

predicting age-associated diseases by exploring the role of biophotonic communication in senescence.

Furthermore, as discussed in detail in Chapter 1, senescence is also observed in a range of diseases (Section 1.3.4), and induction of senescence can contribute to disease management, such as in the case of cancer (Section 1.3.3). Recording the biophotonic communication of cells, especially considering that there is a distinct effect of that communication during senescence, suggests a potential application in detecting diseases such as heart and neurodegenerative conditions (McHugh & Gil, 2018). Additionally, since anti-cancer therapies employ senescence-induction drugs for delaying the progression of cancer (von Kobbe, 2019), monitoring non-invasively the biophotonic communication of the targeted organisms can record the presence of senescence or non-senescence and reveal insights into whether the treatment is successful or can be used in clinical trials for non-invasive evaluation of the efficacy of these drugs.

Furthermore, future research ought to characterise the nature of this biophotonic signal, which is different between senescence and non-senescence cells. By identifying the properties, such as wavelength and intensity, of that emission, one could mimic that signal extracellularly and potentially manipulate the cells non-invasively. This would provide a new approach to senescence-induction or senolytic treatments according to the needs of each patient. Although that proposal is a far-reaching goal, the understanding that non-chemical signalling is different among senescent cells marks the initial steps towards considering that clinical approach.

5.3.6 Conclusion

In conclusion, the exploration of non-chemical communication during senescence offers new insights into the mechanisms of cellular interactions and signalling pathways. This chapter has demonstrated the existence of biophotonic emission and signalling from

mitochondria isolated from senescent cells. The differential effects observed in oxygen consumption rates between senescent and non-senescent populations, as a result of differential biophotonic communication, further highlight the complexity of this phenomenon and its potential implications in ageing-related diseases and conditions. These senescence-associated changes could be used by future studies aiming to employ non-chemical communication as a diagnostic tool and therapeutic target in managing age-related disorders.

Chapter 6 : Effect of External Near-Infrared Light on Senescence

Chapter 6 is an extended version of the published paper "*Selective induction of senescence in cancer cells through near-infrared light treatment via mitochondrial modulation"* (Kalampouka et al., 2024).

6.1 Aims

Photobiomodulation (PBM), utilising non-ionizing light in the visible and NIR spectrum, has been suggested as a potential method for enhancing tissue repair, reducing inflammation, and possibly mitigating cancer-therapy-associated side effects. In this chapter, the effect of PBM (734 nm NIR light) on cellular senescence, in both cancer and non-cancer cellular models was investigated. By examining the cellular and mitochondrial mechanisms and responses to NIR light exposure, this research aimed to increase understanding of how NIR light and PBM can manipulate cellular behaviour, with potential implications for cancer treatment.

6.2 Results

6.2.1 LED light characterization

The first aim of this chapter was to characterize the LED in terms of wavelength and thermal effect. The LED light's maximum wavelength was 734 nm (Figure 6.1A), which lies within the spectrum of NIR (de Sousa, 2017; Pooam et al., 2021). No significant thermal effect (Figure 6.1B) was recorded during LED light treatment at a 40 mm distance on any media used.

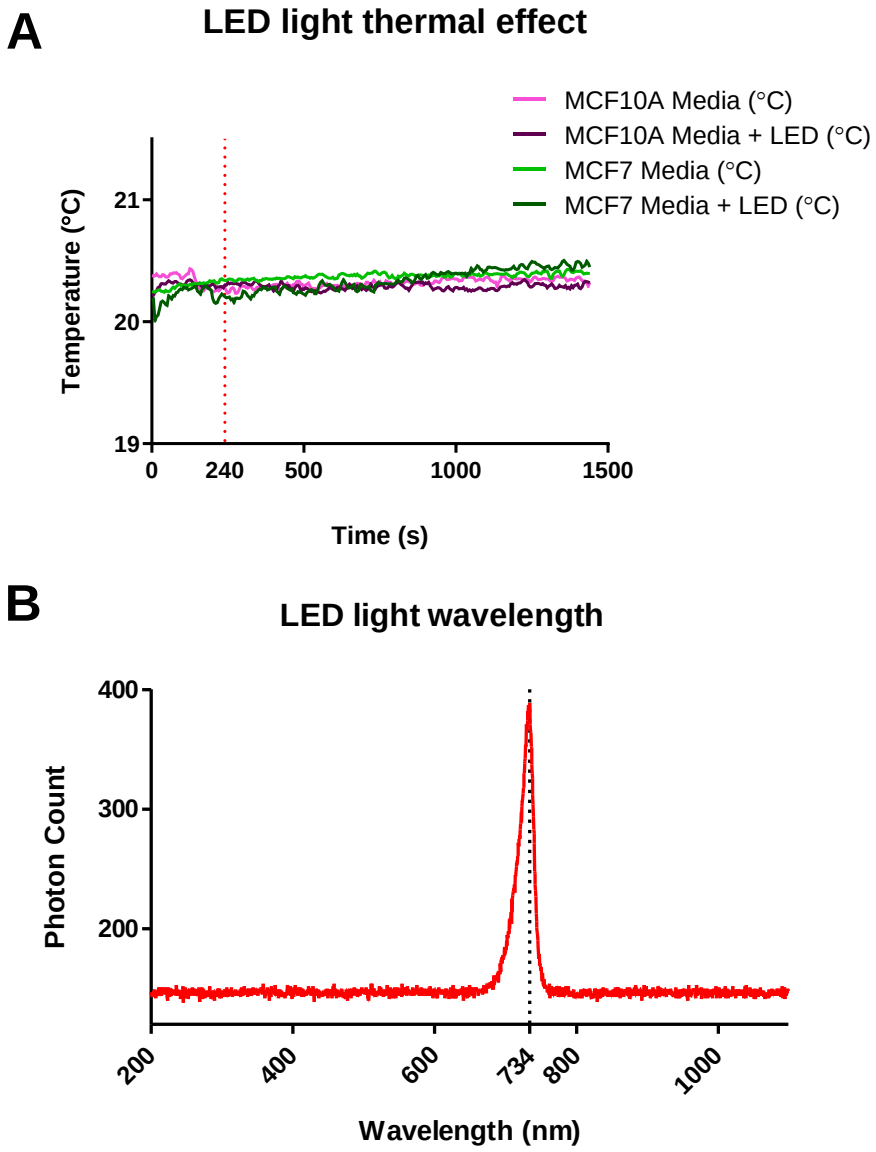

Figure 6.1: LED light characterisation. (A) Thermal measurements of cancer (MCF7, A549) and non-cancer (MCF10A, IMR-90) cell media during 1,440 seconds of monitoring. LED exposure period (240-1,440 seconds) showed no significant temperature changes in any media type tested (N=3 independent repeats per media type). Temperature was recorded using a FireSting optical temperature sensor. (B) Spectral characterization of the LED light source revealed peak emission at 734 nm, confirming near-infrared wavelength classification. Measurements were taken using a high-resolution UV-NIR spectrometer with the LED array positioned 40 mm from the detection point, yielding a power output between 0.328 to 0.420 mW (Fluence ≈ 63 mJ/cm^2, Power density ≈ 0.05 mW/cm^2).

6.2.2 NIR light treatment increases the levels of senescence in cancer cells

The effect of NIR light treatment was examined in control and senescent cancer population. NIR light increases the senescence effect in control MCF7 breast cancer cells by 10.01% ± 5.36 (Figure 6.2A; P = 0.0081) and in A549 lung cancer cells by 14.45% ± 5.54 (Figure 6.3A; P = 0.0026), while in 0.25 μM Dox treated MCF7 cells by 13.72% ± 6.03 (Figure 6.2B; P = 0.0081) and in A549 cells by 203.20% ± 63.19 (Figure 6.3B; P = 0.0026), as measured by β-gal activity using the CellEvent fluorescent stain. Significant interactions between Dox and NIR light treatments were observed only in the A549 cell line among the two tested (Interaction; MCF7: P = 0.6510, A549: P = 0.0080).

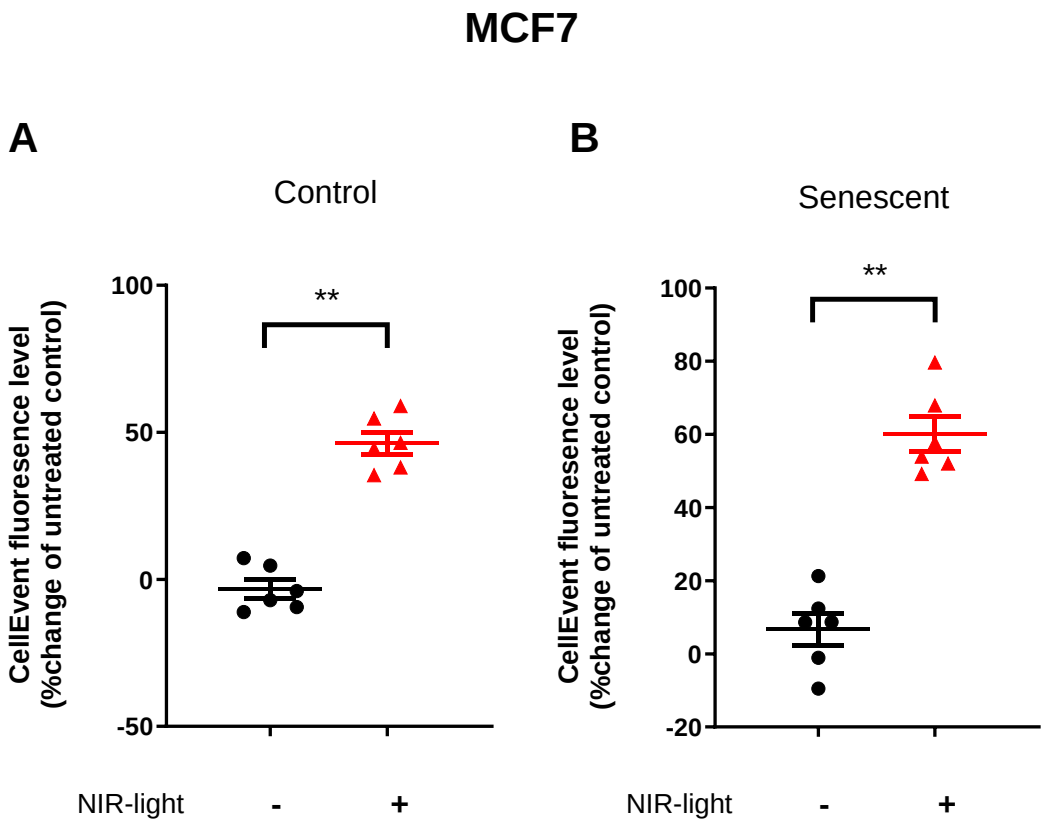

Figure 6.2: The effect of NIR light on levels of senescence in MCF7 cells – Flow cytometry. MCF7 breast cancer cells were cultured in either media alone (A; control population) or treated with 0.25 μM Dox for 24 hours (B; senescent population), followed by 6 days in drug-free media. In parallel, populations were exposed to either no light or daily 20-minute NIR light treatment (734 nm) for 6 days. Senescence levels were quantified by flow cytometry in live cells following CellEvent staining and expressed as a percentage change from untreated control (N=6 independent biological repeats). Statistical significance was determined using two-way ANOVA with post-hoc Bonferroni testing. Data are presented as mean changes compared to untreated control ± SEM. ** : $P \leq 0.01$.

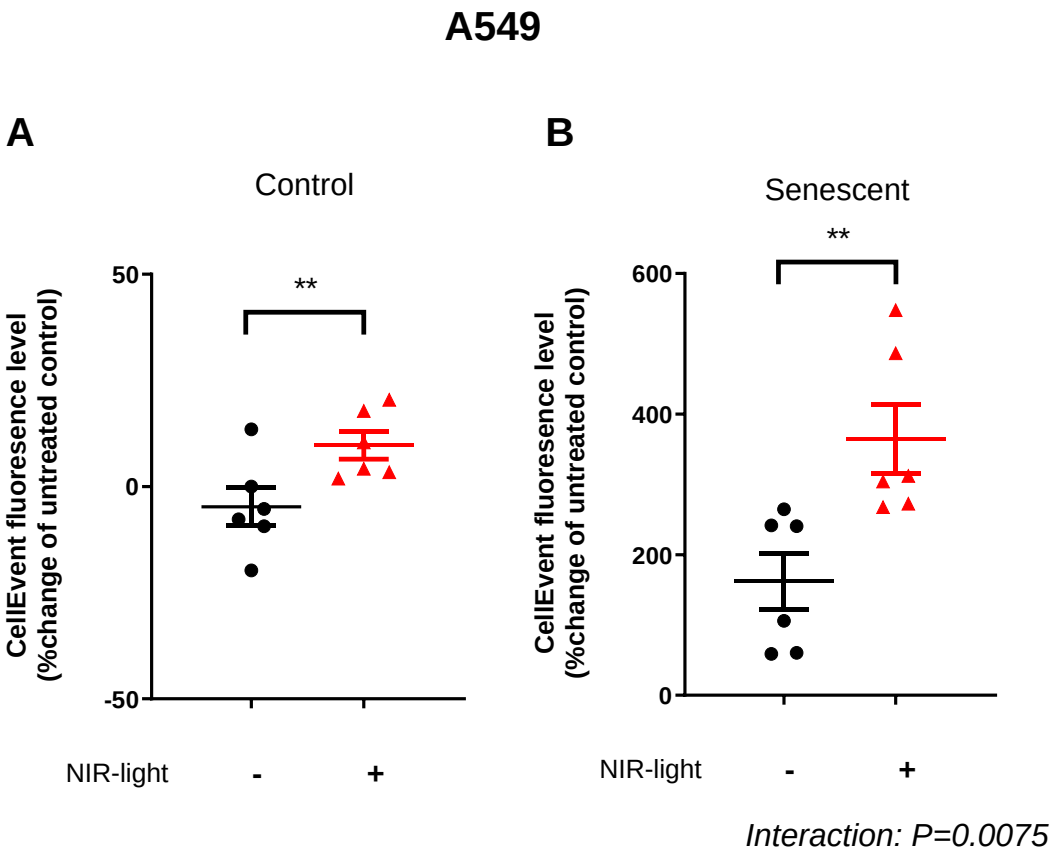

Figure 6.3: The effect of NIR light on levels of senescence in A549 cells – Flow cytometry. A549 lung cancer cells were cultured in either media alone (A; control population) or treated with 0.25 μM Dox for 24 hours (B; senescent population), followed by 6 days in drug-free media. In parallel, populations were exposed to either no light or daily 20-minute NIR light treatment (734 nm) for 6 days. Senescence levels were quantified by flow cytometry in live cells following CellEvent staining and expressed as a percentage change from untreated control (N=6 independent biological repeats). Statistical significance was determined using two-way ANOVA with post-hoc Bonferroni testing. Data are presented as mean changes compared to untreated control ± SEM. ** : P ≤ 0.01.

6.2.3 NIR light treatment doesn't affect the levels of senescence in non-cancer cells

The effect of the same NIR light treatment was examined in control and senescent non-cancer population. In contrast to cancer population, non-cancer cell lines MCF10A (Figure 6.4; P = 0.9725) and IMR-90 (Figure 6.5; P = 0.0727) were unaffected in terms of senescence induction. No significant interactions between Dox and NIR light treatments were observed (Interaction; MCF10A: P = 0.9190, IMR-90: P = 0.5420; Figure 6.2).

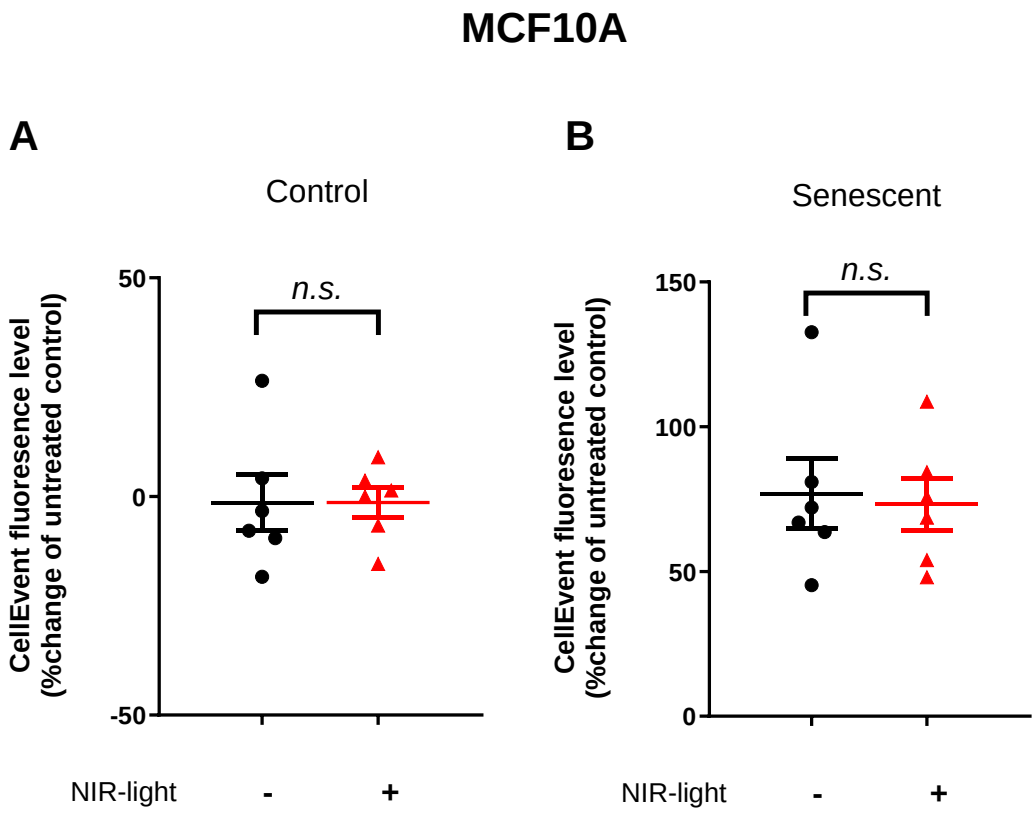

Figure 6.4: The effect of NIR light on levels of senescence in MCF10A cells – Flow cytometry. MCF10A breast cells were cultured in either media alone (A; control population) or treated with 0.25 μM Dox for 24 hours (B; senescent population), followed by 6 days in drug-free media. In parallel, populations were exposed to either no light or daily 20-minute NIR light treatment (734 nm) for 6 days. Senescence levels were quantified by flow cytometry in live cells following CellEvent staining and expressed as a percentage change from untreated control (N=6 independent biological repeats). Statistical significance was determined using two-way ANOVA with post-hoc Bonferroni testing. Data are presented as mean changes compared to untreated control ± SEM.

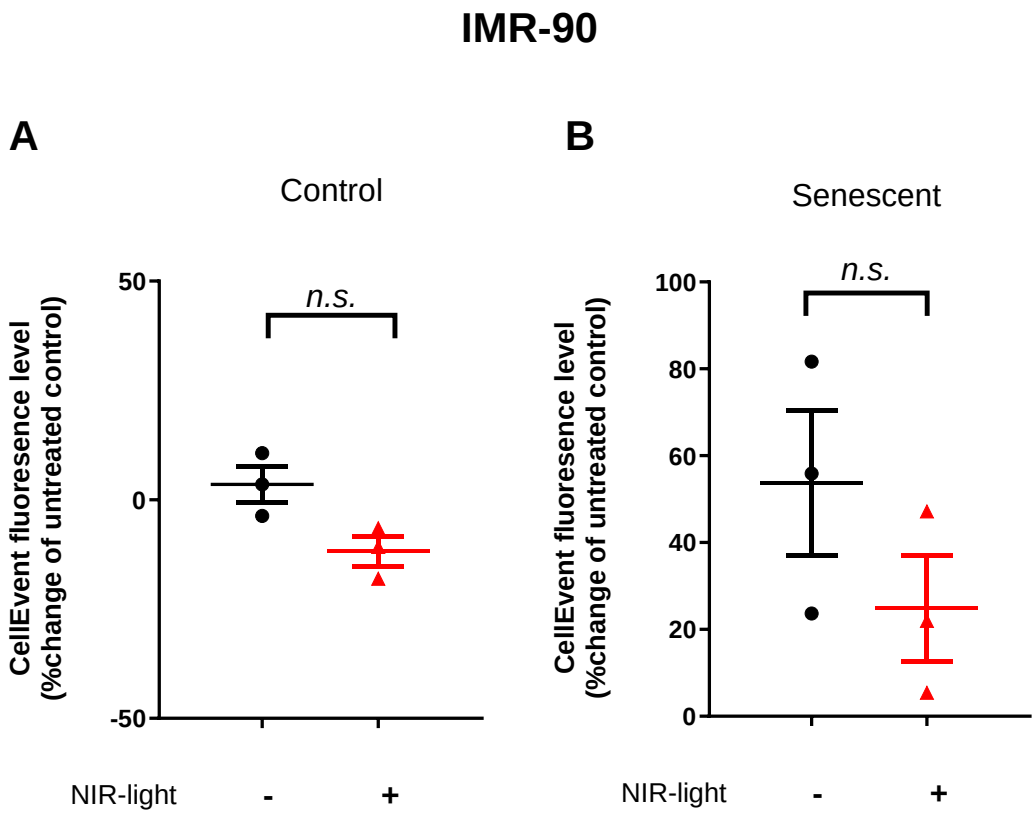

Figure 6.5: The effect of NIR light on levels of senescence in IMR-90 cells – Flow cytometry. IMR-90 lung fibroblast cells were cultured in either media alone (A; control population) or treated with 0.25 μM Dox for 24 hours (B; senescent population), followed by 6 days in drug-free media. In parallel, populations were exposed to either no light or daily 20-minute NIR light treatment (734 nm) for 6 days. Senescence levels were quantified by flow cytometry in live cells following CellEvent staining and expressed as a percentage change from untreated control (N=3 independent biological repeats). Statistical significance was determined using two-way ANOVA with post-hoc Bonferroni testing. Data are presented as mean changes compared to untreated control ± SEM.

6.2.4 NIR light treatment modulates ROS in MCF7 cancer cells

The mitochondria of MCF7 breast cancer and MCF10A breast non-cancer cells were further assessed regarding NIR light treatment for both states of cell populations (control and Dox treated). For the MCF7 cells, the results showed a significant increase ($P = 0.0158$) in cellular ROS production after NIR light treatment, with a 36% ± 11.30 increase in control cells (Figure 6.6A) and 53.90% ± 37.45 in 0.25 μM Dox treated cells (Figure 6.6B).

For the MCF10A cells, there was no significant difference in ROS levels post-NIR light treatment ($P = 0.9353$; Figure 6.7). As expected, Dox alone led to significant changes in ROS levels in both cancer and non-cancer cells (MCF7: 130.20 ± 22.50, $P < 0.0001$; MCF10A: 135.80 ± 37.90 $P < 0.0001$). No Dox – NIR light significant interaction was observed regarding ROS levels (MCF7: $P = 0.2504$, Figure 6.6; MCF10A: $P = 0.7449$; Figure 6.7).

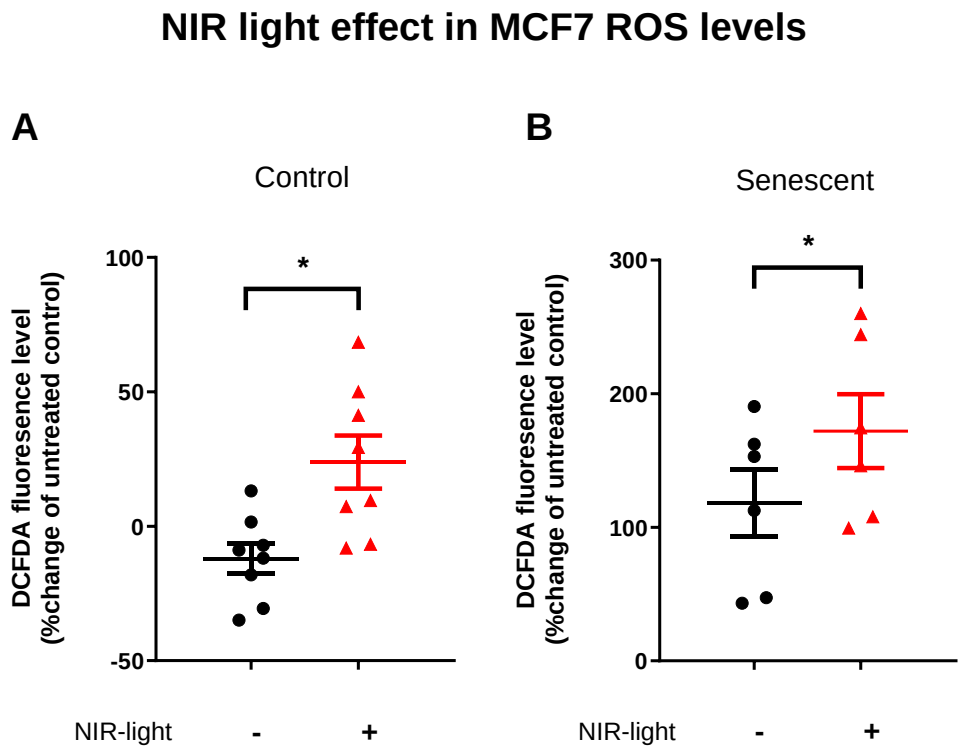

Figure 6.6: The effect of NIR light on cellular ROS production – Flow cytometry. MCF7 breast cancer cells were cultured in either media alone (A; control population) or treated with 0.25 μM Dox for 24 hours (B; senescent population), followed by 6 days in drug-free media. In parallel, populations were exposed to either no light or daily 20-minute NIR light treatment (734 nm) for 6 days. ROS levels were quantified by flow cytometry in live cells following DCFDA staining and expressed as a percentage change from untreated control (N=8 independent biological repeats). Statistical significance was determined using two-way ANOVA with post-hoc Bonferroni testing. Data are presented as mean changes compared to untreated control ± SEM. * : $P \leq 0.05$.

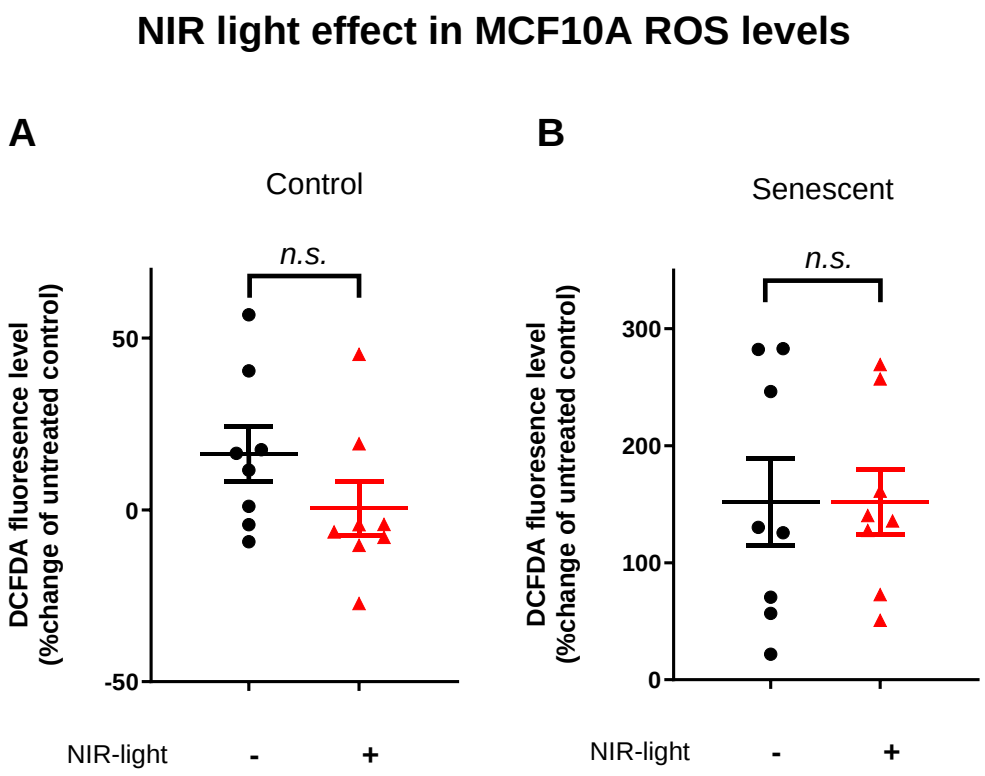

Figure 6.7: The effect of NIR light on cellular ROS production – Flow cytometry. MCF10A breast cells were cultured in either media alone (A; control population) or treated with 0.25 μM Dox for 24 hours (B; senescent population), followed by 6 days in drug-free media. In parallel, populations were exposed to either no light or daily 20-minute NIR light treatment (734 nm) for 6 days. ROS levels were quantified by flow cytometry in live cells following DCFDA staining and expressed as a percentage change from untreated control (N=8 independent biological repeats). Statistical significance was determined using two-way ANOVA with post-hoc Bonferroni testing. Data are presented as mean changes compared to untreated control ± SEM.

6.2.5 NIR light treatment does not affect mitochondrial Ca^{2+} levels

The mitochondrial Ca^{2+} levels of MCF7 breast cancer and MCF10A non-cancer breast cells, exposed to either control or 0.25 μM Dox, were further assessed in terms of NIR light treatment. The results showed no significant effect (MCF7: P = 0.6007, Figure 6.8; MCF10A P = 0.2941, Figure 6.9) on mitochondrial Ca^{2+} levels post-NIR light treatment. As expected, mitochondrial Ca^{2+} levels were significantly increased by 32.10% ± 5.65 (P < 0.0001; Figure 6.8) in MCF7 and by 90.30% ± 23.87 (P < 0.0001; Figure 6.9) in MCF10A cells treated with 0.25 μM Dox in comparison to untreated. No significant Dox–NIR light interaction was observed regarding ROS levels (MCF7: P = 0.8366, Figure 6.8; MCF10A: P = 0.5586, Figure 6.9).

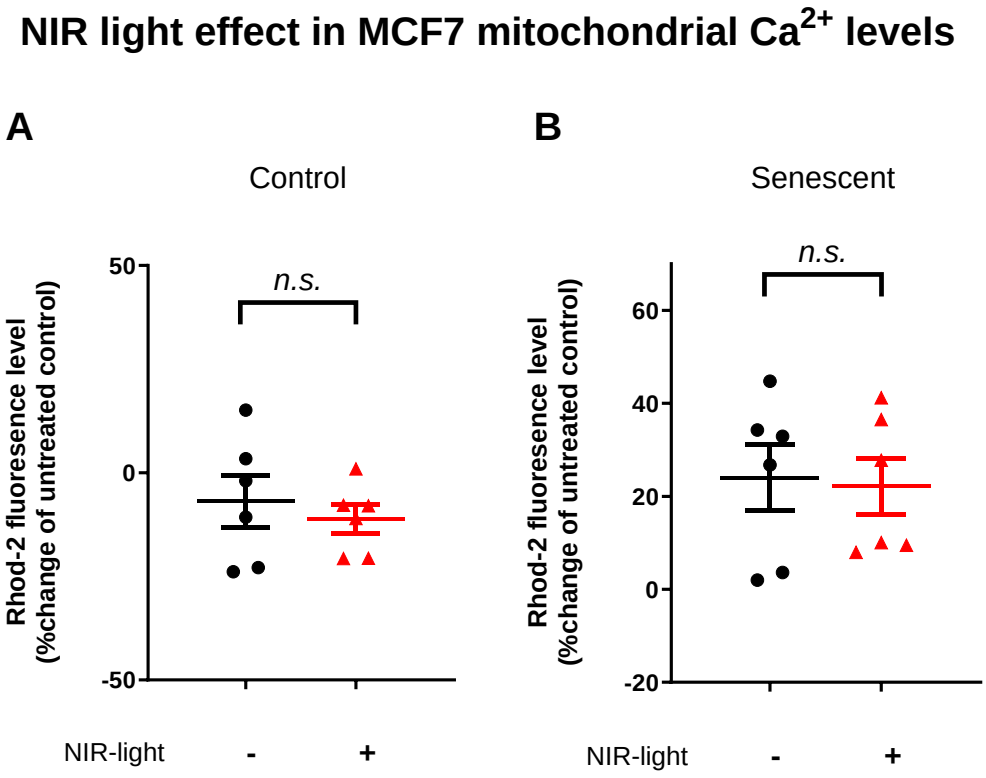

Figure 6.8: The effect of NIR light on mitochondrial Ca^{2+} levels – Flow cytometry. MCF7 breast cancer cells were cultured in either media alone (A; control population) or treated with 0.25 μM Dox for 24 hours (B; senescent population), followed by 6 days in drug-free media. In parallel, populations were exposed to either no light or daily 20-minute NIR light treatment (734 nm) for 6 days. Mitochondrial Ca^{2+} levels were quantified by flow cytometry in live cells following Rhod-2 staining and expressed as a percentage change from untreated control (N=6 independent biological repeats). Statistical significance was determined using two-way ANOVA with post-hoc Bonferroni testing. Data are presented as mean changes compared to untreated control ± SEM.

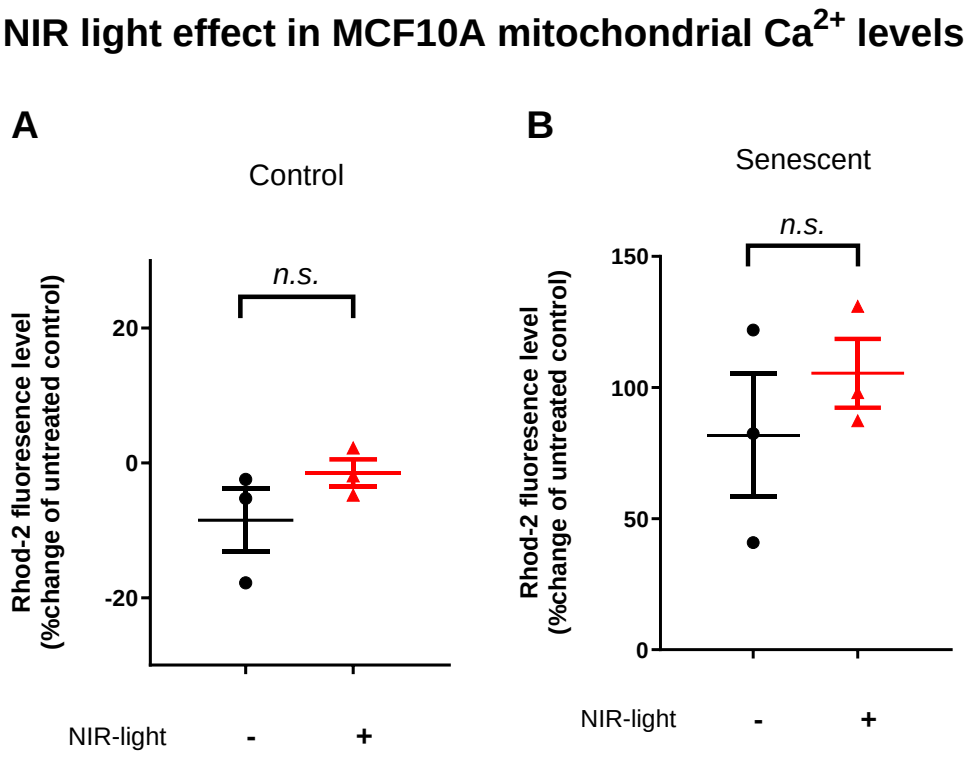

Figure 6.9: The effect of NIR light on mitochondrial Ca^{2+} levels – Flow cytometry. MCF10A breast cells were cultured in either media alone (A; control population) or treated with 0.25 µM Dox for 24 hours (B; senescent population), followed by 6 days in drug-free media. In parallel, populations were exposed to either no light or daily 20-minute NIR light treatment (734 nm) for 6 days. Mitochondrial Ca^{2+} levels were quantified by flow cytometry in live cells following Rhod-2 staining and expressed as a percentage change from untreated control (N=3 independent biological repeats). Statistical significance was determined using two-way ANOVA with post-hoc Bonferroni testing. Data are presented as mean changes compared to untreated control ± SEM.

6.2.6 NIR light treatment modulates MMP in MCF7 cancer cells

The MMP of MCF7 breast cancer cells were further assessed regarding NIR light treatment for two cell treatments (control and 0.25 μM Dox). The results showed a significant increase ($P = 0.0116$) in MMP after NIR light treatment, by 12.96% ± 4.00 in control populations (figure 6.10A) and by 7.08% ± 6.34 in 0.25 μM Dox-treated populations (Figure 6.10B). MMP was not significantly increased between untreated and cells treated with 0.25 μM Dox ($P = 0.4206$; Figure 6.10). No significant Dox – NIR light interaction was observed regarding MMP levels ($P = 0.4278$; Figure 6.10).

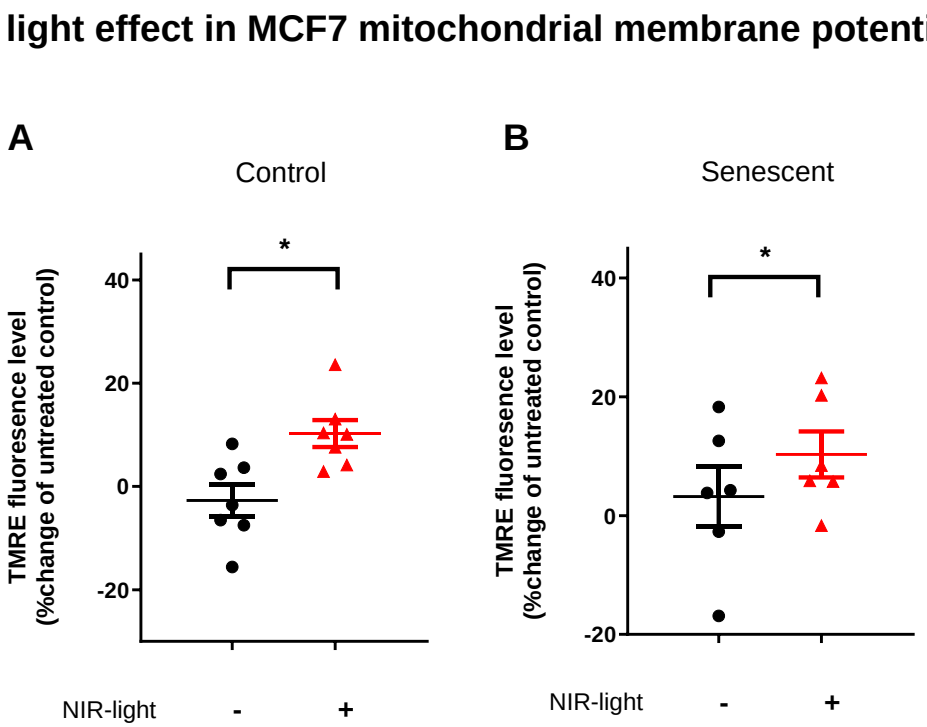

Figure 6.10: The effect of NIR light on MMP – Flow cytometry. MCF7 breast cancer cells were cultured in either media alone (A; control population) or treated with 0.25 μM Dox for 24 hours (B; senescent population), followed by 6 days in drug-free media. In parallel, populations were exposed to either no light or daily 20-minute NIR light treatment (734 nm) for 6 days. Mitochondrial membrane potential was quantified by flow cytometry in live cells following TMRE staining and expressed as a percentage change from untreated control (N=6 independent biological repeats). Statistical significance was determined using two-way ANOVA with post-hoc Bonferroni testing. Data are presented as mean changes compared to untreated control ± SEM. * : $P \leq 0.05$.

6.2.7 NIR light treatment modulates intracellular Ca^{2+} levels in cancer cells

The total intracellular Ca^{2+} levels were assessed post-NIR light treatment in MCF7 breast cancer cells exposed to control or 0.25 μM Dox. The results showed a significant increase ($P = 0.0366$) of intracellular Ca^{2+} post-NIR light treatment, by 13.90% ± 6.40 in control populations (Figure 6.11A) and by 39.38% ± 24.14 in 0.25 μM Dox-treated populations (Figure 6.11B). As expected, total Ca^{2+} was significantly increased between untreated and cells treated with 0.25 μM Dox by 94.65% ± 12.11 ($P < 0.0001$; Figure 6.11). No significant Dox–NIR light interaction was observed in total Ca^{2+} levels ($P = 0.3022$; Figure 6.11).

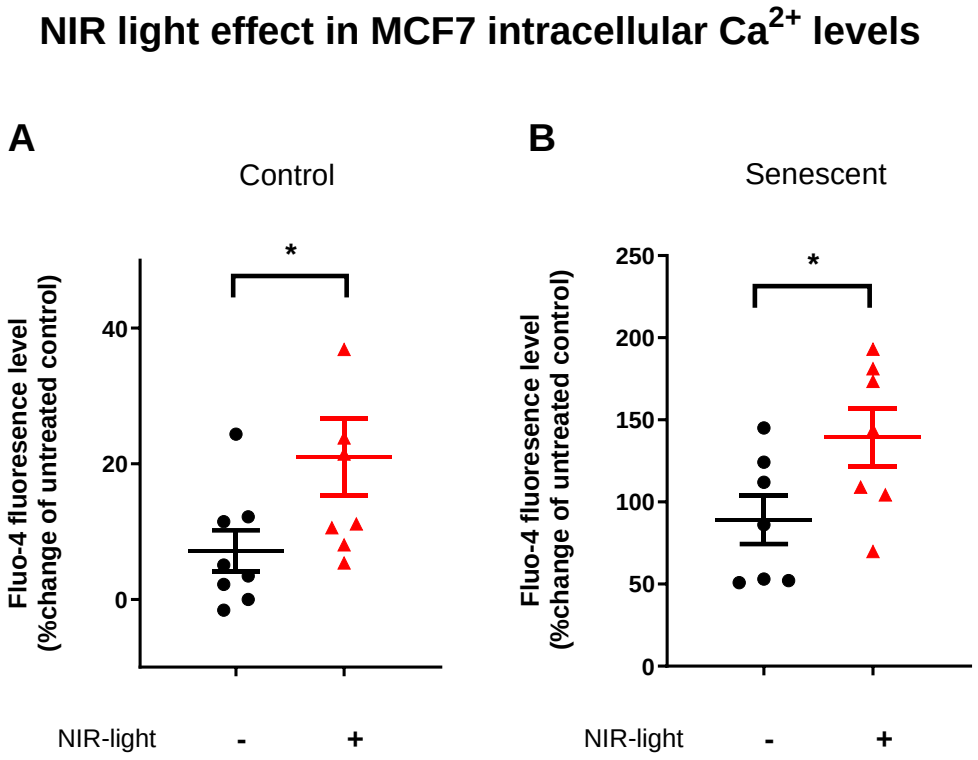

Figure 6.11: The effect of NIR light on intracellular Ca^{2+} levels – Flow cytometry. MCF7 breast cancer cells were cultured in either media alone (A; control population) or treated with 0.25 μM Dox for 24 hours (B; senescent population), followed by 6 days in drug-free media. In parallel, populations were exposed to either no light or daily 20-minute NIR light treatment (734 nm) for 6 days. Total intracellular Ca^{2+} levels were quantified by flow cytometry in live cells following Fluo-4 staining and expressed as a percentage change from untreated control (N=8 independent biological repeats). Statistical significance was determined using two-way ANOVA with post-hoc Bonferroni testing. Data are presented as mean changes compared to untreated control ± SEM. * : $P \leq 0.05$.

To sum up, all tests in this chapter were analysed with two-way ANOVA, where the effects of Dox, NIR light treatment, and their interaction were calculated. The complete list of all changes and statistical interactions is found in Table 6.1. The table summarizes the statistical analysis for all the experiments conducted in this chapter, providing an overview of the effects of Dox and NIR light treatments, both individually and in combination.

Complete table of two-way ANOVA results

Biological Assay	P value		
	Dox	NIR light	Interaction
CellEvent Senescence Green_MCF7	**0.0001**	**0.0081**	0.6508
CellEvent Senescence Green_MC10A	**0.0006**	0.9725	0.9196
CellEvent Senescence Green_A549	**0.0001**	**0.0026**	**0.0075**
CellEvent Senescence Green_IMR-90	**0.0036**	0.0727	0.5423
DCFDA_MCF7	**0.0001**	**0.0145**	0.2504
DCFDA_MCF10A	**0.0001**	0.9353	0.6191
Rhod-2_MCF7	**0.0001**	0.6007	0.8366
Rhod-2_MCF10A	**0.0001**	0.2941	0.5586
Fluo-4_MCF7	**0.0001**	**0.0366**	0.3022
TMRE_MCF7	**0.4206**	**0.0116**	0.4278

Table 6.1: Two-way ANOVA results of biological assays comparing effects of Dox drug and NIR light treatment. The table presents P-values for three factors: Dox treatment effect, NIR light treatment effect, and their interaction across different cell lines and assays. Results include senescence detection (CellEvent), ROS levels (DCFDA), mitochondrial Ca^{2+} (Rhod-2), total cellular Ca^{2+} (Fluo-4), and MMP (TMRE) measurements in cancer (MCF7, A549) and non-cancer (MCF10A, IMR-90) cell lines. Statistical significance ($P \leq 0.05$) is indicated in bold, demonstrating differential responses between cancer and non-cancer cells.

6.3 Discussion

6.3.1 NIR light treatment increases senescence effect in cancer cells

This chapter aimed to investigate the effects of NIR light treatment on senescence induction in both cancer and non-cancer cell lines. The primary objectives were to examine whether NIR light could induce cellular senescence, explore its impact on ROS levels, and assess changes in mitochondrial function and homeostasis.

To achieve this, the effects of NIR light treatment on senescence were investigated in four cell lines. Results showed that NIR light treatment (wavelength: 734 nm; fluence: 63 mJ/cm^2) can lead to significant induction of senescence in cancer cell lines (Figures 6.2 and 6.3) while sparing non-cancer cells (Figures 6.4 and 6.5). Indeed, exposure to NIR light-induced senescence in breast MCF7 and lung A549 cancer cells in the absence of Dox treatment, and also increased the senescence effect of Dox-induced senescent cell lines. Moreover, NIR light treatment exhibited a significant detectable interaction with Dox, leading to increased senescence within the lung cancer A549 model.

Since senescence is a permanent cell cycle arrest, and as demonstrated in Section 3.2.3, a significant decrease in cell proliferation is expected following NIR light exposure. Previous studies have evaluated PBM therapy on cancer cell proliferation but failed to test for senescence. For instance, Hu et al. showed that A2058 melanoma cell lines increased in number in response to PBM (632.8 nm light) but used higher fluences (intensity): 500, 1000, and 2000 mJ/cm^2. The same dose-response increase was observed in the CCO activity of this cell line (Hu et al., 2007). Magrini et al. reported similar results when tested different fluences (5, 28.8, and 1000 mJ/cm2) of 633 nm light treatment on MCF7 breast cancer cells (Magrini et al., 2012). Cell number increased with metabolic activity at a 1000 mJ/cm^2 fluence, while no increase in cell number or metabolic activity was reported at a fluence of 5 mJ/cm^2. In the results of this thesis, though the light characteristic was similar (734 nm) to those used by Hu et al. and Magrini et al., its fluence was lower (63 mJ/cm^2), which may

explain the differential effect of the treatment used in this thesis. Interestingly, when the light treatment used by Magrini et al. decreased to a fluence range (28 mJ/cm^2) similar to that used in this thesis, they observed no increase in cell population, but higher metabolic activity compared to cells treated with light of 5 mJ/cm^2 (Magrini et al., 2012). This would suggest that they may induce senescence in their cell populations, but senescence was not examined in that study.

As mentioned in Section 1.1, senescence signals the irreversible proliferation arrest of the cell, but the cell remains highly metabolically active (Hayflick & Moorhead, 1961; Quijano et al., 2012). These results, together with those previously published, suggest that NIR light senescence induction in cancer cells, but not normal cells, may display a bi-phasic effect, with a fluence "sweet-spot" above 20 mJ/cm^2 and below 300 mJ/cm^2 (Magrini et al., 2012) at wavelengths of 600 – 800 nm (de Freitas and Hamblin, 2016; Wang et al., 2016; Hamblin, 2017), whitin this range, there is a permanent cell cycle arrest with an increase in metabolic activity. However, when the fluence is increased above this range, NIR treatment can increase cellular proliferation and metabolic rates in cancer cells. The overall mechanism of this remains unknown and requires further investigation.

It is well-established that the effectiveness of PBM on a particular target tissue can depend on various factors, including the light source, wavelength, energy density, light pulse structure, and duration of the light application. These parameters significantly determine the optimal treatment outcomes (Kujawa et al., 2014; Yadav & Gupta, 2017). A biphasic dose-response curve, also known as hormesis, illustrates that excessively low or high doses such as fluence (mJ/cm^2), irradiance (mW/cm^2), duration of application, or treatment design may result in no significant effect or opposite inhibitory effects (Huang et al., 2011; Kujawa et al., 2014). Thus, it is likely that NIR light treatment may be hormetic in nature, with cancer cell proliferation increasing at very low/high light fluence but inducing senescence at a specific range.

Of particular interest is the significant interaction between NIR light and Dox in A549 lung cancer cells. This could be attributed to Dox's intrinsic photosensitizing properties. As demonstrated by Greco et al. (2023), Dox, as a chemical structure, serves as a chromophore, which means that it can absorb light in the visible spectrum, making it a potential photosensitizer. If Dox becomes photoactivated, then it can generate ROS (Dolmans et al., 2003; Greco et al., 2023). This light-dependent ROS generation increases Dox's cytotoxic effects higher than conventional chemotherapeutic action (Greco et al., 2023). The combination of NIR light with Dox treatment in A549 cells possibly triggers this dynamic effect, leading to increased oxidative stress and a higher senescence response (Ewald et al., 2010). This significant interaction indicates the potential of Dox's dual role as both a chemotherapeutic agent and a photosensitizer to enhance its anticancer efficacy, particularly in lung cancer models like A549 cells. Further investigation is required to optimize light parameters and drug concentrations that could lead to significant interactions of more cancer models, such as MCF7 breast cancer, and thus, the development of more effective photochemotherapy strategies for cancer treatment (Greco et al., 2023; Hamblin et al., 2018).

6.3.2 NIR light does not affect senescence levels in non-cancer cell lines

The same dose-response differential effect appears to be applied between cells of different origins. As cancer cells indicate a significant permanent cell cycle arrest after the NIR light treatment, the MCF10A breast non-cancer cells and IMR-90 lung fibroblasts show no significant change. This confirms that although the overall phenotype of senescent cells is similar, it depends on the senescence induction mechanism, the molecular pathway and the origin of the cell (Gorgoulis et al., 2019; Toussaint et al., 2002).

Numerous studies have reported that PBM treatment at high doses of over 1000 mJ/cm^2 can significantly increase the proliferation of non-cancer cells of different origins, including stem cells from human teeth (Fernandez et al., 2016), human osteoblast-like cells (Khadra

et al., 2005), melanocytes (Yu et al., 2003), human adipose stem cells (Abrahamse et al., 2010) and skin fibroblasts WS1 (de Villiers et al., 2011). Similar effects have also been reported in healthy human umbilical cord blood-derived mesenchymal stem cells (Kim et al., 2019) and healthy canine epidermal keratinocyte progenitors (Gagnon et al., 2016) following PBM treatment with fluence ranges of 300 - 100 mJ/cm^2; the latter fluence being closer to the NIR light characteristic of this thesis. At present, it is unclear why there is a discrepancy between the results of the current study and those reported in the literature. Still, it indicates that the response of non-cancer cells to PBM may be related to tissue origin (Laakso et al., 1993), with different cell types showing differential activation “sweet-spots”.

6.3.3 NIR light treatment increases ROS levels in cancer but not in non-cancer cells

It has been previously suggested that modulation of ROS levels is one of the primary effects of PBM (Amaroli et al., 2022). It was, therefore, hypothesised that increasing intracellular ROS with NIR light should lead to senescence induction in cancer cells since their metabolism is more complex than normal cells, and they can switch readily between glycolysis and oxidative phosphorylation (Pavlova & Thompson, 2016). The results showed significantly higher ROS levels in breast cancer cells, with ROS levels increasing almost three times higher in the Dox-induced senescent population than in the control population. On the other hand, there was no change in ROS levels in the breast non-cancer populations post-NIR light treatment (Figures 6.6 and 6.7).

Both *in vivo* and *in vitro* studies have established the essential role of mitochondria and ROS as drivers of cellular senescence (Correia-Melo & Passos, 2015; Höhn et al., 2017; Passos et al., 2010). ROS exhibits a bidirectional influence on cellular senescence, as the senescence process itself rapidly increases ROS levels, worsening oxidative stress due to complications of cellular OXPHOS (Höhn et al., 2017). This reciprocal role not only explains the significant increase in ROS levels post-Dox treatment but also elucidates why the

senescent population exhibited such a high increase in ROS levels—this is a consequence of both NIR light exposure and the induction of senescence.

As discussed in Section 1.9.1, mitochondria dynamics and ROS levels are pivotal in senescence and PBM. CCO, an important chromophore in cells, is located within the mitochondria. ROS can mediate between mitochondria and the nucleus, activating various transcription factors, such as nuclear factor kappa B (NF-kB). NF-kB can influence the expression of numerous genes responsible for cellular functions, including stress-induced responses and survival (Baichwal & Baeuerle, 1997; Wang et al., 2002). Thus, PBS can activate signalling pathways that lead to the upregulation or downregulation of gene expression via these mediators.

Notably, NF-kB regulates the expression of more than a hundred genes, including those that promote antioxidant, anti-apoptotic, pro-proliferation, and pro-migration functions (Hamblin, 2018a). Indeed, a burst of ROS due to PBM has been shown to activate the NF-kB signalling pathway (Hamblin, 2018a). Margini et al. (2012) proposed that ROS production in red light-treated MCF7 mitochondria altered cellular metabolism via interactions with nuclear transcription factors, including the nuclear signalling agent NF-kB (Magrini et al., 2012). Additionally, ROS production due to NF-kB activation after PBM therapy has been observed in other studies, including non-cancer cell models, such as mouse embryonic fibroblasts (Chen et al., 2011).

It is well described that redox plays a key role in the cell cycle, controlling cell growth, proliferation and death (Menon & Goswami, 2007). Therefore, it is unsurprising that cellular senescence involves activation of the nuclear factor kappa B (NF-kB) (Fallah et al., 2019; Rovillain et al., 2011). Fahla et al., using rat cardiac tissue, reported higher ROS levels, decreased mitochondrial function, and a highly significant increase of NF-kB expression following treatment with doses of Dox that were likely to induce senescence. The same effects were not observed in untreated tissues or treated with lower Dox doses, which did not induce senescence (Fallah et al., 2019). This would suggest that the observed increase

in senescence in cancer cells, but not in non-cancer cells, in the current results, was a direct consequence of the elevation in ROS production associated with PBM, which in turn would lead to NF-kB signalling pathway activation and thus senescence.

6.3.4 NIR light changes MCF7 cancer cell homeostasis and mitochondria function

It has been previously suggested that retrograde signalling originating from mitochondria after light absorption can be mediated by changes in ROS, MMP and altered Ca^{2+} levels (Kim, 2014). In line with this concept, results from this thesis revealed significant modulation of all three mediators by PBM in MCF7 breast cancer cells (Figures 6.6, 6.10 and 6.11), except mitochondrial Ca^{2+} levels, which demonstrated no change. On the other hand, no ROS or intracellular Ca^{2+} levels were altered post-NIR light treatment in MCF10A breast non-cancer cells (Figures 6.7 and 6.9), highlighting the intricate impact of PBM on a cellular level (de Freitas & Hamblin, 2016; Kujawa et al., 2014). Together with the effectiveness of PBM, which depends on several factors (Section 3.1.3), the light treatment parameters and the origin of the tissue/cell line influence the molecular mechanisms that regulate transcription factors differently.

In this thesis, MMP increased in cancer cells after NIR light treatment. It is generally accepted that ROS production and MMP are highly correlated (Suski et al., 2012). Indeed, as suggested by Aon and colleagues in their redox-optimised ROS balance hypothesis, mitochondria have evolved to optimise energy production while minimising ROS production by operating at an intermediate redox state, where electron flow and antioxidant balance systems are critical. This hypothesis explains why both an increase in MMP, for example, during hypoxia, and a decrease, as seen with excessive uncoupling, give rise to ROS (Aon et al., 2010). Korshunov et al., using isolated mitochondria from rat cardiac muscle, showed that even a slight increase in MMP was sufficient to produce H_2O_2 in mitochondria (Korshunov et al., 1997). Hence, PBM may induce a rise in the MMP due to an increase in the electron transport chain, which can increase ROS levels (Hamblin, 2018b; Suski et al.,

2012). Additionally, decreasing MMP is correlated with mitochondrial dysfunction and increased ROS production, which are both key signals for mitochondrial turnover but can contribute to tissue damage (Hamblin, 2018a). This suggests that senescence induction after NIR exposure results from ROS as a secondary messenger, not general mitochondrial dysfunction.

Although no change in mitochondrial Ca^{2+} levels was recorded in this thesis, there was a significant increase in intracellular Ca^{2+} levels post-NIR light exposure. PBM and the use of non-thermal NIR light notably influence cellular Ca^{2+} levels, as demonstrated across various studies, including cervical cancer HeLa cells (Golovynska et al., 2019), neuroblastoma, neuron cells (Golovynska et al., 2021) and osteoblasts (Tani et al., 2018). Studies by Amaroli et al. (2022) demonstrate that specific wavelengths and energies of light impact Ca^{2+} influx, either directly or by affecting mitochondrial activity. The interplay between ROS and Ca^{2+} signalling, as highlighted by Görlach et al., suggests a bidirectional relationship, where oxidative stress triggers Ca^{2+} influx from different cell sources, while Ca^{2+} can increase ROS production (Görlach et al., 2015). Finally, as Ca^{2+} serves as a critical cellular secondary messenger (Berridge, 2012), changes in Ca^{2+} levels induced by NIR light may regulate senescence in cancer cells. As mitochondria are central to Ca^{2+} signalling (Szabadkai & Duchen, 2008), it is surprising that I did not see any changes in mitochondrial Ca^{2+}; however, it is entirely possible that the effects were too small to measure or occurred very quickly. Ca^{2+} influx into mitochondria would stimulate their activity, potentially raising their MMP, but the flow of Ca^{2+} in and out of the mitochondrion is tightly controlled. Thus, further research is required to understand their precise role in the observed shifts in intracellular Ca^{2+}.

6.3.5 Potential mechanisms of NIR light treatment

Mechanistically, two primary mechanisms are most widely accepted in the literature to explain the initial interaction of red to NIR light with cells, leading to PBM effects. The first

and most widely recognized mechanism involves CCO as the primary chromophore (Karu, 2008). CCO, located in the inner mitochondrial membrane as part of complex IV in the electron transport chain, is believed to be the first molecule to interact and absorb light in the range of 600-850 nm (Hamblin, 2016b). This absorption can lead to increased electron transport chain activity, resulting in increased ROS and Ca^{2+} levels, enhanced ATP production and altered metabolic homeostasis (Hamblin, 2016b; Karu, 2008). The second mechanism, as suggested by Wang et al., involves the activation of light-sensitive ion channels, which are thought to be activated by wavelengths in the range of 980-1064 nm, increasing the intracellular Ca^{2+} levels, which then act as signalling molecules to induce cellular physiological changes (Dompe et al., 2020; Wang et al., 2017a). However, this mechanism becomes more relevant for wavelengths beyond the primary absorption range of CCO.

A third, more recent theory proposed by Sommer et al. (2015) suggests that nanoscopic interfacial water layers within and around mitochondria play a crucial role in NIR light absorption. According to this theory, NIR light may reduce the viscosity of these water molecules and expand the volume of water layers, potentially affecting the efficiency of the ATP synthase motor. Interestingly, the water layer modulation seemed to be more dynamic in hydrophilic surfaces, such as mitochondrial inner membrane, intermembrane space, cristae and the F1 part of ATP synthase (Sommer et al., 2015), highlighting the role of mitochondria in PBM.

It is important to note that the first two proposed mechanisms are associated with different wavelength ranges. Although the results of this thesis show increased intracellular Ca^{2+} levels, which both theories can potentially explain, the distinction in wavelengths suggests that the CCO theory is more likely applicable to the findings presented here. This is because the wavelength used in this study (734 nm) falls within the range typically associated with CCO absorption (600 - 850 nm). Additionally, the potential role of interfacial water layers within the mitochondria, as proposed by Sommer et al. (2015), should not be discounted.

This mechanism may contribute to the observed effects, given the structural changes that occur in mitochondria during cellular senescence. As described in Section 1.7.2, mitochondria in senescent cells often appear swollen (Ziegler et al., 2015) and exhibit increased mass and altered cristae structure (Correia-Melo & Passos, 2015). These changes primarily affect the hydrophilic compartments of mitochondria, including the matrix and the intracristal space. Consequently, in the case of senescent MCF7 cells exposed to NIR light treatment, the effects of PBM might be amplified due to the increased presence of these hydrophilic regions. According to Sommer's theory, this NIR light interaction with interfacial water layers of the mitochondria from senescent cells could modulate their viscosity, potentially enhancing the impact of PBM. This hypothesis could explain the observed heightened response to PBM in already senescent MCF7 cells, as the structural changes in their mitochondria may provide a larger arena for light-water interactions.

Furthermore, in comparison to the observations of biophotonic emission in isolated mitochondria (Chapter 5), it's important to note that the current experiments on NIR light treatment were conducted on whole cells. In this context, the NIR light might travel along the microtubule network, potentially sending light signals far into the cells. This concept aligns with theories proposed by Thar and Kuhl (2004) and Kurian et al. (2017), suggesting that microtubules could act as waveguides for light propagation within cells. Thar and Kuhl (2004) described mitochondria as a multi-layer optical system with alternating refractive indices, which could support coherent light propagation and even amplification. Kurian et al. (2017) proposed that the arrangement of aromatic amino acids in tubulin could support quantum coherent energy transfer, potentially extending to mitochondrial proteins.

In summary, it is likely that these various mechanisms work in concert to produce the observed effects of PBM. The initial photon absorption by CCO and/or other chromophores triggers a cascade of events, including changes in mitochondrial function, ROS production, increased membrane potential and accumulation of Ca^{2+} signalling. These changes can then lead to the activation of various transcription factors and signalling pathways, such as

NF-kB (Butow and Avadhani, 2004), ultimately resulting in cellular responses, such as increased senescence in cancer cells.

Further research is needed to fully explore the relative contributions of these mechanisms and how they interact in different cellular contexts, particularly in the context of senescence induction in cancer cells versus non-cancer cells. Understanding these mechanisms more comprehensively could lead to more targeted and effective applications of PBM in various therapeutic contexts.

6.3.6 Differential response of cancerous and non-cancerous cells to PBM

The results in this chapter demonstrate that the potential differences between cancerous and non-cancerous cells are associated with mitochondria and ROS. Warburg was the first to describe what is now known as the "Warburg effect"—the phenomenon whereby cancer cells, despite the presence of oxygen, seem to rely on glycolysis, so-called “aerobic glycolysis”, instead of OXPHOS (Vaupel & Multhoff, 2021; Warburg, 1956). Warburg also identified the enzyme CCO during an experiment he was conducting, suggesting CCO to be a crucial player in cellular energy metabolism. The energy from ingested glucose is extracted through glycolysis, and the resulting pyruvate enters mitochondria through a transporter on the outer membrane. In the last step, CCO controls OXPHOS to produce ATP with the help of oxygen (Kim, 2014).

A more recent study revealed that defects in CCO can cause a metabolic shift to glycolysis (Warburg effect induction) and promote cancer progression. The loss of CCO activity results in the activation of several oncogenic signalling pathways and the upregulation of genes involved in cell signalling, cell migration, and extracellular matrix interactions (Srinivasan et al., 2016) This occurs through multiple mechanisms, including increased production of ROS, stabilization of hypoxia-inducible factor 1α (HIF-1α), activation of AMP-activated protein kinase (AMPK), and induction of retrograde signalling from mitochondria to the

nucleus. Together these changes contribute to the metabolic reprogramming characteristic of cancer cells, promoting their survival, proliferation, and metastatic potential. Since CCO has previously been suggested as containing chromophores that could be responsible for PBM (Section 6.3.5), it explains why cancer cells and normal cells might exhibit varied responses to PBM (Dompe et al., 2020; Hamblin et al., 2018). In cancer cells, PBM can increase energy demand, metabolism, and ROS activity, which activates transcription factors, potentially exacerbating their altered metabolic state. On the other hand, in non-cancer cells, PBM may induce a small burst of ROS that triggers protective mechanisms and minimises damage, placing the cell in a position that overcomes stress and escapes senescence induction.

In parallel, during senescence, the amount of ATP produced by mitochondria decreases, and more is produced through glycolysis. This compensatory response to the change in mitochondrial function due to senescence results in an increase in mitochondrial abundance and a shift towards glycolytic ATP production (Korolchuk et al., 2017). In a study using alpha mouse liver 12 cells, the senescent population had greater glycolytic potential, together with increased mitochondrial activity and damage due to proton leak—this did not increase ATP production despite the increased mitochondrial activity in senescent cells (Singh et al., 2020). Interestingly, a study investigating the metabolic effects of acute 780 nm LED light of 5 J/cm^2 on healthy human dermal fibroblasts neonatal and squamous carcinoma cells demonstrated that the cancer cells were more glycolytic. Only a few hours after treatment, the cancer cells showed increased ROS production and ATP levels, whereas the healthy cells did not; while 24 hours post-treatment, healthy cells increased proliferation, whereas cancer cells did not (Gonçalves de Faria et al., 2021). This suggests that the initial ROS increase and the increase in metabolic demand might play a role in decreased proliferation rates compared to healthy non-cancer cells.

Lastly, the differential response to PBM between cancer and non-cancer cells may be attributed to a differential mechanism of NIR light absorption. Cancer cells, with their altered

mitochondrial function and reliance on glycolysis (Warburg effect), might respond differently to the proposed mechanisms of PBM. For instance, the CCO theory suggests that light absorption by CCO increases electron transport chain activity. In cancer cells, where CCO activity is often compromised (Srinivasan et al., 2016), this mechanism might lead to a more pronounced increase in ROS production compared to non-cancer cells with normal CCO function. This excessive ROS generation in cancer cells could trigger stress responses and potentially lead to increased senescence. Additionally, the water viscosity theory proposed by Sommer et al. (2015) could also have differential effects. Cancer cells often exhibit altered mitochondrial morphology and increased mitochondrial mass (Vyas et al., 2016), which might change the distribution and properties of interfacial water layers. This could potentially enhance the effects of NIR light on water viscosity in cancer cells, leading to more pronounced changes in mitochondrial function.

In conclusion, the differential responses to PBM between cancer and non-cancer cells may result from their distinct metabolic profiles, mitochondrial characteristics, and chromophore compositions. These differences have significant implications for PBM therapy, suggesting that treatment parameters may need to be optimised specifically for cancer or non-cancer applications to achieve optimal outcomes. However, it's important to note that our understanding of these mechanisms is still evolving. The complex interplay between PBM and cellular metabolism creates challenges in generalizing these findings. Further research is needed to explore the precise molecular pathways involved in PBM responses across various cell types and cancer subtypes, and to determine how these origin-related NIR light effects can be translated into more effective and targeted PBM therapies.

6.3.7 Conclusion

Senescence is a multi-step process triggered by various stimuli, including oxidative damage, and different cell types can exhibit different senescence characteristics (Gorgoulis et al., 2019). In this study, NIR light, at a daily dose of 63 mJ/cm^2 over a six-days period,

induced senescence selectively in MCF7 breast and A549 lung cancer cells but not in non-cancer MCF10A breast cells and IMR-90 lung fibroblasts. The proposed mechanism, primarily based on the wavelength spectrum of the light treatment (734 nm), may involve CCO as the primary chromophore. The absorption of NIR light by CCO, as detailed in the literature on PBM action, appears to involve an increase in ROS production and Ca^{2+} levels (Aggarwal et al., 2019; Perillo et al., 2020), a finding confirmed by the results of this thesis.

This selective cancer vs non-cancer response considers the Warburg effect, where cancer cells have a greater shift towards glycolysis, leading to increased ROS levels. The combination of the already elevated ROS levels in cancer cells and PBM-induced ROS increase activates a signal cascade towards senescence and permanent cell cycle arrest as a stress response (Figure 6.12). This mitochondrial/ROS-based mechanism would support the well-described anti-inflammatory and wound-healing properties observed with PBM. However, part of the limitations of this study is that it focused on a single NIR light parameter, which may not capture the full spectrum of cellular responses across different cancer types or light treatment conditions. Future work is needed to establish the optimal fluence and wavelength for PBM and determine its potential as a cancer-selective therapy, as well as the precise location of ROS production.

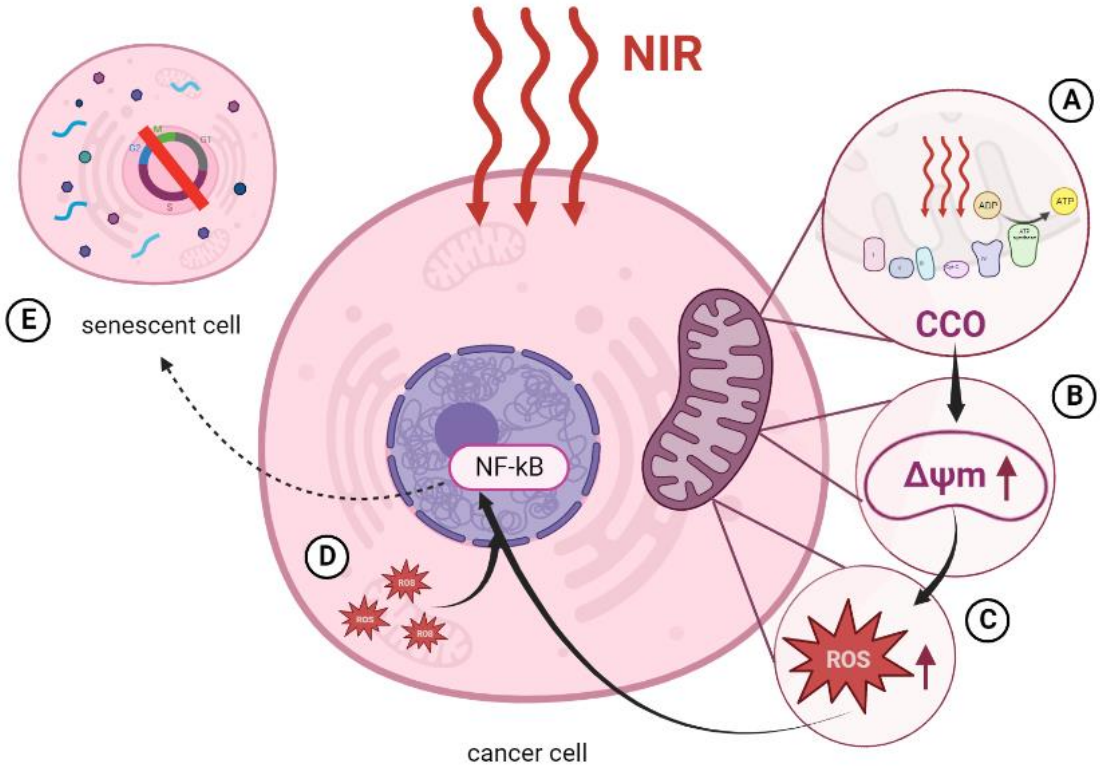

Figure 6.12: Schematic diagram of the proposed mechanism of NIR-induced senescence. Illustration showing cellular responses to 734 nm NIR light exposure in cancer cells. (A) NIR photons penetrate the cell and interact with cytochrome c oxidase (CCO) in mitochondria. (B) This interaction leads to increased mitochondrial membrane potential (MMP) and subsequently (C) elevated ROS production. ROS acts as a signalling messenger between mitochondria and the nucleus, while (D) inherently high baseline ROS levels in cancer cells contribute to the total oxidative burden. The combined ROS accumulation activates the NF-κB signalling pathway in the nucleus, ultimately resulting in (E) cellular senescence. Each stage is indicated by numbered arrows showing the progression of the mechanistic pathway. (Image created with biorender.com)

These findings hold significant benefits for potential clinical applications in the field of cancer therapy and ageing-related conditions. By elucidating the differential response of cancerous and non-cancerous cells to NIR light treatment, this research opens avenues for the development of targeted therapeutic strategies. The selective induction of senescence in cancer cells while sparing non-cancer cells suggests a promising approach for enhancing the efficacy of anti-cancer treatments. Combining PBM therapy with conventional cancer therapies could potentially enhance the senescence-inducing effects, leading to improved outcomes and potentially reducing side effects for cancer patients, as senescence induction could be used to target only the cancerous populations selectively. Furthermore, the protective effect observed in non-cancer cells highlights the potential for NIR light treatment to mitigate age-related pathologies and promote healthy ageing.

One additional limitation is that, despite the promising findings, the experiments were conducted *in vitro*, which may not fully represent the complexity of *in vivo* systems. For example, it has been shown that red to NIR light below 810 nm can be absorbed by blood and skin components (Yadav & Gupta, 2017). Since the NIR light treatment of this study was applied to *in vitro* cell culture, different light parameters might be more effective in *in vivo* models, such as, a higher wavelength penetrating deeper into the tissue. Translating the findings of this thesis from *in vitro* to *in vivo* can potentially enhance cancer treatment and age-related disease management, offering new approaches for improving patient outcomes.

Lastly, while changes in ROS levels and mitochondrial function were observed, the exact molecular mechanisms underlying the differential response between cancer and non-cancer cells require further investigation. Future studies should address these limitations by expanding to a wider range of cell types, exploring various NIR light parameters, and conducting *in vivo* experiments to validate the therapeutic potential of NIR light treatment in cancer and age-related conditions.

Chapter 7 : Thesis Conclusion

7.1 Overview of key findings

This thesis explores the relationship between senescent cells and light; the different aspects of cellular senescence, with a focus on mitochondrial function, non-chemical communication, and the effects of NIR light treatment. The key findings arising from my research are summarised below:

During my research, I successfully developed and refined a Dox-based senescence induction protocol for various cell lines, encompassing both non-cancer (MCF10A breast cells and IMR-90 lung fibroblasts) and cancer (MCF7 breast cancer and A549 lung cancer cells) models. The senescence-associated changes included the expected decrease in proliferation, increased lysosomal content, and morphological alterations. Notably, I observed a substantial increase in ROS levels, MMP, and mitochondrial Ca^{2+} levels, signifying a profound shift in cellular metabolism. These findings enhance our understanding of the underlying mechanisms driving cellular senescence, emphasizing the pivotal role of mitochondrial homeostasis.

I went on to establish the existence of non-chemical communication during cellular senescence. Specifically, I isolated highly metabolically active mitochondria from senescent cells to investigate this phenomenon. Notably, differences in oxygen consumption rates provided compelling evidence for this unique mode of communication. To further validate my findings, I conducted an experiment where these isolated senescent mitochondria were placed in an ultra-sensitive light detector. The outcome was significant photon emission, confirming that the means of non-chemical communication during senescence is light-based. Importantly, I observed that this photonic, non-chemical communication effect exhibited distinct characteristics between senescent and non-senescent states, suggesting

the presence of a specific “biophotonic fingerprint” associated with the senescent cellular condition.

Finally, I successfully achieved selective induction of senescence in cancer cells using near-infrared (NIR) light irradiation, specifically at 734 nm and 63 mJ/cm^2. Remarkably, this NIR light treatment induced senescence in MCF7 and A549 cancer cells while sparing MCF10A and IMR-90 non-cancer cells. The selective effect observed in cancer cells was accompanied by notable changes, including increased ROS levels, altered MMP, and elevated intracellular Ca^{2+} concentrations in MCF7 cells. These findings suggest a potential mitochondria/ROS-mediated mechanism underlying the senescence induction, specifically in cancer cells, via NIR light exposure.

7.2 Significance and Implications

This research provides significant insights into the role of non-chemical biophotonic communication of mitochondria during senescence and the potential applications of intra- or extracellular light to affect mitochondria and further cell homeostasis. The demonstration of non-chemical communication between mitochondria from senescent cells represents a novel area of investigation in cellular signalling. This finding suggests that biophotons emitted by mitochondria may play a crucial role in intercellular and intracellular communication, particularly in the context of cellular senescence. This discovery could potentially have implications for developing non-invasive diagnostic tools for age-related diseases and monitoring the efficacy of senescence-inducing treatments for cancer.

Furthermore, the selective induction of senescence in cancer cells by NIR light treatment, while sparing non-cancer cells, potentially holds promise for anti-cancer therapy. By combining NIR light with conventional treatments, it may be possible to enhance senescence-inducing effects and improve patient outcomes. Additionally, the protective

effect observed in non-cancer cells suggests potential applications in mitigating age-related pathologies and promoting healthy ageing.

7.3 Limitations

This research provides valuable insights into senescence, non-chemical communication, and the effects of NIR light treatment. However, it is important to acknowledge several limitations that impact the scope and interpretation of the findings. A primary limitation of this study is its reliance on *in vitro* cell models. While these models offer controlled experimental conditions, they may not fully recapitulate the complexity of *in vivo* systems. This limitation applies to all experiments conducted across the thesis and underscores the need for caution when extrapolating these results to physiological contexts.

The method of senescence induction also presents a limitation. Dox-induced senescence represents premature senescence, which may not fully reflect the complexities of age-related senescence. Adding a replicative senescence model would have been beneficial for a more comprehensive understanding of senescence processes. However, such a model was not feasible due to the time constraints inherent in a PhD project. While multiple senescence markers were assessed, the study could benefit from examining additional markers and pathways. For instance, the inclusion of epigenetic changes and SASPs measurements would provide a more comprehensive characterization of the senescent phenotype. This limitation extends to the analysis of mitochondrial function, where ATP levels were not measured due to time constraints. Such measurements could have provided additional insights into the metabolic changes associated with senescence.

The study's focus on three main cell lines (MCF10A, MCF7, and A549) limits the generalizability of the findings. Expanding to include a non-cancer lung cell line would have provided a more comprehensive comparison, especially for the non-chemical

communication and NIR-light exposure experiments. Furthermore, the lack of testing for MMP, mitochondrial Ca^{2+}, and intracellular Ca^{2+} in A549 lung cancer cells presents an opportunity for future research to explore mitochondrial function across different cell types during senescence.

The characterization of biophotonic emission during senescence presented a particular challenge. Due to technological limitations, it was not possible to determine the specific parameters of this emission, such as wavelength and intensity. This limitation prevents the full acceptance of the hypothesis that there is a unique biophotonic signature associated with senescence.

In the context of NIR light treatment, the study focused on a single PBM parameter, which may not capture the full spectrum of cellular responses across different cancer types or light treatment conditions. Additionally, the precise chromophores that react with either the NIR light or the biophotons, initially absorbing the light and activating the cascade of molecular pathways to induce a physiological change in the cell, remain unidentified.

These limitations were primarily due to the constraints inherent in a PhD project, including limited time and funding. Despite these constraints, the research provides valuable insights and lays the groundwork for future studies in these areas. Detailed suggestions for addressing some of these limitations are described in the following section.

7.4 Future research

Based on the findings from this thesis, several areas of future research have been identified which warrant further investigation. While *in vitro* studies have provided valuable insights, future research should focus on bridging the gap between laboratory observations and clinical applications.

A promising avenue for future research involves the study of free-circulating mitochondria isolated from human plasma. As mitochondria are known to emit light, this approach could verify biophotonic emission in human models (Blalock et al., 2024; Stier, 2021). Furthermore, investigating the effects of NIR light treatment on the function and bioenergetics of these isolated mitochondria could provide valuable insights into the impact of PBM on human mitochondria *in vivo*.

To further explore the mechanisms underlying non-chemical communication between senescent and non-senescent cells, additional studies using the ultra-sensitive light detector are necessary. Comparing light emission from the mitochondria of senescent and non-senescent cells could reveal important differences. Given that ROS are a primary source of biophotonic production, exploring the relationship between ROS increase and biophotonic emission could provide mechanistic insights. Recording the biophotonic emission from whole cells instead of isolated mitochondria might also provide mechanistic insides into the biophotonic production and absorption mechanism. Additionally, examining biophotonic production in cancer cell mitochondria and comparing it with non-cancer cells could help explain the differential effects observed in non-chemical communication.

Since this study hinted at a differential effect of biophotonic communication during senescence, by exploring the unique emission during senescence, we could be able to mimic such light signals and potentially influence cellular function completely non-invasively, thus considering the possibility of its use as a diagnostic or therapeutic target. While current technology limits our ability to measure the exact wavelength and intensity of minimal photon emissions, characterizing the precise nature of the "biophotonic fingerprint" during senescence could have significant implications for ageing research and quantum biology.

Further research should also focus on optimizing NIR light treatment parameters for both senescent and non-senescent cells. This includes investigating different wavelengths,

fluence, and treatment regimens to maximize the selective induction of senescence in cancer cells while minimizing potential side effects. Additionally, by exploring the potential synergistic effects of combining NIR light treatment with existing cancer therapies or senescence-inducing drugs, we could potentially aim to develop more effective and targeted treatment strategies.

Lastly, as technology advances, developing more sensitive methods to detect and characterize biophotonic emissions from cells and mitochondria will be crucial. This could include improvements in spectroscopic techniques or the development of new sensing technologies capable of detecting and analyzing extremely low-level light emissions.

7.5 Concluding remarks

This thesis has significantly advanced our understanding of the relationship between mitochondrial function, cellular senescence and light. The findings highlight the potential of utilizing light, either in the form of biophotons or as a form of PBM, as tools to influence mitochondria or to understand their physiological and metabolic state. Published literature highlights the importance and health benefits of the use of NIR light (Dompe et al., 2020; Hamblin et al., 2018), and recently, light-based non-chemical communication has gained interest (Mackenzie et al., 2024; Mould et al., 2024). Uniquely, this thesis explored the relationship between light and cellular senescence. Senescence, as an effect of antagonistic pleiotropy, can be both a weapon against mutations, diseases, wounds, and immunopathology, as well as an agent of organismal dysfunction and ageing. Fully comprehending the signalling processes that occur before and during senescence is essential. This knowledge could serve as a powerful tool for optimizing human health and countering health risks, effectively playing a dual role.

Exploring light and its relationship with biological systems could potentially open avenues for developing non-invasive, novel diagnostic and therapeutic approaches for age-related diseases and cancer. While further research is necessary to address the limitations and expand upon these findings, this work represents a significant contribution to the field of cellular senescence and opens exciting possibilities for translational applications in healthcare.

References

Abrahamse, H., Houreld, N. N., S Muller, S., & Ndlovu, L. (2010). Fluence and wavelength of low intensity laser irradiation affect activity and proliferation of human adipose derived stem cells. *Medical Technology SA*, *24*(2). https://doi.org/https://journals.co.za/doi/abs/10.10520/EJC74247

Acosta, J. C., Banito, A., Wuestefeld, T., Georgilis, A., Janich, P., Morton, J. P., Athineos, D., Kang, T.-W., Lasitschka, F., Andrulis, M., Pascual, G., Morris, K. J., Khan, S., Jin, H., Dharmalingam, G., Snijders, A. P., Carroll, T., Capper, D., Pritchard, C., … Gil, J. (2013). A complex secretory program orchestrated by the inflammasome controls paracrine senescence. *Nature Cell Biology*, *15*(8), 978–990. https://doi.org/10.1038/ncb2784

Adams, P. D. (2007). Remodeling of chromatin structure in senescent cells and its potential impact on tumor suppression and aging. *Gene*, *397*(1–2), 84–93. https://doi.org/10.1016/j.gene.2007.04.020

Adewoye, A. B., Tampakis, D., Follenzi, A., & Stolzing, A. (2020). Multiparameter flow cytometric detection and quantification of senescent cells in vitro. *Biogerontology*, *21*(6), 773–786. https://doi.org/10.1007/s10522-020-09893-9

Afifi, M. M., Crncec, A., Cornwell, J. A., Cataisson, C., Paul, D., Ghorab, L. M., Hernandez, M. O., Wong, M., Kedei, N., & Cappell, S. D. (2023). Irreversible cell cycle exit associated with senescence is mediated by constitutive MYC degradation. *Cell Reports*, *42*(9), 113079. https://doi.org/10.1016/j.celrep.2023.113079

Ailioaie, L. M., Ailioaie, C., & Litscher, G. (2023). Photobiomodulation in Alzheimer's Disease—A Complementary Method to State-of-the-Art Pharmaceutical Formulations and Nanomedicine? *Pharmaceutics*, *15*(3), 916. https://doi.org/10.3390/pharmaceutics15030916

Albrecht-Buehler, G. (1992). Rudimentary form of cellular 'vision'. *Proceedings of the National Academy of Sciences*, *89*(17), 8288–8292. https://doi.org/10.1073/pnas.89.17.8288

Allen, R. G., Tresini, M., Keogh, B. P., Doggett, D. L., & Cristofalo, V. J. (1999). Differences in electron transport potential, antioxidant defenses, and oxidant generation in young and senescent fetal lung fibroblasts (WI-38). *Journal of Cellular Physiology*, *180*(1), 114–122. https://doi.org/10.1002/(SICI)1097-4652(199907)180:1<114::AID-JCP13>3.0.CO;2-0

Amaroli, A., Pasquale, C., Zekiy, A., Benedicenti, S., Marchegiani, A., Sabbieti, M. G., & Agas, D. (2022). Steering the multipotent mesenchymal cells towards an anti-inflammatory and osteogenic bias via photobiomodulation therapy: How to kill two birds with one stone. *Journal of Tissue Engineering*, *13*, 204173142211101. https://doi.org/10.1177/20417314221110192

Anders, J. J., Lanzafame, R. J., & Arany, P. R. (2015). Low-Level Light/Laser Therapy Versus Photobiomodulation Therapy. *Photomedicine and Laser Surgery*, *33*(4), 183–184. https://doi.org/10.1089/pho.2015.9848

Aon, M. A., Cortassa, S., & O'Rourke, B. (2010). Redox-optimized ROS balance: A unifying hypothesis. *Biochimica et Biophysica Acta (BBA) - Bioenergetics*, *1797*(6–7), 865–877. https://doi.org/10.1016/j.bbabio.2010.02.016

Arnandis, T., Monteiro, P., Adams, S. D., Bridgeman, V. L., Rajeeve, V., Gadaleta, E., Marzec, J., Chelala, C., Malanchi, I., Cutillas, P. R., & Godinho, S. A. (2018). Oxidative Stress in Cells with Extra Centrosomes Drives Non-Cell-Autonomous Invasion. *Developmental Cell*, *47*(4), 409-424.e9. https://doi.org/10.1016/j.devcel.2018.10.026

Ash, C., Dubec, M., Donne, K., & Bashford, T. (2017). Effect of wavelength and beam width on penetration in light-tissue interaction using computational methods. *Lasers in Medical Science*, *32*(8), 1909–1918. https://doi.org/10.1007/s10103-017-2317-4

Ashapkin, V. V., Kutueva, L. I., Kurchashova, S. Y., & Kireev, I. I. (2019). Are There Common Mechanisms Between the Hutchinson–Gilford Progeria Syndrome and Natural Aging? *Frontiers in Genetics*, *10*. https://doi.org/10.3389/fgene.2019.00455

Avci, P., Gupta, A., Sadasivam, M., Vecchio, D., Pam, Z., Pam, N., & Hamblin, M. R. (2013). Low-level laser (light) therapy (LLLT) in skin: stimulating, healing, restoring. *Seminars in Cutaneous Medicine and Surgery*, *32*(1), 41–52.

Baichwal, V. R., & Baeuerle, P. A. (1997). Apoptosis: Activate NF-κB or die? *Current Biology*, *7*(2), R94–R96. https://doi.org/10.1016/S0960-9822(06)00046-7

Baker, D. J., Childs, B. G., Durik, M., Wijers, M. E., Sieben, C. J., Zhong, J., A. Saltness, R., Jeganathan, K. B., Verzosa, G. C., Pezeshki, A., Khazaie, K., Miller, J. D., & van Deursen, J. M. (2016). Naturally occurring p16Ink4a-positive cells shorten healthy lifespan. *Nature*, *530*(7589), 184–189. https://doi.org/10.1038/nature16932

Baker, D. J., Wijshake, T., Tchkonia, T., LeBrasseur, N. K., Childs, B. G., van de Sluis, B., Kirkland, J. L., & van Deursen, J. M. (2011). Clearance of p16Ink4a-positive senescent cells delays ageing-associated disorders. *Nature*, *479*(7372), 232–236. https://doi.org/10.1038/nature10600

Barja, G., & Herrero, A. (2000). Oxidative damage to mitochondrial DNA is inversely related to maximum life span in the heart and brain of mammals. *The FASEB Journal*, *14*(2), 312–318. https://doi.org/10.1096/fasebj.14.2.312

Barolet, D., Roberge, C. J., Auger, F. A., Boucher, A., & Germain, L. (2009). Regulation of Skin Collagen Metabolism In Vitro Using a Pulsed 660nm LED Light Source: Clinical Correlation with a Single-Blinded Study. *Journal of Investigative Dermatology*, *129*(12), 2751–2759. https://doi.org/10.1038/jid.2009.186

Bartkova, J., Rezaei, N., Liontos, M., Karakaidos, P., Kletsas, D., Issaeva, N., Vassiliou, L.-V. F., Kolettas, E., Niforou, K., Zoumpourlis, V. C., Takaoka, M., Nakagawa, H., Tort, F., Fugger, K., Johansson, F., Sehested, M., Andersen, C. L., Dyrskjot, L., Ørntoft, T., … Gorgoulis, V. G. (2006). Oncogene-induced senescence is part of the tumorigenesis barrier imposed by DNA damage checkpoints. *Nature*, *444*(7119), 633–637. https://doi.org/10.1038/nature05268

Bat'yanov, A. P. (1984). Distant-optical interaction of mitochondria through quartz. *Bulletin of Experimental Biology and Medicine*, *97*(6), 740–742. https://doi.org/10.1007/BF00804160

Bereiter-Hahn, J. (1990). *Behavior of Mitochondria in the Living Cell* (pp. 1–63). https://doi.org/10.1016/S0074-7696(08)61205-X

Berridge, M. J. (2012). Calcium signalling remodelling and disease. *Biochemical Society Transactions*, *40*(2), 297–309. https://doi.org/10.1042/BST20110766

Bielak-Zmijewska, A., Wnuk, M., Przybylska, D., Grabowska, W., Lewinska, A., Alster, O., Korwek, Z., Cmoch, A., Myszka, A., Pikula, S., Mosieniak, G., & Sikora, E. (2014). A comparison of replicative senescence and doxorubicin-induced premature senescence of vascular smooth muscle cells isolated from human aorta. *Biogerontology*, *15*(1), 47–64. https://doi.org/10.1007/s10522-013-9477-9

Birch, J., & Passos, J. F. (2017). Targeting the SASP to combat ageing: Mitochondria as possible intracellular allies? *BioEssays*, *39*(5), 1600235. https://doi.org/10.1002/bies.201600235

Birch-Machin, M. A. (2006). The role of mitochondria in ageing and carcinogenesis. *Clinical and Experimental Dermatology*, *31*(4), 548–552. https://doi.org/10.1111/j.1365-2230.2006.02161.x

Blalock, Z. N., Wu, G. W. Y., Lindqvist, D., Trumpff, C., Flory, J. D., Lin, J., Reus, V. I., Rampersaud, R., Hammamieh, R., Gautam, A., Ressler, K. J., Yang, R., Muhie, S., Daigle, B. J., Bierer, L. M., Hood, L., Wang, K., Lee, I., Dean, K. R., … Mellon, S. H. (2024). Circulating cell-free mitochondrial DNA levels and glucocorticoid sensitivity in a cohort of male veterans with and without combat-related PTSD. *Translational Psychiatry*, *14*(1), 22. https://doi.org/10.1038/s41398-023-02721-x

Bodnar, P. M., Peshko, A. O., Prystupiuk, O. M., Voronko, A. A., Kyriienko, D. V, Mykhal'chyshyn, H. P., & Naumova, M. I. (1999). Laser therapy in diabetes mellitus. *Likars'ka Sprava*, *6*, 125–128.

Bojko, A., Czarnecka-Herok, J., Charzynska, A., Dabrowski, M., & Sikora, E. (2019). Diversity of the Senescence Phenotype of Cancer Cells Treated with Chemotherapeutic Agents. *Cells*, *8*(12), 1501. https://doi.org/10.3390/cells8121501

Bókkon, I., Salari, V., Tuszynski, J. A., & Antal, I. (2010). Estimation of the number of biophotons involved in the visual perception of a single-object image: Biophoton intensity can be considerably higher inside cells than outside. *Journal of Photochemistry and Photobiology B: Biology*, *100*(3), 160–166. https://doi.org/10.1016/j.jphotobiol.2010.06.001

Borodkina, A. V., Shatrova, A. N., Deryabin, P. I., Griukova, A. A., Abushik, P. A., Antonov, S. M., Nikolsky, N. N., & Burova, E. B. (2016). Calcium alterations signal either to senescence or to autophagy induction in stem cells upon oxidative stress. *Aging*, *8*(12), 3400–3418. https://doi.org/10.18632/aging.101130

Bowen, J. M., Chamley, L., Keelan, J. A., & Mitchell, M. D. (2002). Cytokines of the Placenta and Extra-placental Membranes: Roles and Regulation During Human Pregnancy and Parturition. *Placenta*, *23*(4), 257–273. https://doi.org/10.1053/plac.2001.0782

Burgos, R. C. R., Schoeman, J. C., Winden, L. J. van, Červinková, K., Ramautar, R., Van Wijk, E. P. A., Cifra, M., Berger, R., Hankemeier, T., & Greef, J. van der. (2017). Ultra-weak photon emission as a dynamic tool for monitoring oxidative stress

metabolism. *Scientific Reports*, *7*(1), 1229. https://doi.org/10.1038/s41598-017-01229-x

Burton, D. G. A., & Krizhanovsky, V. (2014). Physiological and pathological consequences of cellular senescence. *Cellular and Molecular Life Sciences*, *71*(22), 4373–4386. https://doi.org/10.1007/s00018-014-1691-3

Bussian, T. J., Aziz, A., Meyer, C. F., Swenson, B. L., van Deursen, J. M., & Baker, D. J. (2018). Clearance of senescent glial cells prevents tau-dependent pathology and cognitive decline. *Nature*, *562*(7728), 578–582. https://doi.org/10.1038/s41586-018-0543-y

Butow, R. A., & Avadhani, N. G. (2004). Mitochondrial Signaling. *Molecular Cell*, *14*(1), 1–15. https://doi.org/10.1016/S1097-2765(04)00179-0

Cahu, J., & Sola, B. (2013). A Sensitive Method to Quantify Senescent Cancer Cells. *Journal of Visualized Experiments*, *78*. https://doi.org/10.3791/50494-v

Calabrese, E. J., & Mattson, M. P. (2017). How does hormesis impact biology, toxicology, and medicine? *Npj Aging and Mechanisms of Disease*, *3*(1), 13. https://doi.org/10.1038/s41514-017-0013-z

Campisi, J. (2003). Cancer and ageing: rival demons? *Nature Reviews Cancer*, *3*(5), 339–349. https://doi.org/10.1038/nrc1073

Campisi, J. (2013). Aging, Cellular Senescence, and Cancer. *Annual Review of Physiology*, *75*(1), 685–705. https://doi.org/10.1146/annurev-physiol-030212-183653

Campisi, J., & d'Adda di Fagagna, F. (2007). Cellular senescence: when bad things happen to good cells. *Nature Reviews Molecular Cell Biology*, *8*(9), 729–740. https://doi.org/10.1038/nrm2233

Cardoso, F. dos S., Barrett, D. W., Wade, Z., Gomes da Silva, S., & Gonzalez-Lima, F. (2022). Photobiomodulation of Cytochrome c Oxidase by Chronic Transcranial Laser in Young and Aged Brains. *Frontiers in Neuroscience*, *16*. https://doi.org/10.3389/fnins.2022.818005

Chang, B. D., Broude, E. V, Dokmanovic, M., Zhu, H., Ruth, A., Xuan, Y., Kandel, E. S., Lausch, E., Christov, K., & Roninson, I. B. (1999). A senescence-like phenotype distinguishes tumor cells that undergo terminal proliferation arrest after exposure to anticancer agents. *Cancer Research*, *59*(15), 3761–3767.

Chen, A. C.-H., Arany, P. R., Huang, Y.-Y., Tomkinson, E. M., Sharma, S. K., Kharkwal, G. B., Saleem, T., Mooney, D., Yull, F. E., Blackwell, T. S., & Hamblin, M. R. (2011). Low-Level Laser Therapy Activates NF-kB via Generation of Reactive Oxygen Species in Mouse Embryonic Fibroblasts. *PLoS ONE*, *6*(7), e22453. https://doi.org/10.1371/journal.pone.0022453

Chen, J.-H., Ozanne, S. E., & Hales, C. N. (2007). *Methods of Cellular Senescence Induction Using Oxidative Stress* (pp. 179–189). https://doi.org/10.1007/978-1-59745-361-5_14

Chen, Q., Fischer, A., Reagan, J. D., Yan, L. J., & Ames, B. N. (1995). Oxidative DNA damage and senescence of human diploid fibroblast cells. *Proceedings of the National Academy of Sciences*, *92*(10), 4337–4341. https://doi.org/10.1073/pnas.92.10.4337

Chien, Y., Scuoppo, C., Wang, X., Fang, X., Balgley, B., Bolden, J. E., Premsrirut, P., Luo, W., Chicas, A., Lee, C. S., Kogan, S. C., & Lowe, S. W. (2011). Control of the senescence-associated secretory phenotype by NF-κB promotes senescence and enhances chemosensitivity. *Genes & Development*, *25*(20), 2125–2136. https://doi.org/10.1101/gad.17276711

Childs, B. G., Baker, D. J., Wijshake, T., Conover, C. A., Campisi, J., & van Deursen, J. M. (2016). Senescent intimal foam cells are deleterious at all stages of atherosclerosis. *Science*, *354*(6311), 472–477. https://doi.org/10.1126/science.aaf6659

Childs, B. G., Durik, M., Baker, D. J., & van Deursen, J. M. (2015). Cellular senescence in aging and age-related disease: from mechanisms to therapy. *Nature Medicine*, *21*(12), 1424–1435. https://doi.org/10.1038/nm.4000

Chinnery, P. F., & Schon, E. A. (2003). Mitochondria. *Journal of Neurology, Neurosurgery & Psychiatry*, *74*(9), 1188–1199. https://doi.org/10.1136/jnnp.74.9.1188

Chuprin, A., Gal, H., Biron-Shental, T., Biran, A., Amiel, A., Rozenblatt, S., & Krizhanovsky, V. (2013). Cell fusion induced by ERVWE1 or measles virus causes cellular senescence. *Genes & Development*, *27*(21), 2356–2366. https://doi.org/10.1101/gad.227512.113

Cifra, M., & Pospíšil, P. (2014). Ultra-weak photon emission from biological samples: Definition, mechanisms, properties, detection and applications. *Journal of Photochemistry and Photobiology B: Biology*, *139*, 2–10. https://doi.org/10.1016/j.jphotobiol.2014.02.009

Clement, M., Daniel, G., & Trelles, M. (2005). Optimising the design of a broad-band light source for the treatment of skin. *Journal of Cosmetic and Laser Therapy*, *7*(3–4), 177–189. https://doi.org/10.1080/14764170500344575

Cohen, S., & Popp, F. , A. (2003). Biophon emission of human body. *Indian Journal Fo Experimental Biology*, *41*, 440–445.

Cole, L. A. (2016). Adenosine Triphosphate Energetics. *Biology of Life*, 65–77. https://doi.org/10.1016/B978-0-12-809685-7.00010-1

Coppé, J.-P., Desprez, P.-Y., Krtolica, A., & Campisi, J. (2010). The Senescence-Associated Secretory Phenotype: The Dark Side of Tumor Suppression. *Annual Review of Pathology: Mechanisms of Disease*, *5*(1), 99–118. https://doi.org/10.1146/annurev-pathol-121808-102144

Coppé, J.-P., Patil, C. K., Rodier, F., Sun, Y., Muñoz, D. P., Goldstein, J., Nelson, P. S., Desprez, P.-Y., & Campisi, J. (2008). Senescence-Associated Secretory Phenotypes Reveal Cell-Nonautonomous Functions of Oncogenic RAS and the p53 Tumor Suppressor. *PLoS Biology*, *6*(12), e301. https://doi.org/10.1371/journal.pbio.0060301

Correia-Melo, C., Marques, F. D., Anderson, R., Hewitt, G., Hewitt, R., Cole, J., Carroll, B. M., Miwa, S., Birch, J., Merz, A., Rushton, M. D., Charles, M., Jurk, D., Tait, S. W., Czapiewski, R., Greaves, L., Nelson, G., Bohlooly-Y, M., Rodriguez-Cuenca, S., … Passos, J. F. (2016). Mitochondria are required for pro-ageing features of the senescent phenotype. *The EMBO Journal*, *35*(7), 724–742. https://doi.org/10.15252/embj.201592862

Correia-Melo, C., & Passos, J. F. (2015). Mitochondria: Are they causal players in cellular senescence? *Biochimica et Biophysica Acta (BBA) - Bioenergetics*, *1847*(11), 1373–1379. https://doi.org/10.1016/j.bbabio.2015.05.017

Courtois-Cox, S., Jones, S. L., & Cichowski, K. (2008). Many roads lead to oncogene-induced senescence. *Oncogene*, *27*(20), 2801–2809. https://doi.org/10.1038/sj.onc.1210950

Craddock, T. J. A., Friesen, D., Mane, J., Hameroff, S., & Tuszynski, J. A. (2014). The feasibility of coherent energy transfer in microtubules. *Journal of The Royal Society Interface*, *11*(100), 20140677. https://doi.org/10.1098/rsif.2014.0677

Crowe, E. P., Nacarelli, T., Bitto, A., Lerner, C., Sell, C., & Torres, C. (2014). *Detecting Senescence: Methods and Approaches* (pp. 425–445). https://doi.org/10.1007/978-1-4939-0888-2_23

da Silva, P. F. L., Ogrodnik, M., Kucheryavenko, O., Glibert, J., Miwa, S., Cameron, K., Ishaq, A., Saretzki, G., Nagaraja-Grellscheid, S., Nelson, G., & von Zglinicki, T. (2019). The bystander effect contributes to the accumulation of senescent cells in vivo. *Aging Cell*, *18*(1), e12848. https://doi.org/10.1111/acel.12848

de Freitas, L. F., & Hamblin, M. R. (2016). Proposed Mechanisms of Photobiomodulation or Low-Level Light Therapy. *IEEE Journal of Selected Topics in Quantum Electronics : A Publication of the IEEE Lasers and Electro-Optics Society*, *22*(3). https://doi.org/10.1109/JSTQE.2016.2561201

de Sousa M. V. P. (2017). What is low-level laser (light) therapy? . In Michael R. Hamblin, Tanupriya Agrawal, & Marcelo de Sousa (Eds.), *Handbook of Low-Level Laser Therapy*. Pan Stanford Publishing Pte. Ttd.

de Villiers, J. A., Houreld, N. N., & Abrahamse, H. (2011). Influence of Low Intensity Laser Irradiation on Isolated Human Adipose Derived Stem Cells Over 72 Hours and Their Differentiation Potential into Smooth Muscle Cells Using Retinoic Acid. *Stem Cell Reviews and Reports*, *7*(4), 869–882. https://doi.org/10.1007/s12015-011-9244-8

Debacq-Chainiaux, F., Erusalimsky, J. D., Campisi, J., & Toussaint, O. (2009). Protocols to detect senescence-associated beta-galactosidase (SA-βgal) activity, a biomarker of senescent cells in culture and in vivo. *Nature Protocols*, *4*(12), 1798–1806. https://doi.org/10.1038/nprot.2009.191

Demaria, M., Ohtani, N., Youssef, S. A., Rodier, F., Toussaint, W., Mitchell, J. R., Laberge, R.-M., Vijg, J., Van Steeg, H., Dollé, M. E. T., Hoeijmakers, J. H. J., de Bruin, A., Hara, E., & Campisi, J. (2014). An Essential Role for Senescent Cells in Optimal Wound Healing through Secretion of PDGF-AA. *Developmental Cell*, *31*(6), 722–733. https://doi.org/10.1016/j.devcel.2014.11.012

DePinho, R. A. (2000). The age of cancer. *Nature*, *408*(6809), 248–254. https://doi.org/10.1038/35041694

Di Micco, R., Fumagalli, M., Cicalese, A., Piccinin, S., Gasparini, P., Luise, C., Schurra, C., Garre', M., Giovanni Nuciforo, P., Bensimon, A., Maestro, R., Giuseppe Pelicci, P., & d'Adda di Fagagna, F. (2006). Oncogene-induced senescence is a DNA damage response triggered by DNA hyper-replication. *Nature*, *444*(7119), 638–642. https://doi.org/10.1038/nature05327

Di Micco, R., Krizhanovsky, V., Baker, D., & d'Adda di Fagagna, F. (2021). Cellular senescence in ageing: from mechanisms to therapeutic opportunities. *Nature Reviews Molecular Cell Biology*, *22*(2), 75–95. https://doi.org/10.1038/s41580-020-00314-w

Di Mitri, D., & Alimonti, A. (2016). Non-Cell-Autonomous Regulation of Cellular Senescence in Cancer. *Trends in Cell Biology*, *26*(3), 215–226. https://doi.org/10.1016/j.tcb.2015.10.005

Di Mitri, D., Toso, A., Chen, J. J., Sarti, M., Pinton, S., Jost, T. R., D'Antuono, R., Montani, E., Garcia-Escudero, R., Guccini, I., Da Silva-Alvarez, S., Collado, M., Eisenberger, M., Zhang, Z., Catapano, C., Grassi, F., & Alimonti, A. (2014). Tumour-infiltrating Gr-1+ myeloid cells antagonize senescence in cancer. *Nature*, *515*(7525), 134–137. https://doi.org/10.1038/nature13638

Dimri, G. P., Itahana, K., Acosta, M., & Campisi, J. (2000). Regulation of a Senescence Checkpoint Response by the E2F1 Transcription Factor and p14 ^{ARF} Tumor Suppressor. *Molecular and Cellular Biology*, *20*(1), 273–285. https://doi.org/10.1128/MCB.20.1.273-285.2000

Dimri, G. P., Lee, X., Basile, G., Acosta, M., Scott, G., Roskelley, C., Medrano, E. E., Linskens, M., Rubelj, I., & Pereira-Smith, O. (1995). A biomarker that identifies senescent human cells in culture and in aging skin in vivo. *Proceedings of the National Academy of Sciences*, *92*(20), 9363–9367. https://doi.org/10.1073/pnas.92.20.9363

Dolmans, D. E. J. G. J., Fukumura, D., & Jain, R. K. (2003). Photodynamic therapy for cancer. *Nature Reviews Cancer*, *3*(5), 380–387. https://doi.org/10.1038/nrc1071

Dompe, C., Moncrieff, L., Matys, J., Grzech-Leśniak, K., Kocherova, I., Bryja, A., Bruska, M., Dominiak, M., Mozdziak, P., Skiba, T., Shibli, J., Angelova Volponi, A., Kempisty, B., & Dyszkiewicz-Konwińska, M. (2020). Photobiomodulation—Underlying Mechanism and Clinical Applications. *Journal of Clinical Medicine*, *9*(6), 1724. https://doi.org/10.3390/jcm9061724

Dreesen, O. (2020). Towards delineating the chain of events that cause premature senescence in the accelerated aging syndrome Hutchinson–Gilford progeria (HGPS). *Biochemical Society Transactions*, *48*(3), 981–991. https://doi.org/10.1042/BST20190882

Du, J., Deng, T., Cao, B., Wang, Z., Yang, M., & Han, J. (2023). The application and trend of ultra-weak photon emission in biology and medicine. *Frontiers in Chemistry*, *11*. https://doi.org/10.3389/fchem.2023.1140128

Duchen, M. R. (2000). Mitochondria and calcium: from cell signalling to cell death. *The Journal of Physiology*, *529*(1), 57–68. https://doi.org/10.1111/j.1469-7793.2000.00057.x

Duran, I., Pombo, J., Sun, B., Gallage, S., Kudo, H., McHugh, D., Bousset, L., Barragan Avila, J. E., Forlano, R., Manousou, P., Heikenwalder, M., Withers, D. J., Vernia, S., Goldin, R. D., & Gil, J. (2024). Detection of senescence using machine learning algorithms based on nuclear features. *Nature Communications*, *15*(1), 1041. https://doi.org/10.1038/s41467-024-45421-w

El-Far, A. H., Darwish, N. H. E., & Mousa, S. A. (2020). Senescent Colon and Breast Cancer Cells Induced by Doxorubicin Exhibit Enhanced Sensitivity to Curcumin, Caffeine, and Thymoquinone. *Integrative Cancer Therapies*, *19*, 153473541990116. https://doi.org/10.1177/1534735419901160

Evan, G. I., & d'Adda di Fagagna, F. (2009). Cellular senescence: hot or what? *Current Opinion in Genetics & Development*, *19*(1), 25–31. https://doi.org/10.1016/j.gde.2008.11.009

Ewald, J. A., Desotelle, J. A., Wilding, G., & Jarrard, D. F. (2010). Therapy-Induced Senescence in Cancer. *JNCI: Journal of the National Cancer Institute*, *102*(20), 1536–1546. https://doi.org/10.1093/jnci/djq364

Fagagna, F. d'Adda di, Reaper, P. M., Clay-Farrace, L., Fiegler, H., Carr, P., von Zglinicki, T., Saretzki, G., Carter, N. P., & Jackson, S. P. (2003). A DNA damage checkpoint response in telomere-initiated senescence. *Nature*, *426*(6963), 194–198. https://doi.org/10.1038/nature02118

Fallah, M., Mohammadi, H., Shaki, F., Hosseini-Khah, Z., Moloudizargari, M., Dashti, A., Ziar, A., Mohammadpour, A., Mirshafa, A., Modanloo, M., & Shokrzadeh, M. (2019). Doxorubicin and liposomal doxorubicin induce senescence by enhancing nuclear factor kappa B and mitochondrial membrane potential. *Life Sciences*, *232*, 116677. https://doi.org/10.1016/j.lfs.2019.116677

Fan, X., He, Y., Wu, G., Chen, H., Cheng, X., Zhan, Y., An, C., Chen, T., & Wang, X. (2023). Sirt3 activates autophagy to prevent DOX-induced senescence by inactivating PI3K/AKT/mTOR pathway in A549 cells. *Biochimica et Biophysica Acta (BBA) - Molecular Cell Research*, *1870*(2), 119411. https://doi.org/10.1016/j.bbamcr.2022.119411

Faragher, R. G. A. (2021). Simple Detection Methods for Senescent Cells: Opportunities and Challenges. *Frontiers in Aging*, *2*. https://doi.org/10.3389/fragi.2021.686382

Farhadi, A., Forsyth, C., Banan, A., Shaikh, M., Engen, P., Fields, J. Z., & Keshavarzian, A. (2007). Evidence for non-chemical, non-electrical intercellular signaling in intestinal epithelial cells. *Bioelectrochemistry*, *71*(2), 142–148. https://doi.org/10.1016/j.bioelechem.2007.03.001

Fernandez, A. P., Junqueira, M. de A., Marques, N. C. T., Machado, M. A. A. M., Santos, C. F., Oliveira, T. M., & Sakai, V. T. (2016). Effects of low-level laser therapy on stem cells from human exfoliated deciduous teeth. *Journal of Applied Oral Science*, *24*(4), 332–337. https://doi.org/10.1590/1678-775720150275

Finsen N. O. (1902). *Om Bekæmpelse af Lupus vulgaris med en Redegørelse for de i Danmark opnaaede Resultater.* . Gyldendalske Boghandels Forlag.

Finsen, N. R. (2023). *The Nobel Prize in Physiology or Medicine 1903*. NobelPrize.Org. https://www.nobelprize.org/prizes/medicine/1903/summary/

Fleiss, A., & Sarkisyan, K. S. (2019). A brief review of bioluminescent systems (2019). *Current Genetics*, *65*(4), 877–882. https://doi.org/10.1007/s00294-019-00951-5

Fonteriz, R. I., de la Fuente, S., Moreno, A., Lobatón, C. D., Montero, M., & Alvarez, J. (2010). Monitoring mitochondrial [Ca2+] dynamics with rhod-2, ratiometric pericam and aequorin. *Cell Calcium*, *48*(1), 61–69. https://doi.org/10.1016/j.ceca.2010.07.001

Foo, A. S. C., Soong, T. W., Yeo, T. T., & Lim, K.-L. (2020). Mitochondrial Dysfunction and Parkinson's Disease—Near-Infrared Photobiomodulation as a Potential Therapeutic Strategy. *Frontiers in Aging Neuroscience*, *12*. https://doi.org/10.3389/fnagi.2020.00089

Foo, M. X. R., Ong, P. F., & Dreesen, O. (2019). Premature aging syndromes: From patients to mechanism. *Journal of Dermatological Science*, *96*(2), 58–65. https://doi.org/10.1016/j.jdermsci.2019.10.003

Freund, A., Patil, C. K., & Campisi, J. (2011). p38MAPK is a novel DNA damage response-independent regulator of the senescence-associated secretory phenotype. *The EMBO Journal*, *30*(8), 1536–1548. https://doi.org/10.1038/emboj.2011.69

Friedman, J. R., & Nunnari, J. (2014). Mitochondrial form and function. *Nature*, *505*(7483), 335–343. https://doi.org/10.1038/nature12985

Fumagalli, M., Rossiello, F., Mondello, C., & d'Adda di Fagagna, F. (2014). Stable Cellular Senescence Is Associated with Persistent DDR Activation. *PLoS ONE*, *9*(10), e110969. https://doi.org/10.1371/journal.pone.0110969

Gabe, Y., Osanai, O., & Takema, Y. (2014). The relationship between skin aging and steady state ultraweak photon emission as an indicator of skin oxidative stress *in vivo*. *Skin Research and Technology*, *20*(3), 315–321. https://doi.org/10.1111/srt.12121

Gasek, N. S., Kuchel, G. A., Kirkland, J. L., & Xu, M. (2021). Strategies for targeting senescent cells in human disease. *Nature Aging*, *1*(10), 870–879. https://doi.org/10.1038/s43587-021-00121-8

Gee, K. R., Brown, K. A., Chen, W.-N. U., Bishop-Stewart, J., Gray, D., & Johnson, I. (2000). Chemical and physiological characterization of fluo-4 Ca2+-indicator dyes. *Cell Calcium*, *27*(2), 97–106. https://doi.org/10.1054/ceca.1999.0095

Giles, R. E., Blanc, H., Cann, H. M., & Wallace, D. C. (1980). Maternal inheritance of human mitochondrial DNA. *Proceedings of the National Academy of Sciences*, *77*(11), 6715–6719. https://doi.org/10.1073/pnas.77.11.6715

Golovynska, I., Golovynskyi, S., Stepanov, Y. V., Garmanchuk, L. V., Stepanova, L. I., Qu, J., & Ohulchanskyy, T. Y. (2019). Red and near-infrared light induces intracellular Ca $^{2+}$ flux via the activation of glutamate *N* -methyl-D-aspartate receptors. *Journal of Cellular Physiology*, *234*(9), 15989–16002. https://doi.org/10.1002/jcp.28257

Golovynska, I., Golovynskyi, S., Stepanov, Y. V., Stepanova, L. I., Qu, J., & Ohulchanskyy, T. Y. (2021). Red and near-infrared light evokes Ca2+ influx, endoplasmic reticulum release and membrane depolarization in neurons and cancer cells. *Journal of Photochemistry and Photobiology B: Biology*, *214*, 112088. https://doi.org/10.1016/j.jphotobiol.2020.112088

Gonçalves de Faria, C. M., Ciol, H., Salvador Bagnato, V., & Pratavieira, S. (2021). Effects of photobiomodulation on the redox state of healthy and cancer cells. *Biomedical Optics Express*, *12*(7), 3902. https://doi.org/10.1364/BOE.421302

Gorgoulis, V., Adams, P. D., Alimonti, A., Bennett, D. C., Bischof, O., Bishop, C., Campisi, J., Collado, M., Evangelou, K., Ferbeyre, G., Gil, J., Hara, E., Krizhanovsky, V., Jurk, D., Maier, A. B., Narita, M., Niedernhofer, L., Passos, J. F., Robbins, P. D., …

Demaria, M. (2019). Cellular Senescence: Defining a Path Forward. *Cell*, *179*(4), 813–827. https://doi.org/10.1016/j.cell.2019.10.005

Gorgoulis, V. G., & Halazonetis, T. D. (2010). Oncogene-induced senescence: the bright and dark side of the response. *Current Opinion in Cell Biology*, *22*(6), 816–827. https://doi.org/10.1016/j.ceb.2010.07.013

Görlach, A., Bertram, K., Hudecova, S., & Krizanova, O. (2015). Calcium and ROS: A mutual interplay. *Redox Biology*, *6*, 260–271. https://doi.org/10.1016/j.redox.2015.08.010

Greco, G., Ulfo, L., Turrini, E., Marconi, A., Costantini, P. E., Marforio, T. D., Mattioli, E. J., Di Giosia, M., Danielli, A., Fimognari, C., & Calvaresi, M. (2023). Light-Enhanced Cytotoxicity of Doxorubicin by Photoactivation. *Cells*, *12*(3), 392. https://doi.org/10.3390/cells12030392

Grzech-Leśniak, K. (2017). Making Use of Lasers in Periodontal Treatment: A New Gold Standard? *Photomedicine and Laser Surgery*, *35*(10), 513–514. https://doi.org/10.1089/pho.2017.4323

Gurwitsch, A. (1923). Die Natur des spezifischen Erregers der Zellteilung. *Archiv Für Mikroskopische Anatomie Und Entwicklungsmechanik*, *100*(1–2), 11–40. https://doi.org/10.1007/BF02111053

Hagens, R., Khabiri, F., Schreiner, V., Wenck, H., Wittern, K., Duchstein, H., & Mei, W. (2008). Non-invasive monitoring of oxidative skin stress by ultraweak photon emission measurement. II: biological validation on ultraviolet A-stressed skin. *Skin Research and Technology*, *14*(1), 112–120. https://doi.org/10.1111/j.1600-0846.2007.00207.x

Hamblin, M. R. (2016a). Photobiomodulation or low-level laser therapy. *Journal of Biophotonics*, *9*(11–12), 1122–1124. https://doi.org/10.1002/jbio.201670113

Hamblin, M. R. (2016b). Shining light on the head: Photobiomodulation for brain disorders. *BBA Clinical*, *6*, 113–124. https://doi.org/10.1016/j.bbacli.2016.09.002

Hamblin, M. R. (2017a). Mechanisms and applications of the anti-inflammatory effects of photobiomodulation. *AIMS Biophysics*, *4*(3), 337–361. https://doi.org/10.3934/biophy.2017.3.337

Hamblin, M. R. (2017b). Mechanisms and applications of the anti-inflammatory effects of photobiomodulation. *AIMS Biophysics*, *4*(3), 337–361. https://doi.org/10.3934/biophy.2017.3.337

Hamblin, M. R. (2018a). Mechanisms and Mitochondrial Redox Signaling in Photobiomodulation. *Photochemistry and Photobiology*, *94*(2), 199–212. https://doi.org/10.1111/php.12864

Hamblin, M. R. (2018b). Photobiomodulation for traumatic brain injury and stroke. *Journal of Neuroscience Research*, *96*(4), 731–743. https://doi.org/10.1002/jnr.24190

Hamblin, M. R., Nelson, S. T., & Strahan, J. R. (2018). Photobiomodulation and Cancer: What Is the Truth? *Photomedicine and Laser Surgery*, *36*(5), 241–245. https://doi.org/10.1089/pho.2017.4401

Harley, C. B., Futcher, A. B., & Greider, C. W. (1990). Telomeres shorten during ageing of human fibroblasts. *Nature*, *345*(6274), 458–460. https://doi.org/10.1038/345458a0

Harman, D. (1956). Aging: A Theory Based on Free Radical and Radiation Chemistry. *Journal of Gerontology*, *11*(3), 298–300. https://doi.org/10.1093/geronj/11.3.298

Hatefi, Y. (1985). THE MITOCHONDRIAL ELECTRON TRANSPORT AND OXIDATIVE PHOSPHORYLATION SYSTEM. *Annual Review of Biochemistry*, *54*(1), 1015–1069. https://doi.org/10.1146/annurev.bi.54.070185.005055

Hayflick, L., & Moorhead, P. S. (1961). The serial cultivation of human diploid cell strains. *Experimental Cell Research*, *25*(3), 585–621. https://doi.org/10.1016/0014-4827(61)90192-6

He, S., & Sharpless, N. E. (2017). Senescence in Health and Disease. *Cell*, *169*(6), 1000–1011. https://doi.org/10.1016/j.cell.2017.05.015

Helman, A., Klochendler, A., Azazmeh, N., Gabai, Y., Horwitz, E., Anzi, S., Swisa, A., Condiotti, R., Granit, R. Z., Nevo, Y., Fixler, Y., Shreibman, D., Zamir, A., Tornovsky-Babeay, S., Dai, C., Glaser, B., Powers, A. C., Shapiro, A. M. J., Magnuson, M. A., … Ben-Porath, I. (2016). p16Ink4a-induced senescence of pancreatic beta cells enhances insulin secretion. *Nature Medicine*, *22*(4), 412–420. https://doi.org/10.1038/nm.4054

Herbig, U., Ferreira, M., Condel, L., Carey, D., & Sedivy, J. M. (2006). Cellular Senescence in Aging Primates. *Science*, *311*(5765), 1257–1257. https://doi.org/10.1126/science.1122446

Herbig, U., Jobling, W. A., Chen, B. P. C., Chen, D. J., & Sedivy, J. M. (2004). Telomere Shortening Triggers Senescence of Human Cells through a Pathway Involving ATM, p53, and p21CIP1, but Not p16INK4a. *Molecular Cell*, *14*(4), 501–513. https://doi.org/10.1016/S1097-2765(04)00256-4

Hernandez-Segura, A., Nehme, J., & Demaria, M. (2018a). Hallmarks of Cellular Senescence. *Trends in Cell Biology*, *28*(6), 436–453. https://doi.org/10.1016/j.tcb.2018.02.001

Hernandez-Segura, A., Brandenburg, S., & Demaria, M. (2018b). Induction and Validation of Cellular Senescence in Primary Human Cells. *Journal of Visualized Experiments*, *136*. https://doi.org/10.3791/57782

Herskind, C., & Rodemann, H. P. (2000). Spontaneous and radiation-induced differentiationof fibroblasts. *Experimental Gerontology*, *35*(6–7), 747–755. https://doi.org/10.1016/S0531-5565(00)00168-6

Höhn, A., Weber, D., Jung, T., Ott, C., Hugo, M., Kochlik, B., Kehm, R., König, J., Grune, T., & Castro, J. P. (2017). Happily (n)ever after: Aging in the context of oxidative stress, proteostasis loss and cellular senescence. *Redox Biology*, *11*, 482–501. https://doi.org/10.1016/j.redox.2016.12.001

Hooten, N. N., & Evans, M. K. (2017). Techniques to Induce and Quantify Cellular Senescence. *Journal of Visualized Experiments*, *123*. https://doi.org/10.3791/55533

Hou, J.-G., Jeon, B.-M., Yun, Y.-J., Cui, C.-H., & Kim, S.-C. (2019). Ginsenoside Rh2 Ameliorates Doxorubicin-Induced Senescence Bystander Effect in Breast Carcinoma

Cell MDA-MB-231 and Normal Epithelial Cell MCF-10A. *International Journal of Molecular Sciences*, *20*(5), 1244. https://doi.org/10.3390/ijms20051244

Hu, W.-P., Wang, J.-J., Yu, C.-L., Lan, C.-C. E., Chen, G.-S., & Yu, H.-S. (2007). Helium–Neon Laser Irradiation Stimulates Cell Proliferation through Photostimulatory Effects in Mitochondria. *Journal of Investigative Dermatology*, *127*(8), 2048–2057. https://doi.org/10.1038/sj.jid.5700826

Huang, W., Hickson, L. J., Eirin, A., Kirkland, J. L., & Lerman, L. O. (2022). Cellular senescence: the good, the bad and the unknown. *Nature Reviews Nephrology*, *18*(10), 611–627. https://doi.org/10.1038/s41581-022-00601-z

Huang, Y.-Y., Sharma, S. K., Carroll, J., & Hamblin, M. R. (2011). Biphasic Dose Response in Low Level Light Therapy – an Update. *Dose-Response*, *9*(4), dose-response.1. https://doi.org/10.2203/dose-response.11-009.Hamblin

Hutter, E., Renner, K., Pfister, G., Stockl, P., Jansen-Durr, P., & Gnaiger, E. (2004). Senescence-associated changes in respiration and oxidative phosphorylation in primary human fibroblasts. *Biochemical Journal*, *380*(3), 919–928. https://doi.org/10.1042/bj20040095

Iida, T. , Yoshiki, Y. , Someya, S. , & Okubo, K. (2002). Generation of Reactive Oxygen Species and Photon Emission from a Browned Product. *Bioscience, Biotechnology, and Biochemistry*, *66*(8), 1641–1645. https://doi.org/10.1271/bbb.66.1641

Inagaki, H. , Ishida, Y. , U. A. , Kato, K. , Kageyama, C. , Iyozumi, H. , & Nukui, H. ,. (2008). Difference in ultraweak photon emissions between sulfonylurea-resistant and sulfonylurea-susceptible biotypes of Scirpus juncoides following the application of a sulfonylurea herbicide. *Weed Biology and Management*, *8*(2), 78–84. https://doi.org/10.1111/j.1445-6664.2008.00278.x

Jeon, O. H., Kim, C., Laberge, R.-M., Demaria, M., Rathod, S., Vasserot, A. P., Chung, J. W., Kim, D. H., Poon, Y., David, N., Baker, D. J., van Deursen, J. M., Campisi, J., & Elisseeff, J. H. (2017). Local clearance of senescent cells attenuates the development of post-traumatic osteoarthritis and creates a pro-regenerative environment. *Nature Medicine*, *23*(6), 775–781. https://doi.org/10.1038/nm.4324

Jochems, F., Thijssen, B., De Conti, G., Jansen, R., Pogacar, Z., Groot, K., Wang, L., Schepers, A., Wang, C., Jin, H., Beijersbergen, R. L., Leite de Oliveira, R., Wessels, L. F. A., & Bernards, R. (2021). The Cancer SENESCopedia: A delineation of cancer cell senescence. *Cell Reports*, *36*(4), 109441. https://doi.org/10.1016/j.celrep.2021.109441

Johnstone, D. M., Moro, C., Stone, J., Benabid, A.-L., & Mitrofanis, J. (2016). Turning On Lights to Stop Neurodegeneration: The Potential of Near Infrared Light Therapy in Alzheimer's and Parkinson's Disease. *Frontiers in Neuroscience*, *9*. https://doi.org/10.3389/fnins.2015.00500

Jost, T., Heinzerling, L., Fietkau, R., Hecht, M., & Distel, L. V. (2021). Palbociclib Induces Senescence in Melanoma and Breast Cancer Cells and Leads to Additive Growth Arrest in Combination With Irradiation. *Frontiers in Oncology*, *11*. https://doi.org/10.3389/fonc.2021.740002

Jun, J.-I., & Lau, L. F. (2010). The matricellular protein CCN1 induces fibroblast senescence and restricts fibrosis in cutaneous wound healing. *Nature Cell Biology*, *12*(7), 676–685. https://doi.org/10.1038/ncb2070

Kalampouka, I., Mould, R. R., Botchway, S. W., Mackenzie, A. M., Nunn, A. V., Thomas, E. L., & Bell, J. D. (2024). Selective induction of senescence in cancer cells through near-infrared light treatment via mitochondrial modulation. *Journal of Biophotonics*. https://doi.org/10.1002/jbio.202400046

Kamal, A. H. M., & Komatsu, S. (2016). Proteins involved in biophoton emission and flooding-stress responses in soybean under light and dark conditions. *Molecular Biology Reports*, *43*(2), 73–89. https://doi.org/10.1007/s11033-015-3940-4

Karu, T. I. (2008). Mitochondrial Signaling in Mammalian Cells Activated by Red and Near-IR Radiation. *Photochemistry and Photobiology*, *84*(5), 1091–1099. https://doi.org/10.1111/j.1751-1097.2008.00394.x

Kaynezhad, P., Tachtsidis, I., & Jeffery, G. (2016). Optical monitoring of retinal respiration in real time: 670 nm light increases the redox state of mitochondria. *Experimental Eye Research*, *152*, 88–93. https://doi.org/10.1016/j.exer.2016.09.006

Kaznacheev, A. V. P., Mikhailova, L. P., & Kartashov, N. B. (1980). Distant intercellular electromagnetic interaction between two tissue cultures. *Bulletin of Experimental Biology and Medicine*, *89*(3), 345–348. https://doi.org/10.1007/BF00834249

Khadra, M., Lyngstadaas, S. P., Haanæs, H. R., & Mustafa, K. (2005). Effect of laser therapy on attachment, proliferation and differentiation of human osteoblast-like cells cultured on titanium implant material. *Biomaterials*, *26*(17), 3503–3509. https://doi.org/10.1016/j.biomaterials.2004.09.033

Kim, H., Esser, L., Hossain, M. B., Xia, D., Yu, C.-A., Rizo, J., van der Helm, D., & Deisenhofer, J. (1999). Structure of Antimycin A1, a Specific Electron Transfer Inhibitor of Ubiquinol−Cytochrome *c* Oxidoreductase. *Journal of the American Chemical Society*, *121*(20), 4902–4903. https://doi.org/10.1021/ja990190h

Kim, H. P. (2014). Lightening up Light Therapy: Activation of Retrograde Signaling Pathway by Photobiomodulation. *Biomolecules & Therapeutics*, *22*(6), 491–496. https://doi.org/10.4062/biomolther.2014.083

Kim, J. E., Woo, Y. J., Sohn, K. M., Jeong, K. H., & Kang, H. (2017). Wnt/β-catenin and ERK pathway activation: A possible mechanism of photobiomodulation therapy with light-emitting diodes that regulate the proliferation of human outer root sheath cells. *Lasers in Surgery and Medicine*, *49*(10), 940–947. https://doi.org/10.1002/lsm.22736

Kim, K., Lee, J., Jang, H., Park, S., Na, J., Myung, J., Kim, M.-J., Jang, W.-S., Lee, S.-J., Kim, H., Myung, H., Kang, J., & Shim, S. (2019). Photobiomodulation Enhances the Angiogenic Effect of Mesenchymal Stem Cells to Mitigate Radiation-Induced Enteropathy. *International Journal of Molecular Sciences*, *20*(5), 1131. https://doi.org/10.3390/ijms20051131

Kim, K.-H., Chen, C.-C., Monzon, R. I., & Lau, L. F. (2013). Matricellular Protein CCN1 Promotes Regression of Liver Fibrosis through Induction of Cellular Senescence in Hepatic Myofibroblasts. *Molecular and Cellular Biology*, *33*(10), 2078–2090. https://doi.org/10.1128/MCB.00049-13

Kobayashi, M., Kikuchi, D., & Okamura, H. (2009). Imaging of Ultraweak Spontaneous Photon Emission from Human Body Displaying Diurnal Rhythm. *PLoS ONE*, *4*(7), e6256. https://doi.org/10.1371/journal.pone.0006256

Kobayashi, M., Sasaki, K., Enomoto, M., & Ehara, Y. (2006). Highly sensitive determination of transient generation of biophotons during hypersensitive response to cucumber mosaic virus in cowpea. *Journal of Experimental Botany*, *58*(3), 465–472. https://doi.org/10.1093/jxb/erl215

Koopman, W. J. H., Distelmaier, F., Smeitink, J. A., & Willems, P. H. (2012). OXPHOS mutations and neurodegeneration. *The EMBO Journal*, *32*(1), 9–29. https://doi.org/10.1038/emboj.2012.300

Korolchuk, V. I., Miwa, S., Carroll, B., & von Zglinicki, T. (2017). Mitochondria in Cell Senescence: Is Mitophagy the Weakest Link? *EBioMedicine*, *21*, 7–13. https://doi.org/10.1016/j.ebiom.2017.03.020

Korshunov, S. S., Skulachev, V. P., & Starkov, A. A. (1997). High protonic potential actuates a mechanism of production of reactive oxygen species in mitochondria. *FEBS Letters*, *416*(1), 15–18. https://doi.org/10.1016/S0014-5793(97)01159-9

Krishan, A. (1975). Rapid flow cytofluorometric analysis of mammalian cell cycle by propidium iodide staining. *The Journal of Cell Biology*, *66*(1), 188–193. https://doi.org/10.1083/jcb.66.1.188

Krizhanovsky, V., Yon, M., Dickins, R. A., Hearn, S., Simon, J., Miething, C., Yee, H., Zender, L., & Lowe, S. W. (2008). Senescence of Activated Stellate Cells Limits Liver Fibrosis. *Cell*, *134*(4), 657–667. https://doi.org/10.1016/j.cell.2008.06.049

Kuilman, T., Michaloglou, C., Mooi, W. J., & Peeper, D. S. (2010). The essence of senescence. *Genes & Development*, *24*(22), 2463–2479. https://doi.org/10.1101/gad.1971610

Kuilman, T., & Peeper, D. S. (2009). Senescence-messaging secretome: SMS-ing cellular stress. *Nature Reviews Cancer*, *9*(2), 81–94. https://doi.org/10.1038/nrc2560

Kujawa, J., Pasternak, K., Zavodnik, I., Irzmański, R., Wróbel, D., & Bryszewska, M. (2014). The effect of near-infrared MLS laser radiation on cell membrane structure and radical generation. *Lasers in Medical Science*, *29*(5), 1663–1668. https://doi.org/10.1007/s10103-014-1571-y

Kumari, R., & Jat, P. (2021). Mechanisms of Cellular Senescence: Cell Cycle Arrest and Senescence Associated Secretory Phenotype. *Frontiers in Cell and Developmental Biology*, *9*. https://doi.org/10.3389/fcell.2021.645593

Kurian, P., Obisesan, T. O., & Craddock, T. J. A. (2017). Oxidative species-induced excitonic transport in tubulin aromatic networks: Potential implications for neurodegenerative disease. *Journal of Photochemistry and Photobiology B: Biology*, *175*, 109–124. https://doi.org/10.1016/j.jphotobiol.2017.08.033

Kurz, D. J., Decary, S., Hong, Y., & Erusalimsky, J. D. (2000). Senescence-associated (beta)-galactosidase reflects an increase in lysosomal mass during replicative ageing of human endothelial cells. *Journal of Cell Science*, *113*(20), 3613–3622. https://doi.org/10.1242/jcs.113.20.3613

Laakso, L., Richardson, C., & Cramond, T. (1993). Factors affecting Low Level Laser Therapy. *Australian Journal of Physiotherapy*, *39*(2), 95–99. https://doi.org/10.1016/S0004-9514(14)60473-6

Laberge, R.-M., Sun, Y., Orjalo, A. V., Patil, C. K., Freund, A., Zhou, L., Curran, S. C., Davalos, A. R., Wilson-Edell, K. A., Liu, S., Limbad, C., Demaria, M., Li, P., Hubbard, G. B., Ikeno, Y., Javors, M., Desprez, P.-Y., Benz, C. C., Kapahi, P., … Campisi, J. (2015). MTOR regulates the pro-tumorigenic senescence-associated secretory phenotype by promoting IL1A translation. *Nature Cell Biology*, *17*(8), 1049–1061. https://doi.org/10.1038/ncb3195

Lackner, L. L. (2013). Determining the shape and cellular distribution of mitochondria: the integration of multiple activities. *Current Opinion in Cell Biology*, *25*(4), 471–476. https://doi.org/10.1016/j.ceb.2013.02.011

Lee, A. C., Fenster, B. E., Ito, H., Takeda, K., Bae, N. S., Hirai, T., Yu, Z.-X., Ferrans, V. J., Howard, B. H., & Finkel, T. (1999). Ras Proteins Induce Senescence by Altering the Intracellular Levels of Reactive Oxygen Species. *Journal of Biological Chemistry*, *274*(12), 7936–7940. https://doi.org/10.1074/jbc.274.12.7936

Lee, B. Y., Han, J. A., Im, J. S., Morrone, A., Johung, K., Goodwin, E. C., Kleijer, W. J., DiMaio, D., & Hwang, E. S. (2006). Senescence-associated β-galactosidase is lysosomal β-galactosidase. *Aging Cell*, *5*(2), 187–195. https://doi.org/10.1111/j.1474-9726.2006.00199.x

Leite de Oliveira, R., & Bernards, R. (2018). Anti-cancer therapy: senescence is the new black. *The EMBO Journal*, *37*(10). https://doi.org/10.15252/embj.201899386

Levine, M. E. (2013). Modeling the Rate of Senescence: Can Estimated Biological Age Predict Mortality More Accurately Than Chronological Age? *The Journals of Gerontology Series A: Biological Sciences and Medical Sciences*, *68*(6), 667–674. https://doi.org/10.1093/gerona/gls233

Liao, C., Xiao, Y., & Liu, L. (2020). The Dynamic Process and Its Dual Effects on Tumors of Therapy-Induced Senescence. *Cancer Management and Research*, *Volume 12*, 13553–13566. https://doi.org/10.2147/CMAR.S285083

López-Otín, C., Blasco, M. A., Partridge, L., Serrano, M., & Kroemer, G. (2013). The Hallmarks of Aging. *Cell*, *153*(6), 1194–1217. https://doi.org/10.1016/j.cell.2013.05.039

Lowe, S. W., Cepero, E., & Evan, G. (2004). Intrinsic tumour suppression. *Nature*, *432*(7015), 307–315. https://doi.org/10.1038/nature03098

Lujambio, A. (2016). To clear, or not to clear (senescent cells)? That is the question. *BioEssays*, *38*, S56–S64. https://doi.org/10.1002/bies.201670910

Mackenzie, A. M., Smith, H. E., Mould, R. R., Bell, J. D., Nunn, A. V. W., & Botchway, S. W. (2024). Rooting out ultraweak photon emission a-mung bean sprouts. *Journal of Photochemistry and Photobiology*, *19*, 100224. https://doi.org/10.1016/j.jpap.2023.100224

Magrini, T. D., dos Santos, N. V., Milazzotto, M. P., Cerchiaro, G., & da Silva Martinho, H. (2012). Low-level laser therapy on MCF-7 cells: a micro-Fourier transform infrared spectroscopy study. *Journal of Biomedical Optics*, *17*(10), 1015161. https://doi.org/10.1117/1.JBO.17.10.101516

Marais, A., Adams, B., Ringsmuth, A. K., Ferretti, M., Gruber, J. M., Hendrikx, R., Schuld, M., Smith, S. L., Sinayskiy, I., Krüger, T. P. J., Petruccione, F., & van Grondelle, R. (2018). The future of quantum biology. *Journal of The Royal Society Interface*, *15*(148), 20180640. https://doi.org/10.1098/rsif.2018.0640

Martin, N., & Bernard, D. (2018). Calcium signaling and cellular senescence. *Cell Calcium*, *70*, 16–23. https://doi.org/10.1016/j.ceca.2017.04.001

Martin, N., Zhu, K., Czarnecka-Herok, J., Vernier, M., & Bernard, D. (2023). Regulation and role of calcium in cellular senescence. *Cell Calcium*, *110*, 102701. https://doi.org/10.1016/j.ceca.2023.102701

Martini, H., & Passos, J. F. (2023). Cellular senescence: all roads lead to mitochondria. *The FEBS Journal*, *290*(5), 1186–1202. https://doi.org/10.1111/febs.16361

McCarthy, D. A., Clark, R. R., Bartling, T. R., Trebak, M., & Melendez, J. A. (2013). Redox Control of the Senescence Regulator Interleukin-1α and the Secretory Phenotype. *Journal of Biological Chemistry*, *288*(45), 32149–32159. https://doi.org/10.1074/jbc.M113.493841

McHugh, D., & Gil, J. (2018). Senescence and aging: Causes, consequences, and therapeutic avenues. *Journal of Cell Biology*, *217*(1), 65–77. https://doi.org/10.1083/jcb.201708092

Menon, S. G., & Goswami, P. C. (2007). A redox cycle within the cell cycle: ring in the old with the new. *Oncogene*, *26*(8), 1101–1109. https://doi.org/10.1038/sj.onc.1209895

Mester, E., Ludany, G., Selyei, M., Szende, B., & Total, G. J. (1968a). The stimulating effect of low power laser rays on biological systems. *Laser Rev.*, *1*(3).

Mester, E., Szende, B., & Gärtner, P. (1968b). The effect of laser beams on the growth of hair in mice. *Radiobiologia, Radiotherapia*, *9*(5), 621–626.

Mijares, A., Allen, P. D., & Lopez, J. R. (2021). Senescence Is Associated With Elevated Intracellular Resting [Ca2 +] in Mice Skeletal Muscle Fibers. An in vivo Study. *Frontiers in Physiology*, *11*. https://doi.org/10.3389/fphys.2020.601189

Milczarek, M. (2020). The Premature Senescence in Breast Cancer Treatment Strategy. *Cancers*, *12*(7), 1815. https://doi.org/10.3390/cancers12071815

Minuzzi, L. G., Rama, L., Chupel, M. U., Rosado, F., Dos Santos, J. V., Simpson, R., Martinho, A., Paiva, A., & Teixeira, A. M. (2018). Effects of lifelong training on senescence and mobilization of T lymphocytes in response to acute exercise. *Exercise Immunology Review*, *24*, 72–84.

Mitrofanis, J., & Jeffery, G. (2018). Does photobiomodulation influence ageing? *Aging*, *10*(9), 2224–2225. https://doi.org/10.18632/aging.101556

Miwa, S., Kashyap, S., Chini, E., & von Zglinicki, T. (2022). Mitochondrial dysfunction in cell senescence and aging. *Journal of Clinical Investigation*, *132*(13). https://doi.org/10.1172/JCI158447

Mizutani, S., & Tomoda Y. (1996). Effects of placental proteases on maternal and fetal blood pressure in normal pregnancy and preeclampsia. *American Journal of Hypertension*, *9*(6), 591–597. https://doi.org/10.1016/0895-7061(96)00016-7

Moore, A. S., & Holzbaur, E. L. (2018). Mitochondrial-cytoskeletal interactions: dynamic associations that facilitate network function and remodeling. *Current Opinion in Physiology*, *3*, 94–100. https://doi.org/10.1016/j.cophys.2018.03.003

Morris-Hanon, O., Marazita, M. C., Romorini, L., Isaja, L., Fernandez-Espinosa, D. D., Sevlever, G. E., Scassa, M. E., & Videla-Richardson, G. A. (2019). Palbociclib Effectively Halts Proliferation but Fails to Induce Senescence in Patient-Derived Glioma Stem Cells. *Molecular Neurobiology*, *56*(11), 7810–7821. https://doi.org/10.1007/s12035-019-1633-z

Moskalev, A., Guvatova, Z., Lopes, I. D. A., Beckett, C. W., Kennedy, B. K., De Magalhaes, J. P., & Makarov, A. A. (2022). Targeting aging mechanisms: pharmacological perspectives. *Trends in Endocrinology & Metabolism*. https://doi.org/10.1016/j.tem.2022.01.007

Mould, R. R., Kalampouka, I., Thomas, E. L., Guy, G. W., Nunn, A. V. W., & Bell, J. D. (2023). Non-chemical signalling between mitochondria. *Frontiers in Physiology*, *14*. https://doi.org/10.3389/fphys.2023.1268075

Mould, R. R., Mackenzie, A. M., Kalampouka, I., Nunn, A. V. W., Thomas, E. L., Bell, J. D., & Botchway, S. W. (2024). Ultra weak photon emission—a brief review. *Frontiers in Physiology*, *15*. https://doi.org/10.3389/fphys.2024.1348915

Mould, R. R., Thomas, E. T., Guy, G., Nunn, A., & Bell, J. (2022). Cell-cell death communication by signals passing through non-aqueous environments: A reply. *Results in Chemistry*, *4*, 100538. https://doi.org/10.1016/j.rechem.2022.100538

Muñoz-Espín, D., Cañamero, M., Maraver, A., Gómez-López, G., Contreras, J., Murillo-Cuesta, S., Rodríguez-Baeza, A., Varela-Nieto, I., Ruberte, J., Collado, M., & Serrano, M. (2013). Programmed Cell Senescence during Mammalian Embryonic Development. *Cell*, *155*(5), 1104–1118. https://doi.org/10.1016/j.cell.2013.10.019

Muñoz-Espín, D., & Serrano, M. (2014). Cellular senescence: from physiology to pathology. *Nature Reviews Molecular Cell Biology*, *15*(7), 482–496. https://doi.org/10.1038/nrm3823

Murata, D., Arai, K., Iijima, M., & Sesaki, H. (2020). Mitochondrial division, fusion and degradation. *The Journal of Biochemistry*, *167*(3), 233–241. https://doi.org/10.1093/jb/mvz106

Murugan, N. J., Persinger, M. A., Karbowski, L. M., & Dotta, B. T. (2020). Ultraweak Photon Emissions as a Non-Invasive, Early-Malignancy Detection Tool: An In Vitro and In Vivo Study. *Cancers*, *12*(4), 1001. https://doi.org/10.3390/cancers12041001

Myrianthopoulos, V., Evangelou, K., Vasileiou, P. V. S., Cooks, T., Vassilakopoulos, T. P., Pangalis, G. A., Kouloukoussa, M., Kittas, C., Georgakilas, A. G., & Gorgoulis, V. G. (2019). Senescence and senotherapeutics: a new field in cancer therapy. *Pharmacology & Therapeutics*, *193*, 31–49. https://doi.org/10.1016/j.pharmthera.2018.08.006

Naeser, M. A., Zafonte, R., Krengel, M. H., Martin, P. I., Frazier, J., Hamblin, M. R., Knight, J. A., Meehan, W. P., & Baker, E. H. (2014). Significant Improvements in Cognitive Performance Post-Transcranial, Red/Near-Infrared Light-Emitting Diode Treatments in Chronic, Mild Traumatic Brain Injury: Open-Protocol Study. *Journal of Neurotrauma*, *31*(11), 1008–1017. https://doi.org/10.1089/neu.2013.3244

Narita, M., Nuñez, S., Heard, E., Narita, M., Lin, A. W., Hearn, S. A., Spector, D. L., Hannon, G. J., & Lowe, S. W. (2003). Rb-Mediated Heterochromatin Formation and Silencing of E2F Target Genes during Cellular Senescence. *Cell*, *113*(6), 703–716. https://doi.org/10.1016/S0092-8674(03)00401-X

Niggli, H. J. (1992). Ultraweak photons emitted by cells: Biophotons. *Journal of Photochemistry and Photobiology B: Biology*, *14*(1–2), 144–146. https://doi.org/10.1016/1011-1344(92)85090-H

Nitiss, J. L. (2009). Targeting DNA topoisomerase II in cancer chemotherapy. *Nature Reviews Cancer*, *9*(5), 338–350. https://doi.org/10.1038/nrc2607

Noppe, G., Dekker, P., de Koning-Treurniet, C., Blom, J., van Heemst, D., Dirks, R. W., Tanke, H. J., Westendorp, R. G. J., & Maier, A. B. (2009). Rapid flow cytometric method for measuring senescence associated β-galactosidase activity in human fibroblasts. *Cytometry Part A*, *75A*(11), 910–916. https://doi.org/10.1002/cyto.a.20796

Nunn, A. V. W., Guy, G. W., Botchway, S. W., & Bell, J. D. (2020). From sunscreens to medicines: Can a dissipation hypothesis explain the beneficial aspects of many plant compounds? *Phytotherapy Research*, *34*(8), 1868–1888. https://doi.org/10.1002/ptr.6654

Ohya, T., Kurashige, H., Okabe, H., & Kai, S. (2000). Early Detection of Salt Stress Damage by Biophotons in Red Bean Seedling. *Japanese Journal of Applied Physics*, *39*(Part 1, No. 6A), 3696–3700. https://doi.org/10.1143/JJAP.39.3696

Ohya, T., Yoshida, S., Kawabata, R., Okabe, H., & Kai, S. (2002). Biophoton Emission Due to Drought Injury in Red Beans: Possibility of Early Detection of Drought Injury. *Japanese Journal of Applied Physics*, *41*(Part 1, No. 7A), 4766–4771. https://doi.org/10.1143/JJAP.41.4766

Ortega-Ojeda, F., Calcerrada, M., Ferrero, A., Campos, J., & Garcia-Ruiz, C. (2018). Measuring the Human Ultra-Weak Photon Emission Distribution Using an Electron-Multiplying, Charge-Coupled Device as a Sensor. *Sensors*, *18*(4), 1152. https://doi.org/10.3390/s18041152

Passarella, S., & Karu, T. (2014). Absorption of monochromatic and narrow band radiation in the visible and near IR by both mitochondrial and non-mitochondrial photoacceptors results in photobiomodulation. *Journal of Photochemistry and Photobiology B: Biology*, *140*, 344–358. https://doi.org/10.1016/j.jphotobiol.2014.07.021

Passos, J. F., Nelson, G., Wang, C., Richter, T., Simillion, C., Proctor, C. J., Miwa, S., Olijslagers, S., Hallinan, J., Wipat, A., Saretzki, G., Rudolph, K. L., Kirkwood, T. B. L., & von Zglinicki, T. (2010). Feedback between p21 and reactive oxygen production is necessary for cell senescence. *Molecular Systems Biology*, *6*(1), 347. https://doi.org/10.1038/msb.2010.5

Passos, J. F., & von Zglinicki, T. (2005). Mitochondria, telomeres and cell senescence. *Experimental Gerontology*, *40*(6), 466–472. https://doi.org/10.1016/j.exger.2005.04.006

Pathak, R. U., Soujanya, M., & Mishra, R. K. (2021). Deterioration of nuclear morphology and architecture: A hallmark of senescence and aging. *Ageing Research Reviews*, *67*, 101264. https://doi.org/10.1016/j.arr.2021.101264

Pavlova, N. N., & Thompson, C. B. (2016). The Emerging Hallmarks of Cancer Metabolism. *Cell Metabolism*, *23*(1), 27–47. https://doi.org/10.1016/j.cmet.2015.12.006

Petrova, N. V., Velichko, A. K., Razin, S. V., & Kantidze, O. L. (2016). Small molecule compounds that induce cellular senescence. *Aging Cell*, *15*(6), 999–1017. https://doi.org/10.1111/acel.12518

Pinheiro J, Bates D, DebRoy S, Sarkar D, & R Core Team. (2020). *(https://CRAN.R-project.org/package=nlme)*.

Pooam, M., Aguida, B., Drahy, S., Jourdan, N., & Ahmad, M. (2021). Therapeutic application of light and electromagnetic fields to reduce hyper-inflammation triggered by COVID-19. *Communicative & Integrative Biology*, *14*(1), 66–77. https://doi.org/10.1080/19420889.2021.1911413

Popp, F. A., Nagl, W., Li, K. H., Scholz, W., Weingärtner, O., & Wolf, R. (1984). Biophoton emission. *Cell Biophysics*, *6*(1), 33–52. https://doi.org/10.1007/BF02788579

Popp, F.-A. (1992). Some Essential Questions of Biophoton Research and Probable Answers. In *Recent Advances in Biophoton Research and Its Applications* (pp. 1–46). WORLD SCIENTIFIC. https://doi.org/10.1142/9789814439671_0001

Popp, F.-A. (2003a). Biophotons — Background, Experimental Results, Theoretical Approach and Applications. In *Integrative Biophysics* (pp. 387–438). Springer Netherlands. https://doi.org/10.1007/978-94-017-0373-4_12

Popp, F.-A. (2003b). Properties of biophotons and their theoretical implications. *Indian J Exp Biol.*, *41*(5), 391–402.

Pospíšil, P., Prasad, A., & Rác, M. (2019). Mechanism of the Formation of Electronically Excited Species by Oxidative Metabolic Processes: Role of Reactive Oxygen Species. *Biomolecules*, *9*(7), 258. https://doi.org/10.3390/biom9070258

Potapovich, A., & Kostyuk, V. (2021). Cell cell death communication by signals passing through non-aqueous environments. *Results in Chemistry*, *3*, 100107. https://doi.org/10.1016/j.rechem.2021.100107

Powner, M. B., & Jeffery, G. (2024). Light stimulation of mitochondria reduces blood glucose levels. *Journal of Biophotonics*, *17*(5). https://doi.org/10.1002/jbio.202300521

Prasad, A., & Pospišil, P. (2011). Two-dimensional imaging of spontaneous ultra-weak photon emission from the human skin: role of reactive oxygen species. *Journal of Biophotonics*, *4*(11–12), 840–849. https://doi.org/10.1002/jbio.201100073

Prasad, A., & Pospíšil, P. (2013). Towards the two-dimensional imaging of spontaneous ultra-weak photon emission from microbial, plant and animal cells. *Scientific Reports*, *3*(1), 1211. https://doi.org/10.1038/srep01211

Quarta, M., & Demaria, M. (2024). On the past, present and future of senotherapeutics. *Npj Aging*, *10*(1), 11. https://doi.org/10.1038/s41514-024-00139-3

Quijano, C., Cao, L., Fergusson, M. M., Romero, H., Liu, J., Gutkind, S., Rovira, I. I., Mohney, R. P., Karoly, E. D., & Finkel, T. (2012). Oncogene-induced senescence results in marked metabolic and bioenergetic alterations. *Cell Cycle*, *11*(7), 1383–1392. https://doi.org/10.4161/cc.19800

R Core Team. (2021). *R: A language and environment for statistical computing.* R Foundation for Statistical Computing, Vienna, Austria. URL: Https://Www.R-Project.Org/. https://www.R-project.org/

Rabinowitz, Z. M., & Cui, L. (2023). Detecting cellular senescence in vivo: Imagining imaging better. *Aging and Cancer*, *4*(3–4), 97–110. https://doi.org/10.1002/aac2.12067

Rahnama, M. , Tuszynski, J. A. , Bókkon, I. , Cifra, M. , Sardar, P. , & Salari, V. (2011). Emission Of Mitochondrial Biophotons And Their Effect On Electrical Activity Of Membrane Via Microtubules. *Journal of Integrative Neuroscience*, *10*(01), 65–88. https://doi.org/10.1142/S0219635211002622

Rajagopalan, S., & Long, E. O. (2012). Cellular senescence induced by CD158d reprograms natural killer cells to promote vascular remodeling. *Proceedings of the National Academy of Sciences*, *109*(50), 20596–20601. https://doi.org/10.1073/pnas.1208248109

Rastogi, A., & Pospíšil, P. (2010). Ultra-weak photon emission as a non-invasive tool for monitoring of oxidative processes in the epidermal cells of human skin: comparative study on the dorsal and the palm side of the hand. *Skin Research and Technology*. https://doi.org/10.1111/j.1600-0846.2010.00442.x

Rastogi, A., & Pospíšil, P. (2012). Production of hydrogen peroxide and hydroxyl radical in potato tuber during the necrotrophic phase of hemibiotrophic pathogen Phytophthora infestans infection. *Journal of Photochemistry and Photobiology B: Biology*, *117*, 202–206. https://doi.org/10.1016/j.jphotobiol.2012.10.001

Raynard, C., Tessier, N., Huna, A., Warnier, M., Flaman, J.-M., Van Coppenolle, F., Ducreux, S., Martin, N., & Bernard, D. (2022). Expression of the Calcium-Binding Protein CALB1 Is Induced and Controls Intracellular Ca2+ Levels in Senescent Cells. *International Journal of Molecular Sciences*, *23*(16), 9376. https://doi.org/10.3390/ijms23169376

Roets, B. (2023). Potential application of PBM use in hair follicle organoid culture for the treatment of androgenic alopecia. *Materials Today Bio*, *23*, 100851. https://doi.org/10.1016/j.mtbio.2023.100851

Rogers, G. W., Brand, M. D., Petrosyan, S., Ashok, D., Elorza, A. A., Ferrick, D. A., & Murphy, A. N. (2011). High Throughput Microplate Respiratory Measurements Using Minimal Quantities Of Isolated Mitochondria. *PLoS ONE*, *6*(7), e21746. https://doi.org/10.1371/journal.pone.0021746

Rojas, J. C., & Gonzalez-Lima, F. (2013). Neurological and psychological applications of transcranial lasers and LEDs. *Biochemical Pharmacology*, *86*(4), 447–457. https://doi.org/10.1016/j.bcp.2013.06.012

Rojas, J. C., Lee, J., John, J. M., & Gonzalez-Lima, F. (2008). Neuroprotective Effects of Near-Infrared Light in an *In Vivo* Model of Mitochondrial Optic Neuropathy. *The*

Journal of Neuroscience, *28*(50), 13511–13521. https://doi.org/10.1523/JNEUROSCI.3457-08.2008

Rossi, C., Foletti, A., Magnani, A., & Lamponi, S. (2011). New perspectives in cell communication: Bioelectromagnetic interactions. *Seminars in Cancer Biology*, *21*(3), 207–214. https://doi.org/10.1016/j.semcancer.2011.04.003

Rovillain, E., Mansfield, L., Caetano, C., Alvarez-Fernandez, M., Caballero, O. L., Medema, R. H., Hummerich, H., & Jat, P. S. (2011). Activation of nuclear factor-kappa B signalling promotes cellular senescence. *Oncogene*, *30*(20), 2356–2366. https://doi.org/10.1038/onc.2010.611

Roy, M., Reddy, P. H., Iijima, M., & Sesaki, H. (2015). Mitochondrial division and fusion in metabolism. *Current Opinion in Cell Biology*, *33*, 111–118. https://doi.org/10.1016/j.ceb.2015.02.001

Salama, R., Sadaie, M., Hoare, M., & Narita, M. (2014). Cellular senescence and its effector programs. *Genes & Development*, *28*(2), 99–114. https://doi.org/10.1101/gad.235184.113

Sangita Devi, A., & Thokchom, S. (2017). Children Living with Progeria. *Nursing & Care Open Access Journal*, *3*(4). https://doi.org/10.15406/ncoaj.2017.03.00077

Schafer, M. J., White, T. A., Iijima, K., Haak, A. J., Ligresti, G., Atkinson, E. J., Oberg, A. L., Birch, J., Salmonowicz, H., Zhu, Y., Mazula, D. L., Brooks, R. W., Fuhrmann-Stroissnigg, H., Pirtskhalava, T., Prakash, Y. S., Tchkonia, T., Robbins, P. D., Aubry, M. C., Passos, J. F., … LeBrasseur, N. K. (2017). Cellular senescence mediates fibrotic pulmonary disease. *Nature Communications*, *8*(1), 14532. https://doi.org/10.1038/ncomms14532

Schieber, M., & Chandel, N. S. (2014). ROS Function in Redox Signaling and Oxidative Stress. *Current Biology*, *24*(10), R453–R462. https://doi.org/10.1016/j.cub.2014.03.034

Schmidt, S., Schneider, L., Essmann, F., Cirstea, I. C., Kuck, F., Kletke, A., Jänicke, R. U., Wiek, C., Hanenberg, H., Ahmadian, M. R., Schulze-Osthoff, K., Nürnberg, B., & Piekorz, R. P. (2010). The centrosomal protein TACC3 controls paclitaxel sensitivity by modulating a premature senescence program. *Oncogene*, *29*(46), 6184–6192. https://doi.org/10.1038/onc.2010.354

Scialò, F., Fernández-Ayala, D. J., & Sanz, A. (2017). Role of Mitochondrial Reverse Electron Transport in ROS Signaling: Potential Roles in Health and Disease. *Frontiers in Physiology*, *8*. https://doi.org/10.3389/fphys.2017.00428

Scordino, A., Baran, I., Gulino, M., Ganea, C., Grasso, R., Niggli, J. H., & Musumeci, F. (2014). Ultra-weak Delayed Luminescence in cancer research: A review of the results by the ARETUSA equipment. *Journal of Photochemistry and Photobiology B: Biology*, *139*, 76–84. https://doi.org/10.1016/j.jphotobiol.2014.03.027

Sefati, N., Esmaeilpour, T., Salari, V., Zarifkar, A., Dehghani, F., Ghaffari, M. K., Zadeh-Haghighi, H., Császár, N., Bókkon, I., Rodrigues, S., & Oblak, D. (2024). Monitoring Alzheimer's disease via ultraweak photon emission. *IScience*, *27*(1), 108744. https://doi.org/10.1016/j.isci.2023.108744

Serrano, M., Lin, A. W., McCurrach, M. E., Beach, D., & Lowe, S. W. (1997). Oncogenic ras Provokes Premature Cell Senescence Associated with Accumulation of p53 and p16INK4a. *Cell*, *88*(5), 593–602. https://doi.org/10.1016/S0092-8674(00)81902-9

Severino, J., Allen, R. G., Balin, S., Balin, A., & Cristofalo, V. J. (2000). Is β-Galactosidase Staining a Marker of Senescence in Vitro and in Vivo? *Experimental Cell Research*, *257*(1), 162–171. https://doi.org/10.1006/excr.2000.4875

Sharpless, N. E., & Sherr, C. J. (2015). Forging a signature of in vivo senescence. *Nature Reviews Cancer*, *15*(7), 397–408. https://doi.org/10.1038/nrc3960

Shay, J. W., & Wright, W. E. (2000). Hayflick, his limit, and cellular ageing. *Nature Reviews Molecular Cell Biology*, *1*(1), 72–76. https://doi.org/10.1038/35036093

Shay, J. W., & Wright, W. E. (2019). Telomeres and telomerase: three decades of progress. *Nature Reviews Genetics*, *20*(5), 299–309. https://doi.org/10.1038/s41576-019-0099-1

Shen, X., Mei, W., & Xu, X. (1994). Activation of neutrophils by a chemically separated but optically coupled neutrophil population undergoing respiratory burst. *Experientia*, *50*(10), 963–968. https://doi.org/10.1007/BF01923488

Shinhmar, H., Grewal, M., Sivaprasad, S., Hogg, C., Chong, V., Neveu, M., & Jeffery, G. (2020). Optically Improved Mitochondrial Function Redeems Aged Human Visual Decline. *The Journals of Gerontology: Series A*, *75*(9), e49–e52. https://doi.org/10.1093/gerona/glaa155

Shinhmar, H., Hogg, C., Neveu, M., & Jeffery, G. (2021). Weeklong improved colour contrasts sensitivity after single 670 nm exposures associated with enhanced mitochondrial function. *Scientific Reports*, *11*(1), 22872. https://doi.org/10.1038/s41598-021-02311-1

Singh, B. K., Tripathi, M., Sandireddy, R., Tikno, K., Zhou, J., & Yen, P. M. (2020). Decreased autophagy and fuel switching occur in a senescent hepatic cell model system. *Aging*, *12*(14), 13958–13978. https://doi.org/10.18632/aging.103740

Sivapathasuntharam, C., Sivaprasad, S., Hogg, C., & Jeffery, G. (2017). Aging retinal function is improved by near infrared light (670 nm) that is associated with corrected mitochondrial decline. *Neurobiology of Aging*, *52*, 66–70. https://doi.org/10.1016/j.neurobiolaging.2017.01.001

Sivapathasuntharam, C., Sivaprasad, S., Hogg, C., & Jeffery, G. (2019). Improving mitochondrial function significantly reduces the rate of age related photoreceptor loss. *Experimental Eye Research*, *185*, 107691. https://doi.org/10.1016/j.exer.2019.107691

Smogorzewska, A. (2002). Different telomere damage signaling pathways in human and mouse cells. *The EMBO Journal*, *21*(16), 4338–4348. https://doi.org/10.1093/emboj/cdf433

Sommer, A. P., Haddad, M. Kh., & Fecht, H.-J. (2015). Light Effect on Water Viscosity: Implication for ATP Biosynthesis. *Scientific Reports*, *5*(1), 12029. https://doi.org/10.1038/srep12029

Srdic-Rajic, T., Santibañez, J. F., Kanjer, K., Tisma-Miletic, N., Cavic, M., Galun, D., Jevric, M., Kardum, N., Konic-Ristic, A., & Zoranovic, T. (2017). Iscador Qu inhibits

doxorubicin-induced senescence of MCF7 cells. *Scientific Reports*, *7*(1), 3763. https://doi.org/10.1038/s41598-017-03898-0

Srinivasan, S., Guha, M., Dong, D. W., Whelan, K. A., Ruthel, G., Uchikado, Y., Natsugoe, S., Nakagawa, H., & Avadhani, N. G. (2016). Disruption of cytochrome c oxidase function induces the Warburg effect and metabolic reprogramming. *Oncogene*, *35*(12), 1585–1595. https://doi.org/10.1038/onc.2015.227

Stab, B. R., Martinez, L., Grismaldo, A., Lerma, A., Gutiérrez, M. L., Barrera, L. A., Sutachan, J. J., & Albarracín, S. L. (2016). Mitochondrial Functional Changes Characterization in Young and Senescent Human Adipose Derived MSCs. *Frontiers in Aging Neuroscience*, *8*. https://doi.org/10.3389/fnagi.2016.00299

Stier, A. (2021). Human blood contains circulating cell-free mitochondria, but are they really functional? *American Journal of Physiology-Endocrinology and Metabolism*, *320*(5), E859–E863. https://doi.org/10.1152/ajpendo.00054.2021

Stoldt, S., Wenzel, D., Kehrein, K., Riedel, D., Ott, M., & Jakobs, S. (2018). Spatial orchestration of mitochondrial translation and OXPHOS complex assembly. *Nature Cell Biology*, *20*(5), 528–534. https://doi.org/10.1038/s41556-018-0090-7

Storer, M., Mas, A., Robert-Moreno, A., Pecoraro, M., Ortells, M. C., Di Giacomo, V., Yosef, R., Pilpel, N., Krizhanovsky, V., Sharpe, J., & Keyes, W. M. (2013). Senescence Is a Developmental Mechanism that Contributes to Embryonic Growth and Patterning. *Cell*, *155*(5), 1119–1130. https://doi.org/10.1016/j.cell.2013.10.041

Suda, K., Moriyama, Y., Razali, N., Chiu, Y., Masukagami, Y., Nishimura, K., Barbee, H., Takase, H., Sugiyama, S., Yamazaki, Y., Sato, Y., Higashiyama, T., Johmura, Y., Nakanishi, M., & Kono, K. (2024). Plasma membrane damage limits replicative lifespan in yeast and induces premature senescence in human fibroblasts. *Nature Aging*, *4*(3), 319–335. https://doi.org/10.1038/s43587-024-00575-6

Suh, D. H., Kim, M.-K., Kim, H. S., Chung, H. H., & Song, Y. S. (2013). Mitochondrial permeability transition pore as a selective target for anti-cancer therapy. *Frontiers in Oncology*, *3*. https://doi.org/10.3389/fonc.2013.00041

Suski, J. M., Lebiedzinska, M., Bonora, M., Pinton, P., Duszynski, J., & Wieckowski, M. R. (2012a). *Relation Between Mitochondrial Membrane Potential and ROS Formation* (pp. 183–205). https://doi.org/10.1007/978-1-61779-382-0_12

Świder, K., Dominiak, M., Grzech-Leśniak, K., & Matys, J. (2019). Effect of Different Laser Wavelengths on Periodontopathogens in Peri-Implantitis: A Review of In Vivo Studies. *Microorganisms*, *7*(7), 189. https://doi.org/10.3390/microorganisms7070189

Szabadkai, G., & Duchen, M. R. (2008). Mitochondria: The Hub of Cellular Ca^{2+} Signaling. *Physiology*, *23*(2), 84–94. https://doi.org/10.1152/physiol.00046.2007

Tai, H., Wang, Z., Gong, H., Han, X., Zhou, J., Wang, X., Wei, X., Ding, Y., Huang, N., Qin, J., Zhang, J., Wang, S., Gao, F., Chrzanowska-Lightowlers, Z. M., Xiang, R., & Xiao, H. (2017). Autophagy impairment with lysosomal and mitochondrial dysfunction is an important characteristic of oxidative stress-induced senescence. *Autophagy*, *13*(1), 99–113. https://doi.org/10.1080/15548627.2016.1247143

Takeda, M., Kobayashi, M., Takayama, M., Suzuki, S., Ishida, T., Ohnuki, K., Moriya, T., & Ohuchi, N. (2004a). Biophoton detection as a novel technique for cancer imaging. *Cancer Science*, *95*(8), 656–661. https://doi.org/10.1111/j.1349-7006.2004.tb03325.x

Takeda, M., Kobayashi, M., Takayama, M., Suzuki, S., Ishida, T., Ohnuki, K., Moriya, T., & Ohuchi, N. (2004b). Biophoton detection as a novel technique for cancer imaging. *Cancer Science*, *95*(8), 656–661. https://doi.org/10.1111/j.1349-7006.2004.tb03325.x

Tam, S. Y., Tam, V. C. W., Ramkumar, S., Khaw, M. L., Law, H. K. W., & Lee, S. W. Y. (2020). Review on the Cellular Mechanisms of Low-Level Laser Therapy Use in Oncology. *Frontiers in Oncology*, *10*. https://doi.org/10.3389/fonc.2020.01255

Tani, A., Chellini, F., Giannelli, M., Nosi, D., Zecchi-Orlandini, S., & Sassoli, C. (2018). Red (635 nm), Near-Infrared (808 nm) and Violet-Blue (405 nm) Photobiomodulation Potentiality on Human Osteoblasts and Mesenchymal Stromal Cells: A Morphological and Molecular In Vitro Study. *International Journal of Molecular Sciences*, *19*(7), 1946. https://doi.org/10.3390/ijms19071946

Thapa, R. K., Nguyen, H. T., Jeong, J.-H., Kim, J. R., Choi, H.-G., Yong, C. S., & Kim, J. O. (2017). Progressive slowdown/prevention of cellular senescence by CD9-targeted delivery of rapamycin using lactose-wrapped calcium carbonate nanoparticles. *Scientific Reports*, *7*(1), 43299. https://doi.org/10.1038/srep43299

Thar, R., & Kühl, M. (2004). Propagation of electromagnetic radiation in mitochondria? *Journal of Theoretical Biology*, *230*(2), 261–270. https://doi.org/10.1016/j.jtbi.2004.05.021

ThermoFisher Scientific. (2019). *CellEvent™ Senescence Green Flow Cytometry Assay Kit User Guide*. Thermo Fisher Scientific Inc. https://www.thermofisher.com/document-connect/document-connect.html?url=https://assets.thermofisher.com/TFS-Assets%2FLSG%2Fmanuals%2FMAN0018281_CellEvent_Senescence_Green_Flow_Cytometry_Assay_Kit_PIS.pdf

Toussaint, O., Royer, V., Salmon, M., & Remacle, J. (2002). Stress-induced premature senescence and tissue ageing. *Biochemical Pharmacology*, *64*(5–6), 1007–1009. https://doi.org/10.1016/S0006-2952(02)01170-X

Tsuchida, K., & Kobayashi, M. (2020). Oxidative stress in human facial skin observed by ultraweak photon emission imaging and its correlation with biophysical properties of skin. *Scientific Reports*, *10*(1), 9626. https://doi.org/10.1038/s41598-020-66723-1

Turrens, J. F. (2003). Mitochondrial formation of reactive oxygen species. *The Journal of Physiology*, *552*(2), 335–344. https://doi.org/10.1113/jphysiol.2003.049478

van Deursen, J. M. (2014). The role of senescent cells in ageing. *Nature*, *509*(7501), 439–446. https://doi.org/10.1038/nature13193

Van Wijk, R., & Van Wijk, E. (2023). Integrating Ultraweak Photon Emission in Mitochondrial Research. In *Ultra-Weak Photon Emission from Biological Systems* (pp. 461–474). Springer International Publishing. https://doi.org/10.1007/978-3-031-39078-4_28

Van Wijk, R., Van Wijk, E. P. A., Wiegant, F. A. C., & Ives, J. (2008). Free radicals and low-level photon emission in human pathogenesis: state of the art. *Indian Journal of Experimental Biology*, *46*(5), 273–309.

Vasileiou, P., Evangelou, K., Vlasis, K., Fildisis, G., Panayiotidis, M., Chronopoulos, E., Passias, P.-G., Kouloukoussa, M., Gorgoulis, V., & Havaki, S. (2019). Mitochondrial

Homeostasis and Cellular Senescence. *Cells*, *8*(7), 686. https://doi.org/10.3390/cells8070686

Vaupel, P., & Multhoff, G. (2021). Revisiting the Warburg effect: historical dogma *versus* current understanding. *The Journal of Physiology*, *599*(6), 1745–1757. https://doi.org/10.1113/JP278810

Vermeulen, K., Van Bockstaele, D. R., & Berneman, Z. N. (2005). Apoptosis: mechanisms and relevance in cancer. *Annals of Hematology*, *84*(10), 627–639. https://doi.org/10.1007/s00277-005-1065-x

Volodyaev, I., van Wijk, E., Cifra, M., & Vladimirov, Y. A. (2023). *Ultra-Weak Photon Emission from Biological Systems* (I. Volodyaev, E. van Wijk, M. Cifra, & Y. A. Vladimirov, Eds.). Springer International Publishing. https://doi.org/10.1007/978-3-031-39078-4

von Kobbe, C. (2019). Targeting senescent cells: approaches, opportunities, challenges. *Aging*, *11*(24), 12844–12861. https://doi.org/10.18632/aging.102557

von Zglinicki, T. (2002). Oxidative stress shortens telomeres. *Trends in Biochemical Sciences*, *27*(7), 339–344. https://doi.org/10.1016/S0968-0004(02)02110-2

von Zglinicki, T., Saretzki, G., Döcke, W., & Lotze, C. (1995). Mild Hyperoxia Shortens Telomeres and Inhibits Proliferation of Fibroblasts: A Model for Senescence? *Experimental Cell Research*, *220*(1), 186–193. https://doi.org/10.1006/excr.1995.1305

Vyas, S., Zaganjor, E., & Haigis, M. C. (2016). Mitochondria and Cancer. *Cell*, *166*(3), 555–566. https://doi.org/10.1016/j.cell.2016.07.002

Wang, C., Jurk, D., Maddick, M., Nelson, G., Martin-Ruiz, C., & Von Zglinicki, T. (2009). DNA damage response and cellular senescence in tissues of aging mice. *Aging Cell*, *8*(3), 311–323. https://doi.org/10.1111/j.1474-9726.2009.00481.x

Wang, T., Zhang, X., & Li, J. J. (2002). The role of NF-κB in the regulation of cell stress responses. *International Immunopharmacology*, *2*(11), 1509–1520. https://doi.org/10.1016/S1567-5769(02)00058-9

Wang, T.-H., Chen, C.-C., Leu, Y.-L., Lee, Y.-S., Lian, J.-H., Hsieh, H.-L., & Chen, C.-Y. (2021). Palbociclib induces DNA damage and inhibits DNA repair to induce cellular senescence and apoptosis in oral squamous cell carcinoma. *Journal of the Formosan Medical Association*, *120*(9), 1695–1705. https://doi.org/10.1016/j.jfma.2020.12.009

Wang, X., Tian, F., Soni, S. S., Gonzalez-Lima, F., & Liu, H. (2016). Interplay between up-regulation of cytochrome-c-oxidase and hemoglobin oxygenation induced by near-infrared laser. *Scientific Reports*, *6*(1), 30540. https://doi.org/10.1038/srep30540

Wang, Y., Huang, Y.-Y., Wang, Y., Lyu, P., & Hamblin, M. R. (2017a). Photobiomodulation of human adipose-derived stem cells using 810 nm and 980 nm lasers operates via different mechanisms of action. *Biochimica et Biophysica Acta (BBA) - General Subjects*, *1861*(2), 441–449. https://doi.org/10.1016/j.bbagen.2016.10.008

Wang, Y., Huang, Y.-Y., Wang, Y., Lyu, P., & Hamblin, M. R. (2017b). Red (660 nm) or near-infrared (810 nm) photobiomodulation stimulates, while blue (415 nm), green

(540 nm) light inhibits proliferation in human adipose-derived stem cells. *Scientific Reports*, *7*(1), 7781. https://doi.org/10.1038/s41598-017-07525-w

Warburg, O. (1956). On Respiratory Impairment in Cancer Cells. *Science*, *124*(3215), 269–270. https://doi.org/10.1126/science.124.3215.269

Wheaton, K., Campuzano, D., Ma, W., Sheinis, M., Ho, B., Brown, G. W., & Benchimol, S. (2017). Progerin-Induced Replication Stress Facilitates Premature Senescence in Hutchinson-Gilford Progeria Syndrome. *Molecular and Cellular Biology*, *37*(14). https://doi.org/10.1128/MCB.00659-16

Wicher, S. A., Roos, B. B., Teske, J. J., Fang, Y. H., Pabelick, C., & Prakash, Y. S. (2021). Aging increases senescence, calcium signaling, and extracellular matrix deposition in human airway smooth muscle. *PLOS ONE*, *16*(7), e0254710. https://doi.org/10.1371/journal.pone.0254710

Wikramanayake, T. C., Rodriguez, R., Choudhary, S., Mauro, L. M., Nouri, K., Schachner, L. A., & Jimenez, J. J. (2012). Effects of the Lexington LaserComb on hair regrowth in the C3H/HeJ mouse model of alopecia areata. *Lasers in Medical Science*, *27*(2), 431–436. https://doi.org/10.1007/s10103-011-0953-7

Wiley, C. D., & Campisi, J. (2021). The metabolic roots of senescence: mechanisms and opportunities for intervention. *Nature Metabolism*, *3*(10), 1290–1301. https://doi.org/10.1038/s42255-021-00483-8

Wiley, C. D., Velarde, M. C., Lecot, P., Liu, S., Sarnoski, E. A., Freund, A., Shirakawa, K., Lim, H. W., Davis, S. S., Ramanathan, A., Gerencser, A. A., Verdin, E., & Campisi, J. (2016). Mitochondrial Dysfunction Induces Senescence with a Distinct Secretory Phenotype. *Cell Metabolism*, *23*(2), 303–314. https://doi.org/10.1016/j.cmet.2015.11.011

Williams, G. C. (1957). Pleiotropy, Natural Selection, and the Evolution of Senescence. *Evolution*, *11*(4), 398. https://doi.org/10.2307/2406060

Witham, M. D., Granic, A., Miwa, S., Passos, J. F., Richardson, G. D., & Sayer, A. A. (2023). New Horizons in cellular senescence for clinicians. *Age and Ageing*, *52*(7). https://doi.org/10.1093/ageing/afad127

Yadav, A., & Gupta, A. (2017). Noninvasive red and near-infrared wavelength-induced photobiomodulation: promoting impaired cutaneous wound healing. *Photodermatology, Photoimmunology & Photomedicine*, *33*(1), 4–13. https://doi.org/10.1111/phpp.12282

Yegorov, Y. E., Akimov, S. S., Hass, R., Zelenin, A. V., & Prudovsky, I. A. (1998). Endogenous β-Galactosidase Activity in Continuously Nonproliferating Cells. *Experimental Cell Research*, *243*(1), 207–211. https://doi.org/10.1006/excr.1998.4169

Yoon, Y.-S., Yoon, D.-S., Lim, I. K., Yoon, S.-H., Chung, H.-Y., Rojo, M., Malka, F., Jou, M.-J., Martinou, J.-C., & Yoon, G. (2006). Formation of elongated giant mitochondria in DFO-induced cellular senescence: Involvement of enhanced fusion process through modulation of Fis1. *Journal of Cellular Physiology*, *209*(2), 468–480. https://doi.org/10.1002/jcp.20753

Yosef, R., Pilpel, N., Tokarsky-Amiel, R., Biran, A., Ovadya, Y., Cohen, S., Vadai, E., Dassa, L., Shahar, E., Condiotti, R., Ben-Porath, I., & Krizhanovsky, V. (2016).

Directed elimination of senescent cells by inhibition of BCL-W and BCL-XL. *Nature Communications*, *7*(1), 11190. https://doi.org/10.1038/ncomms11190

Yu, H.-S., Wu, C.-S., Kao, Y.-H., Chiou, M.-H., & Yu, C.-L. (2003). Helium–Neon Laser Irradiation Stimulates Migration and Proliferation in Melanocytes and Induces Repigmentation in Segmental-Type Vitiligo. *Journal of Investigative Dermatology*, *120*(1), 56–64. https://doi.org/10.1046/j.1523-1747.2003.12011.x

Zamani, A. R. N., Saberianpour, S., Geranmayeh, M. H., Bani, F., Haghighi, L., & Rahbarghazi, R. (2020). Modulatory effect of photobiomodulation on stem cell epigenetic memory: a highlight on differentiation capacity. *Lasers in Medical Science*, *35*(2), 299–306. https://doi.org/10.1007/s10103-019-02873-7

Zapata, F., Pastor-Ruiz, V., Ortega-Ojeda, F., Montalvo, G., Ruiz-Zolle, A. V., & García-Ruiz, C. (2021). Human ultra-weak photon emission as non-invasive spectroscopic tool for diagnosis of internal states – A review. *Journal of Photochemistry and Photobiology B: Biology*, *216*, 112141. https://doi.org/10.1016/j.jphotobiol.2021.112141

Zhao, X., van Wijk, E., Yan, Y., van Wijk, R., Yang, H., Zhang, Y., & Wang, J. (2016). Ultra-weak photon emission of hands in aging prediction. *Journal of Photochemistry and Photobiology B: Biology*, *162*, 529–534. https://doi.org/10.1016/j.jphotobiol.2016.07.030

Zhong, G., Qin, S., Townsend, D., Schulte, B. A., Tew, K. D., & Wang, G. Y. (2019). Oxidative stress induces senescence in breast cancer stem cells. *Biochemical and Biophysical Research Communications*, *514*(4), 1204–1209. https://doi.org/10.1016/j.bbrc.2019.05.098

Zhou, L., Chen, X., Liu, T., Gong, Y., Chen, S., Pan, G., Cui, W., Luo, Z.-P., Pei, M., Yang, H., & He, F. (2015). Melatonin reverses H2O2 -induced premature senescence in mesenchymal stem cells via the SIRT1-dependent pathway. *Journal of Pineal Research*, *59*(2), 190–205. https://doi.org/10.1111/jpi.12250

Zhu, Q., Xiao, S., Hua, Z., Yang, D., Hu, M., Zhu, Y.-T., & Zhong, H. (2021). Near Infrared (NIR) Light Therapy of Eye Diseases: A Review. *International Journal of Medical Sciences*, *18*(1), 109–119. https://doi.org/10.7150/ijms.52980

Zhu, Y., Tchkonia, T., Pirtskhalava, T., Gower, A. C., Ding, H., Giorgadze, N., Palmer, A. K., Ikeno, Y., Hubbard, G. B., Lenburg, M., O'Hara, S. P., LaRusso, N. F., Miller, J. D., Roos, C. M., Verzosa, G. C., LeBrasseur, N. K., Wren, J. D., Farr, J. N., Khosla, S., … Kirkland, J. L. (2015). The Achilles' heel of senescent cells: from transcriptome to senolytic drugs. *Aging Cell*, *14*(4), 644–658. https://doi.org/10.1111/acel.12344

Ziegler, D. V., Wiley, C. D., & Velarde, M. C. (2015). Mitochondrial effectors of cellular senescence: beyond the free radical theory of aging. *Aging Cell*, *14*(1), 1–7. https://doi.org/10.1111/acel.12287

Zorova, L. D., Popkov, V. A., Plotnikov, E. Y., Silachev, D. N., Pevzner, I. B., Jankauskas, S. S., Babenko, V. A., Zorov, S. D., Balakireva, A. V., Juhaszova, M., Sollott, S. J., & Zorov, D. B. (2018). Mitochondrial membrane potential. *Analytical Biochemistry*, *552*, 50–59. https://doi.org/10.1016/j.ab.2017.07.009